Partial Insertion Effects in Time Domain Reflectometry Waveform Interpretation for Soil Characterization: A Novel Approach and Analysis

Effet de l'insertion partielle sur l'interprétation du signal réfléchi dans le domaine du temps: une approche et une analyse nouvelles

A Thesis Submitted to the Division of Graduate Studies
Of the Royal Military College of Canada
by

Abdelhakim Zahzam

In Partial Fulfillment of the Requirements for the Degree of
Master of Applied Science

September 2024

ACKNOWLEDGMENT

ABSTRACT

Time Domain Reflectometry (TDR) is a popular method used in soil science, geotechnical, and geo-environmental engineering to determine soil properties both in situ and in laboratory tests. The waveform produced by TDR contains information about the electrical properties of the tested soil. These properties include soil permittivity and soil conductivity, which affect the speed and shape of the reflected electrical pulse. By analyzing the TDR waveform, information about soil characteristics such as water content and soil density is obtained. The TDR waveform results depend on the interpretation method and other factors that can impact the waveform, such as pulse frequency and instrument parameters.

The waveform can be interpreted by various methods to determine the tested soil's characteristics such as the tangent method, the Heimovaara method, and Schwartz Adaptive Waveform Interpretation with Gaussian Filtering (AWIGF). All of these existing interpretation methods consider full-length probe insertion in the soil. Using TDR in a Plexiglas column experiment by inserting the TDR probes through the column's cell wall thickness means that the probe is only partially inserted in the soil and partially surrounded by the Plexiglas and the rubber o rings fittings considered here as part of the cell's wall, on a length equal to its thickness. This partial insertion in the soil-Plexiglas column experiment has not been thoroughly discussed or developed in the literature. Therefore, the contribution to the TDR waveform of the cell's wall, reflected by its apparent length on the waveform, has to be found. The electromagnetic properties of the cell's wall are found separately using reference materials of known permittivity.

A novel waveform partitioning method is proposed in this research to extract the correct apparent length of the actual insertion length of the probe in the soil. Two different permittivity averaging methods, refractive index and arithmetic mean, are simultaneously considered in this proposed interpretation method. However, in this study, the refractive index method led to a better fit for most of the obtained waveforms compared to the arithmetic mean method.

This study shows that ignoring the partial insertion of the TDR probes in the tested soil leads to erroneous waveform interpretation underestimating the soil permittivity by as much as 30% for the experimental setup used.

RÉSUMÉ

La réflectométrie temporelle (TDR) est une méthode populaire utilisée en science des sols, en géotechnique et géo-environnement, pour déterminer les propriétés du sol par les essais en place et en laboratoire. Le signal produit par la TDR contient des informations sur les propriétés électriques du sol testé. Ces propriétés comprennent la permittivité et la conductivité électrique du sol, qui affectent la vitesse et la forme de l'impulsion électrique réfléchie dans le milieu. L'analyse du signal TDR permet d'obtenir des informations sur les caractéristiques du sol telles que la teneur en eau et la densité du sol. Les résultats du signal TDR dépendent de la méthode d'interprétation et d'autres facteurs impactant le signal, tels que la fréquence d'impulsion et les paramètres de l'instrument.

Le signal peut être interprété par différentes méthodes pour déterminer les caractéristiques du sol testé, parmi lesquelles la méthode de la tangente, la méthode de Heimovaara et la méthode d'interprétation adaptative du signal de Schwartz avec filtrage gaussien (AWIGF). Toutes ces méthodes d'interprétation existantes prennent en compte l'insertion de la sonde sur toute sa longueur dans le sol. L'utilisation du TDR dans une colonne de plexiglas en insérant les sondes TDR à travers l'épaisseur de la paroi de la colonne signifie que la sonde n'est que partiellement insérée dans le sol et que partiellement entourée par le plexiglas et les joints en caoutchouc. Les joints à l'extérieur de la cellule sont considérés ici comme faisant partie de la paroi de la cellule, sur une longueur égale à l'épaisseur de celle-ci. Cette insertion partielle dans l'expérience de la colonne de sol-Plexiglas n'a pas été discutée ou développée de manière approfondie dans la littérature. Par conséquent, la contribution du signal TDR de la paroi de la cellule, reflétée par sa longueur apparente sur le signal, doit être trouvée. Les propriétés électromagnétiques de la paroi de la cellule sont déterminées séparément en utilisant des matériaux de référence dont la permittivité est connue.

Une nouvelle méthode de partitionnement du signal est proposée dans cette recherche pour extraire la longueur apparente correcte de la longueur d'insertion réelle de la sonde dans le sol. Deux méthodes différentes de calcul de permittivité moyenne, l'indice de réfraction et la moyenne arithmétique, sont prises en compte simultanément dans la méthode d'interprétation proposée. Cependant, dans cette étude, l'indice de réfraction a permis une meilleure adéquation pour la majorité des signaux obtenus par rapport à la méthode de la moyenne arithmétique.

Cette étude montre que le fait d'ignorer l'insertion partielle des sondes TDR dans le sol testé conduit à une interprétation erronée du signal, sous-estimant la permittivité du sol de 30 % pour la configuration expérimentale utilisée.

TABLE OF CONTENTS

LIST OF TABLES

LIST OF FIGURES

LIST OF SYMBOLS

c	Speed in vacuum constant (3×10^8 m/s)
c_j	Given coefficient for each data point ρ_j [-]
Cc	Coefficient of Curvature [-]
Cu	Uniformity Coefficient [-]
d	Smoothing constant to evaluate V'_{max2} [-]
e	Smoothing constant to evaluate t_1 [-]
ECb	Bulk electrical conductivity [L^{-3} M^{-1} T^3 I^2]
$ECpw$	Pore water electrical conductivity [L^{-3} M^{-1} T^3 I^2]
f_2	Fraction of points in the waveform [-]
$f_i(K_{a2}/K_{a1})$	Layer 1 and layer 2 apparent permittivity ratio function [-]
	• i = number of the function
Gs	Specific gravity of soil [-]
$g(t;\sigma)$	Gaussian kernel with a standard deviation at time t [-]
$g'(t;\sigma)$	First order Gaussian derivative kernel with a standard deviation at time t [-]
$h(t)$	Gaussian smoothed waveform at time t [-]
$h'(t)$	Gaussian smoothed waveform first derivate at time t [-]
$h''(t)$	Gaussian smoothed waveform second derivate at time t [-]
i	Center of a moving window [-]

i_{max2}	Waveform point associated with $t_{V'max2}$ [-]
i_{max1}	Waveform point associated with $t_{V'max1}$ [-]
i_b	Last point of the baseline before the local amplitude minimum [-]
j	$(-1)^{0.5}$
K_a	Apparent relative dielectric permittivity also presented as K [-]
K_{aA}	Apparent relative dielectric permittivity of air [-]
K_{a2}/K_{a1}	Layer 2 to layer 1 apparent relative dielectric permittivity ratio [-]
K_{aB}	Apparent relative dielectric permittivity of column's wall [-]
K_{aS}	Apparent relative dielectric permittivity of soil [-]
K_{aS1}/K_{aS2}	Layer 2 to layer 1 apparent relative dielectric permittivity of soil ratio [-]
$K_{aR'}$	Apparent relative dielectric permittivity of reference material when the TDR is partially inserted [-]
K_{ijk}	Measured apparent relative dielectric permittivity [-]

- i = Setup number (1 to 10)
- j = TDR number (1, 2, 3)
- k = Vertically inserted (V), Laterally inserted (L)

K_{aT}	Total apparent relative dielectric permittivity [-]
K_{ai}	Apparent relative dielectric permittivity of i [-]

- i = L1 for layer 1, L2 for layer 2

K^*	Dielectric relative dielectric permittivity [-]
K'	Real part of the relative dielectric permittivity [-]

K'' Imaginary part of the relative dielectric permittivity [-]

L_a Apparent length [L]

L_{aR} Apparent length of reference material along a fully inserted TDR probe [L]

$L_{aR'}$ Apparent length of reference material along a partially inserted TDR probe [L]

$L_{aB+R'}$ Apparent length of column's wall and the reference material along the TDR probe [L]

L_{aB} Apparent length of column's wall along a partially inserted TDR probe [L]

L_{aS} Apparent length of soil along a partially inserted TDR probe [L]

L_{aT} Total apparent length [L]

L_i Layer i [-]

- i = 1 for layer 1, 2 for layer 2, 2' for layer 2 found with the tangent method on the vertical insertion waveform

L_r Real length [L]

L_{rT} Real total length [L]

L_{ri} Real length of each layer along TDR probe [L]

- i = L1 for layer 1, L2 for layer 2

L_{rR} Real length of reference material along a fully inserted TDR probe [L]

$L_{rR'}$ Real length of reference material along a partially inserted TDR probe [L]

L_{rB} Real length of column's wall along a partially inserted TDR probe [L]

L_{rS} Real length of soil along a partially inserted TDR probe [L]

L_{rA} Real length of air along a partially inserted TDR probe [L]

$L_{rB+R'}$ Real length of column's wall and reference material along TDR probe [L]

L_{rT}	Real total length [L]
L_{ri}/L_{rT}	Layer's length fraction along the TDR probe [-]
	• i = number of the layer
L_{r1}/L_{r2}	Layer 1 to layer 2 length ratio along the TDR probe [-]
m_2	Half width of points in $h''(t)$ to fit parabola and estimate $t_{V''max2}$ [-]
N_p	Number of sampling points in the waveform $V(t)$ [-]
R^2	Coefficient of determination [-]
S	Sampling interval [T]
T	Temperature [°C]
t_1	Time of the first reflection on the TDR's waveform [T]
t_{1-i}	Time of the first reflection on the waveform of TDR [T]
	• i = number of the TDR
t_2	Time of the second reflection on the TDR's waveform [T]
t'_1	Time of the first reflection of the column's wall on the waveform [T]
t'_2	Time of the second reflection of the column's wall on the waveform [T]
t_j	Time of the reflection ρ_j [T]
$t_{V'max2}$	Highest point in $h'(t)$ [T]
$t_{V'max2}$	Time of the highest h'(t) associated with i_{max2} [T]
t_{Vmin2}	Time in V(t) associated with $t_{V'min2}$ [T]
$t_{V'min2}$	Time when h'(t) is equal to zero [T]
$t_{V''max2}$	Time of the maximum second derivative [T]

t_{x2}	Time at the intersection of the tangents [T]
t_{+w}	Furthest time on the right of a moving window [T]
t_{-w}	Furthest time on the left of a moving window [T]
V_0	Measured pulse's amplitude at the end of the waveform [-]
V	Measured amplitude at time t that is converted to ρ [-]
V	Vertical fully inserted TDR total permittivity [-]
$V1$	Calculated vertical total relative permittivity (layer 1+layer 2) using lateral TDRs' measured permittivity [-]
$V2$	Calculated vertical total relative permittivity (layer 1+layer 2) using vertical TDR obtained waveform [-]
V'_{max2}	Maximum amplitude gradient of $h'(t)$ [T^{-1}]
V'_{0max2}	Maximum amplitude gradient obtained in air [T^{-1}]
$V(t)$	Obtained waveform from TDR [V]
w	Half of moving window length [T]
$+w$	Right half of a moving window length [T]
$-w$	Left half of a moving window length [T]
Δ	Calculated difference
Δt	Total time travel [T]
Δt_s	Travel time of partially inserted TDR probe into the soil [T]
Δt_T	Total travel time [T]
Δt_B	Travel time of partially inserted TDR probe into the reference material [T]

$\Delta t_{B+R'}$	Travel time in column's wall with reference material [T]
$\Delta t_{R'}$	Travel time of partially inserted TDR probe into the reference material [T]
Δt_R	Travel time of fully inserted TDR probe into the reference material [T]
Δt_p	Total travel time of the full length probe [T]
Δt_0	Correction term used to describe the epoxy part of the TDR in (Heimovaara 1993) [T]
α	Fitted characteristic noise level [T]
β	Fitted exponent [-]
γ	Constant given for the highest smoothing level [-]
λ	Wavelength [L]
σ	Standard deviation or half width of the Gaussian kernel [T]
σ_a	Standard deviation of the Gaussian kernel that scales the minimum smoothing level [T]
σ_b	Standard deviation of the Gaussian kernel that scales the maximum smoothing level [T]
σ_{dc}	Zero frequency conductivity $[\mathrm{L}^{-3}\,\mathrm{M}^{-1}\,\mathrm{T}^3\,\mathrm{I}^2]$
ρ	Reflection coefficient [-]
ρ_d	Soil's dry density $[\mathrm{M}\,\mathrm{V}^{-3}]$
ρ_j	Reflection coefficient at a time t in a window [-]
ρ_i	Average reflection coefficient obtained within the window [-]
ω	Angular frequency $[\mathrm{T}^{-1}]$
ε_w	Water's permittivity [-]
ε_0	Free-space permittivity (8.854 x 10^{-12} F/m)

$\bar{v}$ Normalized velocity [L/T]

v_{EMT} Velocity calculated with electromagnetic theory [LT^{-1}]

v_{meas} Velocity calculated with electromagnetic theory [LT^{-1}]

v_{ray} Velocity calculated with ray theory [LT^{-1}]

Chapter 1: Introduction

1.1. Background

Time-domain reflectometry (TDR) is widely employed in geotechnical engineering to determine soil properties. One of its primary applications is to determine soil moisture in experiments studying water movement and distribution, such as in vadose zones. It has also been used to determine and monitor other soil characteristics, such as density and contaminants. Using TDR in soil columns offers multiple advantages over traditional soil analysis methods: TDR is a non-destructive real-time measurement method for soil properties, allowing users to monitor soil conditions without disturbing the soil. TDR can be easily implemented in other soil analysis experiments. TDR enables measurements of soil properties along vertical profiles within soil columns, making it commonly used. However, despite its common usage in columns, very little available information in literature approaches the subject of the column's wall effect on the TDR waveform. It is considered negligible or not presented, unlike other literature using TDR on soil columns where the subject is not discussed.

1.2. Objective of the research

The objective of this research is to develop a partial insertion method that considers both refractive index and arithmetic mean permittivity averaging methods for different interpretation techniques. Multiple experiments will be conducted to demonstrate how various TDR characteristics and column usage affect the results. Since several waveform interpretation methods exist, three approaches are considered and compared. This involves identifying differences in results and determining parameters that contribute to discrepancies beyond the interpretation method itself. The methods under consideration include the tangent method, commonly used in early TDR applications, the Heimovaara method, which relies on calibration with known permittivity materials, and the Schwartz method, an advanced automated technique for determining permittivity. The literature indicates that TDR usage in multilayer columns is primarily in vertical and lateral positions. A comparison of these layouts will be conducted to assess their respective advantages and disadvantages. Furthermore, identifying errors associated with TDR usage in

columns is another objective of this research. This information is crucial for future corrections and improvements, ultimately leading to better results.

1.3. Research program

The research program consists of four main phases following the literature review. These phases include familiarization with the TDR, construction of columns, experiments, and result analysis.

The first phase involves familiarization with the TDR, where tests are conducted on different materials to master waveform interpretation and to understand the effect of material characteristics on the waveforms and permittivity.

The second phase is column construction. It begins with constructing a small column to test the construction method before constructing the other columns. Subsequently, tests are conducted on the columns with water and soil to address any issues.

The third phase comprises experiments. Once the procedures are prepared, a blank test is conducted to identify areas for improvement. After refining the experimental procedure, up to three tests are conducted before the experiments commence. In the case of more extended experiments with repetitive procedures, multiple repetitions are performed before the experiments.

The fourth phase involves results analysis, which includes waveform interpretation, data compilation, and discussion of the obtained results.

1.4. Thesis organization

Chapter 1: Introduction

The use of TDR in soil test columns is introduced and the research objectives and methodology are presented.

Chapter 2: Literature review

The literature review is presented to explain how the TDR works, to show the different interpretation method and its application in laboratory experiments.

Chapter 3: Method theory to determine the permittivity of soil in a cell

The general method of partial insertion is explained and then, the applied method on different interpretation methods is explained.

Chapter 4: Experimental setup

The construction of the column is presented with the modifications that were done during the upgrade. The TDR, the variable energy rammer, soils and the thermometer are described.

Chapter 5: Experimental procedure

The gradual insertion, the multi setups and the multi layers experiments' procedures are presented.

Chapter 6: Results and discussion

The results and discussion of the following points are presented:

- The obtained results of the Heimovaara interpretation method.
- The obtained permittivity of the column's wall using different interpretation methods.
- Results from multiple TDR setups experiments.
- Comparison of refractive index and arithmetic mean, and multi-layer experiments.

Subsequently, the sources of errors related to TDR usage in columns are presented and discussed.

Chapter 7: Conclusion

The key points about the partial insertion correction method, the experiments, permittivity averaging methods, and waveform interpretation methods are discussed, along with recommendations and future work.

Chapter 2: Literature review

TDR (Time Domain Reflectometry) is a technique that evaluates the reflectometry of pulse travel using the time domain. Initially introduced in the 60s, it was used mainly to measure the distance of a discontinuity in electrical and communication lines. In the 70s, research about TDR to determine the soil's properties emerged (Davis and Annan 1977) until (Topp et al. 1980) popularized TDR usage in the geotechnical engineering field. Topp et al. (1980) work consists of obtaining multiple permittivity at different volumetric water contents to obtain an empirical permittivity-dependent equation. This opened the way for more TDR-related work in geotechnical engineering, such as wetting front detection (Christiansen 1995), contaminants detection (Chenaf and Amara 2004), and other monitoring TDR work where the TDR signal is related to soil condition.
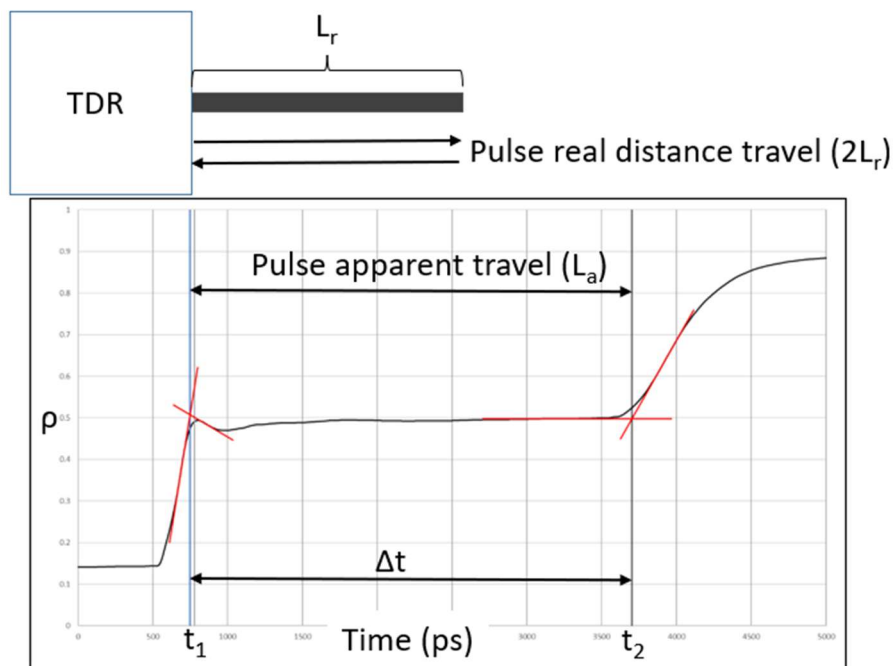
Figure 1.4.1: Illustration of a waveform obtained from a TDR

The TDR works by sending an electrical pulse down a cable or probe and measuring the reflections changes of the pulse during the travel. The TDR device or pulse generator generates an electrical pulse with different properties, such as the pulse frequency and frequency bandwidth. Then, it is sent down the medium, such as a cable or probe inserted in a material. That pulse travels at a known

velocity, which is determined by the properties of the medium. During the travel, the amplitude of the pulse changes with the environment's condition change around the medium. In Figure 1.4.1, the amplitude of the waveform is converted to the reflection coefficient ρ, which is the reflected voltage to the transmitted voltage ratio. Otherwise, the equation of ρ, as used in Schwartz et al. (2016), can be described as reflection coefficient ρ, which is the reflected voltage to the transmitted voltage ratio. Otherwise, the equation of ρ, as used in Schwartz et al. (2016), can be described as

$$\rho = \frac{2V - V_0}{V_0} \qquad\qquad (2.1)$$

Where V_0 is the incident pulse amplitude that is the measured amplitude at the plateau at the end of the waveform (around 20 000ps) obtained in air (open circuit). V is the reflected pulse amplitude measured at time t on the waveform.

As the pulse encounters a change in the dielectric constant or a discontinuity in the cable, a portion of the pulse is reflected back toward the TDR device. The reflected pulse is detected by the TDR device, and the time taken for the pulse to travel from the TDR device to the discontinuity and back is measured. In the case of a TDR probe, the total physical travelled distance is twice the probe length L_r. In order to determine the apparent relative permittivity K_a of a material with a Time Domain Reflectometry (TDR) apparatus, a Δt is obtained from the waveform shown in Figure 1.4.1 by determining the position of t_1 and t_2. Note that only the relative permittivity is used in this thesis and is represented with variable K. The Δt is the time needed for the pulse to travel the real probe length (L_r) that is inserted in the material and to return. Thus, the first reflection at t_1 is the time at which the pulse enters part of the probe in the material, and the second reflection at t_2 is when it ends the travel at the end of the probe. With those measured parameters of the waveform, K_a can be calculated using the equation below.

$$K_a^{0.5} = \frac{c\,\Delta t}{2\,L_r} = \frac{L_a}{2\,L_r} \qquad\qquad (2.2)$$

Where c is the speed in the vacuum (3×10^8 m/s) and L_r is the TDR real length inside the material. The $K_a^{0.5}$ is also defined as a ratio of the apparent length L_a to the total real travel length. The L_a is the measured length of the reflected signal, which is obtained by multiplying c by Δt measured on the waveform, as shown in equation (2.2) and Figure 1.4.1. The application of the equation (2.1

) can be applied for transverse electromagnetic electromagnetic wave which require TDRs that have at least two conductors like the one used in this thesis that has 3 probes.

In Topp et al. (1980), the dielectric permittivity K^* of a material defined in equation (2.3) has two components. The real part K' represents the ability of a material to store electrical energy, and the imaginary part K'' represents the ability of the material to dissipate electrical energy. The dissipated energy is the electrical loss due to frequency-dependent loss mechanisms such as dielectric relaxation and ionic conductivity. The TDR can only measure the real part of the dielectric permittivity because it is made to measure the pulse properties variation in time. However, for this reason, the permittivity in equation (2.2) is called apparent permittivity K_a. The imaginary part of the dielectric permittivity of the material can be estimated (Topp et al. 2000), and other methods, such as frequency domain reflectometry, can also be used. For most soils except for clay, the imaginary part has negligible impact on the dielectric permittivity when the probe is fully inserted in a soil, making $K^* \approx K'$ at pulse frequency above 1 GHz. Also, as a part of the imaginary part of the equation (2.3), the σ_{dc} is the zero-frequency conductivity, the ω is the angular frequency, ϵ_0 is the free-space permittivity, and j is $(-1)^{0.5}$.

$$K^* = K' + j\left[K'' + \left(\frac{\sigma_{dc}}{\omega\,\epsilon_0}\right)\right] \tag{2.3}$$

2.1   Determining t_1 and t_2 (Waveform interpretation methods)

Multiple methods to determine t_1 and t_2 exist, from which the most commonly used methods are the tangent method and Heimovaara (1993) method. Furthermore, some TDR apparatus, such as (Schwartz et al. 2014), are programmed to determine the Δt to give the K_a of soil which is called the Schwartz method in this thesis.

Initially, the obtained waveform from the TDR contained the section of the cable that connects to the probes. So, a manual analysis is done to determine the probe section of the waveform in order to determine Δt of that section and calculate the permittivity. Generally, the t_1 is the first peak of that section from which the apex is found at the intersection of two tangent lines that are on each side of the peak. Then, the second reflection at the next high increase of ρ, t_2 is found by using the

intersection of the tangent of the curve preceding the curve change and the tangent of the increase, as shown in Figure 1.4.1. When the permittivity changes, both t_1 and t_2 change when the Tangents method is used.

Most of the TDR probes in early literature were hand-made, and were maintained with epoxy resin. That epoxy part of TDR has a certain length section of the probe in it, which creates a lag since the pulse passes through the epoxy section before going into the free probe section. Thus, using the Tangent method in that situation leads to erroneous results (Robinson et al. 2003) when the first reflection is used as t_1. Heimovaara (1993) developed a correction method to remediate the problem, as shown in the equation below.

$$\Delta t_s = \Delta t_p - \Delta t_0 \tag{2.4}$$

Where Δt_s is the travel time in the soil, Δt_p is the total travel time obtained from a fully inserted TDR in soil, and Δt_0 is the correction term used to describe the epoxy section of the TDR. The correction term is found by inserting the TDR in a known material with a known permittivity, such as air with a permittivity of 1 and water with a permittivity following the equation below (Hasted 1973)

$$\varepsilon_{water}(T) = 87.740 - 0.40008\,T + 9.398\;x\;10^{-4}\,T^2 - 1.410\;x\;10^{-6}\,T^3 \tag{2.5}$$

Where T is the temperature in $°C$. Knowing the temperature during the insertion of the TDR probes, the permittivity of water is calculated using equation (2.5). With the obtained permittivity of water at temperature T and the TDR probe length inside the water, the Δt is found by isolating it using equation (2.2). Then, the water's Δt is substracted from the total Δt of the fully inserted in water TDR giving the Δt_0. Same is done with air.

The discussed waveform interpretation method below can't be accurate if the waveform smoothing is high or low, especially during waveform interpretation. Multiple waveform smoothing methods exist to remove noise, such as wavelet analysis, Gaussian Kernel, moving polynomial regression, moving median, and Kalman, using Matlab, Python, and other signal processing software. However, their application depends on the type of waveform, either on the frequency domain or

time domain. However, in the case of TDR waveforms, three main smoothing methods are presented in the literature, which are the moving average, Savitzky-Golay filter and Gaussian filter in the adaptive waveform interpretation with Gaussian filtering (AWIGF).

Starting with the simplest one, the moving average filter, which consists of calculating the average value inside a moving window. The window in this context is the number of data points where a higher number of data gives a higher smoothing effect. This method of smoothing was used in Heimovaara and Bouten (1990a) on a 251 data points waveform to develop an automated analysis. The author applied smoothing, where the window length was adjusted for each sensor. Then, a first derivative is done in order to find the inflection point of the rising section following the beginning and the end of the sensor section of the waveform. This is used to determine a range of data points to calculate the linear regression that will be used as a tangent in the automated analysis. However, for a waveform that has the same axis as Figure 1.4.1, the moving average follows the equation below

$$\rho_i = \frac{\sum_{j=i-w}^{i+w} \rho_j}{2w + 1} \qquad\qquad (2.6)$$

Where ρ_j is the reflection coefficient at a time t_j, w is the half of the window length, and ρ_i is the reflection coefficient obtained by the average within the window. This filtering method is fast, but it can affect the accuracy of the waveform interpretation by flattening highly negative or positive peaks. This happens when there is a high difference between one point and the rest of the data point within the window.
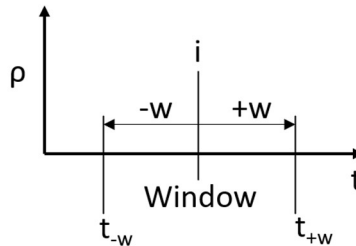
Figure 2.1.1: Visual representation of a window in moving average

The Savitzky-Golay filter is another smoothing filter that was applied to waveforms. It uses the same principle of the window as the moving average. But instead of using an average value, it uses a polynomial of a chosen degree to fit the data points within the window. Then, the smoothed point value at data point i is found on that polynomial curve. The method's equation is below

$$\rho_i = \sum_{j=i-w}^{i+w} c_j \, \rho_j \qquad\qquad (2.7)$$

Where c_j is the given coefficient for each data point ρ_j that depends on the window width, the polynomial degree and the derivation degree. The method can also be used to determine maxima and minima data points by using the first derivative and to find the inflection point by using second derivative coefficients. In S. R. Evett (2000), the user can choose between 0 and 21 data points for smoothing the initial waveform and 0 to 19 data points for the derivative of the waveform.

The Gaussian filter is a filter that can be applied on one dimension, such as a TDR signal, and can also be applied on two dimensions application. The Gaussian filter consists of using Gaussian function to smooth the waveform (AWIGF), as shown in the equation below for one dimension (Schwartz et al. 2014)

$$g(t\,;\,\sigma) = \frac{1}{\sqrt{2\pi\sigma}} \, exp\left(\frac{-t^2}{2\sigma^2}\right) \qquad\qquad (2.8)$$

Where t is time, and σ is the standard deviation or half-width of the Gaussian kernel. The AWIGF method consists of a convolution of the waveform $V(t)$ using the Gaussian in equation (2.8) to obtain the smoothed waveform $h(t)$ shown in Figure 2.1.2. The convolution of Gaussian-derivative kernels $g'(t;\sigma)$ in equation (2.9) with $h(t)$ is done to obtain the first derivative of the smoothed waveform $h'(t)$. When the convolution of $h'(t)$ is done with $g'(t;\sigma)$, the second derivative of the smoothed waveform $h''(t)$ is obtained (the third waveform in Figure 2.1.2), where its usage is explained later in this chapter.

$$g'(t \; ; \; \sigma) = \frac{-2t}{\sqrt{2\pi\sigma}} \; exp\left(\frac{-t^2}{2\sigma^2}\right) \qquad\qquad (2.9)$$

In equation (2.9), the standard deviation σ is defined as

$$\sigma = e\sqrt{\frac{\alpha}{S}} \qquad\qquad (2.10)$$

Where e is a constant-dependent on the rise time of the signal to evaluate t_1, S is the sampling interval, and α is a fitted characteristic noise level associated with a given step pulse generator and background noise environment. S and α are a time unit while the constant e is unitless, and both α and e are instrument-dependent. Once the waveform is smooth and the derivations are done, the t_1 is found by evaluating the part in the waveform where the first reflection is present.

To determine the characteristics of the second reflection, the right window is defined as f_2N_p on waveform $V(t)$, where N_p is the number of sampling points in the waveform $V(t)$, and f_2 is the fraction of these points. In Schwartz et al. (2014), f_2 is set at 0.72 for all analyses. That window is then smoothed to obtain $h'(t)$ using equation (2.11) to calculate σ where d is set to 2.0 to allow the maximum of the derivative of the smoothed signal V'_{max2} to be determined at a consistent level of smoothing.

$$\sigma = d\sqrt{\frac{\alpha}{S}} \qquad\qquad (2.11)$$

Then, V'_{max2} is found within f_2N_p, and σ is calculated using equation (2.12). Because of V'_{max2} variation, with the amplitude scale and rise time of the step pulse generator, Schwartz et al. (2014) propose an adaptive scaled Gaussian kernel. Equation (2.12) uses parameter β, which is a fitted exponent used to evaluate the smoothing level of the Gaussian kernel and ratio of the obtained V'_{max2} to the equivalent maximum gradient obtained with TDR measurement in air V'_{0max2}, V'_{max2}/V'_{0max2}.

$$\frac{\sigma - \sigma_a}{\sigma_b - \sigma_a} = exp\left(-\beta \frac{V'_{max2}}{V'_{0\,max2}}\right) - exp(-\beta) \qquad (2.12)$$

The standard deviation of the Gaussian kernel that scales the minimum smoothing level in time, unit σ_a is assumed to be $(\alpha/S)^{0.5}$ to avoid excessive smoothing. As for the standard deviation of the Gaussian kernel that scales the maximum smoothing level in time unit σ_b is defined as $\gamma \sigma_a$ where γ is a constant that gives the highest smoothing level. In Schwartz et al. (2014), the chosen value of γ is 6. The obtained σ in equation (2.12) is then used to smooth the right window in order to obtain $h''(t)$.
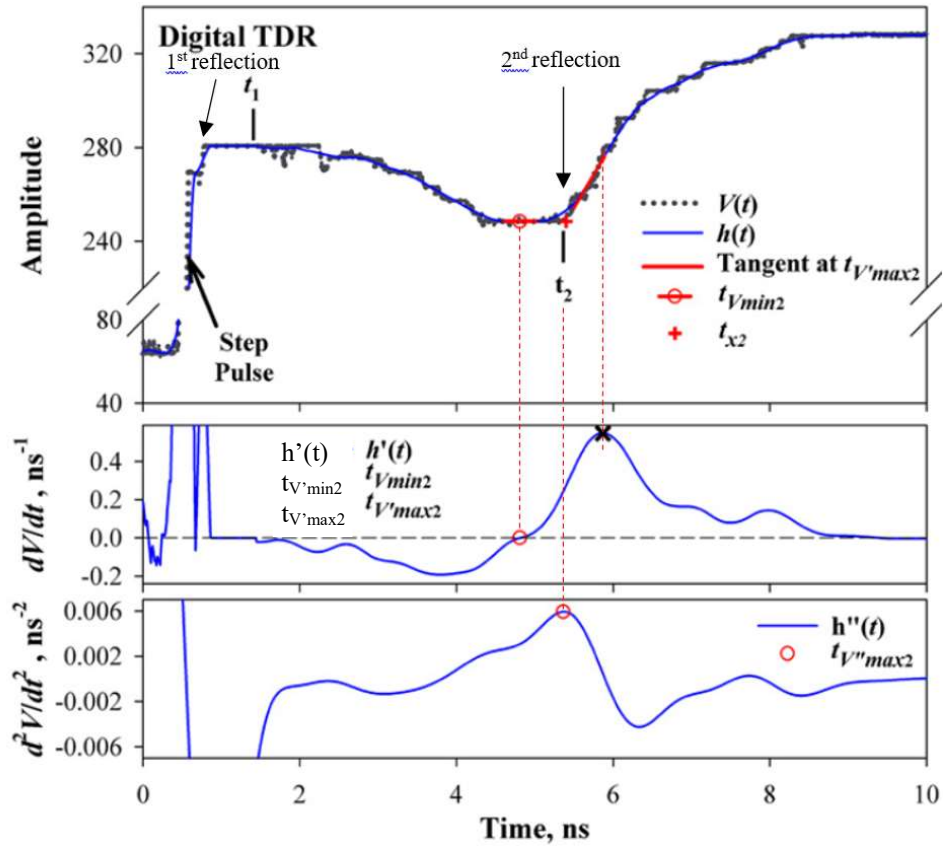
Figure 2.1.2: An example of AWIGF waveform interpretation (Schwartz et al. 2014)

As presented in Schwartz (2014), in $h'(t)$ shown in Figure 2.1.2, the time of the highest point $t_{V'max2}$ is associated with i_{max2} in $V(t)$, and $t_{V'min2}$ is the point where $h'(t)$ is equal to 0 which is associated with t_{Vmin2} in $V(t)$ before the second reflection. The $t_{V'max2}$ and t_{Vmin2} are used to determine the

intersection of the tangents t_{x2}. The tangent to $t_{V'max2}$ after the second reflection is found by an approximation where a linear fit of five points centred on the point i_{max2}. The tangent before the second reflection of $h(t)$ at t_{Vmin2} is found by using a second-order Taylor series approximation. In the case where $t_{V'min2}$ in $h'(t)$ doesn't exist, the intersection of both AWIGF tangents t_{x2} is obtained by using tangent at $t_{V'max2}$ and a tangent line of seven $h(t)$ waveform points. The last point of the 7 points i_b is positioned at

$$i_b = i_{max1} + \lfloor 0.7(i_{max2} - i_{max1}) \rfloor \qquad (2.13)$$

Where i_{max1} is the point identified with the time $t_{V'max1}$, which is the highest point in the $h'(t)$ waveform at the beginning of the transmission line. In the case of an oscillation caused by the heterogeneity of the material condition along the probes, which can result in multiple local minimums, the t_{Vmin2} just before the second reflection is chosen and a linear fit to the baseline is done. In order to remove error relative to the usage of t_{x2} to find t_2 because of the waveform attenuation, the time $t_{V''max2}$ at the highest point i_{2d} in waveform $h''(t)$ is used following equation (2.14). It is found by calculating the maximum of a parabola with $\pm m_2$ points on each side of the maximum. Where the m_2 is defined as $m_2 = ||(N-1)/4||$. Once t_2 is found, the travel time Δt is calculated.

$$t_2 = \begin{cases} t_{V''max2} \ for \ t_{Vmin2} \leq t_{V''max2} \leq t_{x2} \\ t_{Vmin2} \ for \ t_{Vmin2} > t_{V''max2} \\ t_{x2} \ for \ t_{V''max2} > t_{x2} \end{cases} \qquad (2.14)$$

2.2   TDR usage standard

As for most experiments or instrument usage, norms should exist in order to ensure accurate usage and results. In the case of the TDR, there is an ASTM standard test method for water content and density of soil in situ by TDR (D6780/D6780M-19). The standard consists of using multiple rod probes, coaxial head, and TDR apparatus to obtain the apparent relative dielectric constant K_a of the soil in situ. Then, the soil where the measurement is done is excavated to be compacted in a

mould where the same measurement is done with the same coaxial head and TDR. With the obtained K_a of both in situ and in the mould, the water content and the dry density are calculated. The standard doesn't require any specific type of TDR, but articles are proposed for waveform interpretation (Yu and Drnevich 2004, Jung et al. 2013) and automated waveform interpretation (Baker and Allmaras 1990, Heimovaara and Bouten 1990b, Or and Wraith 1999, Feng et al. 1999). However, this standard doesn't go in-depth about waveform interpretation, where someone with a different TDR can have some difficulties. Moreover, the proposed articles can't be applied to all TDRs because the waveforms can be different. The difference in waveforms can be caused by the fact that the pulse is sent through a cable before getting into the probes or different TDR characteristics, such as the step pulse characteristic. In order to understand how to interpret the TDR waveforms, a literature review is not enough because of the TDR apparatus difference. It is suggested to experiment with deionized water, where its electrical properties are largely documented.

2.3 TDR application methods in Lab experiments

As introduced in this chapter, the TDR can be used as an instrument to monitor change in the soil where the TDR is calibrated for a specific condition, considering all the parameters that affect the calibration. For example, to calibrate TDR for soil volumetric water content measurements, the TDR tests are done at multiple values of water content and temperatures (Or and Wraith 1999, Schanz et al. 2011). The TDR can also be used to detect changes in the material's initial condition. For example, TDR is used for landslide detection (Thuro et al. 2010, Chung et al. 2022), where a coaxial cable is inserted into a hole that crosses enough distance to cover the shear zone. Then, the deformation is detected when the last obtained waveform spikes, as shown in Figure 2.3.1 (B) which demonstrates the initial waveform doesn't. Moreover, the depth can be determined by the coaxial cable properties and the waveform.
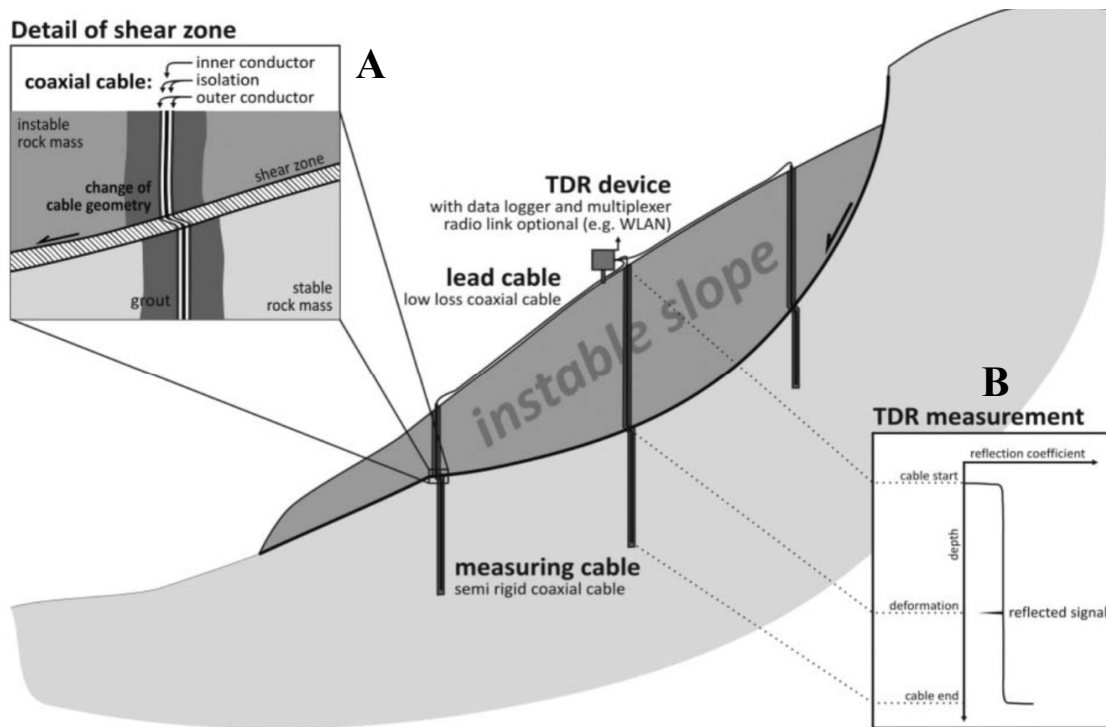
Figure 2.3.1: Illustration of TDR usage to monitor slope stability (Thuro et al. 2010)
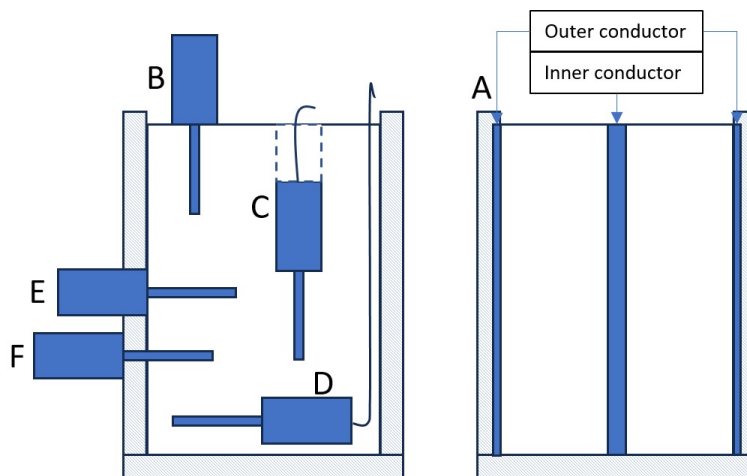
Figure 2.3.2: The different possible layouts of TDR in a cell

At the beginning of the TDR usage in soil mechanics and geotechnical domains, the TDR was mostly inserted in soil only. But with increased popularity, the TDR was intensively used in experiments necessitating columns. It depends on its application, the TDR can be inserted in a soil

cell in different orientations and positions as shown in Figure 2.3.2. The TDR can be installed on a column as layouts B, C, D E and F or it can be the column itself as layout A shown in Figure 2.3.2.

 The Figure 2.3.2 layout A consists of a coaxial cell that is built with an inner conductor and an outer conductor, the same as a coaxial cable. The inner conductor is a probe that is connected to a cable through which the pulse is sent. The outer conductor is used to have an accurate reading by protecting the inner conductor from external interferences and to lower noise. The TDR cell works the same way as the other TDRs that are built to be inserted. This means that the waveform interpretation is the same, where a t_1 and t_2 are found in order to determine the permittivity. This apparatus was used in different experiments such as (Topp et al. 1980, Chan and Knight 2001a) for volumetric water content and multilayer experiments. The advantage of this TDR cell is its customizability. Like in (Chan and Knight 2001a), the coaxial cell can be built to have different heights by using threaded sections of inner and outer conductors. It also has no external interferences because of the outer conductor where the TDR with probes can have their waveform affected by external objects in their electromagnetic field. The soil can also be installed easily, and depending on how the cell is built, no insertion is needed. The disadvantage of the coaxial cell is the difficulty of adding other instruments to the cell because of the risk of interfering with the electromagnetic field. The waveform interpretation can be hard depending on the experiment because the inner conductor passes through layers. The cost to build the apparatus can be high, and it requires extensive calibration in order to be used.
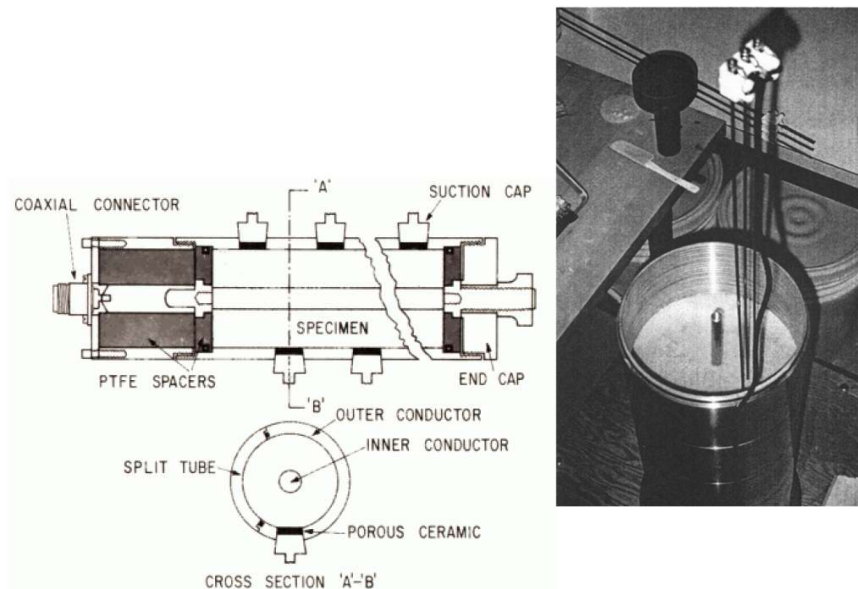
Figure 2.3.3:left) TDR apparatus diagram from (Topp et al. 1980); right) TDR apparatus from (Chan and Knight 2001b)

The usage of TDR at the surface; layout B in figure 2.3.2 is probably the simplest used method. This layout has multiple applications, such as measuring water content for one layer or multilayer (Schaap et al. 2003), waterfront detection (Topp et al. 1982), water pressure by height measurement (Dowding et al. 1996) and other experiments. This layout can cause an error if there is wobbling that is caused by highly dense soil. The reason is the wobbling creates a void around the probes. In the case where the soil is not dense, a movement of the TDR's coaxial cable can also create a void. This layout, like the coaxial cell, can also have a hard waveform interpretation if it crosses multiple layers. However, this layout has an advantage with its simplicity where the TDR is inserted and doesn't necessitate any modification of the column and the fact that the insertion can be done at multiple places in order to obtain multiple measurements. In the case where the horizontal position variation is not enough, the vertical insertion at different depths shown in Figure 2.3.2 C can also be done in order to have measurement in 3D. It consists of digging a hole at different depths and inserting the TDR to do the measurement. This method can be repeated at different depths, which makes it practical to take measurements of the layers. The other way to apply this method is to dig a trench large enough to insert the TDR laterally in the case of a bigger experiment. This method's

disadvantage is the request of digging, which is a destructive measurement method. It is not the case if the soil is used as a sample. The other disadvantage is the disruption of the soil before TDR insertion during soil removal. Otherwise, the advantage of reading at multiple positions is good especially when a high number of TDRs can't be obtained to make multiple measurements. Figure 2.3.2 D layout is a good way to use TDR for monitoring soil conditions at multiple points. It consists of burying the TDR horizontally at a certain depth in the soil and comparing the measurements of the soil condition in time with the initial measurement (Bhuyan et al. 2018). In this layout, the TDR can't be installed vertically because it can be damaged when the hole is back filled. Bhuyan et al. (2018) used this layout to calibrate the soil density in order to monitor soil under roads. A box large enough, as shown in Figure 2.3.4, was filled with soil in two layers with the TDR in between. The TDR can be buried at different positions for monitoring for water content profiling (Greco 2006) and for soil monitoring around the pipe (Curioni et al. 2019). So, this layout is good for multiple-point soil monitoring, but it needs a calibration that considers every aspect of the experiment and depending on the experiment, it can be expansive. On a large scale, the TDR can be damaged if there is too much pressure, the TDR is not sealed enough for the water pressure or a combination of both. However, this layout, compared to the layout in Figure 2.3.2 C, doesn't disrupt the soil.
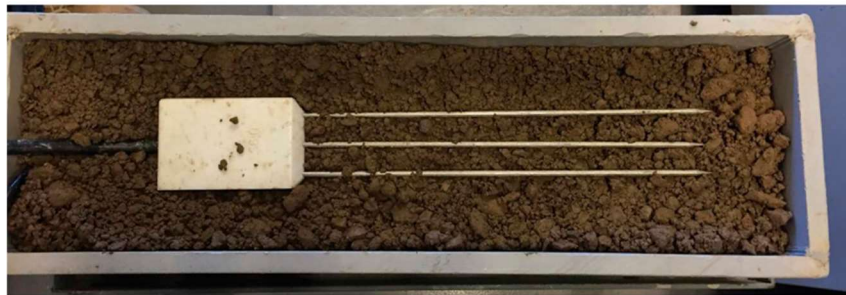
Figure 2.3.4: TDR layout calibration for different density and water content (Bhuyan et al. 2018)

For the lateral insertion of TDR in cells, the TDR can be embedded as in layout D or be inserted through holes, as in layouts E and F shown in Figure 2.3.3. An Example of embedded TDR in soil is shown in Figure 2.3.4 where the whole probe length is inserted into the soil. Depending on the type of the cell, the embedded TDR can be advantageous in a square tank where the height is dynamic (Technion 2023). Meaning that the TDR stays at the same position in the soil during soil compaction by sliding along the wall. To do so, Technion (2023) built a slot high enough to install

soft spacers, TDR and aluminum profile in order to have vertical movement only, as shown in Figure 2.3.4. So, when the compaction produces movement, the spacers start to compress at the same time. Otherwise, the height of the TDR in this layout doesn't change, and each TDR has its own slot (Ghavam-Nasiri et al. 2017). The same for layout F was used in a lot of experiments, such as in Keng and Topp (1983) and Heimovaara et al. (1993). The advantage of these layouts is the accessibility of lateral measurements on the cell without disruption of the soil inside the cell. The disadvantage of the lateral insertions is the water leakage, which can make the construction of this layout difficult. Generally, most experiments use rubber to seal the connection of the TDR with the cell, as in Heimovaara et al. (1993) or Yang et al. (2004). The insertion slot construction can be difficult especially if layout F is applied to a cylindrical column. Because of the holes' drilling accuracy, a small difference in hole position or in hole diameter can make the TDR either hard to install or hard to keep in place. This may also result in the presence of wobbling depending on the cell wall thickness. So, for these reasons, it requires accurate machining during construction.
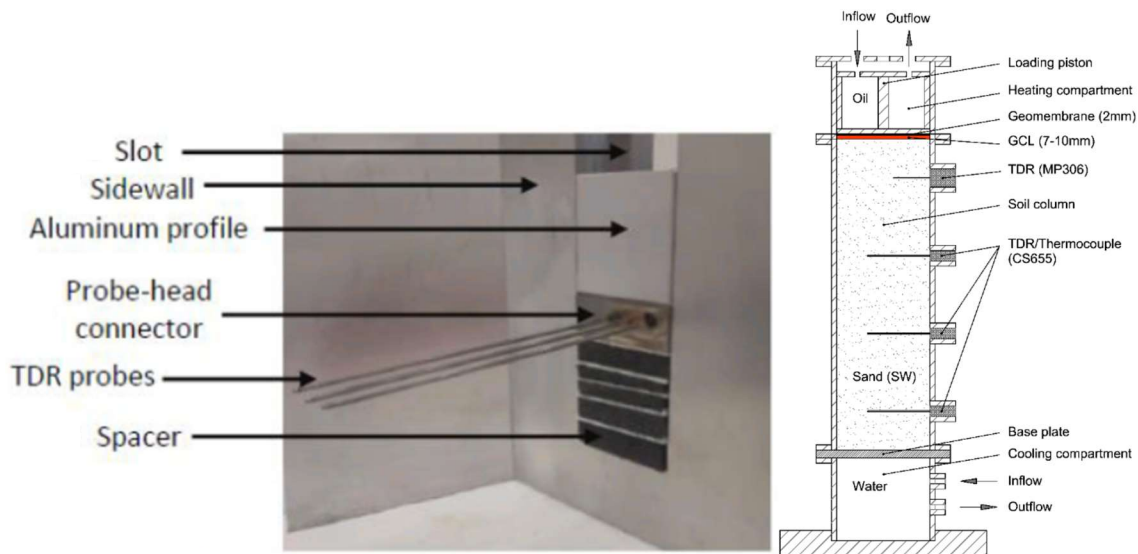
Figure 2.3.5:TDR layout of (Technion 2023) on the left and (Ghavam-Nasiri et al. 2017) on the right

2.4   Permittivity through material layers

Determining the permittivity of a homogeneous material and heterogeneous material is a simple task when the material covers the whole TDR probes' length. Conversely, when multiple layers cover the TDR's probe, the impact of the permittivity from the previous layer is noticeable. Thus,

an average permittivity is needed to calculate the real total permittivity of all the layers. In order to determine the average permittivity, two common methods exist: the Arithmetic method and the refractive index method. The arithmetic method or the effective medium theory EMT equation shown below is the weighted arithmetic mean of the permittivities and their length ratio to the full probe length

$$K_{aT} = \sum_{i=1}^{N} K_{ai} \left(\frac{L_{ri}}{L_{rT}} \right)$$ (2.15)

In the equation (2.15) the K_{aT} is the total permittivity which is the average permittivity of the mix, K_{ai} is the permittivity of each layer, L_{ri} is the real length covered by the layer and L_{rT} is the total length covered by the multilayer. Technically, in the case of a partially covered probe, i.e., TDR half inserted into water, the probe needs to be considered as fully covered with air and water.

The second method is the refractive index or ray theory (Chan and Knight 1999, 2001a) described by equation (2.16), which has the same coefficients as equation (2.15) with the addition of exponent $n=0.5$. Mathematically, the Arithmetic mean method is a weighted arithmetic mean with an exponent n of 1, while the refractive index is also a weighted arithmetic mean with an exponent n of 0.5. Introduced by (Birchak et al. 1974), the method is based on the model that demonstrates the effect of layering orientation on the permittivity (Brown 1956). Depending on the layering orientation to the electromagnetic wave, the exponent n has a value ranging from -1 when the layering is perpendicular to 1 when the layering is parallel.

$$(K_{aT})^n = \sum_{i=1}^{N} (K_{ai})^n \left(\frac{L_{ri}}{L_{rT}} \right)$$ (2.16)

In Birchak et al. (1974), the value of n is 0.5 with frequencies between 4 GHz and 6 GHz, but other authors found different values, such as $n=0.65$ (Dobson et al. 1985) at frequencies between 1.4 GHz and 18 GHz and $n=1/3$ (Looyenga 1965) where the frequencies are not mentioned. Hilhorst (1998) represented this as being accidental and related to the selected frequency used during the testing. This value of n is inversely proportional to the frequency, meaning that a lower frequency

gives a higher value of *n* and vice versa. Furthermore, the value of *n* is dependent on the frequency used as bound water affects the relaxation frequency, which increases energy loss when the relaxation frequency decreases. However, the most frequent value of *n* is 0.5 for the majority of soils. In Chan and Knight (1999, 2001a), both averaging methods can be applied depending on the wavelength-to-layer thickness (*λ/L*) ratio. The reason for the *λ/L* usage for the multilayered media is the electromagnetic wave velocity varies with the layer's materials and thickness. The author used the normalized electromagnetic velocity $\bar{v}$ shown in equation (2.17) to *λ/L* ratio in order to determine the *λ/L* range for each method.

$$\bar{v} = \frac{v_{EMT} - v_{meas}}{v_{EMT} - v_{ray}} \qquad\qquad (\ 2.17\ )$$

Where the v_{EMT} is the velocity using the electromagnetic theory, v_{meas} is the measured velocity and v_{ray} is the velocity using ray theory. In other words, the ray theory is the refractive index and the EMT is the arithmetic mean. The transition between the Arithmetic mean and refractive index is from *λ/L* of 3 and 6, and more data was needed to find the transition, but numerical study results gave a transition around 4. Thus, the refractive index method is used when *λ/L*≤ 4, and the arithmetic mean is used when *λ/L* ≥ 4. To calculate the EM wave velocity, the frequency is needed and the broadband frequency varies between TDRs. In Chan and Knight (1999, 2001a), the central frequency of the broadband frequencies of the Tektronix (750 MHz) was used to determine the v_{meas}. The v_{meas} is equal to the ratio of the wavelength to the frequency. However, Schaap et al. (2003) simulated the multilayer system by using modelled waveforms to show the averaging of average permittivity limits. The results confirmed that the averaging methods do depend not only on the permittivity of the layer or its thickness but also on the frequency, the bandwidth, and the periodicity in layering. Thus, at a lower frequency (<50 MHz), all the multilayers followed the arithmetic mean regime because of a high delay. Above 50 MHz, the number of layers 2 and 4 followed the refractive index regime, while the 40 and 80 layers followed the arithmetic regime. According to the author, the arithmetic regime of those multilayers is explained by the increase of delay created by the signal resonance at many impedance mismatches that cause the increase in the apparent permittivity. As for the layer thickness, the result was similar to (Chan and Knight 2001a), where layers <0.015 m showed an arithmetic mean and > 0.015 m showed a refractive index mean.

Schaap et al. (2003) represented the results as a normalized electromagnetic velocity vs layer graph thickness, unlike Chan and Knight (2001a) λ/L ratio.

Other authors were confronted to the multilayers when they inserted the TDR laterally through the column cell. In order to obtain the signal of the material inside the column, different methods were used. Starting with Keng and Topp (1983) where a TDR was used on a soil column with the gamma-ray attenuation technique to measure soil's water content. By subtracting the measured travel time of air, water, and paraffin mix from the travel time of the column's wall with each of these materials, the travel time of the column's wall can be calculated. The polycarbonate plastic column, with a thickness of 0.64 cm, has an average travel time of 0.05 ns. Due to the low resolution of the TDR, the effect of the wall was neglected. Stähli and Stadler (1997) also discussed obtaining the permittivity of soil in an insulated column. Their method involves measuring the permittivity of water at 20°C for the full probe length. Then, when the TDR is inserted through the column full of water, the apparent length of water at 20°C is subtracted from the apparent length of water and the column on the waveform to obtain the transmission line's apparent length. The author's assumption that the apparent length of the line was constant caused an error of 0.01 m^3-m^3 in volumetric water content during the freezing-thawing cycle. However, the method to determine the apparent length of the column using the refractive index is intuitive, but in reality, the arithmetic method also needs to be considered. The application of an averaging method depends on multiple parameters of the material layers and the TDR. For these reasons, research on the correction method is done.

Chapter 3: Method theory to determine permittivity of soil in a cell

The methodology in this chapter is presented comprehensively to elucidate the removal of the cell's wall from the signal. The Refractive Index method is presented in the general methodology, where the utilization of lengths aids in understanding the waveform concept. Additionally, the Arithmetic Mean method is employed for comparison with the refractive index method. Subsequently, the methodology is delineated for the Tangents, Heimovaara, and Schwartz methods.

3.1 General method

In this chapter, lengths presented in figure 3.1.1 are used to facilitate the understanding of the correction method described in this chapter. During the experiment, the Δt and K_a are used instead of the apparent length L_a.

$$L_a = c \, \Delta t \tag{3.1}$$

The idea is to obtain a ratio of the reference actual length L_{rR} to the reference apparent length $L_{a\,R}$ of the full-length probe in a homogenous material of known permittivity such as air or water, as permittivity of a homogenous material in a cell remains constant under same conditions. If conditions change, a permittivity for each condition is required. However, the use of the ratio below in equation (3.3) to obtain the apparent length of the probe inside the reference material into the cell $L_{aR'}$ that is from a measured actual length of the probe inside the reference material into the cell $L_{rR'}$ can be done.

$$\frac{L_{r\,R'}}{L_{a\,R'}} = \left(\frac{L_{r\,R}}{L_{a\,R}}\right) \tag{3.2}$$

$$L_{a\,R'} = \left(\frac{L_{r\,R'}}{L_{r\,R}}\right) L_{a\,R} \tag{3.3}$$

$$\Delta t_{R\prime} = \left(\frac{L_{r\,R\prime}}{L_{r\,R}}\right)\Delta t_R \qquad (3.4)$$
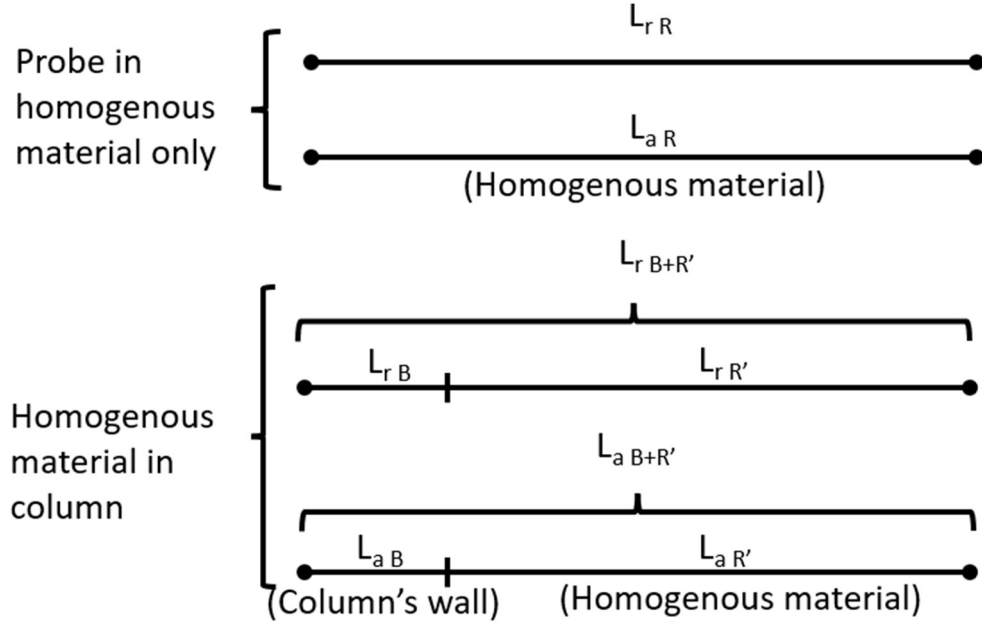
Figure 3.1.1: Measured lengths when the TDR probe is inserted in homogenous materials and when it is inserted in a column full of homogenous material

With the $L_{a\,R\prime}$, the apparent length of the column's wall can be obtained by subtracting the homogenous material apparent length $L_{a\,R\prime}$ in the column to the full apparent length of the waveform $L_{a\,B+R\prime}$.

$$L_{a\,B} = L_{a\,B+R\prime} - L_{a\,R\prime} = L_{a\,B+R\prime} - \left(\frac{L_{r\,R\prime}}{L_{r\,R}}\right)L_{a\,R} \qquad (3.5)$$

$$\Delta t_B = \Delta t_{B+R\prime} - \Delta t_{R\prime} \qquad (3.6)$$

Thus, whatever the homogenous material is in the column, the column's wall apparent length L_{aB} is the same because there is no change in its material's conditions, and it is in the same condition as the calibration. The apparent permittivity of the column's wall L_{aB} can be determined by using

the apparent permittivity of the Column's wall K_{aB}, which gives the L_{aB}. That L_{aB} will be used to determine the apparent length of soil L_{aS} during the test with soils where the equation is

$$L_{a\,S} = L_{a\,T} - L_{a\,B} = L_{a\,T} - \left(L_{a\,B+R'} - \left(\frac{L_{r\,R'}}{L_{r\,R}}\right)L_{a\,R}\right)$$ (3.7)

$$\Delta t_S = \Delta t_T - \Delta t_B$$ (3.8)
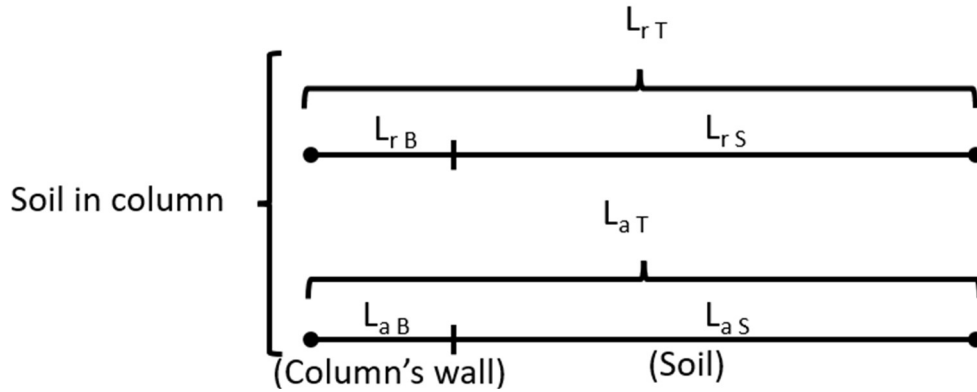
Figure 3.1.2: Measured length when TDR probe is inserted into a column full of soil

Thus, with the Δt_S, K_{aS} can be calculated with equation (2.2). It is essential to know that soils can't be used as a reference material since the signal is affected by the compaction level and pore heterogeneity that can affect the signal which makes it difficult to reproduce. Also, L_{rB} in Figure 3.1.1 and Figure 3.1.2 regroups all the materials of the column's wall. For example, in the a case of multiple material such as rubber O-ring and column's Plexiglas should all be considered in one L_{rB} and not fragmented by individual lengths. Furthermore, if a compressible material is used at the column's wall such as rubber, it is important to keep the same length for more accuracy or find a K_{aB} for each column's wall length. Because it might be possible that the concentration of the material used as a column's wall can affect the K_{aB}. If the K_{aB} is variable, a K_{aB} can be used for each condition of the material. In order to obtain Δt the equation below can be used

$$\Delta t_B = \frac{K_{aB}^{0.5}\,2\,L_{rB}}{c}$$ (3.9)

The procedure explained below where the Δt are substracted is the refractive index mean permittivity method since the Arithmetic meaning method can't used Δt summation. Thus using K_a and Δt on the experiments data was done. This correction method is applied to two layers, in this case, the Column's wall and the material inside the cell. Theoretically, for three layers and more, the equation using different averaging methods (arithmetic mean and refractive index) to obtain the K_{aS} below can be used.

$$K_{aT}^n = K_{a1}^n \left(\frac{L_{r1}}{L_{rT}}\right) + K_{a2}^n \left(\frac{L_{r2}}{L_{rT}}\right) + \cdots + K_{aS}^n \left(\frac{L_{rS}}{L_{rT}}\right) \tag{3.10}$$

$$K_{aT}^n = \sum_{i=1}^{N} K_{ai}^n \left(\frac{L_{ri}}{L_{rT}}\right) + K_{aS}^n \left(\frac{L_{rS}}{L_{rT}}\right) \tag{3.11}$$

$$K_{aS} = \left[\left[K_{aT}^n - \sum_{i=1}^{N} K_{ai}^n \left(\frac{L_{ri}}{L_{rT}}\right)\right]\left(\frac{L_{rT}}{L_{rS}}\right)\right]^{1/n} \tag{3.12}$$

Where i is the material's layer. The K_a of the materials that precede the soil should be known to obtain the K_{aS}. Otherwise, there will be too much unknown K_a for one equation.

3.2 Determining permittivity of soil with different methods of interpretation

The method to determine K_{aS}, explained in the preceding chapter, is similar for all waveform interpretation methods (Schawrtz, Tangents and Heimovaara). It is five steps that consist of

- Determining reference material's L_{rR}, Δt_R and K_{aR} with full TDR probe length
- Determining L_{rB} , $L_{rR'}$, $\Delta t_{R'}$ and K_{aT} with the probe inserted into the cell
- Determining Δt_B or calculate K_{aB} using different permittivity meaning methods
- Repeating the preceding steps for each condition of the cell's wall in case of variable L_{rB}
- Determining Δt_S and K_{aS} of the soil in a cell using different permittivity meaning methods

3.2.1   Tangents method

First, the full length of the TDR probe should pass through only air or deionized water where the waveforms are obtained. For each homogenous material and for each TDR, a Δt_R is measured on the obtained waveform, as shown in Figure 3.2.1. At the end of this step, L_{rR} and Δt_R are known to calculate the apparent permittivity of the reference material K_{aR}.   The Conventional method depends on the conditions of the reference material in the first step, which needs to be the same in step 2. If it is hard to have the same condition, a calibration including different parameter variations should be done. In the case of water, the permittivity must be measured at different temperatures, so the permittivity of water vs temperature can be used in step 2.
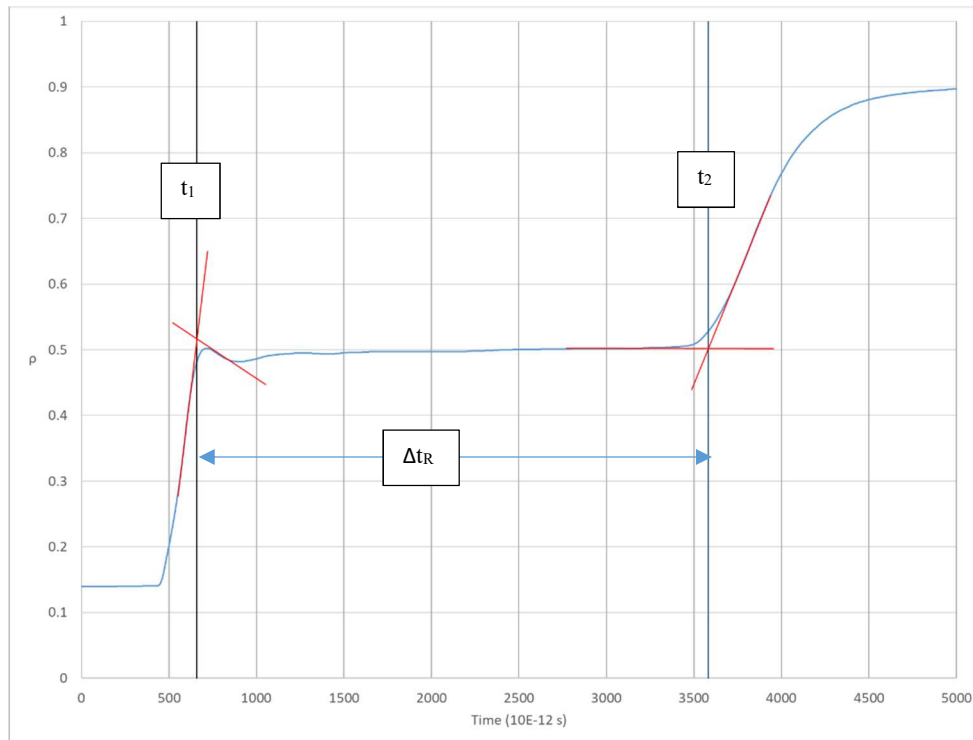
Figure 3.2.1: TDR 305-143 waveform interpretation of water at 22.7 °C (Tangent method)

Secondly, when inserting the TDR on the side of the cell, it should be done in the same way as when inserted into a soil-filled cell. This means that the rubber O-ring, as shown in Figure 3.2.2, should have approximately the same length along the probe when inserted. Then, determine the actual length of the column's wall L_{rB} by measuring the length of the cell's Plexiglas and the rubber O-rings from which the $L_{rR'}$ can be calculated by subtracting the length of the probe L_{rT} from L_{rB}.
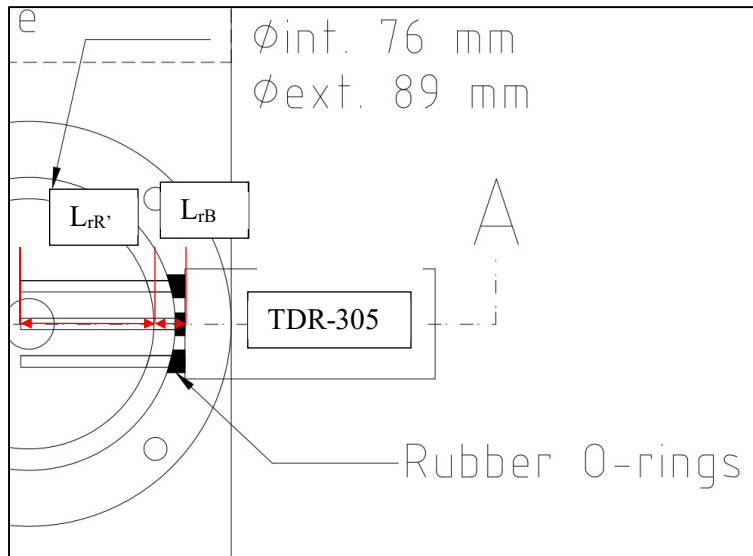
Figure 3.2.2: top) L_rB and L_rR' of the TDR-305 probes inserted in the small column (SC) shown at the (bottom) picture

Once the measurement is done, the homogenous material is inserted into the cell, and the waveforms are obtained, as shown in Figure 3.2.3. The obtained waveform is different from the waveform of the homogenous material. When the waveforms of water and water+column's wall are superposed, as in Figure 3.2.3, some similarities and differences are noticeable. At the beginning of the waveforms at point 1, there is a small difference between the t_1 and a difference of about 0.1 in the coefficient of reflection (ρ) because of different materials. At the lowest ρ, the probe's electromagnetic field is in water, while at the highest ρ, the electromagnetic field is in the rubber O-ring and air. At point 2, both waveforms have the same slope because they are in the same material. Finally, at point 3, both waveforms don't have the same t_2 because of the column's wall. The apparent length changes with the material along the probe, changing the t_2 of the waveforms.
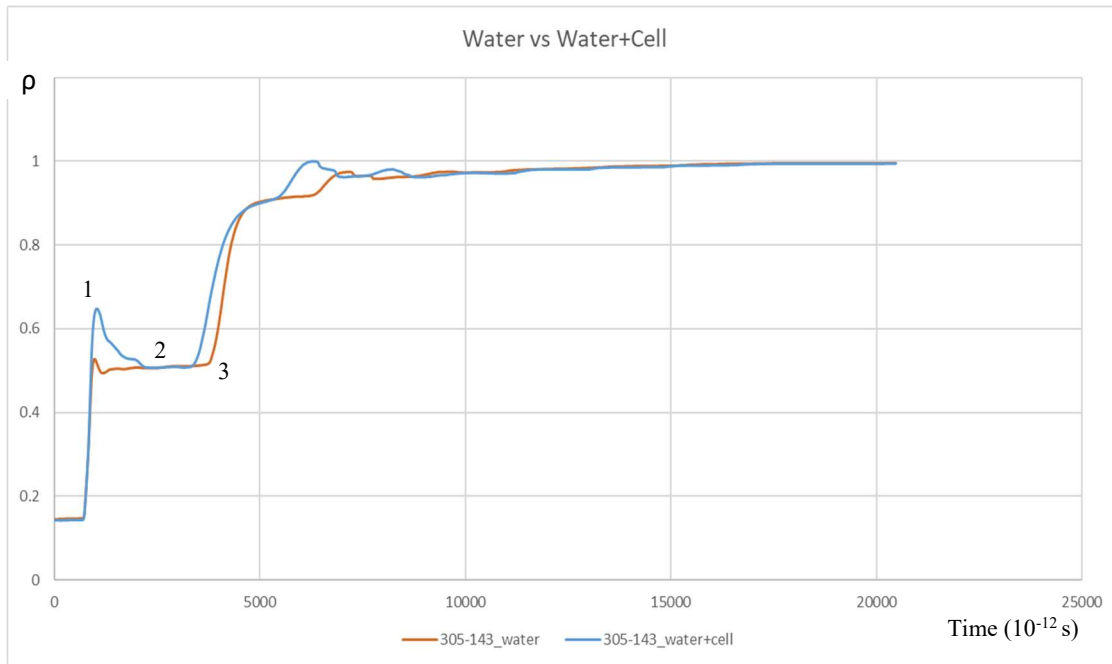
Figure 3.2.3: Water waveforms with and without the column's wall obtained from TDR 305-143

Thirdly, the determination of K_{aB} is done by using the graph in Figure 3.2.4 and by following the steps described in the Chapter 2. It consists of:

- Finding t_2 ;
- Finding the t_1 by subtracting $\Delta t_{R'}$ found earlier in step 2 of the procedure by using equation (3.4) ;
- Finding t_1 of the column's wall (t_1') with the Conventional methods, which consist of the first apex ;
- Calculating Δt_B by subtracting t_2' to t_1' ; and
- Calculating K_{aB} .
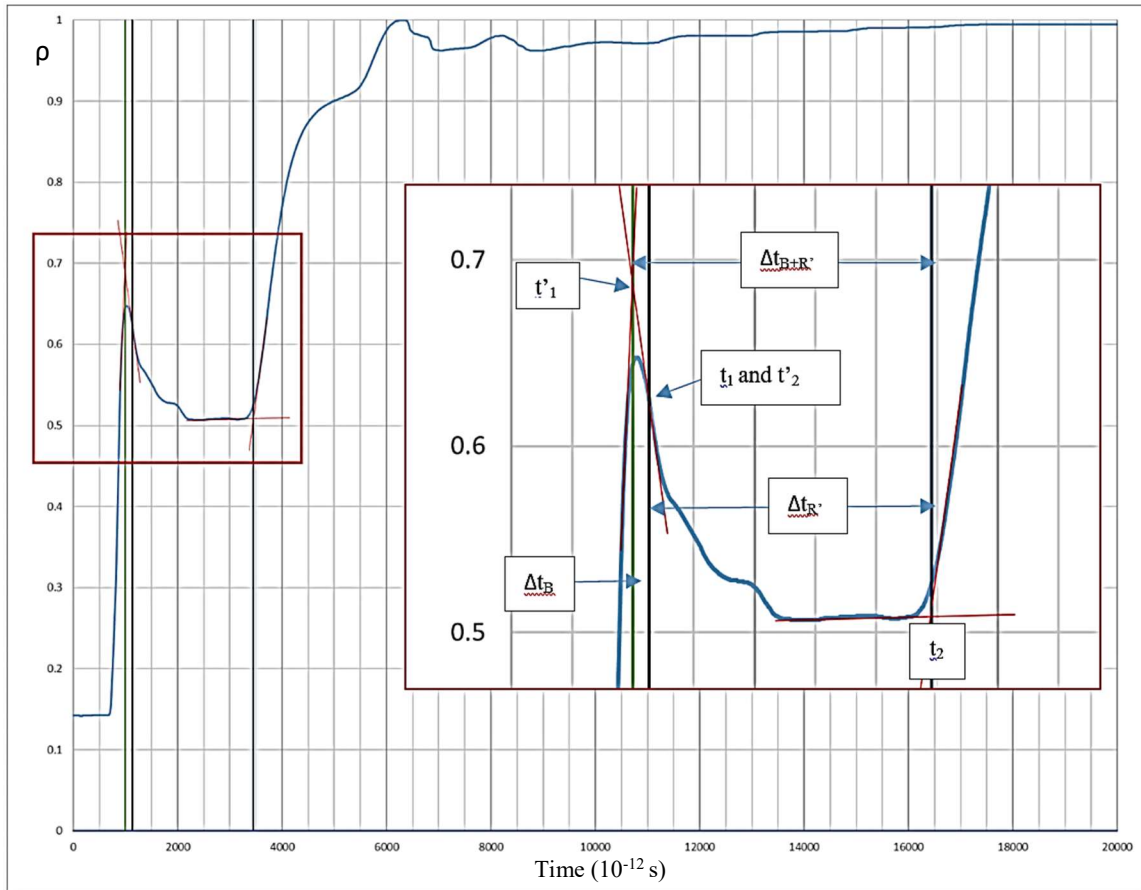
Figure 3.2.4: Graphic method to determine Δt_B using Tangent method

Finally, when K_{aB} is determined in the precedent step, the experiment with the column filled with soil can be done. As shown in Figure 3.2.5, the K_{aS} is determined by finding t_2 and t'_1 first. Then, by using equation (3.9), the $Δt_B$ is calculated to be used in equation (3.8) to find $Δt_S$. Thus, it gives the K_{aS} of the soil inside the column by using equation (2.2).
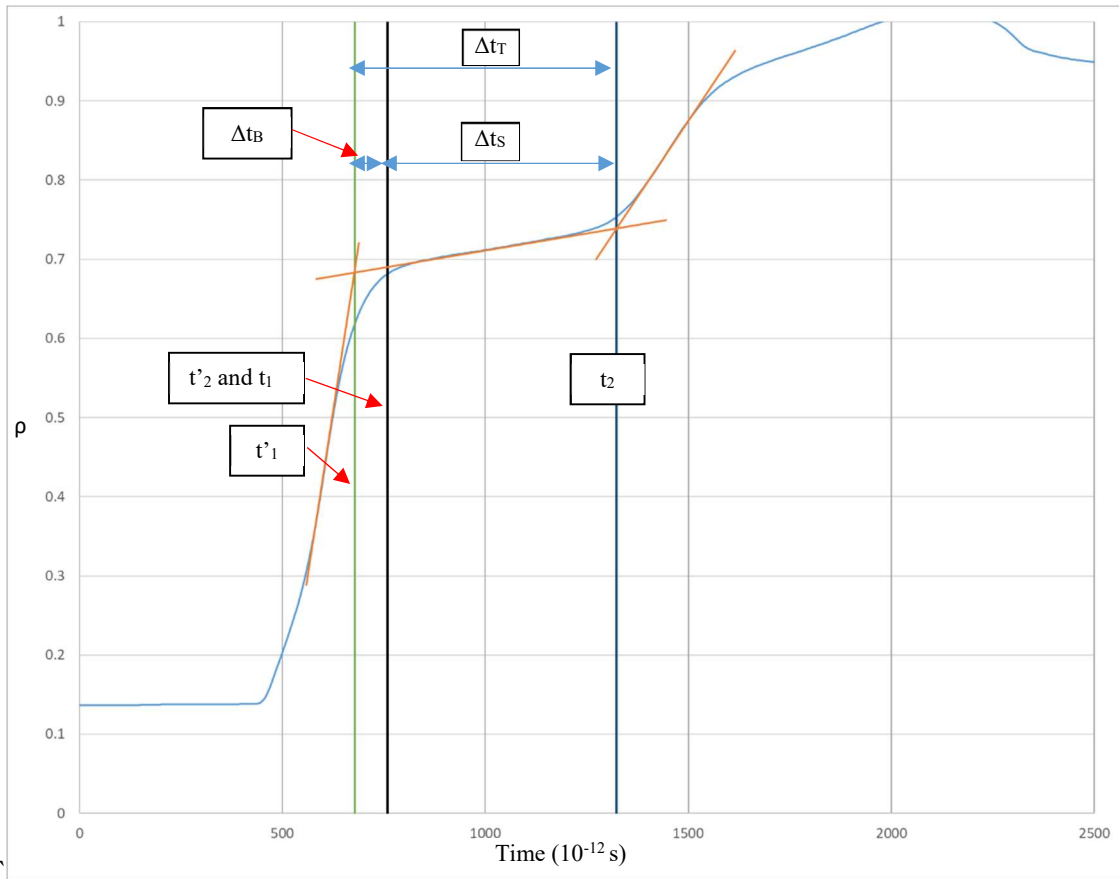
Figure 3.2.5: Waveform obtained from TDR-305 inserted into the small column (SC) filled with moist sand

3.2.2 Heimovaara method

The Heimovaara method consists of using Heimovaara (1993) calibration method to calibrate the t_1 of the waveform by using water or air. The opposite of the tangent method, the Heimovaara method depends on the literature to find the permittivity of the water-based method on (Hasted 1973). Thus, making the first step to be the calibration of t_1. As shown in Figure 3.2.6, the first step consists of finding the permittivity of water at a temperature T in which the full TDR probe is inserted. Hasted (1973) equation is

$$\varepsilon_w(T) = 87.740 - 0.40008T + 9.398 \times 10^{-4}\, T^2 - 1.410 \times 10^{-6}T^3 \qquad (3.13)$$

With the permittivity of water obtained with equation (3.13) and the permittivity of air ≈ 1, the $\varDelta t_R$ is found with equation (2.2) by isolating $\varDelta t_R$. Then, it is subtracted to t_2 to find the t_1, as shown in Figure 3.2.6. The t_1 is fixed for the whole experiment. This means that in step 2, when the reference material is filled into the column, t_1' is equal to t_1 found in the first step, as shown in Figure 3.2.6 and in Figure 3.2.7. Using air as a reference to determine t_1 is more accurate since the temperature has a negligible effect on the permittivity. Thus, making it less dependent on literature than other materials. However, depending on the material of the TDR probes, temperature variations may cause changes in the probe length, L_r, leading to errors in the calibration of t_1. In this study, stainless steel probes were used, which makes temperature-related variations negligible.
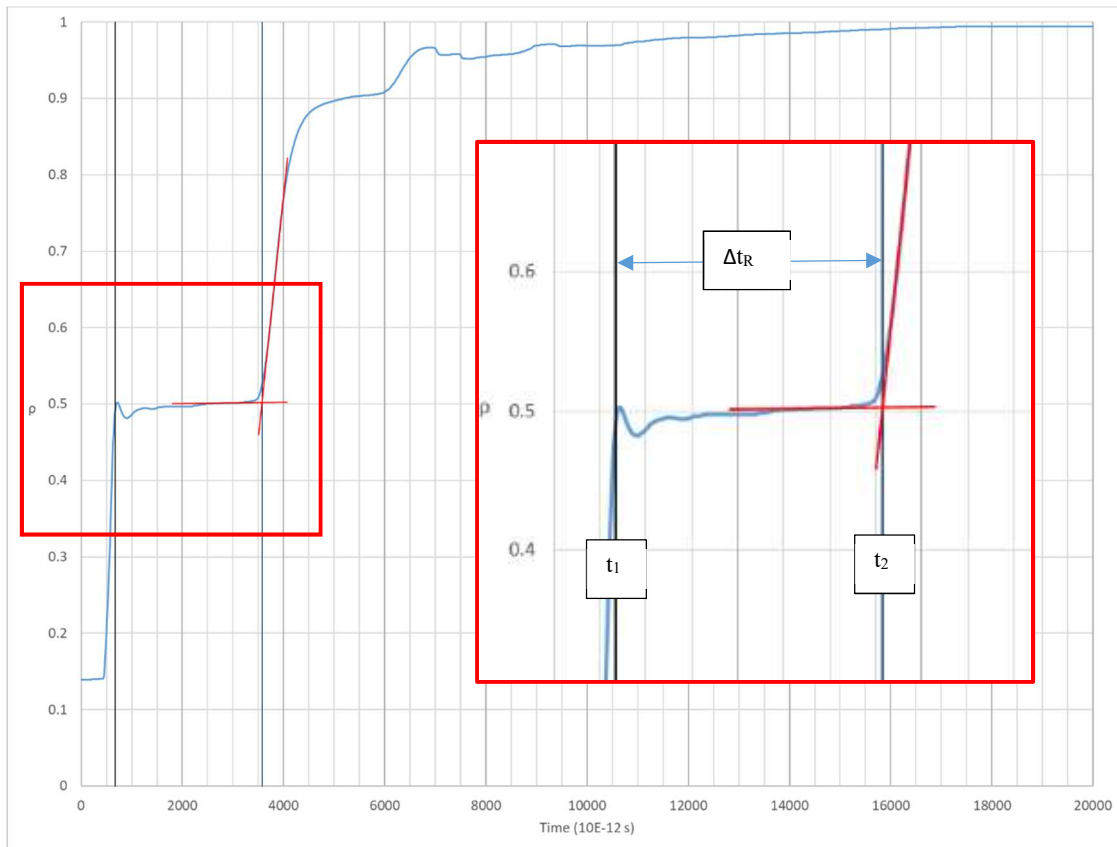
Figure 3.2.6: Heimovaara method to calibrate t_1 with water at 22.7°C

The procedure to separate the column's wall with Heimovaara can be simplified by going straight to step 2. After finding t_2, $\varDelta t_{R'}$ is calculated with equation (2.2) from the known permittivity of the reference materials. Then, the t_1 that is obtained from the subtraction of $\varDelta t_{R'}$ to t_2 is fixed, and

Δt_B doesn't need to be found. But, for this experiment, the Δt_B is determined. When the K_{aB} is calculated and the probe is inserted into a column filled with soil, the K_{aS} can be found in the same way as in the conventional method.
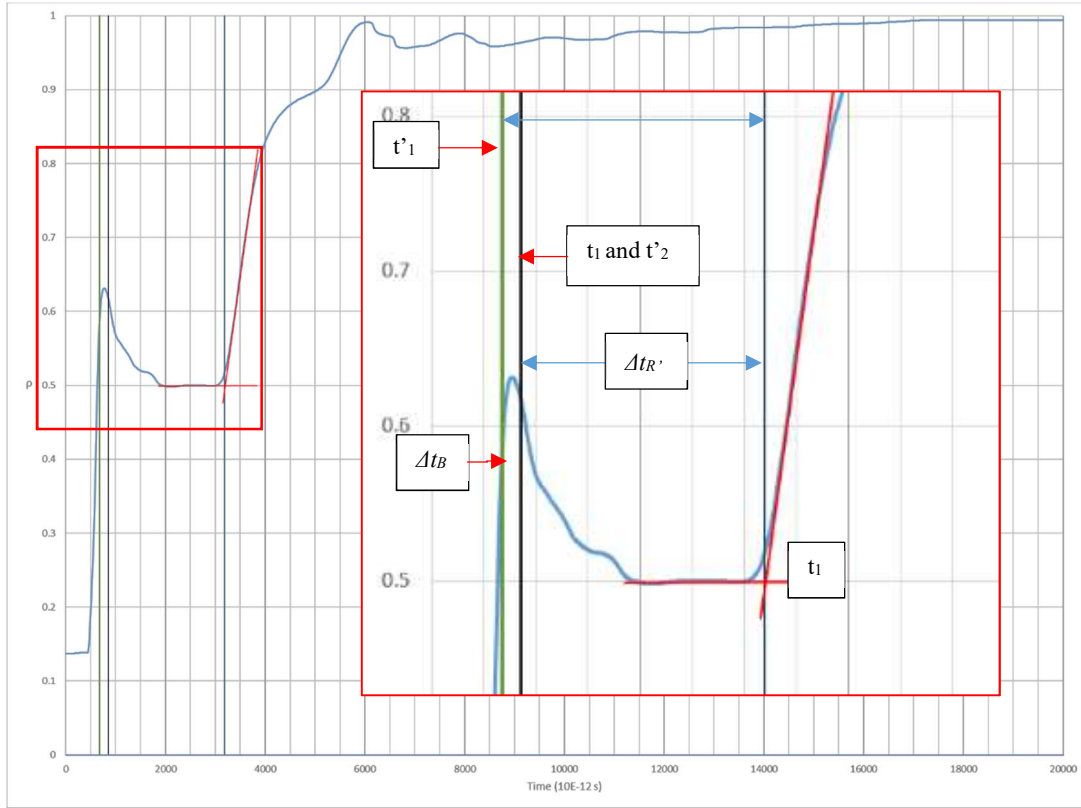
Figure 3.2.7: Graphic method to determine Δt_B using Heimovaara method

3.2.3 Schwartz method

The Schwartz method consists of taking the reading of the TDR of the K_{aR} of water and air at temperature T. Similar to the tangent method, but with automated waveform interpretation, the TDR probe is inserted into the reference material-filled column to obtain the permittivity obtained for both materials $K_{aB+R'}$. With the measured L_{rB} and $L_{rR'}$, the K_{aB} can be obtained with the equation below

$$K_{aB} = \left[K_{aB+R'} - K_{aR} \left(\frac{L_{rR'}}{L_{r\,B+R'}} \right) \right] \left(\frac{L_{r\,B+R'}}{L_{r\,B}} \right) \qquad (3.14)$$

32

The equation (3.14) follows the same principle in Birchak et al. (1974) in which K_{aB} was isolated. When the soil is inserted into the column filled with soil, the same equation applies, which gives

$$K_{aS} = \left[K_{aT} - K_{aB}\left(\frac{L_{rB}}{L_{rT}}\right)\right]\left(\frac{L_{rT}}{L_{rS}}\right) \qquad (3.15)$$

Chapter 4: Experimental setup

4.1 Experimental columns

Two Plexiglas columns with different dimensions of diameters and heights are built. The two columns are identified as the small column (SC) and the big column (BC) as shown in Figure 4.1.1. The column SC has an inside diameter of 76 mm, an outside diameter of 89 mm, and a height of 162 mm. While, the column BC has an inside diameter of 114 mm, an outside diameter of 127 mm, and a height of 300 mm. The Plexiglas wall thickness for both cells is 13 mm. Each column is supported at the bottom by a Plexiglas plate and at the top by a 25 mm plywood sheet, which is cut to match the inner diameter of the cells. A 2 mm rubber sheet is placed at the base of each cell in order to seal the cylinder part to the Plexiglas base plate.
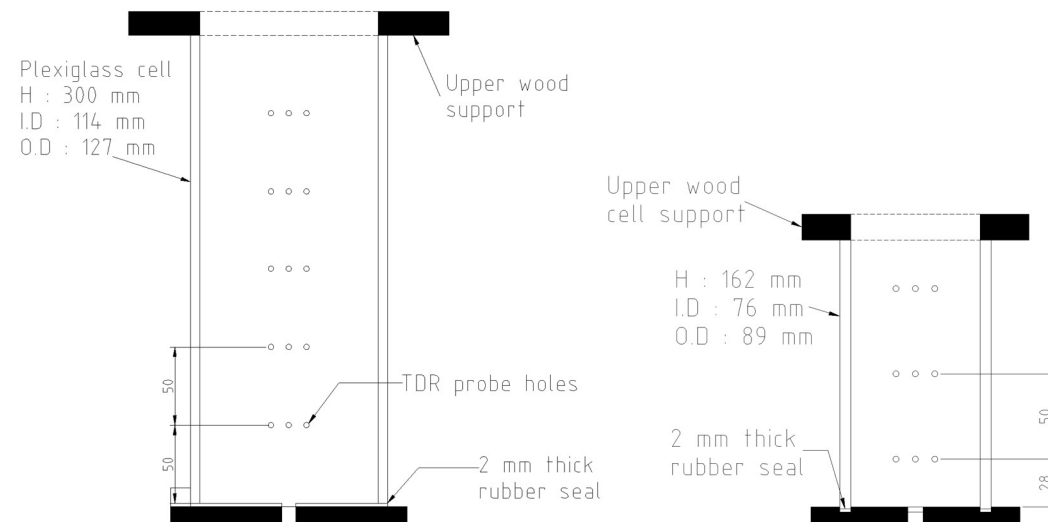
Figure 4.1.1: Left) dimensions of the column BC; Right) dimensions of the column SC

The lateral insertion of the TDR probes in the column is done through three horizontal holes of 3.6 mm in diameter at a height of 28 mm from the column base as shown in Figure 4.1.1. The vertical spacing between the TDR holes is 50 mm, thereafter. The same method to drill TDR holes was used for both columns after a test was done on a Plexiglas cylinder sample. Slight discrepancies in hole diameter or drilling angle can impede TDR probe insertion due to friction by making it hard to insert or deviation by changing the spacing of the rods. The process starts with stabilizing the Plexiglas cylinder in a wood setup as shown in Figure 4.1.2 and then proceeds to hole marking,

where a paper tape is installed along the column to mark the middle TDR probe at specific heights. To mark the position of the probes on each side of the middle probe, the middle hole mark was drilled with a centering drill bit before drilling with a drill press. This will give an accurate marking of the other probes when the TDR is inserted deep enough into the column's wall to mark each outer probe. Once the other holes on each side of the middle hole were marked, the same method was used to drill the holes.
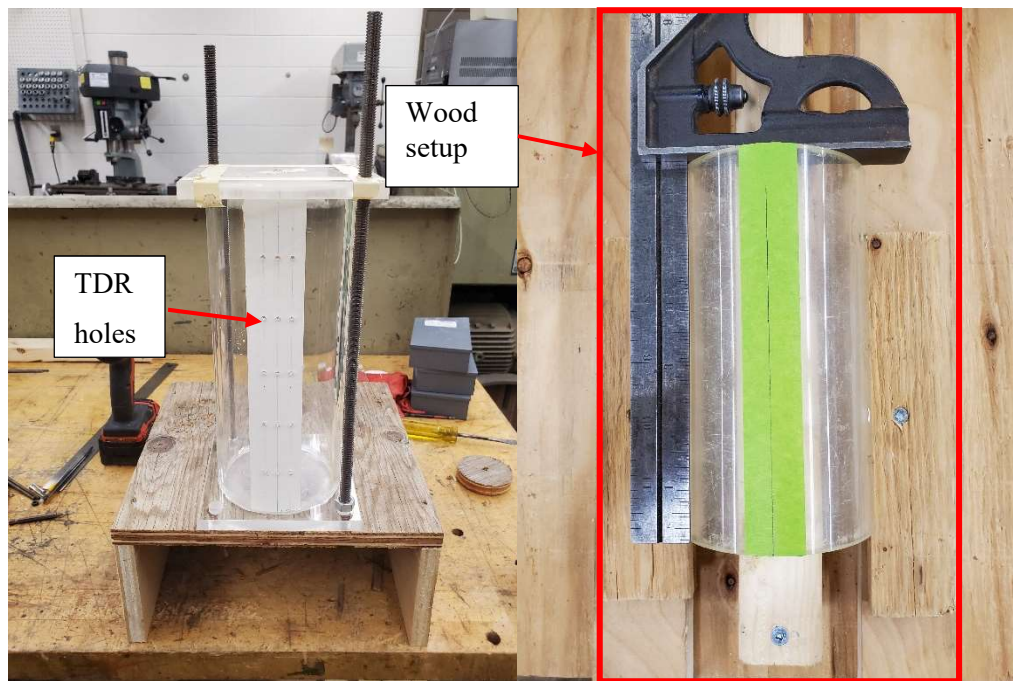
Figure 4.1.2: Left) Column BC with TDR holes; Right) Column's wood support and TDR holes marking before drilling

Drilling the TDR holes was the most challenging part of the column's construction because the TDR holes were either small for the probe, not aligned or not straight. Thus, when the hole was small, a 0.5 mm to 1 mm larger drill bit diameter was used to widen the holes. When the hole is slightly not aligned, the same drill bit diameter was used to enlarge the hole on one side. As for the angled hole, it is probably caused by a slight movement of the drill bit at the beginning of the drilling. The small hole done with the centring drill bit doesn't help with the drilling angle; it only helps keep the drill bit in place to have an accurate position for drilling. To make mass measurements, a scale with a precision of ±0.1g was used. As for temperature measurements, a thermometer with a precision of ±0.1°C is inserted into the soil from the top.

4.1.1 TDR probe orientation

To choose the orientation of the TDR probes, a small column was built with a vertical and horizontal orientation in order to place different soils. Then, a small experiment was done on a test column that was used to test various equipment before building the columns, as shown in Figure 4.1.3. Holes were drilled in a vertical and horizontal alignment at the same height on the column.
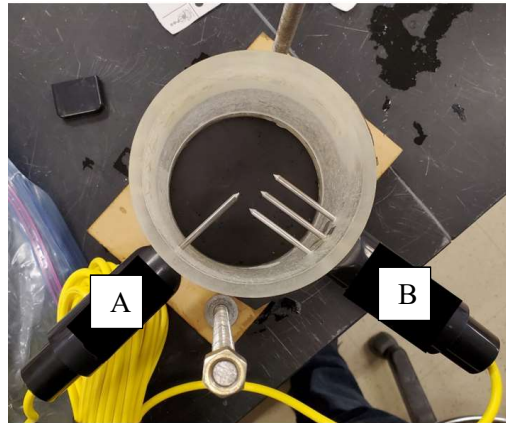
Figure 4.1.3: TDR insertion in the test column A) Vertical alignment and B) Horizontal alignment

Two different soils were used: the first one is poorly graded sand (SP), and the second one is Soil 2, which is retained on sieve #16 (passing sieve #8) from SP sand. Both soils are prepared to have 8% of water content. The SP sand was placed under two different compaction levels. The first one is compacted until there is no displacement, while the second one is not compacted, meaning the soil was just put in the column as is. The soil 2 was compacted enough to be flattened. Thus, a total of three soils were used: compacted SP sand (CSP), non-compacted SP sand (NCSP) and soil 2 (S2).

First, the column is filled with each soil at the time to obtain the waveform from the TDR in each soil's vertical and horizontal positions. Then, two soils were put in layers such as the thickness of the bottom layer is either 63 mm when one of the three rods of the vertically inserted TDR probes is in this layer (here indicated as 1/3 insertion) and the two other rods in the upper soil layer (Figure 4.1.3A) or has a thickness of 75 mm if two of the three rods are in the layer and the third rod in the

upper layer (here indicated as 2/3 insertion) (Figure 4.1.4). The NCSP was used in the upper layer in all settings to remains non-compacted.
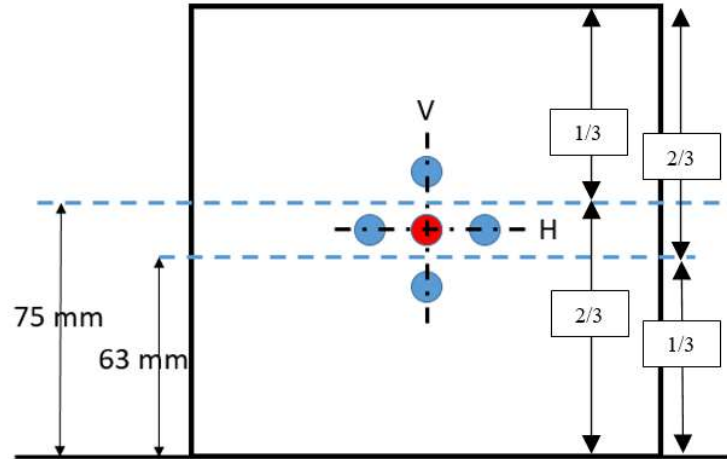
Figure 4.1.4: TDR probes alignment on the test column with the soils separation lines

The installation of the soil at the bottom starts by filling it until the bottom of the first TDR hole. Then, the TDR is inserted to continue filling the soil. The insertion of the TDR probes after the soil installation couldn't be possible because of the risk of damaging the probe when the soil is too dense. During the soil installation after the vertical insertion of the TDR probe, the soil was pushed and compacted between the probes with a spatula, making filling the space around the probes hard. After the soil installation, the permittivity and the waveform were obtained from the TDR. It was decided to use the values of the waveform interpretation done by the TDR software because the results can still be compared even if the results are affected by the Plexiglas layer of the column. This means that the permittivity value is not the true value as it includes the Plexiglas section. Since this error is applied to all readings, it is permissible to use them for comparison. The obtained results from the experiment are shown in Table 4.1.1. For each test, permittivity is found with the TDR. Then, the vertical alignment results are compared with the horizontal alignment values by using the relative difference.

First, the TDR probes alignment was compared in uniformly filled cells for each soil. The obtained results showed that the permittivity from the horizontal position is smaller than the permittivity from vertical position. The maximum calculated absolute difference is 9.7% as reported in Table 4.1.1. These differences are probably due to lower density around the probe because of the

difficulty to compact soil in between the vertically aligned probes. As for the NCSP, where the sand is not compacted, the space between the probes may not properly be filled. As for soil S2, the results of both orientations are the same probably because of the coarser soil is more uniform during the filling.

Secondly, the TDR probes tendency was compared in the cell filled with two different soils. The results in Table 4.1.1 showed that the value of the permittivity tends to the value of the soil that fills 2/3 of the probes. The highest relative difference of the horizontal to the vertical reading is 17.9%. The possible reason for this difference is the distance between the upper limit of the bottom soil CSP (line at 63 mm in Figure 4.1.4) and the horizontal TDR is small, making that space not perfectly filled because of the filling method. Knowing that the 2/3 soil permittivity has the highest influence, it was decided to determine that influence. It consists of calculating the relative percent difference to the one soil-filled cell. For example, a 2% deviation of H_2/3 CSP, 1/3 NCSP means that the 1/3 NCSP had an influence of 2%. If the deviation is negative, it means that the soil with lower permittivity affected the value, while the opposite means that the soil with higher permittivity affected the value. In this case, it was decided that the values 2% and 4% were not significant enough to conclude that the 1/3 soil had an effect. As for the vertical alignment, a deviation of 11% to 22% was obtained and can be caused by the filling method.

Since the effect of the filling method on the results is unknown, the refractive index and arithmetic averaging method were used to confirm the deviation tendency. This consists of using the soils' permittivities on both methods when the column was fully filled with one soil in order to apply the meaning method by using the soils' fractions of 1/3 and 2/3. The refractive index showed a result that is inaccurate because of the unrealistic values where the permittivity should be at least 2.7. Thus, the arithmetic meaning method showed more realistic results, which makes it the chosen method for comparison. Also, it can't be concluded that the orientation of the layer to the electromagnetic wave travel orientation influences the chosen method because they are both soils and not homogenous materials. At the opposite of the deviation of experimental results, the deviation obtained from the arithmetic meaning has the same magnitude for horizontal and vertical orientation because the TDR is about the volume in this case. As for the effect of the 1/3 NCSP and S2 soils, their deviation ranges from -13% to -16% because they have about the same permittivity. The effect of 1/3 CSP ranges from 23% to 31%, which means a higher permittivity has a higher impact than the volume.

Table 4.1.1: Results from the TDR waveform interpretation

	Permittivity	Tendency*	Deviation **	Refractive Index	Arithmetic	Deviation ***
H CSP	5.2		0%	-	-	0%
V CSP	4.7	**Equal**	0%	-	-	0%
% diff. to H	**-9.6%**			-	-	
H NCSP	3.1		0%	-	-	0%
V NCSP	2.8	**Equal**	0%	-	-	0%
% diff. to H	**-9.7%**			-	-	
H S2	2.7		0%	-	-	0%
V S2	2.7	**Equal**	0%	-	-	0%
% diff. to H	**0.0%**			-	-	
H_2/3 C SP, 1/3 NC SP	5.3		2%	2.1	4.5	-13%
V_2/3 C SP, 1/3 NC SP	5.4	**CSP**	15%	2.0	4.1	-13%
% diff. to H	**1.9%**					
H_1/3 C SP, 2/3 NC SP	3		-3%	1.9	3.8	23%
V_1/3 C SP, 2/3 NC SP	3.1	**NCSP**	11%	1.8	3.4	23%
% diff. to H	**3.3%**					
H_2/3 C SP, 1/3 S2	5.1		-2%	2.1	4.4	-16%
V_2/3 C SP, 1/3 S2	4.8	**CSP**	2%	2.0	4.0	-14%
% diff. to H	**-5.9%**					
H_1/3 C SP, 2/3 S2	2.8		4%	1.9	3.5	31%
V_1/3 C SP, 2/3 S2	3.3	**S2**	22%	1.8	3.4	25%
% diff. to H	**17.9%**					

*Tendency of the obtained permittivity
**Percent deviation of the 2/3 soil's value from the uniform soil value
***Difference of the Arithmetic mean value to the Refractive Index value

To conclude the comparison, the horizontal and vertical orientations do not affect the permittivity. However, the orientation affects the experimental method, which can lead to erroneous results by having voids between probes in the case of vertical orientation. Conversely, the horizontal orientation is more favourable, because if the layer is under the TDR probe position, the soil can be compacted uniformly, allowing for insertion of the probe above the layer. This is not feasible with the vertical orientation because there will be one probe inserted into the bottom layer. Also, in the case where the TDR probes are in the middle of the layer, they may be closer to the upper layer and absorb compaction shocks that could damage it, which is not the case for the horizontal orientation. It can be said that the only advantage of the vertical orientation is the construction of the column, where the holes are all done on one line. In the case of the horizontal orientation, it is a little bit more complicated to drill the holes and get them perfectly perpendicular to the column,

which requires manual adjustment with a drill. Even so, since the TDR probes are not perfectly aligned and horizontal, the vertical orientation can have the same difficulty in being built.

4.1.2   TDR probe stabilization and sealing

After the construction of the columns, it was found that some holes were too large to hold the TDR in place. The reason is the TDR is pushed by the O-rings that seal the TDR holes. Thus, the apparatus was modified in order to keep the TDR in place by adding Plexiglas supports, shown in the left picture of Figure 4.1.5. It consists of a Plexiglas plate that has holes that have a diameter smaller than the diameter of the TDRs, which are supported by horizontal Plexiglas support that are attached together with threaded rods. To use the support, the whole cable of the TDR is inserted into the hole so the plate can fit in the back of the TDR. Then, the TDR is inserted into the column in order to install the horizontal supports. In the case of large TDR holes in the columns, this support doesn't eliminate the problem. Because the horizontal supports are installed one by one, it can cause a small movement. However, once it is installed, the length L_{rB} is controlled, and the TDR is stabilized. To seal the TDR holes, multiple setups were tested until the column was sealed. Because of the circular form, the middle has two O-rings that have thicknesses of 2 mm and 1.5 mm. In the outer rods, two 1.5 mm O-rings were added to the 2 mm O-ring. By putting smaller O-rings, the rubber seal can follow the round form as shown in the right picture of Figure 4.1.5.
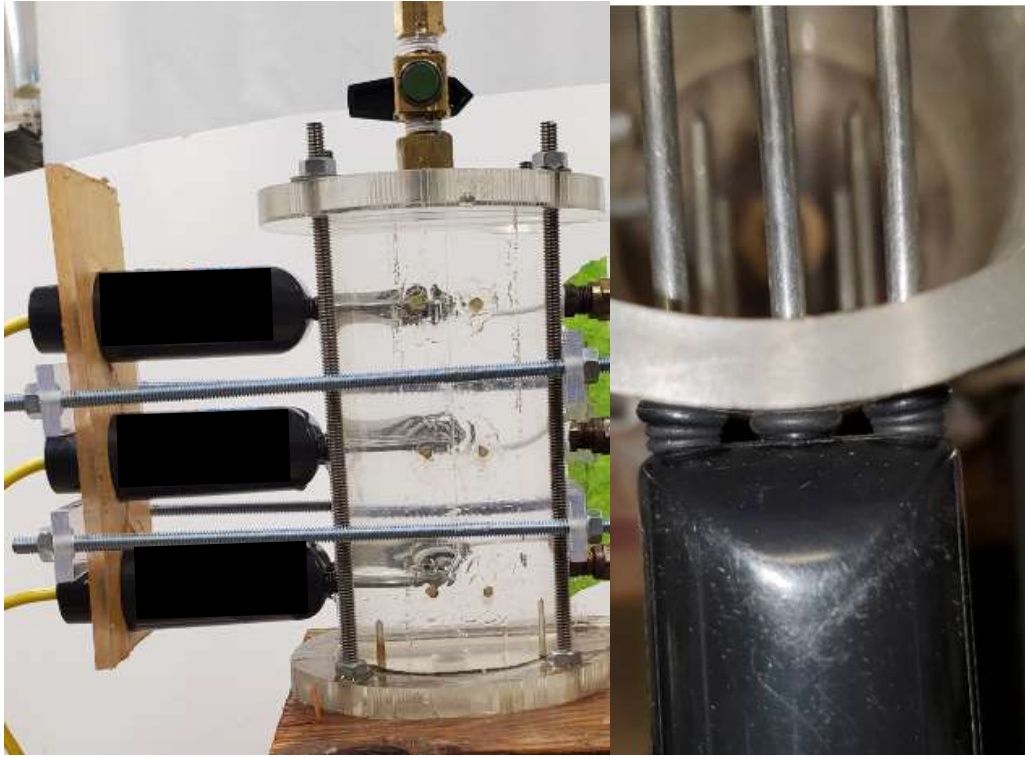
Figure 4.1.5: Left) TDR supports applied on SC during seal test; Right) Close up picture of the rubber O-ring sealing

4.2   TDR Probes

The TDRs that were used for the experiment are Acclima TDR-305H and TDR-310H, as shown in Figure 4.2.1. The TDR-305 has a 3.5 mm Type 304 stainless steel rod with a measured length of 49 mm, and the TDR-310 has a length of 100 mm with a distance between probes of 8 mm. The TDRs send their data through cable to a Data recorder that uses an SDI-12 protocol from which the waveforms are obtained and visualized in the fabricator software. The waveforms have a time steps of 5 ps and a full recording time per waveform (full waveform time length) of ~ 24 000 ps. The permittivity, the bulk electric conductivity (*ECb*), and the pore water electric conductivity (*ECpw*) are also obtained through the fabricator software by an automated waveform interpretation.

Figure 4.2.1: Top) TDR-305; bottom) TDR-310 used for the experiment

4.3   Variable energy rammer

To compact the soil during the experiment, two rammers with adjustable weights were built. The rammer shown in Figure 4.3.1 is a steel cylinder that has an internal component inserted inside. The component is a threaded rod that has a support plate to support the weights. In order to maintain the weights in place, a support screw with a locking washer was added. The locking washer in between helps the screw to stay in place during the vibration caused by the compaction. The support screw is also used to maintain the lateral stabilizer in place. The lateral stabilizer helps to maintain the internal component centred during compaction movement. To control the dropping height, the upward movement restrictor was placed above the lateral stabilizer. It is made with two screws with a locking washer in between. A downward movement restrictor was added at the upper part of the internal component to prevent it from going out. Depending on the rammer, the lower part of the internal component exceeds the cylinder by about 5mm for the small rammer and about 10 mm for the big rammer. The compaction pattern is similar to the Proctor test. Thus, 25 blows were done, starting with four blows, as shown in Figure 4.3.2, then the 21 blows following the clockwise pattern. If more than 25 blows are done, the compaction still starts with four blows, followed by the clockwise compaction pattern.
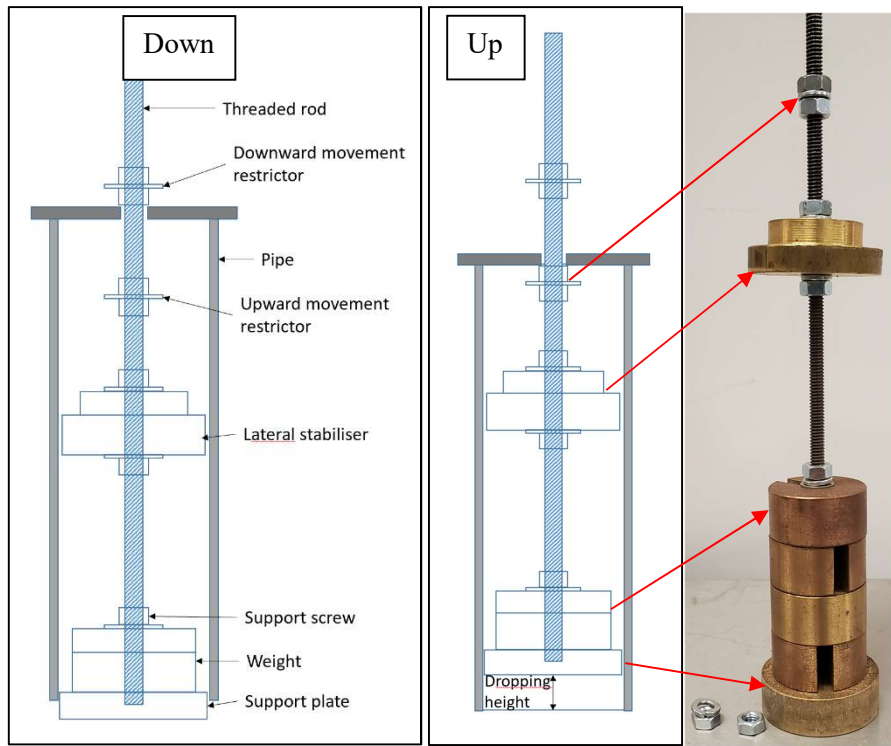
Figure 4.3.1: Rammers diagram
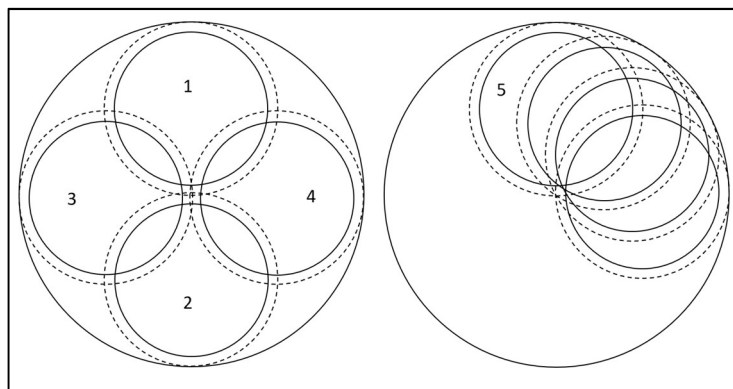
Figure 4.3.2: Compaction pattern used with both rammers

4.4 Materials

The materials that were used during the experiment are air with a known permittivity of 1, deionized water with a permittivity that is temperature dependent, and the soil SF-1, where the grain size distribution is shown in Figure 4.4.1. The soil SF-1 is a poorly graded sand based on the

USCS and has a *Cc* of 0.97 and *Cu* of 4.35. The soil is installed into the cell when it is dry and moistened without the gravitational water and wet with gravitational water. The moistened SF-1 was prepared to have a water content of 4.3% and was mixed before being covered overnight. The wet SF-1 was prepared to have a water content of 12.2%, which makes gravitational water in the cell noticeable. To determine the density of the soil, the ASTM D698-12 procedure was followed, and the results are shown in Figure 4.4.2. The specific gravity of the soil *Gs* was found following the ASTM D854-14 procedure. In order to have a better deaeration, the flask is put into a controlled temperature bath while being connected to a vacuum pump. The total vacuum time was 60 minutes, and the flask was shaken every 10 minutes. The obtained *Gs* of SF-1 soil is 2.721.
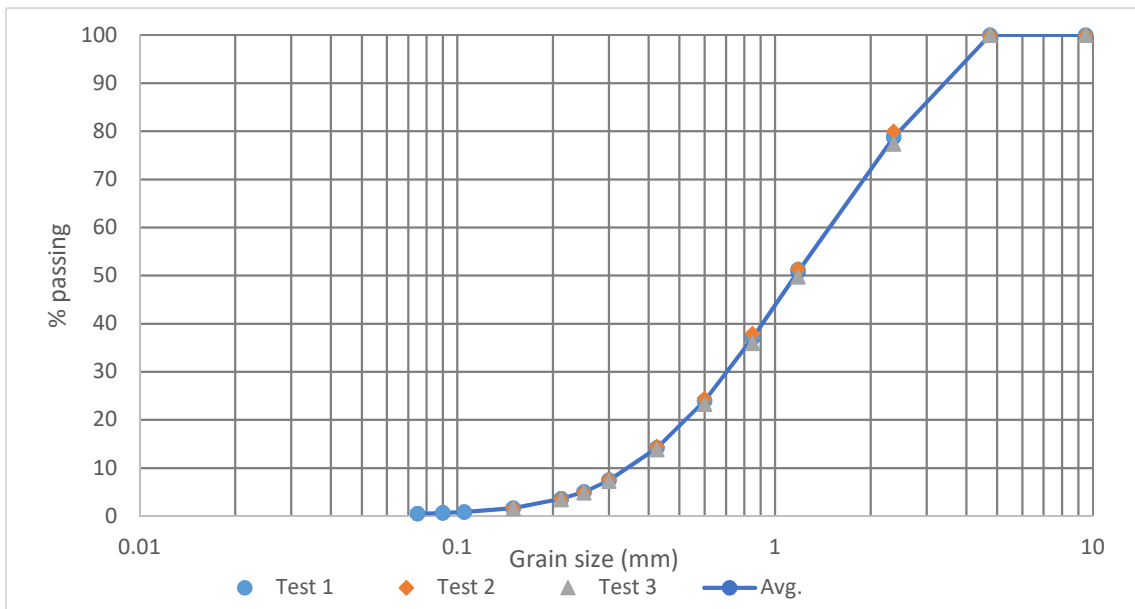
Figure 4.4.1: Grain size distribution of soil SF-1
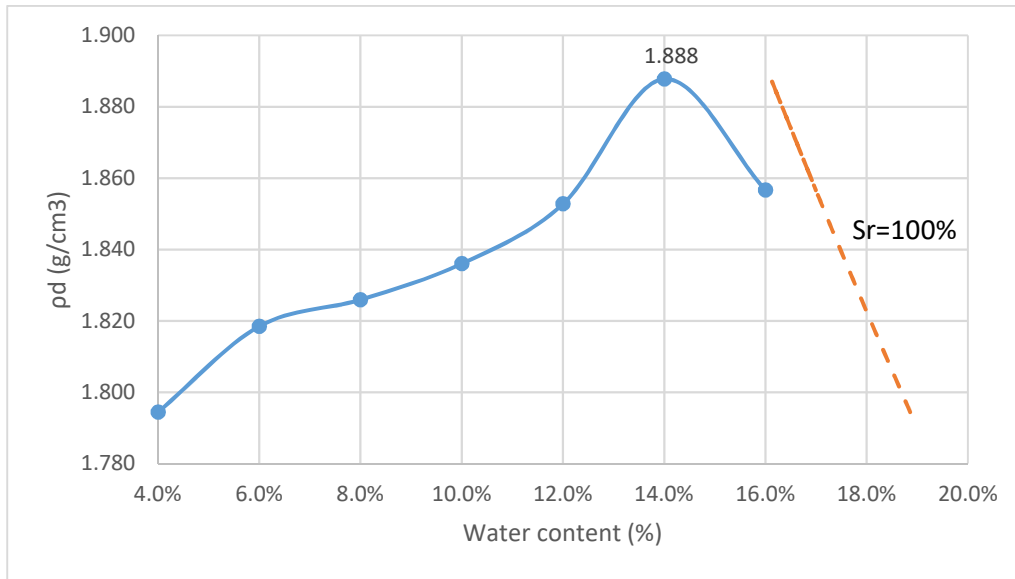
Figure 4.4.2: Proctor test results of SF-1

4.5 Thermometer accuracy verification

In total, three thermometers were used in this thesis. Thermometer 1, with a precision of 0.1°C and an unknown accuracy, was used for all the experiments. Thermometer 2, on the other hand, has a precision of 0.1°C and an accuracy of ±0.2°C, which was determined after the experiments were conducted. Lastly, thermometer 3 with varying precisions and unknown accuracy was also used. The unknown accuracy in this case means that there is no certificate where information about the accuracy from the fabricator is given. However, with the reception of thermometer 2, it was decided to verify if thermometer1 is accurate because it is used in all the experiments. The experiment included thermometer 3, in case where it is needed for future experiments. To determine if the thermometer is accurate, a difference between thermometer 1 and thermometer 2 should be within the accuracy of the thermometer 2 of ±0.2°C for the experiments temperatures ranging between 15°C and 25°C. In cases where the difference is too high, the relation between both is used to calibrate the thermometer. To do so, the temperature was taken with all the thermometers in water at different temperatures, and the results in Table A.1, were plotted for thermometer 1 and thermometer 2 in Figure 4.5.1. For thermometer 1, the difference between temperatures passes the ±0.2°C of the thermometer 2 accuracy around 5.9 °C and 31.3°C. As for the other temperatures, they are considered accurate. In the case of the experiment's temperature, the thermometer 1 is

accurate. As for the thermometer 3, it was more accurate and constant with an average difference of -0.1 °C.

$y = 1.0023x - 0.0354$
$R^2 = 0.9998$
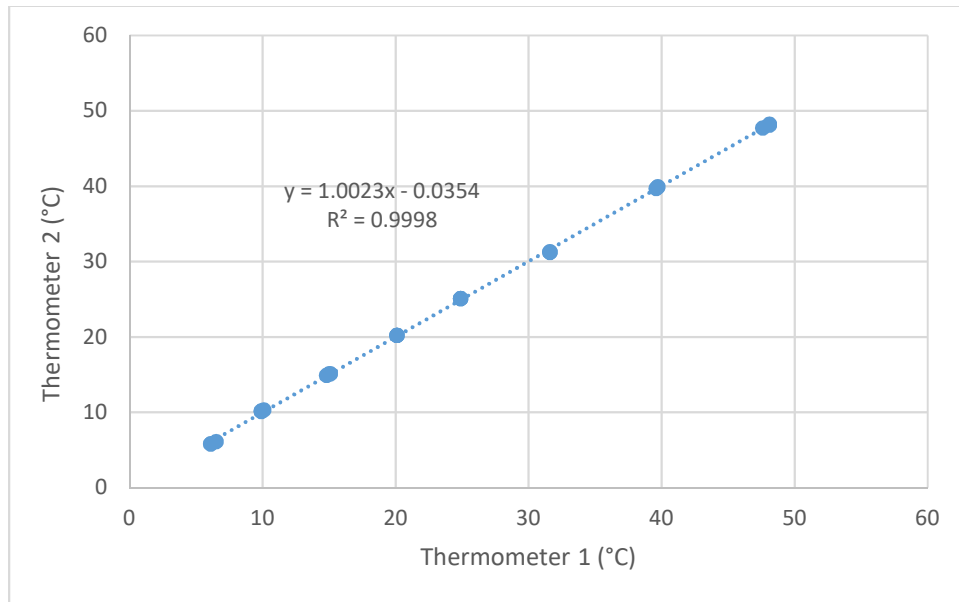
Figure 4.5.1: Thermometer 1 to thermometer 2 relation. Data in Table A.1

Chapter 5: Experimental procedure

There are three experiments where the first one is the gradual insertion of the TDR on the side of the column. This will determine the first reflection apex movement of the waveform and the accuracy of the K_{aS} of the moisture soil when the TDR is partially inserted into the cell. The K_{aS} will be determined using all the interpretation methods described in Chapter 3.

The second experiment consists of 10 setups where, for each setup, the TDRs are placed in a specific way. It determines if there is a presence of interferences between TDRs when multiple TDRs are placed on the column. It is also used to find the K_{aS} of the soil inside the column so the methods described in the preceding chapters can be compared. Finally, the effect of the reinsertion of the probe on K_{aS} is also analyzed to see if it can be a source of error and how it compares to the first insertion.

The third one is the multilayer experiment. The multilayer experiment consists of having two layers in the column BC in which one TDR is inserted laterally into each layer and one TDR is inserted vertically that pass through both layers. This experiment is done to compare the lateral insertion and the vertical insertion. Furthermore, it is also to do a comparison of the meaning method of permittivities and show the vertical insertion complexity.

5.1   Gradual lateral insertion of the TDR in column

First, the empty column is weighted and then filled with wet soil with a water content of 10% in 3 layers of 50 mm. Each layer receives 25 blows, giving a total energy of 62.6 kN-m/m³, 61.6 kN-m/m³ and 65.3 kN-m/m³ for tests #4, #5 and #6. When the soil is installed, and the height H in Figure 5.1.2 is measured, the weight of the column filled with soil is recorded to determine the bulk density. The measured density of the soil during the experiment is 1.69 g/cm³ for test 4 and 1.73 g/cm³ for tests 5 and 6.

During the gradual insertion experiment, the TDR is laterally inserted into the cell in ~10 mm increments until it gets fully inserted. For each increment, the length of the probe in air L_{rA} and the length of L_{rB} are measured and recorded. With those values, the length of the probe in soil L_{rS} is calculated by subtracting the lengths L_{rA} and L_{rB} from L_{rT}. The TDR reading gives the values of

K_{aT}. Then, another reading was done to obtain the waveform from the TDR. At the end of the experiment, the temperature is recorded by inserting the thermometer from the top. The temperature could not be determined for each step to limit the risk of interferences on the TDR's data and the experiment's time was short enough not to affect the temperature.
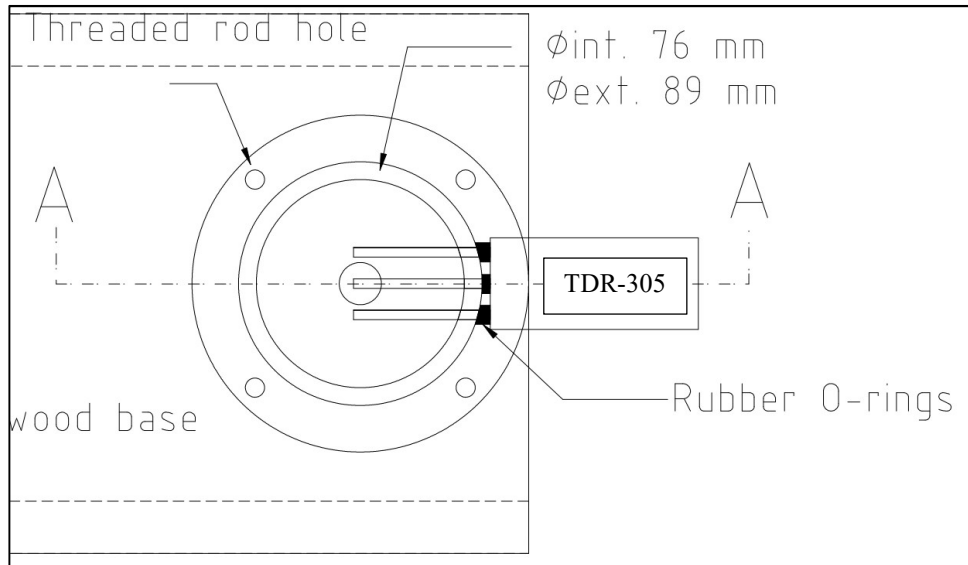
Figure 5.1.1: Plan view of the TDR-305 inserted in the column SC
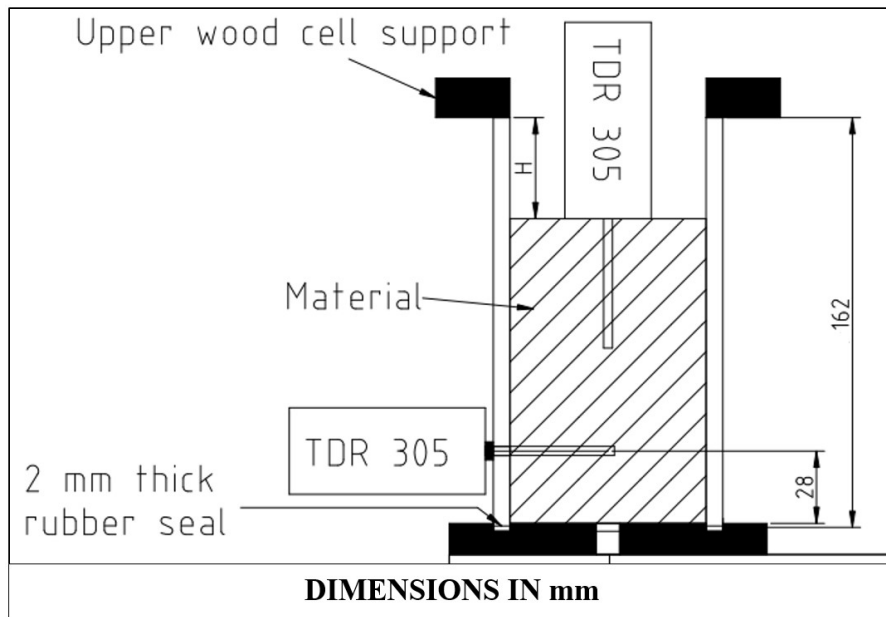
Figure 5.1.2: A-A cut view of the column SC
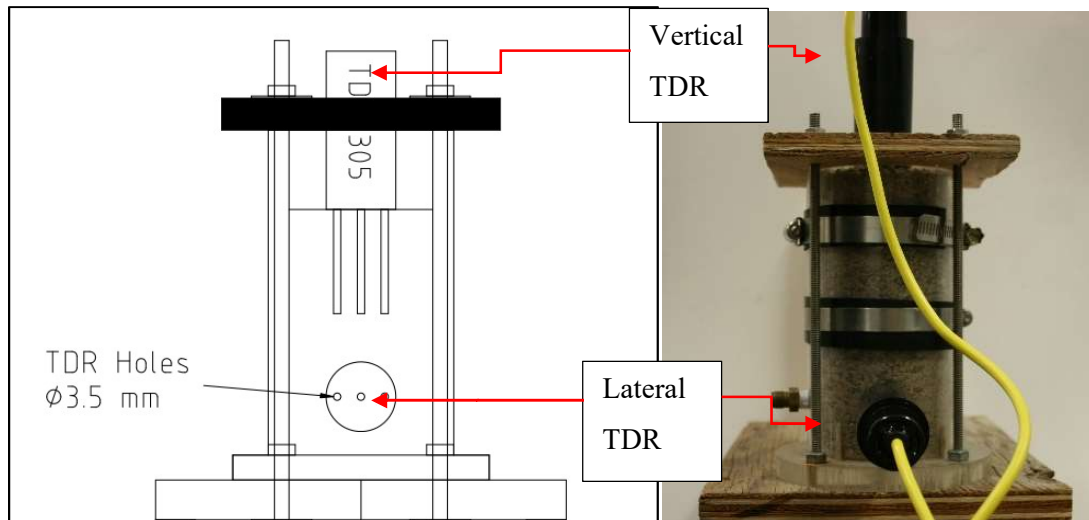
Figure 5.1.3: Front view of the column SC

5.2   Experiment with multiple TDR setups

During the multiple TDR setup experiments, the soil SF-1 is prepared to have three different water contents. The first water content is 0%, where the soil is dry; the second is 4.3%, where the soil is slightly moist; and the third is wet soil, with a water content of 12.2%. First, the soil is filled into the column. During the filling of the dry soil, no compaction was done because the vibration of the compaction makes fines go downward. As shown in Figure 5.2.1, the fine grains are deposited on the bigger grain, and any disturbance makes the grains move downward. Thus, the effect of grain segregation is increased, which may cause a difference in soil conditions between the upper and bottom parts of soil in the cell.

As for the moistened soil and wet soil, the soil is filled into the column in 3 compacted layers with a total energy of 42.7 kN-m/m^3 and 43.8 kN-m/m^3, respectively. This gives a ρ_d of 1.68 g/cm^3 and 1.77 g/cm^3 for the moist soil and wet soil, respectively. A low compaction energy is used to lower the stress on the Plexiglas cell and to be able to insert the TDR probes without damaging the probe. One specimen is taken from the pan to determine the water content of the prepared soil, and one specimen is taken from each of the three layers of the soil in the column. The soil specimen taken from the column is taken at the top, middle, and bottom at the end of the experiment. As for the temperature, it is measured by inserting the thermometer from the top at the end of the experiment. The time of the experiment is short. Thus, it was assumed that the

49

temperature change during the experiment was low. During the experiment, the recorded temperature is 22.0°C and 21.8°C for the moist and wet soil, respectively.

Figure 5.2.1: Dry SF-1 in the column showing segregation
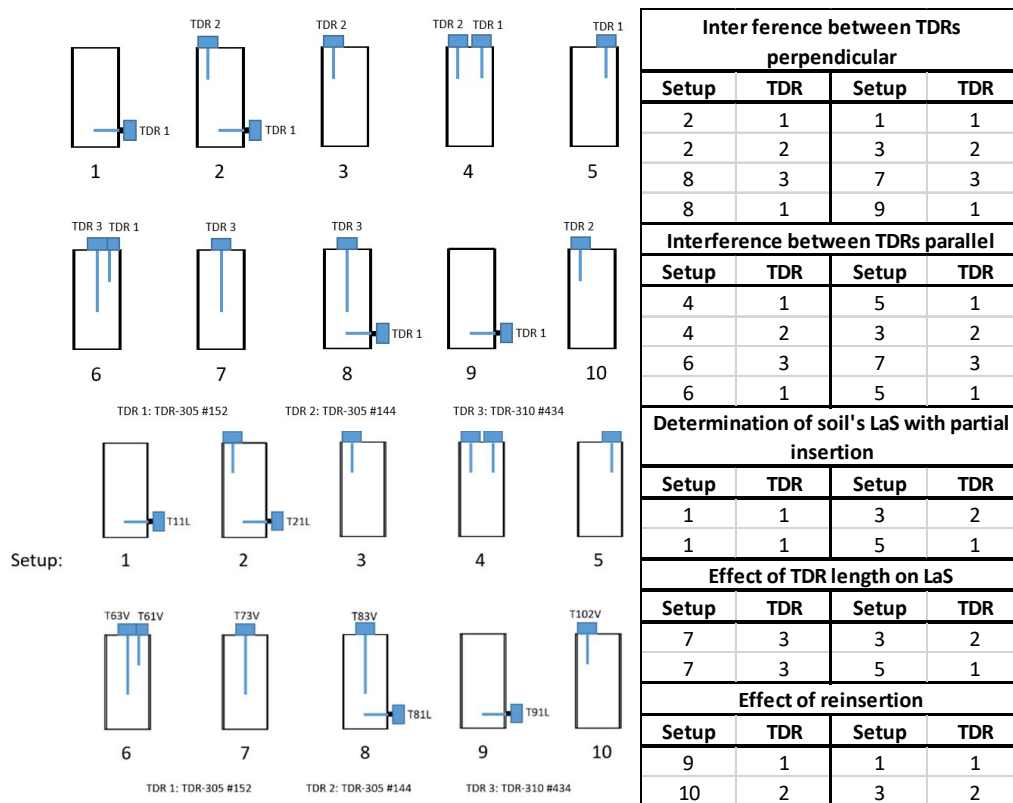
Figure 5.2.2: left) TDR setups during the experiment with position's name; right) Setups comparison for each objective

The setups used during this experiment are shown in Figure 5.2.2 which shows the three TDRs and their placement for each setup.

Setup 1: The TDR1 probe is laterally inserted into the cell filled with soil.

Setup 2: The TDR 1 from Setup 1 is kept in place, and TDR 2 is inserted vertically from the top.

Setup 3: The TDR 1 is removed while the TDR 2 stays in place.

Setup 4: The TDR 2 from Setup 3 is kept in place, and TDR 1 is inserted vertically on the top of the cell.

Setup 5: The TDR 2 is removed, and the TDR 1 is kept.

Setup 6: The TDR1 from Setup 4 is kept, and TDR3 is added.

Setup 7: The TDR 1 is removed, and TDR 3 is kept.

Setup 8: The TDR 1 is laterally reinserted into the cell. Ref Figure 5.2.5

Setup 9: The TDR 3 is removed while TDR 1 stays.

Setup 10: The TDR 1 is removed, and TDR 2 is reinserted at the top.

All the setups were compared for a specific objective. In Figure 5.2.2, each objective has the number of the setup and the number of the TDRs that are compared. For example, to determine if there is an interference between TDRs when they are perpendicular to each other, the TDR 1 of setup 2 is compared to the TDR 1 of setup 1. Therefore, each line represents a comparison of data of two TDRs.

The TDRs are not inserted in the same hole except for setup 9 and setup 10. Thus, the vertically inserted TDRs are inserted following Figure 5.2.3. The figure is printed to fit the dimensions of the cell, then put over the soil where the paper is perforated with a small piece of metal that has a diameter smaller than the TDR probe. So, when the paper is removed, the TDRs are placed accurately for each test. When one TDR is already inserted at the top, another printed layout shown in Figure 5.2.4 is used to mark the next TDR to be inserted.
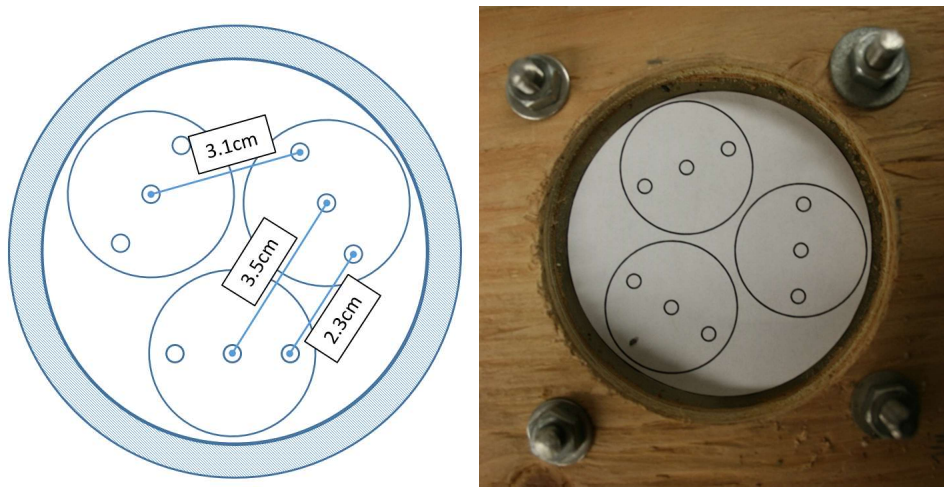
Figure 5.2.3: Left) Layout of the TDR probes when inserted at the top of the cell; Right) Printed TDR Layout put on the Dry soil experiment
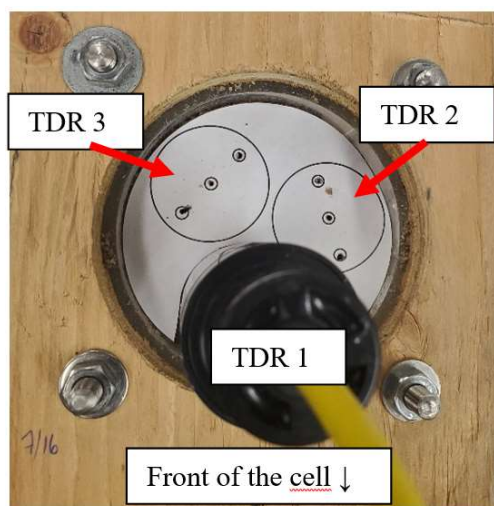
Figure 5.2.4: Paper used to mark the probes insertion when one TDR is inserted

Since the TDRs influence zone can be affected by other TDR probes, the distances between them were measured and calculated depending on the height H shown in Figure 5.1.2. The shortest horizontal distance between the vertically inserted TDRs is 3.1 cm, which is the distance between the middle probe and the outer probe, as shown in Figure 5.2.3. Horizontally, the shortest distance between the vertically inserted TDRs and the laterally inserted TDR1 middle probe is 1.1 cm, as shown in the left drawing in Figure 5.2.5.

On the vertical plane, the vertical distance varies with the TDR probe length and the soil's height. As shown in the right drawing in Figure 5.2.5, where all the vertical distances are shown, the shortest distance is between the TDR1 influence zone and the TDR3 outer rod. During the experiment, the height (H) was 1.2 cm during the wet soil experiment, 0.8 cm during the moist soil experiment, and 0.0 cm during the dry soil experiment. Thus, the closest distance is 2.0 cm for the wet soil, 2.4 cm for the moist soil, and 3.2 cm for the dry soil.
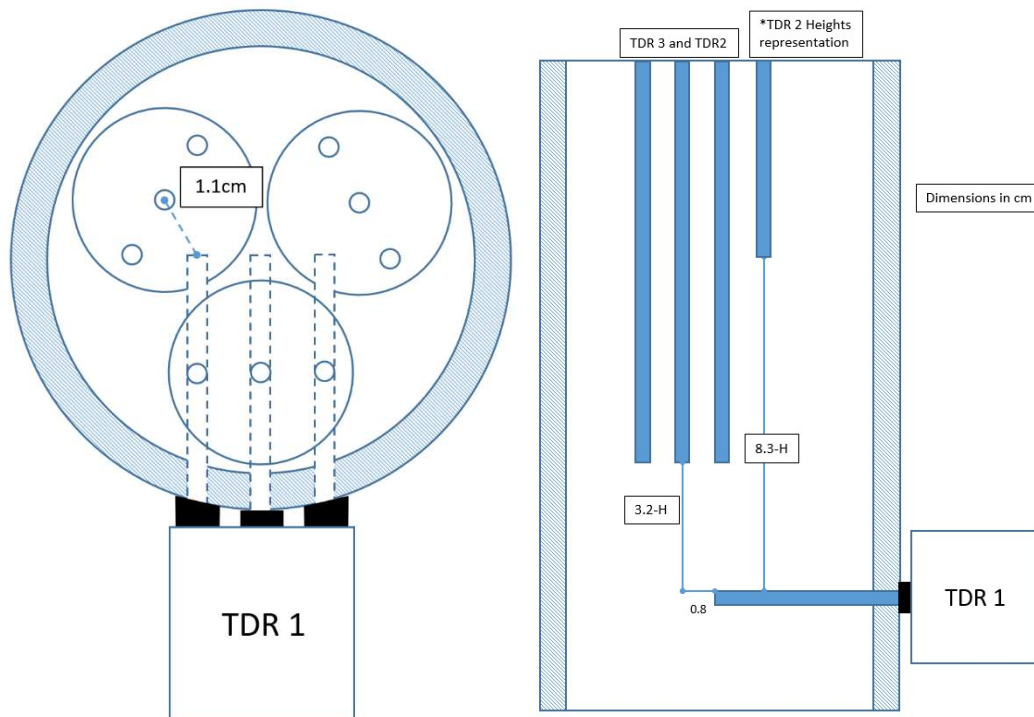
Figure 5.2.5: Left) Closest horizontal distances between TDRs probes and; Right) closest vertical distances between TDRs probes for Setup 2 and Setup 8

5.3   Multilayer of soils experiment

The multilayer of soils experiment consists of filling two layers of SF-1 soil in column BC. The upper layer and the bottom layer have one TDR 305 inserted laterally and one TDR 310 inserted vertically. The soil is prepared to have a water content of 9% and set covered overnight. Both layers are compacted with the same energy of 141.17 kN m/m^3/layer of 50mm. The compaction is done with the big rammer, where 50 blows were done with a weight of 1425.9 g at a drop height of 103 mm. The soil is filled, as shown in Figure 5.3.2, starting with the base layer, which is a highly

compacted layer that is used as a base for the two layers above. The base layer is SF-1 soil with the same water content as the other layers that are added in order to have layers of the same height. After the column was weighed with the base layer, the column was filled with soil to have layer 1 compacted at the specific energy. After the compaction of layer 1, the column is weighed, and the mass is recorded. With the same procedure as layer 1, layer 2 is installed and compacted before weighing. Once the column is filled with the soil's layers, the lateral TDRs are carefully inserted, as shown in Figure 5.3.2. Three TDRs are inserted: TDR#1 in layer 1, TDR#2 in layer 2, and reference TDR (TDR Ref.) above both layers. The TDR Ref. is used to guide the vertical insertion of the TDR#3 since it gives the limits of the Lateral TDRs probes. Thus, it reduces the risk of interference between the vertical TDR and lateral TDR probes. The insertion process of the lateral TDRs is long because the TDRs are slowly inserted, and the lateral supports need to be screwed. So, to avoid the risk of evaporation, a rubber sheet is installed above layer 2 during the process, as shown in Figure 5.3.1.
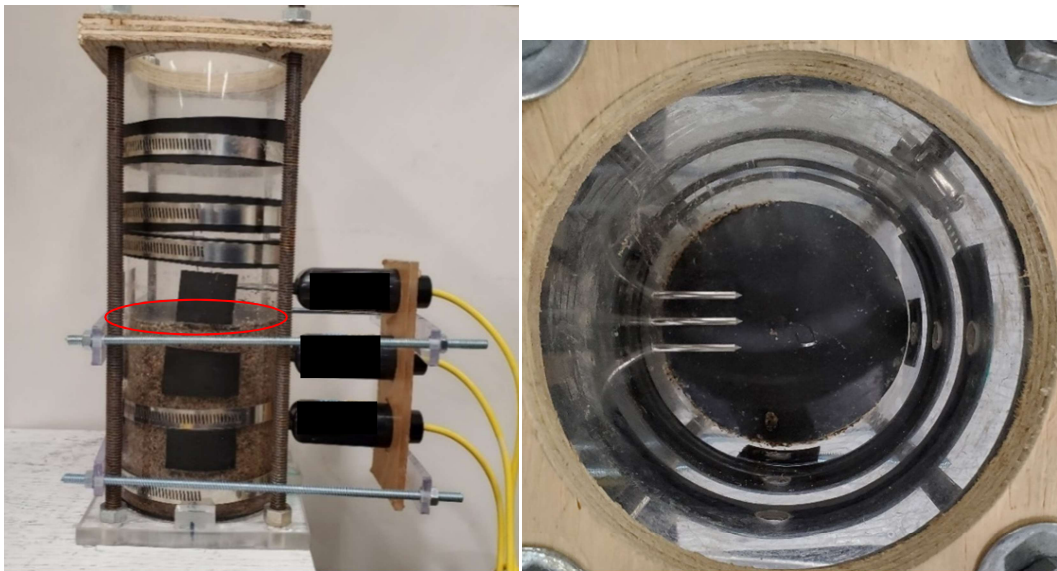
Figure 5.3.1: Side view (left) plan view (right) of the apparatus with the addition of the rubber sheet

The TDR#3 is inserted after the rubber removal. When the installation of the TDR is done, the reading process starts by recording the permittivities and the waveforms from the TDRs. After data recording, the thermometer is inserted and recorded for each layer. This experiment is done to compare lateral TDR insertion and vertical TDR insertion. There will be advantages and

disadvantages to each insertion. Furthermore, the vertical insertion of the TDR will get through two layers of soil where the waveform gives not only one waveform that regroups both layers but also the vertical change in the layers. However, calibration is necessary to monitor the soil's condition and separate both layers in the waveform. Interpreting waveforms is easier with lateral insertion as it provides one layer for each TDR, but only for a horizontal volume into the layer.
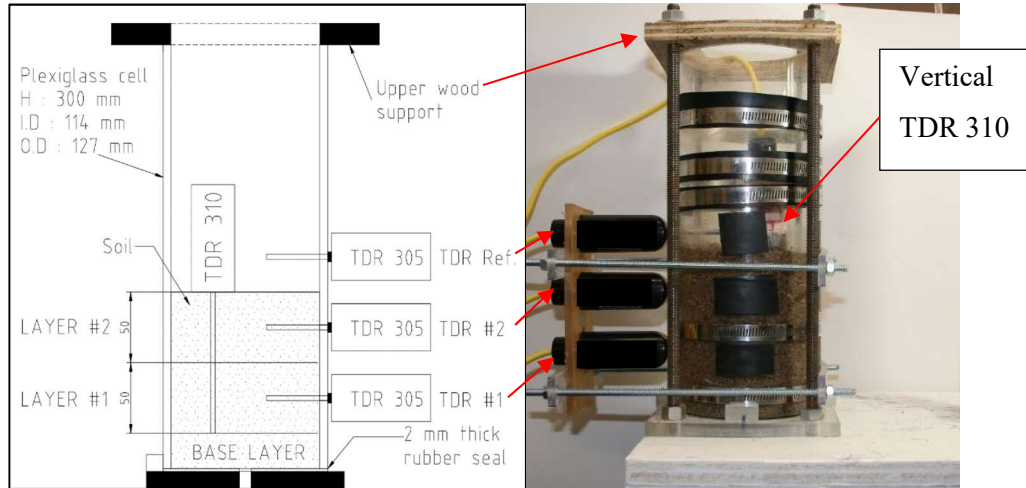
Figure 5.3.2: Setup during the multilayer experiment
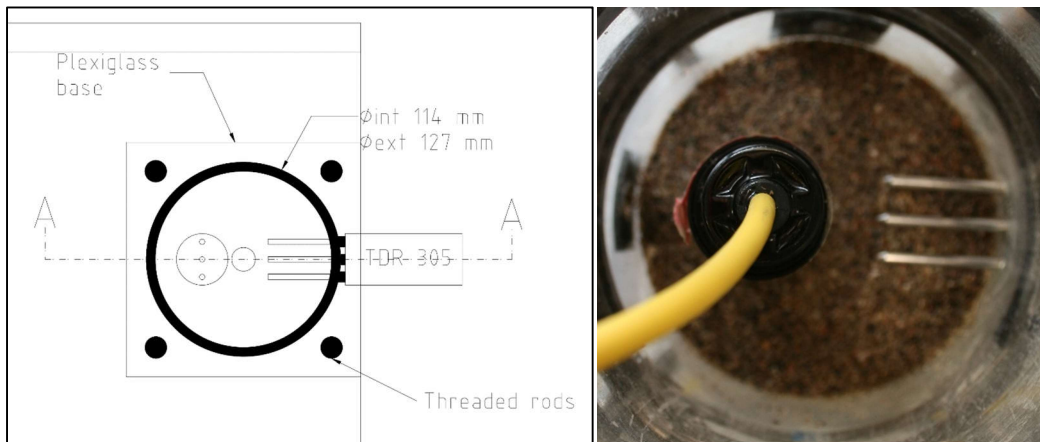
Figure 5.3.3: Plan view of the column BC during the multilayer experiment

Chapter 6: Results and discussion

6.1 Determination of t_1 of the Heimovaara method

As presented in section 3.2.2, the Heimovaara method uses a known permittivity to find t_1 of the waveform. The author didn't discuss his temperature reference choice, so using a different reference source can lead to a different result. To analyze the source of error, Hasted (1973) was compared to Stogryn et al. (1995), which was used as reference permittivity in Schwartz et al. (2009). The Stogryn et al. (1995) permittivity of water at a temperature T is shown below

$$\varepsilon_w = \frac{3.70886 \times 10^4 - 82.168\,T}{4.21854 \times 10^2 + T} \tag{6.1}$$

When both equations are compared, as shown in Table 6.1.1, both equations converge when the temperature rises. Between 10°C and 35°C, a difference of 0.15 to 0.06 was found in the permittivity of water. Conversely, the temperature doesn't change the air permittivity (Schanz et al. 2011).

Table 6.1.1: Difference of water permittivity between Hasted (1973) and Stogryn (1995)

T	Hasted (1973)	Stogryn (1995)	Δε
10	83.83	83.98	0.15
15	81.95	82.08	0.13
20	80.10	80.22	0.12
25	78.30	78.40	0.10
30	76.55	76.63	0.08

An experiment was done to determine if the water temperature has an effect on the Heimovaara method of finding t1. As shown in Figure 6.1.1 (left), the experiment consists of putting two thermometers with a reading precision of 0.1°C and a third thermometer, shown in Figure 6.1.1 (right), with a reading precision of 0.0001°C in a cylinder full of deionized water. The two thermometers on the left picture in Figure 6.1.1 are used to take temperatures, and the third thermometer was added to better monitor temperature variation.

Since it can get more precise, it is more sensitive to temperature change than the two others. The cylinder was put into a temperature-controlled bath. The reason why the experiments can't be done straight into the bath is because of the presence of limestone and other sediments that can affect the results. Then, the tub is set at the desired temperature. The deionized water temperature was monitored with three thermometers. The water was mixed to make sure that the temperature was uniform. When the desired temperature of deionized water is stabilized, the TDR probes are inserted to take data. The temperature increments are approximately 5°C.
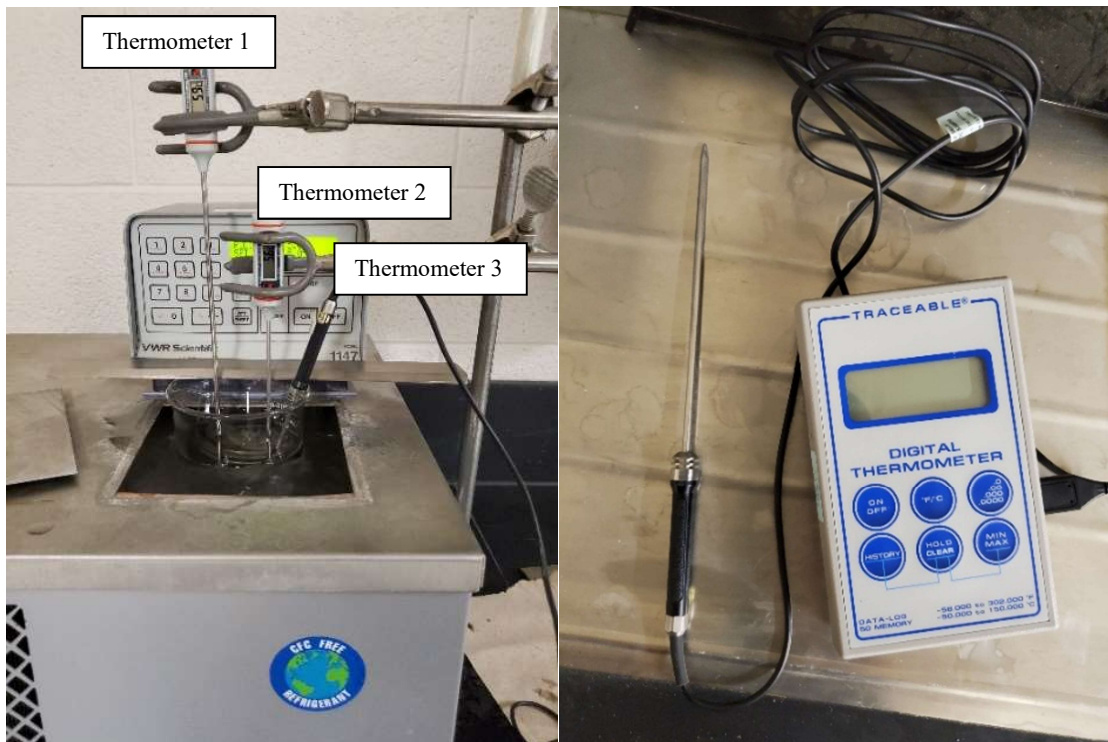
Figure 6.1.1: Left) Apparatus of the experiment to determine the variation of t_1 of Heimovaara method; Right) High precision thermometer 3 used for the experiment

The obtained variation of t_1 and t_2 during the water's temperature change are shown in Figure 6.1.2 to Figure 6.1.8 and in Table 6.1.2. The obtained curves for both t_1 and t_2 are quadratics. However, t_2 curves decrease only compared to t_1 curves, which increase until 25°C for TDR 144 and TDR 152. For the TDR 434, it increases until 30°C before it starts decreasing. The difference is probably due to the TDR's probes lengths.

Ranging from 6°C to 50°C, t_1 variation was between 75 ps and 79 ps for TDR 434 and TDR 144. As for the TDR 152, the variation was between 63 and 64. It was lower than the two others. Similar to points grouping in t_1 vs water temperature graphs, the curve of TDR 152 has an R^2 of 0.62, which is lower than the other TDRs that have values between 0.89 and 0.93. The reason for a low R^2 is unknown; the test was done multiple times, and the same R^2 was obtained.

A maximum spread of 20ps of the data in Figure 6.1.6 at 20°C doesn't affect the accuracy too much. The lowest Δt is about 300 ps for air, which means that spread causes a maximal relative error of 6.7% and decreases with higher Δt such as water and wet soil.
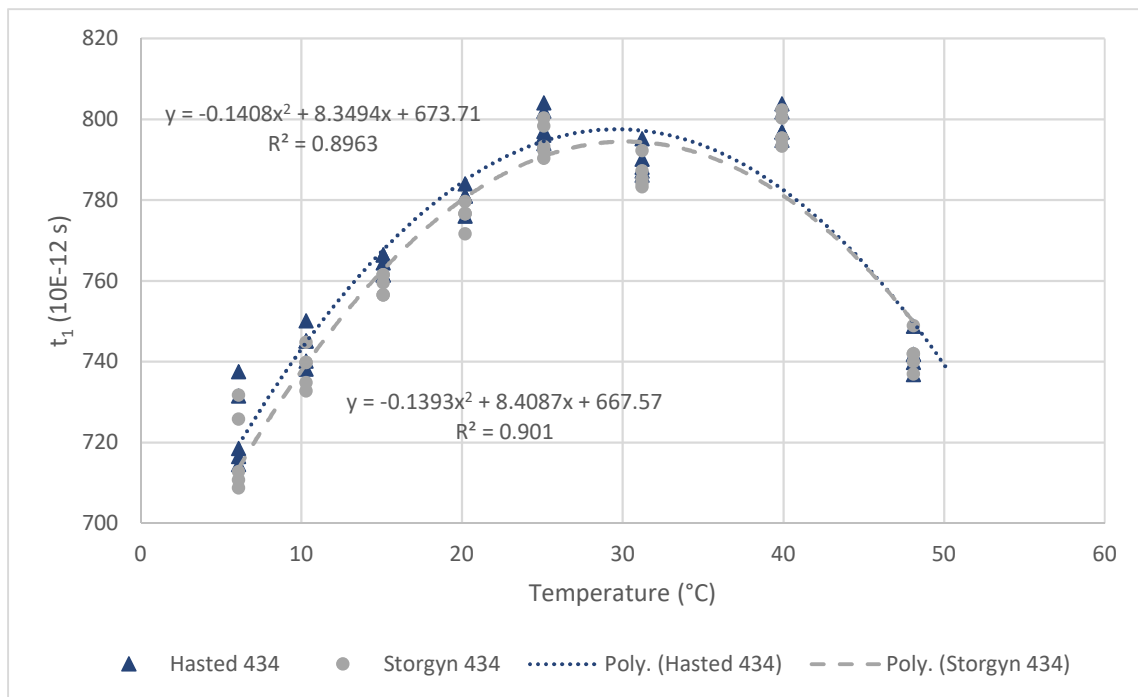
Figure 6.1.2: Heimovaara method's t_1 variation with temperature for TDR #434 (Data in Appendix B Figure B.1 and Figure B.2)
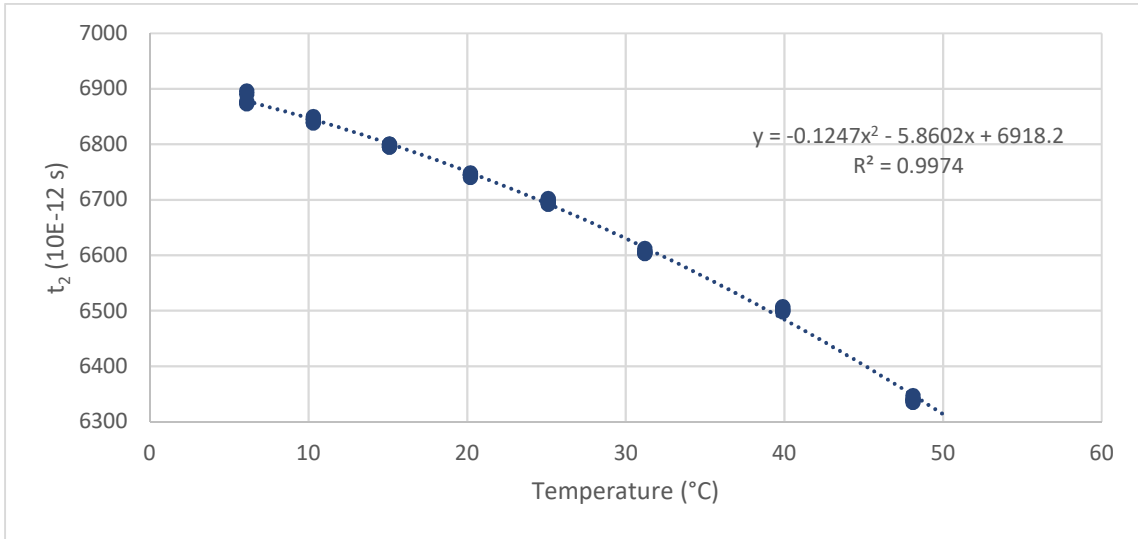
Figure 6.1.3: Variation of t₂ with the temperature of the TDR #434 (Data in Appendix B Figure B.1 and Figure B.2)
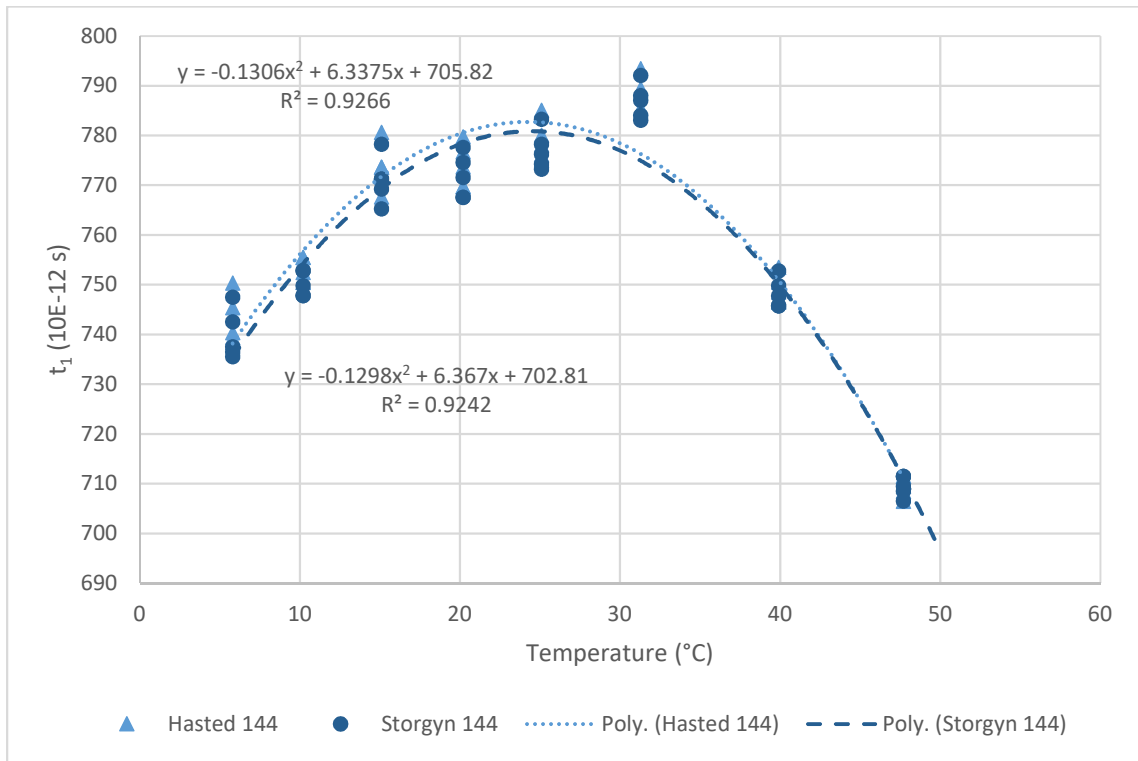
Figure 6.1.4: Heimovaara method's t₁ variation with temperature for TDR #144 (Data in Appendix B Figure B.1 and Figure B.2)
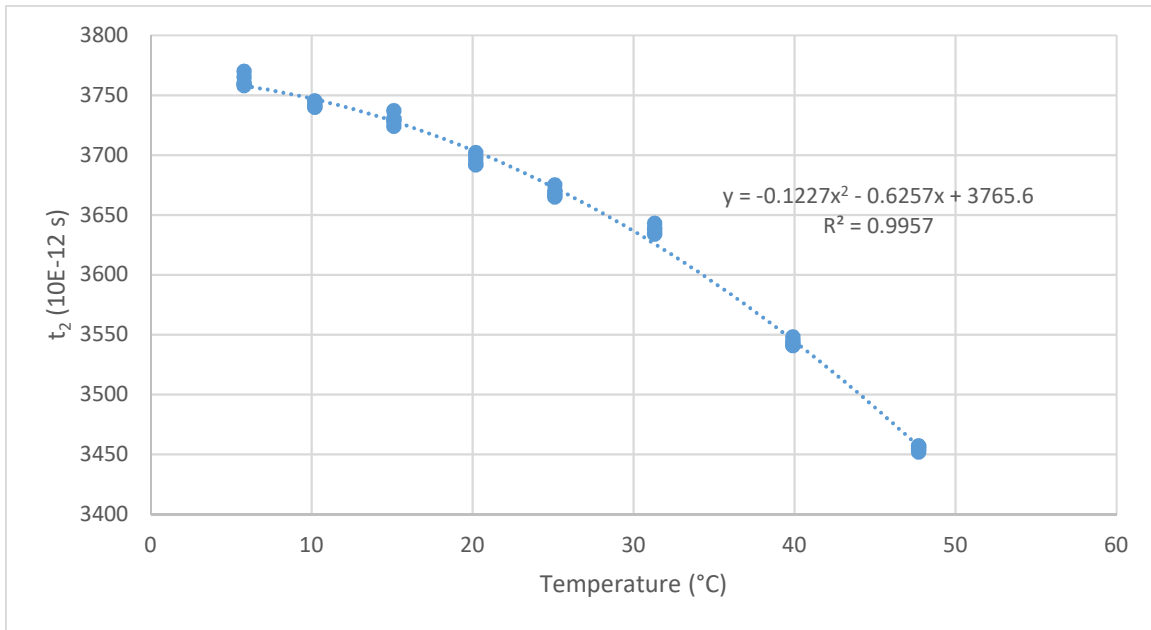
Figure 6.1.5: Variation of t₂ with the temperature of the TDR #144 (Data in Appendix B Figure B.1 and Figure B.2)
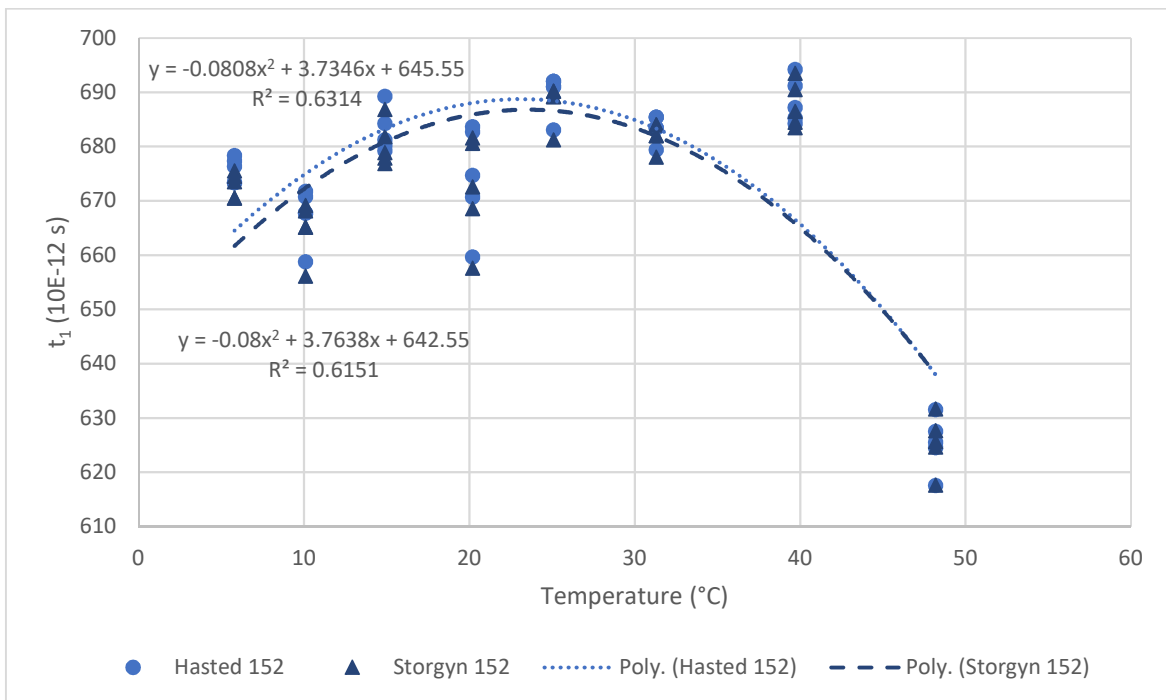
Figure 6.1.6: Heimovaara method's t₁ variation with temperature for TDR #152 during test#3 (Data in Appendix B Figure B.1 and Figure B.2)
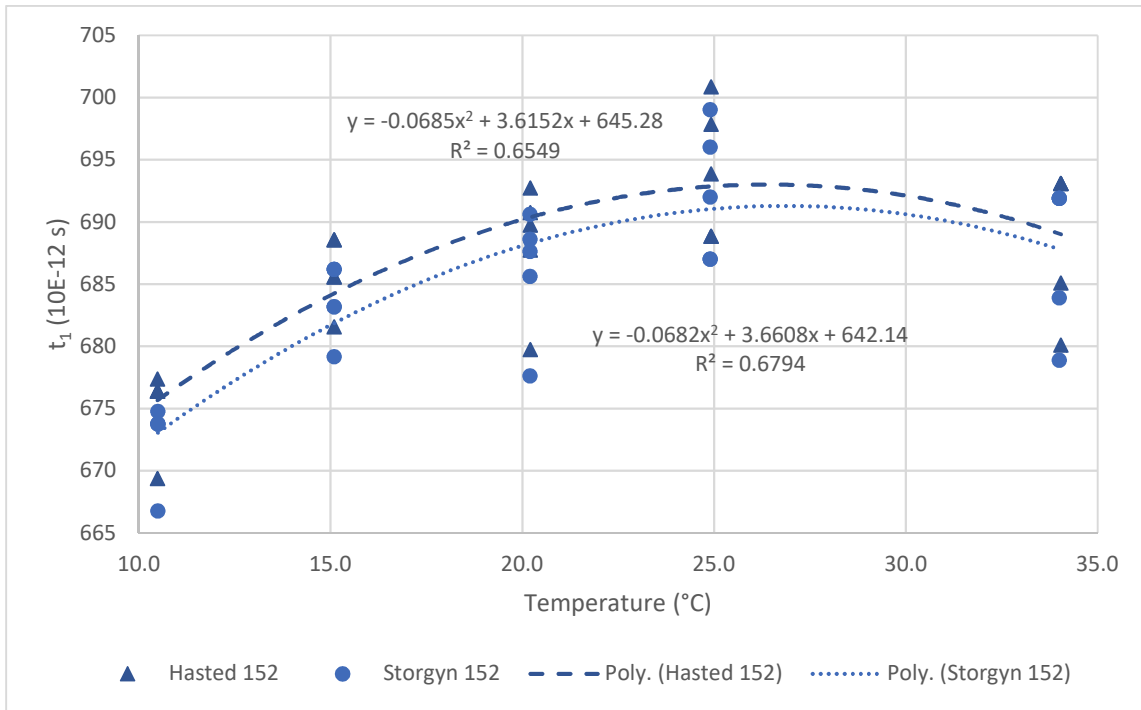
Figure 6.1.7: Heimovaara method's t_1 variation with temperature for TDR #152 during test#1 (Data in Appendix B Figure B.1 and Figure B.2)
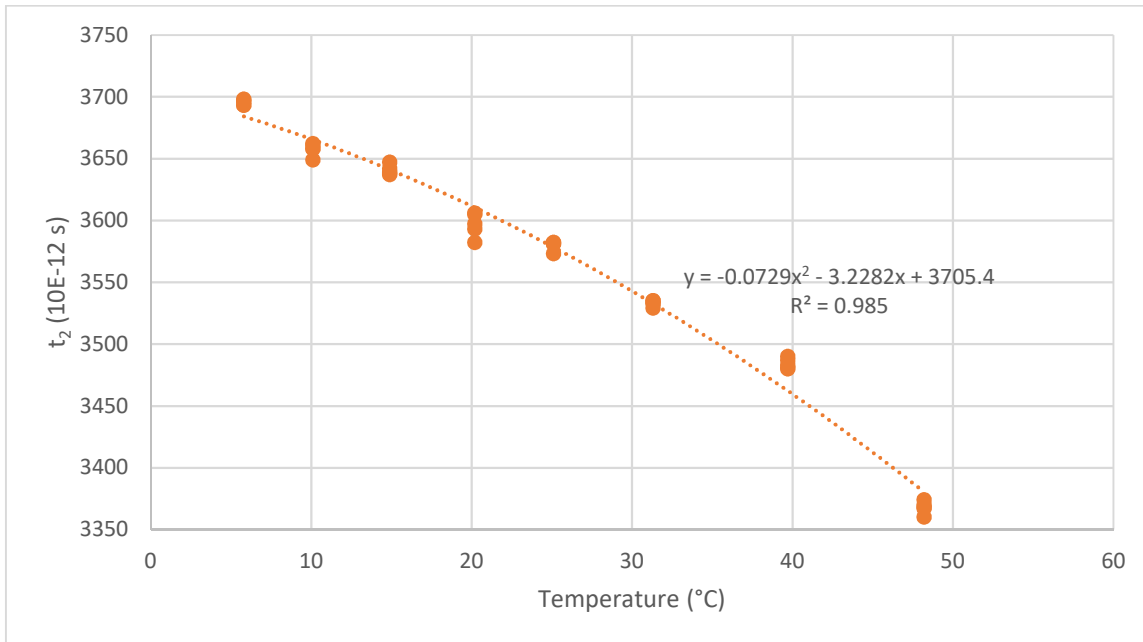
Figure 6.1.8: Variation of t_2 with the temperature of the TDR #152 (Data in Appendix B Figure B.1 and Figure B.2)

Table 6.1.2: Comparison between Hasted (1973) and Stogryn (1995) and maximal variation of t_1 of each TDR

TDR	T	Hasted (1973) ε_w	Stogryn (1995) ε_w	Hasted (1973) avg t_1	Stogryn (1995) avg t_1	Δt_1	t_2
	°C			ps	ps	ps	ps
434	6.1	85.3	85.5	724	718	-6	6882
	10.3	83.7	83.9	744	738	-5	6844
	15.1	81.9	82.0	764	759	-5	6798
	20.2	80.0	80.2	781	776	-4	6745
	25.1	78.3	78.4	799	795	-4	6697
	31.2	76.1	76.2	789	787	-3	6606
	39.9	73.2	73.2	799	797	-1	6502
	48.1	70.5	70.5	742	742	0	6340
			Max. Variation	75	79		542
144	5.8	85.5	85.6	743	740	-3	3762
	10.2	83.8	83.9	753	750	-3	3742
	15.1	81.9	82.0	773	771	-2	3730
	20.2	80.0	80.2	774	772	-2	3696
	25.1	78.3	78.4	779	777	-2	3669
	31.3	76.1	76.2	788	787	-1	3638
	39.9	73.2	73.2	749	748	-1	3544
	47.7	70.6	70.6	709	709	0	3455
			Max. Variation	79	77		307
152	5.8	85.45	85.61	676	673	-3	3695
	10.1	83.79	83.94	667	665	-3	3658
	14.9	81.98	82.12	683	680	-2	3641
	20.2	80.03	80.15	674	672	-2	3597
	25.1	78.27	78.37	690	688	-2	3580
	31.3	76.09	76.17	683	682	-1	3533
	39.7	73.25	73.29	688	688	-1	3484
	48.2	70.48	70.48	625	625	0	3368
			Max. Variation	64	63		328

In Table 6.1.2, the t_1 of both references were compared, and the difference between t_1 values was negligible. On the TDR 434, the highest difference is -6 ps and -3 ps for the smaller TDRs, which is half of the TDR 434. A relation can probably be made with the probe length since the TDR 434 is double the length of the other TDRs. Thus, even if the difference is negligible, the average of both t_1 was chosen. By calculating the average of the regression equations on the t_1 graphs above for each TDR, the equations below were calculated to determine t_1 at a temperature T.

$$t_{1\text{-}434}(T) = -0.1401\ T^2 + 8.3791\ T + 670.64 \qquad\qquad (6.2)$$

$$t_{1\text{-}144}\ (T) = -0.1306\ T^2 + 6.3523\ T + 704.32 \qquad (6.3)$$

$$t_{1\text{-}152}\ (T) = -0.0804\ T^2 + 3.7492\ T + 644.05 \qquad (6.4)$$

To determine the value of t_1 to be used as a reference for the Heimovaara method, the temperature range was chosen to be between 18°C and 22°C. The chosen range is based on the temperature range during experiments. Thus, it was decided to choose 20°C as a reference temperature, which gives a t_1 at 782 ps, 779 ps and 687 ps for the TDR 434, 144 and 152, respectively. Table 6.1.3 shows the average t_1 at 20°C, with the average t_1 at 18°C and 22°C as the minimal and maximal values. When those values are compared with the chosen value of t_1, the highest obtained difference is 6, and the lowest is 1. That difference was used to determine the approx. relative error based on an approximate lowest and the highest value of Δt. The lowest value of Δt is based on air's Δt and the highest on wet soil's Δt. The obtained result of the comparison showed that a maximum approximated error of 0.9% happens if a TDR 144's t_1 at 18°C is used for the lowest Δt. As for the lowest approximated error, it is <0.03% if the TDR 152's t_1 is used for the highest Δt and higher.

Table 6.1.3: Obtained t_1 using water and the approximated relative error

TDR#	Hasted (1973) at 20°C	Stogryn (1995) at 20°C	*Avg.	t_1 at 18°C	t_1 at 22°C	diff. to t_1 at 18°C	diff. to t_1 at 22°C	Lowest Δt (Air)	Highest Δt (Water)	Approx. relative error	
	t_1	t_1	t_1	-	-	-	-	-	-	**Min**	**Max**
	ps	ps	**ps**	ps	ps	ps	ps	ps	ps	%	%
434	784	780	**782**	776	787	6	5	1200	5900	**0.1**	**0.5**
144	780	778	**779**	776	781	3	2	300	2900	**0.1**	**0.9**
152	688	686	**687**	685	688	1	1	300	2900	**0.03**	**0.5**

*Average of Hasted (1973) and Strogyn (1995) t_1

Air was also used to determine the value of t_1 where the results are shown in Table 6.1.4 and compared to the chosen t_1 values found with water. The effect of temperature on t_1 was not tested because it was found that air permittivity doesn't change with the temperature (Schanz et al. 2011). The results show that TDR #434 has a small difference between the reference materials values, while the small TDRs (#144 and #152) have a difference up to -56 ps. This is probably due to the TDR's probe length. When the probe is long, the waveform is elongated enough to find points

accurately, and the opposite is true when the probe is shorter and the material has a small permittivity. As shown in Figure 6.1.9, the obtained waveforms in air from the 100 mm and 49 mm probes were put on the same graph in order to show the different lengths. The t_2 is found for both waveforms, but the t_2 found on the TDR #152 is closer to t_1. Thus, a short probe is not enough to measure a low permittivity.

Consequently, a difference of air's t_1 to water's t_1 of 4ps in the highest Δt for TDR#434 has an absolute approximated difference of 0.1%, and the lowest for the small TDRs is 1.3%. As for the highest absolute approximated difference is 18.8%. Thus, the t_1 that was chosen for the Heimovaara method is the one that was found in water. Even if it varies with the temperature, the water's waveform gives an accurate value of t_2 in order to find the t_1 because of the waveform curve.

Table 6.1.4: Obtained t_1 using air compared to the obtained t_1 using water

TDR	t_1	t_1	Difference to water	Lowest Δt (Air)	Highest Δt (Water)	Abs. approx. relative Difference	
	Air	Water	Δ	-	-	Min	Max
	ps	ps	ps	ps	ps	%	%
434	786	782	4	1200	5900	0.1	0.3
144	723	779	-56	300	2900	1.9	18.8
152	648	687	-39	300	2900	1.3	13.0
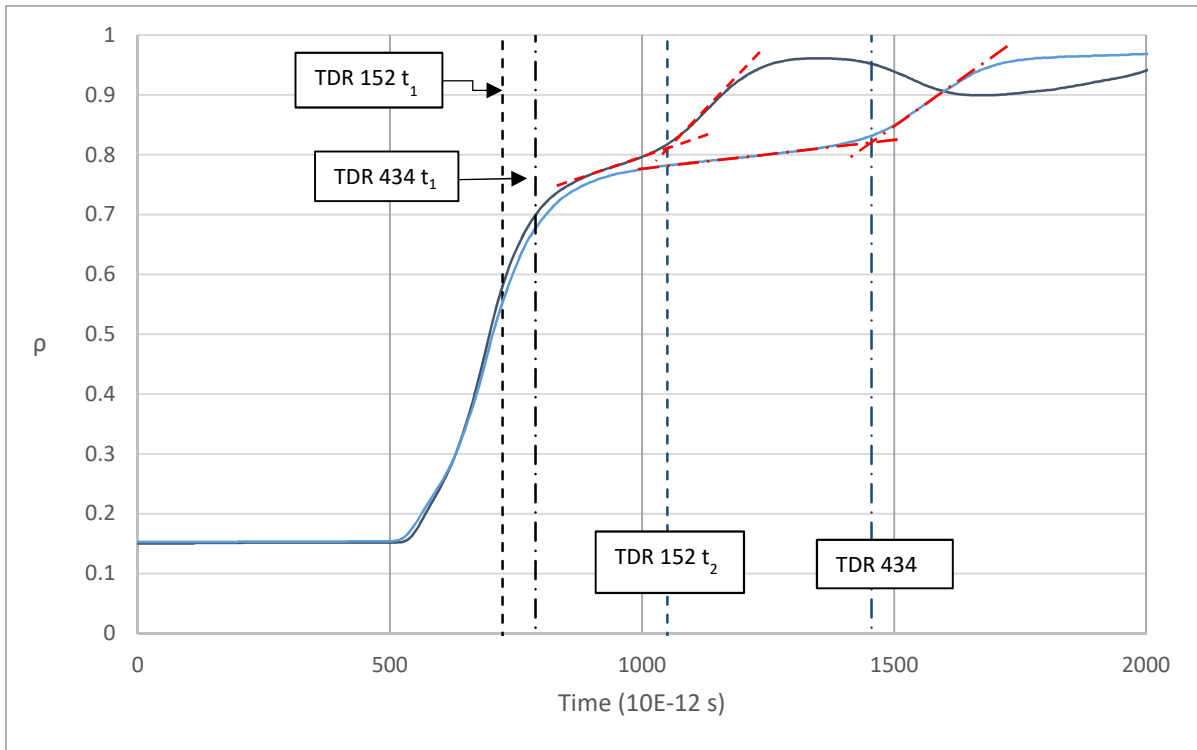
Figure 6.1.9: Length comparison of TDR#152 vs TDR#434 obtained waveforms in air

The fact that the authors chose a known permittivity of water from the literature has led to questioning the TDRs' variation in water permittivity at different temperatures. In the same setup explained in this chapter, the permittivity of water at different temperatures was plotted for the used TDRs and for the literature in Figure 6.1.10 to Figure 6.1.12. For the water permittivity of TDR, the Tangent method and Schwartz method are presented, and the Heimovaara method is indirectly plotted because it uses water permittivity to find t_1.

The figures below show that each TDR has its own curve. Starting with the distance between the Tangent method and the Schwartz method is higher for short TDR probes (#152 and #144) than the longer probes TDR (#434). Both methods converge at higher permittivities for all TDRs and cross the literature curve between 10°C and 30°C. However, the calculation of the relative difference between interpretation methods values to the literature at 20°C resulted in a difference range of -1.4% to 1.7%. Thus, using the literature at that temperature can be acceptable depending on the experiment, but at higher temperatures, the relative difference percentage can reach 3.3%.

From this results, it can be concluded that the values obtained from water's waveforms, especially around 20°, using these interpretation methods are accurate.
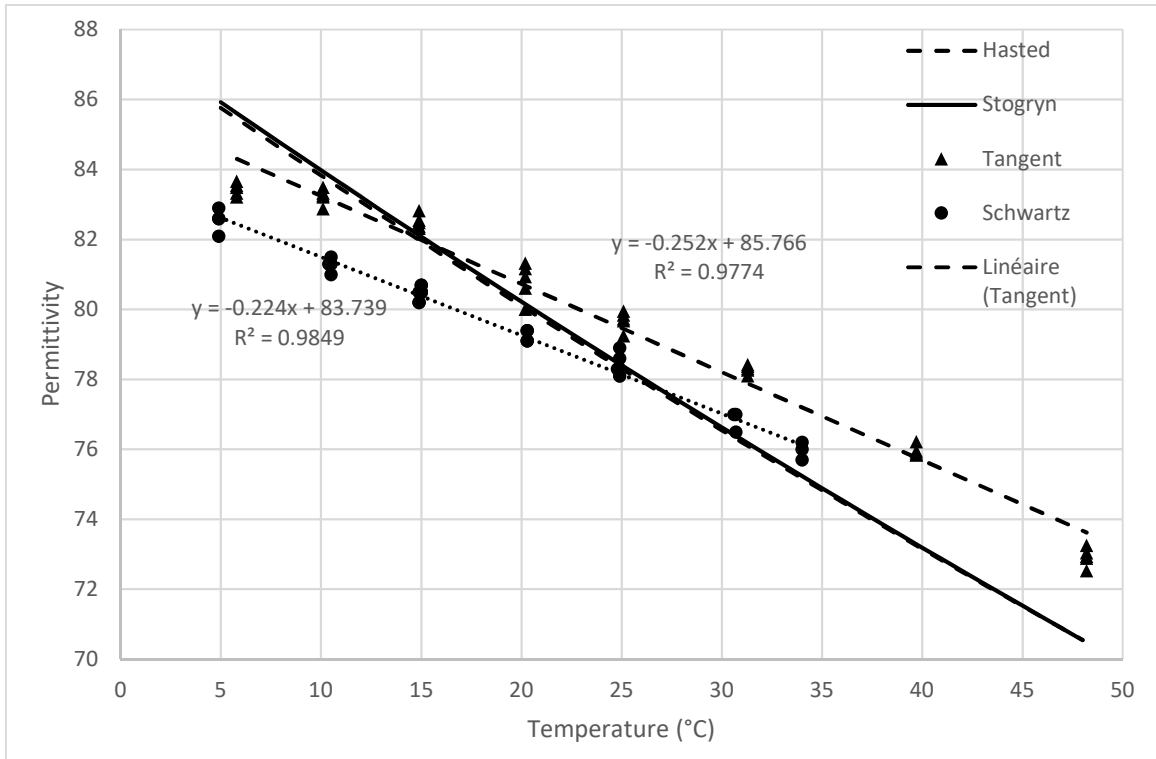
Figure 6.1.10: Graphical comparison of literature water's permittivity at different temperature for TDR#152
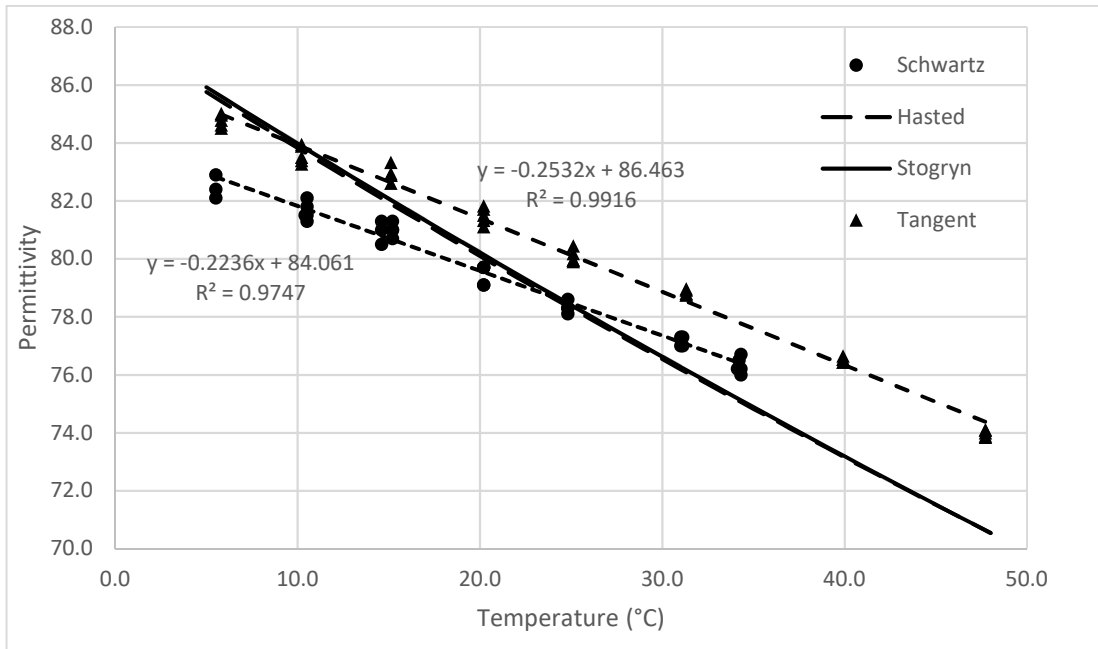
Figure 6.1.11: Graphical comparison of literature water's permittivity at different temperature for TDR#144
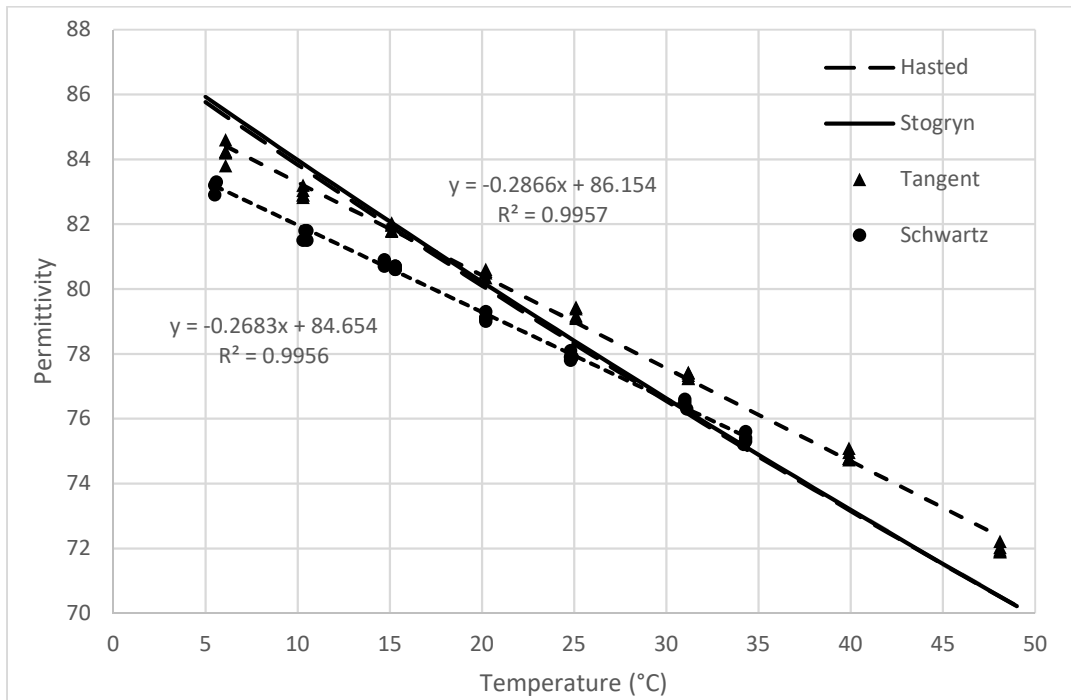
Figure 6.1.12: Graphical comparison of literature water's permittivity at different temperature for TDR#434

6.2　Finding the permittivity of the column's wall

Finding the K_{aB} of the columns SC and BC was done, as explained in Chapter 3. K_{aB} was measured only for TDRs that are inserted laterally on the columns, such as TDR#152 and TDR#144. Initially, air and water were used as reference materials to find K_{aB}, but it appeared that the presence of water in the void had a significant effect on K_{aB}. Thus, the value of K_{aB} found with air as a reference material is used when the void is dry. When the void is wet, the value of K_{aB} found with water is used.

In Figure 6.2.1, the materials around the middle probe are shown. At the outside of the cell, the probe's electromagnetic field contains the rubber O-rings and air. Through the Plexiglas cell wall, the probe's electromagnetic field contains the Plexiglas and a surrounding void of about 1 mm that may contain air, water or soil's fine particles depending on the experiment. In this case, the O-rings, the Plexiglas and the air decreased the total travel time Δt_T of the waveform because of the low permittivity. As for the void, it is filled with water, which should slightly increase Δt_T.
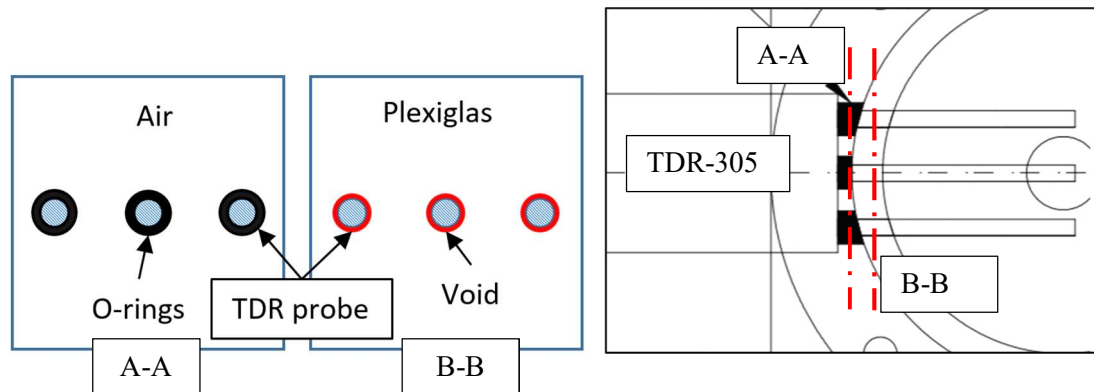
Figure 6.2.1: Middle probe materials around the probes at the rubber O-rings (left) and inside the Plexiglas (right)

For each waveform interpretation method, a K_{aB} is determined for column SC and column BC, and the results are shown in Table 6.2.1 and Table 6.2.3. Both meaning methods are used: the refractive index and the arithmetic mean.

Starting with the K_{aB} of the column SC using the tangent method in Table 6.2.1, where for each reference material and each TDR, the parameters of the experiment are shown. Starting with reference material permittivity and its temperature T found using the tangent method on the

obtained waveform. Then, the length of the TDR probe L_{rR}, the length of the cell's border L_{rB} and the length of the probe inside the reference material $L_{rR'}$ when the probe is inserted into the column. The temperature of the reference material inside the column was also measured, but the same as the T; it was measured only for water since the temperature has no effect on the permittivity of air. The obtained K_{aB} using water as reference material is 2.75 times the K_{aB} of air for the column SC. The same goes for column BC, where the value is 8.68 times the K_{aB} of air using TDR#144 and 10.27 times for TDR#152.

Table 6.2.1: Obtained K_{aB} using Tangent method on column SC and column BC (Waveforms interpretation in Appendix G)

	TDR #	Reference material					Ref. material + Cell					RI	ART
		$K_{aR'}$	T	L_{rR}	L_{rB}	$L_{rR'}$	T	$K_{a\,B+R'}$	$\Delta t_{B+R'}$	$\Delta t_{R'}$	Δt_B	K_{aB}	K_{aB}
			°C	m	m	m	°C		ps	ps	ps		
Column SC													
Air	152	1	-	0.049	0.010	0.039	-	1.0	333	262	71	**1.2**	**1.2**
Water	152	79.9	22.7	0.049	0.010	0.039	22.6	56.7	2460	2342	118	**3.3**	**-37.2**
Column BC													
Air	144	1	-	0.049	0.011	0.040	-	0.97	322	253	69	**0.9**	**0.9**
	152	1	-	0.049	0.011	0.040	-	0.98	322	253	69	**0.9**	**0.9**
Water	144	81.7	21.8	0.049	0.011	0.040	22	58.20	2492	2289	203	**7.6**	**-22.8**
	152	80.6	21.8	0.049	0.011	0.040	22	58.34	2495	2275	220	**9.0**	**-18.6**

The principal idea of this method to find K_{aB} necessitates having the reference material temperature or condition be the same before and after being added to the cell. Meaning that the deionized water needs to be in the same condition in both measurements (with and without column's wall). In the case of the water, it was supposed that impurities in the column, such as fine soil's grain, can change the permittivity of the water. It is certainly a point to consider, but it makes the procedure more complicated. During the experiments, it was difficult to maintain constant temperature in the water when used as a reference material and poured in the cell, in most cases. However, in the experiments reported in Table 6.2.1, the temperature of water changed slightly by 0.1 to 0.2 °C (2.7 to 22.6°C and 21.8 to 22.0°C). Moreover, the same difficulty appeared during the experiment in the cell BC. It is still acceptable since the maximal temperature change is 0.2°C. A better option will be a K_{aB} measurement for each reference temperature, which, in this case, is a calibration with water. It consists of recording a waveform for each water temperature in order to find the permittivity.

Figure 6.2.2 below shows the permittivity obtained with the Schwartz method for each water temperature. The relation obtained from the linear trendline was used to find the water permittivity inside the $K_{aR'}$ cell in order to find K_{aB} in Table 6.2.2. It is important to note that calibration using an interpretation method can't be used with other interpretation methods. There is also a difference in the length of L_{rB} where the tangent method has a length of 0.010 m while the Schwartz method has a length of 0.011 m when tested with air. The difference between those lengths is due to a test that was redone where the tangent method wasn't used because the calibration was sufficient. However, that difference is acceptable since the measurement precision is 0.002 m. More testing with compressible materials can be done to determine its real effect on permittivity K_{aB} as a difference of 0.001 m on a small column's wall gives a difference in K_{aB} of 0.1 in air or 4.7 in water by using results in Table 6.2.2. However, in this case, L_{rB} must be the same for every usage. Furthermore, the permittivity of the Plexiglas is closer to the rubber, which is 3.4 and 3.2, respectively, and the length of L_{rB} affects K_{aB} by changing the air volume in the influence zone, which should lower the permittivity of K_{aB}. As for the obtained result in column BC, it showed that both TDRs used for the experiment have the same value of K_{aB} for both reference materials. It was expected to have different values since there is small variation between the TDR's waveforms. Even between column BC and column SC, the difference is relatively small for both reference materials.
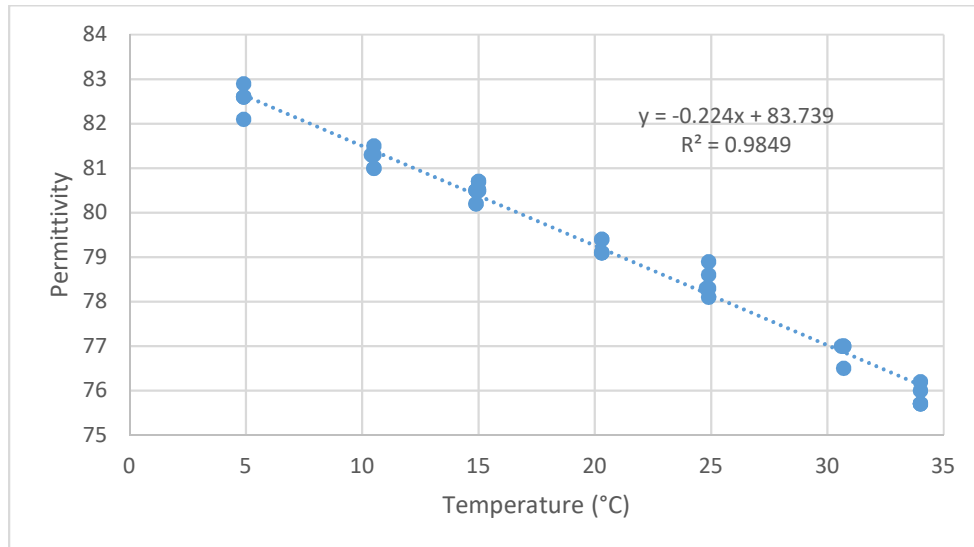
Figure 6.2.2: Schwartz K_a of water at different temperature

Table 6.2.2: Obtained K_{aB} using Schwartz method on column SC and column BC

	TDR#	Reference material				Ref. material + Cell						RI	ART
		*$K_{aR'}$	**T	L_{rR}	Δt_R	K_{aT}	$\Delta t_{B+R'}$	L_{rB}	$L_{rR'}$	$\Delta t_{R'}$	Δt_B	K_{aB}	K_{aB}
			°C	m	ps		ps	m	m	ps	ps		
Column SC													
Air	152	1		0.049	327	1.2	358	**0.011**	0.038	255	103	**2.1**	**1.9**
Water	152	78.7	22.3	0.049	2898	59.7	2524	**0.010**	0.039	2324	200	**9.5**	**-17.3**
Column BC													
AIR	144	1	-	0.049	327	1.1	343	**0.011**	0.038	253	89	**1.5**	**1.4**
	152	1	-	0.049	327	1.1	343	**0.011**	0.038	253	89	**1.5**	**1.4**
Water	144	78.8	22.0	0.049	2900	57.8	2484	**0.011**	0.038	2249	235	**10.2**	**-14.8**
	152	78.8	22.0	0.049	2900	57.8	2484	**0.011**	0.038	2249	235	**10.2**	**-14.8**

*$K_aR'(T)$= -0.224 (T) + 83.739

**Temperature of the reference material inside the cell

Compared to the two other methods, finding K_{aB} with the Heimovaara method is easier because the experiment can be done directly with the TDR inserted in the column during the whole experiment. This requires only the temperature of the reference material inside the cell and the length L_{rB}. As for the $K_{aR'}$ of water, the permittivity of Hasted (1973) was used as a reference during this experiment. The values of the obtained results in Table 6.2.3 are lower than most of the other methods' results, probably because of the fixed t'_1 and t_1 compared to the tangent method where t_1 translates. But also how the Schwartz method procedure works to evaluates t_2. For all the obtained results in Table 6.2.1 to Table 6.2.3, the calculation of K_{aB} using the refractive index (RI) showed a realistic value because the arithmetic mean calculation (ART) gives negative values when water is used as the reference material. This is due to the K_{aT} that is smaller than $K_{aR'}$ (L_{rR}/L_{RT}) which is the fraction of water using the arithmetic mean. Mathematically, it results in negative values and can't be used to obtain K_{aB} but doesn't mean that the Arithmetic method should be neglected for all columns. It is suggested to always verify both methods. When air is used to do the correction, the arithmetic mean results show a realistic value similar to the refractive index because of the expected low permittivity. However, there is no explanation for why the values of K_{aB} of column BC obtained in the air are lower than the permittivity of air in the Heimovaara method and tangent method. Because the permittivity of each of the Plexiglas (cell) and the rubber (O-ring) materials is around 3, which gives a K_{aB} higher than K_a of air like the other methods where the values range from 1.2 to 2.1. A K_{aB} value of 0.9 can be acceptable because it is closer to the permittivity of air, but for the 0.5, at first look, it can be hard to find the reason. The hypothesis of an error in

measurement is false because the TDR was inserted for both measurements with air first and water after. The only plausible source of error in this case is the interpretation method not because of t_1 but because of t_2. To confirm this hypothesis, both the Heimovaara and tangents methods have this problem, but not Schwartz. The possible reason is both methods use the same procedure to find t_2, and in the case of air, it is possible that the smoothing is too high, which makes the value of t_2 too low because the tangents are less steep. It can be also the difference of Heimovaara fixed t_1 obtained from air and from water. This case proves that Schwartz's interpretation method is more realistic and constant by putting conditions on the choice of t_2.

Table 6.2.3: Obtained K_{aB} using Heimovaara method on column SC and column BC (Waveforms interpretation in Appendix G)

	TDR#	Reference material				Reference material + Cell							RI	ART
		$K_{aR'}$	*T	**L_{rR}	L_{rB}	$L_{rR'}$	$t_{1'}$	t_2	$\Delta t_{R'}$	t_1	$\Delta t_{B+R'}$	Δt_B	K_{aB}	K_{aB}
			°C	m	m	m	ps	ps	ps	ps	ps	ps		
Column SC														
Air	152	1	22.6	0.049	**0.010**	0.04	**687**	1010	262	748	323	61	**0.9**	**0.9**
Water	152	79.2	22.6	0.049	**0.010**	0.04	**687**	3190	2331	859	2503	172	**7.1**	**-24.1**
Column BC														
Air	144	1		0.049	**0.011**	0.04	**779**	1086	253	833	307	54	**0.5**	**0.5**
	152	1		0.049	**0.011**	0.04	**687**	1011	253	758	324	71	**0.9**	**0.9**
Water	144	79.4	22	0.049	**0.011**	0.04	**779**	3226	2257	969	2447	190	**6.7**	**-24.3**
	152	79.4	22	0.049	**0.011**	0.04	**687**	3157	2257	900	2470	213	**8.4**	**-19.5**

*Temperature of the reference material inside the cell

**LrR=LrB+R'

RI = Refractive Index mean

ART = Arithmetic meaning

For all waveform interpretation methods, the obtained K_{aB} values of the TDR#152 showed that values of K_{aB} of column SC can be slightly higher with air and lower with water when compared to the values of column BC. Multiple reasons can justify a different value of K_{aB} between column SC and column BC. The first probable reason is that the diameter of the columns changes the volume of Plexiglas around the middle probe of the TDR, as shown in Figure 6.2.3. The logic is a larger diameter has more Plexiglas volume within the influence zone than a smaller diameter. However, when both columns were compared, it appeared that the Plexiglas volume was not

affected by the diameter of the column. On the other hand, the diameter of the column can have an effect on the rubber and air volume. In the case of the highest diameter column, the surface is flatter than the column SC, which makes the rubber of the TDR's outer probes more compressed in order to compress the rubber of the middle probe.

The same can be said with the column SC where the small diameter makes the rubber on the outer rods more compressed on one side. Thus, more rubber volume is created inside the influence zone of the border length. However, the K_{aB} is affected by a larger volume of rubber and less volume of air.
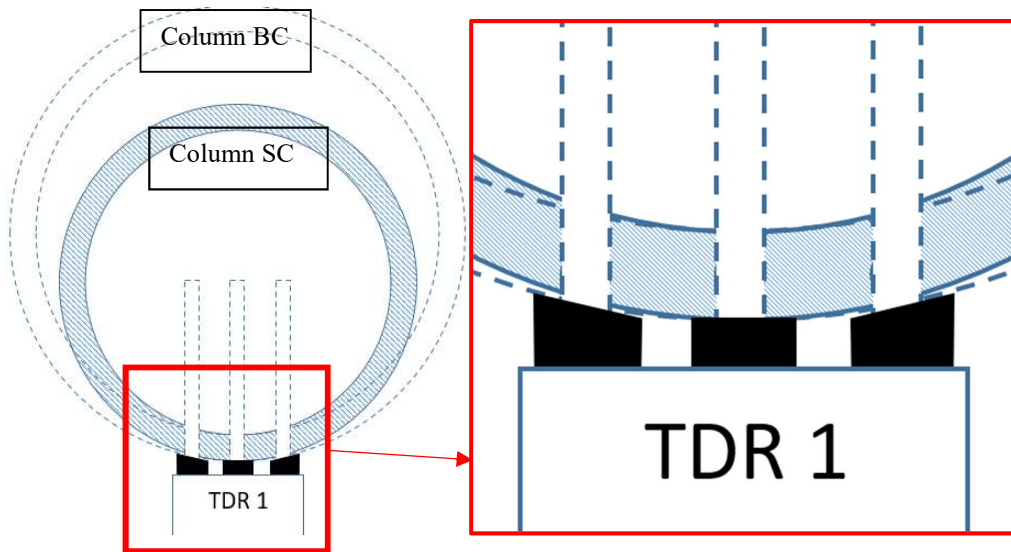
Figure 6.2.3: Differences of column's wall on column SC and BC

However, the first reason doesn't justify the fact that K_{aB} found with water is higher for column BC. Because a higher volume of rubber should give a higher value of K_{aB} found with both air and water since a higher volume of air inside the influence zone will give a lower K_{aB}. Thus, the second plausible reason is that the volume of the void between the TDR probe and the cell Plexiglas can differ between TDR holes. A bigger void will be impacted by the reference material used during the experiment because the material will fill that void. Moreover, the material nearest to the probe surface has the strongest impact on permittivity. In the case of void-filled water, it will give a higher K_{aB} than a TDR hole without void. But technically, it is nearly impossible to make a hole that doesn't leave a void around the probe, and the procedure to determine K_{aB} considers the fact

that the found K_{aB} is for the TDR holes where the correction was done, which can't be generalized for other holes.

6.3 Multiple TDR setups

The multilayer setups experiment consists of putting the TDR in the apparatus with different setups in order to determine if there is interference between TDRs to test the partial insertion method, and also to determine the effect of the TDR length on the obtained K_{aS}. The multiple setups are shown in Chapter 5.2 and all the results are in Appendix C Table C.1. To present the results of the obtained permittivity, a K_{ijk} annotation system was used, where

- i= setup # (1 to 10)
- j= #TDR (1, 2 or 3)
- k= Vertically inserted (V) or Laterally inserted (L)

6.3.1 Interferences between TDRs

During the experiment, the interference can play an important role in the accuracy of the result, and for this reason, it was tested. The test is not about finding which area of the TDR can be affected by the interference. It was tested specifically for the experiment, which is suggested to do before any experiment to make sure that there is no interference between the TDR probes. The result is presented in two tables: Table 6.3.1 shows the results obtained from the perpendicular interferences, and Table 6.3.2 shows the parallel interferences. The perpendicular interferences are the interferences between two TDRs placed perpendicularly. As for the parallel interferences, they are the interferences between two TDRs placed in parallel. For each table, there are three sub-tables of soil condition results: dry, moist, and wet soil. The obtained K_{aS} with all methods of interpretation are shown to be compared with the tangent method and discussed later in section 6.3.5. Then, the difference Δ between K_{aS} values obtained from two parallel TDRs or two perpendicular TDRs is calculated. The gray lines in the next sections are values of the laterally inserted TDRs. Most of the obtained Δ between K_{aS} are between 0.0 and 0.1 for dry and moist soil, which is proof that there are no interferences. The same differences were obtained for the parallel interferences. This makes sense because of the long distance between the probes presented earlier. As for the wet soil, an absolute Δ of 0.4 was obtained; the error is still minimal since it represents about 2% of the K_{aS} value of 20.1. This can be due to the change in soil condition because of the water runoff, which explains why the *K11L* is higher than the *K21L*.

Table 6.3.1: Perpendicular interferences

DRY	K_{aS}				
K ijk	Tangent	Schwartz	Relative diff. to Tangent %	Heimo	Relative diff. to Tangent %
K21L	2.6	2.8	**4%**	2.6	**0%**
K11L	2.6	2.8	**8%**	2.6	**0%**
Abs Δ:	**0.0**	**0.0**		**0.0**	
K22V	2.5	2.8	**12%**	2.2	**-12%**
K32V	2.5	2.8	**12%**	2.2	**-8%**
Abs Δ:	**0.0**	**0.0**		**0.0**	
K83V	3.3	3.3	**0%**	3.4	**0%**
K73V	3.3	3.2	**-3%**	3.4	**0%**
Abs Δ:	**0.0**	**0.1**		**0.0**	
K81L	2.7	2.9	**7%**	2.6	**-4%**
K91L	2.7	2.9	**7%**	2.7	**-4%**
Abs Δ:	**0.0**	**0.0**		**-0.1**	
MOIST	K_{aS}				
K ijk	Tangent	Schwartz	Relative diff. to Tangent %	Heimo	Relative diff. to Tangent %
K21L	4.6	4.7	**0%**	4.7	**0%**
K11L	4.5	4.5	**0%**	4.7	**4%**
Abs Δ:	**0.1**	**0.2**		**0.0**	
K22V	4.5	4.6	**2%**	4.2	**-7%**
K32V	4.5	4.7	**4%**	4.2	**-7%**
Abs Δ:	**0.0**	**0.1**		**0.0**	
K83V	5.7	4.3	**-25%**	5.6	**-2%**
K73V	5.7	4.3	**-25%**	5.6	**-2%**
Abs Δ:	**0.0**	**0.0**		**0.0**	
K81L	4.3	4.4	**2%**	4.4	**2%**
K91L	4.4	4.4	**0%**	4.4	**0%**
Abs Δ:	**0.1**	**0.0**		**0.0**	
WET	K_{aS}				
K ijk	Tangent	Schwartz	Relative diff. to Tangent %	Heimo	Relative diff. to Tangent %
K21L	19.9	17.1	**-14%**	17.8	**-11%**
K11L	20.3	17.2	**-15%**	18.0	**-11%**
Abs Δ:	**0.4**	**0.1**		**0.2**	
K22V	6.2	6.5	**5%**	5.9	**-5%**
K32V	6.1	6.4	**5%**	5.8	**-5%**
Abs Δ:	**0.1**	**0.1**		**0.1**	
K83V	12.6	9.5	**-25%**	12.5	**0%**
K73V	12.6	9.5	**-25%**	12.5	**-1%**
Abs Δ:	**0.0**	**0.0**		**0.0**	
K81L	19.2	16.1	**-16%**	17.0	**-11%**
K91L	19.3	16.1	**-16%**	17.0	**-12%**
Abs Δ:	**0.1**	**0.0**		**0.0**	

Table 6.3.2: Parallel interferences

DRY	K_{aS}				
K ijk	Tangent	Schwartz	Relative diff. to Tangent %	Heimo	Relative diff. to Tangent %
K41V	2.6	2.7	**4%**	2.3	**-15%**
K51V	2.4	2.7	**13%**	2.2	**-8%**
Abs Δ	**0.2**	**0.0**		**0.1**	
K42V	2.6	2.8	**8%**	2.3	**-12%**
K32V	2.5	2.8	**12%**	2.2	**-8%**
Abs Δ	**0.1**	**0.0**		**0.1**	
K63V	3.3	3.2	**-3%**	3.4	**0%**
K73V	3.3	3.2	**-3%**	3.4	**0%**
Abs Δ	**0.0**	**0.0**		**0.0**	
K61V	2.4	2.7	**13%**	2.2	**-8%**
K51V	2.4	2.7	**13%**	2.2	**-8%**
Abs Δ	**0.0**	**0.0**		**0.0**	
MOIST	K_{aS}				
K ijk	Tangent	Schwartz	Relative diff. to Tangent %	Heimo	Relative diff. to Tangent %
K41V	4.5	4.7	**4%**	4.3	**-2%**
K51V	4.5	4.7	**4%**	4.3	**-2%**
Abs Δ	**0.0**	**0.0**		**0.0**	
K42V	4.5	4.7	**4%**	4.2	**-7%**
K32V	4.5	4.7	**4%**	4.2	**-7%**
Abs Δ	**0.0**	**0.0**		**0.0**	
K63V	5.7	4.3	**-25%**	5.6	**-2%**
K73V	5.7	4.3	**-25%**	5.6	**-2%**
Abs Δ	**0.0**	**0.0**		**0.0**	
K61V	4.4	4.7	**7%**	4.2	**-5%**
K51V	4.5	4.7	**4%**	4.3	**-2%**
Abs Δ	**0.0**	**0.0**		**0.1**	
WET	K_{aS}				
K ijk	Tangent	Schwartz	Relative diff. to Tangent %	Heimo	Relative diff. to Tangent %
K41V	6.0	6.3	**5%**	5.8	**-2%**
K51V	5.9	6.2	**5%**	5.7	**-3%**
Abs Δ	**0.1**	**0.1**		**0.1**	
K42V	6.3	6.5	**3%**	5.9	**-5%**
K32V	6.1	6.4	**5%**	5.8	**-5%**
Abs Δ	**0.2**	**0.1**		**0.1**	
K63V	12.6	9.5	**-25%**	12.5	**-1%**
K73V	12.6	9.5	**-25%**	12.5	**-1%**
Abs Δ	**0.0**	**0.0**		**0.0**	
K61V	5.6	5.9	**5%**	5.5	**-2%**
K51V	5.9	6.2	**5%**	5.7	**-3%**
Abs Δ	**0.3**	**0.3**		**0.2**	

6.3.2 *Effect of reinsertion*

The effect of reinsertion results in Table 6.3.3 shows the results obtained in 3 soil conditions using lateral insertion and vertical insertion. For each insertion position, permittivity is obtained during the first and second insertions. A difference is calculated by subtracting the first insertion permittivity from the second one. Then, a method comparison was done and discussed later. Starting with the lateral reinsertion done on dry soil, where the difference between the first insertion is 0.1 for the Schwartz method and 0.0 for the Tangent interpretation method. This difference increases with the water moisture until it reaches -1.1 in wet soil. This is due to two reasons: the stability of movement during insertion and the water content of the soil.

Vertical reinsertion is more affected by the TDR's small wobbling during insertion. The wobbling creates voids around TDR probes, which lower the permittivity. On the other hand, the lateral insertion limits that small movement because of the holes in the Plexiglas cell that support it. However, these results depend on the column construction quality, where more precise drilling can lower the wobbling because of the flush fit. A bad drilling method can increase the wobbling effect, which can increase the risk of errors. Also, the fact that the lateral insertion results in a higher permittivity than the vertical insertion in wet soil proves the presence of free water. This can be the reason why the permittivity of the first insertion, *K32V*, is around 6, and the second insertion, *K102V*, is around 5. Thus, it can be concluded that reinsertion is the cause of that high difference.

As for the effect of water content on the reinsertion, the error caused by the reinsertion in dry soil is the lowest and increases with water content. It is caused by grains rearrangement that is more present in dry soil, which is also the reason behind a higher permittivity of the second insertion than the first insertion. As the water content increases, the cohesion between grains also increases, which leads to a more defined void. In this experiment, the wet soil is not fully saturated. But if this was the case, the permittivity would have increased because the water that has a high permeability would fill the void.

Table 6.3.3: Comparison between first and second insertion of the TDR

DRY	K$_{aS}$				
K ijk	Tangent	Schwartz	Relative diff. to Tangent %	Heimo	Relative diff. to Tangent %
K91L	2.6	2.9	**12%**	2.7	**0%**
K11L	2.6	2.8	**8%**	2.6	**0%**
Δ	**0.0**	**0.1**		**0.1**	
K102V	2.4	2.7	**13%**	2.2	**-13%**
K32V	2.5	2.8	**12%**	2.2	**-8%**
Δ	**-0.1**	**-0.1**		**0.0**	
MOIST	K$_{aS}$				
K ijk	Tangent	Schwartz	Relative diff. to Tangent %	Heimo	Relative diff. to Tangent %
K91L	4.4	4.4	**0%**	4.4	**0%**
K11L	4.5	4.5	**0%**	4.7	**4%**
Δ	**-0.1**	**-0.1**		**-0.3**	
K102V	4.2	4.4	**5%**	4.0	**-5%**
K32V	4.5	4.7	**4%**	4.2	**-7%**
Δ	**-0.3**	**-0.3**		**-0.2**	
WET	K$_{aS}$				
K ijk	Tangent	Schwartz	Relative diff. to Tangent %	Heimo	Relative diff. to Tangent %
K91L	19.3	16.1	**-16%**	17.0	**-12%**
K11L	20.3	17.2	**-15%**	18.0	**-11%**
Δ	**-1.0**	**-1.1**		**-1.0**	
K102V	5.0	5.3	**6%**	4.7	**-6%**
K32V	6.1	6.4	**5%**	5.8	**-5%**
Δ	**-1.1**	**-1.1**		**-1.1**	

6.3.3   *Determining the soil permittivity with partial insertion*

To verify the partial insertion method to obtain the K_{aS}, the lateral TDR's K_{aS} was compared with the vertical TDR's K_{aS}. As in the preceding section, the difference Δ of both K_{aS} was calculated, and the K_{aS} was obtained with all the waveform interpretation methods. The obtained results in Table 6.3.4 showed that the partial insertion method works for the dry soil and moist soil with the highest Δ of +0.5. As for the wet soil, the Δ is higher with a difference of +14.4. The difference is due to the experimental procedure. The reading of the vertical TDR is done on the 3rd layer at the top instead of the same layer as the lateral insertion (1st layer at the bottom). Thus, in wet soil, the water from the top layer runs off to the bottom layer, giving a higher K_{aS} at the bottom. To have a

close comparison, the TDR should be in the same area. However, the results show that the partial insertion method works.

Table 6.3.4: Lateral insertion obtained K_{aS} comparison with vertical insertion results

DRY	K_{aS}				
K ijk	Tangent	Schwartz	Relative diff. to Tangent %	Heimo	Relative diff. to Tangent %
K11L	2.6	2.8	4%	2.6	0%
K32V	2.5	2.8	12%	2.2	-8%
Δ	0.1	0.0		0.4	
K11L	2.6	2.8	8%	2.6	0%
K51V	2.4	2.7	13%	2.2	-8%
Δ	0.2	0.1		0.4	
MOIST	K_{aS}				
K ijk	Tangent	Schwartz	Relative diff. to Tangent %	Heimo	Relative diff. to Tangent %
K11L	4.5	4.5	0%	4.7	4%
K32V	4.5	4.7	4%	4.2	-7%
Δ	0.0	-0.2		0.5	
K11L	4.5	4.5	0%	4.7	4%
K51V	4.5	4.7	4%	4.3	-2%
Δ	0.0	-0.2		0.4	
WET	K_{aS}				
K ijk	Tangent	Schwartz	Relative diff. to Tangent %	Heimo	Relative diff. to Tangent %
K11L	20.3	17.2	-15%	18.0	-11%
K32V	6.1	6.4	5%	5.8	-5%
Δ	14.2	10.8		12.3	
K11L	20.3	17.2	-15%	18.0	-11%
K51V	5.9	6.2	5%	5.7	-3%
Δ	14.4	11.0		12.3	

6.3.4   Effect of TDR length on the permittivity of the soil

The effect of the TDR's probe length on K_{aS} was studied by comparing TDR#1 and TDR#2, which have a probe length of 49 mm, with TDR#3, which has a probe length of 100 mm. All TDR insertions are vertical but not simultaneously inserted. The results obtained in Table 6.3.5 are presented in the same layout as the precedent sections. When the *Δ* are compared, the dry soil has the lowest difference of 0.1 using the tangent method, while the highest difference of 6.8 is in the wet soil using the Heimovaara method. The water runoff makes the water distribution in the layer

uneven and higher water content at the lower level. Thus, the probe with a longer probe doesn't give more accurate results than the TDR with a smaller probe length, but it only has a higher volume. In the case of the wet soil, the TDR with the longest probe passed through a section of the soil with a higher water content. This is why the differences in the dry and moist soil are lower compared to the wet soil. The small differences observed in the dry and moist soil are probably due to the different soil conditions. For dry soil, the difference in soil condition can be explained by the movement of fine grains through the coarser grains. A small vibration and soil filling can cause segregation, which is inevitable. As for the moist soil, the risk of fine movement is lower. So, the difference in soil's condition in moist soil is due to soil compaction because the second layer absorbs the energy from the upper layer. This makes it denser and affects the K_{aS} values of the TDR#3.

Table 6.3.5: Comparison of K_{aS} between different TDR probe lengths

DRY	K_{aS}				
K ijk	Tangent	Schwartz	Relative diff. to Tangent %	Heimo	Relative diff. to Tangent %
K73V	2.6	3.2	**23%**	3.4	**31%**
K32V	2.5	2.8	**12%**	2.2	**-8%**
Δ	**0.1**	**0.4**		**1.2**	
K73V	3.3	3.2	**-3%**	3.4	**0%**
K51V	2.4	2.7	**13%**	2.2	**-8%**
Δ	**0.9**	**0.5**		**1.2**	
MOIST	K_{aS}				
K ijk	Tangent	Schwartz	Relative diff. to Tangent %	Heimo	Relative diff. to Tangent %
K73V	5.7	4.3	**-25%**	5.6	**-2%**
K32V	4.5	4.7	**4%**	4.2	**-7%**
Δ	**1.2**	**-0.4**		**1.4**	
K73V	5.7	4.3	**-25%**	5.6	**-2%**
K51V	4.5	4.7	**4%**	4.3	**-2%**
Δ	**1.2**	**-0.4**		**1.3**	
WET	K_{aS}				
K ijk	Tangent	Schwartz	Relative diff. to Tangent %	Heimo	Relative diff. to Tangent %
K73V	12.6	9.5	**-25%**	12.5	**-1%**
K32V	6.1	6.4	**5%**	5.8	**-5%**
Δ	**6.5**	**3.1**		**6.7**	
K73V	12.6	9.5	**-25%**	12.5	**-1%**
K51V	5.9	6.2	**5%**	5.7	**-3%**
Δ	**6.7**	**3.3**		**6.8**	

6.3.5 Comparison between methods of interpretation

From all the obtained data of the multiple setups experiment, the Schwartz and Heimovaara interpretation method were compared with the tangent method. To make the comparison, a graph was plotted, as shown in Figure 6.3.1. In the graph, the Schwartz and Heimovaara method K_{aS} values is plotted for each Tangent method K_{aS}. Then, a trend line was added for each interpretation method to be compared with the 45° line, which is the 0% difference line.

First, it was noticed that the permittivity deviates from the tangent method at higher values. This is probably due to the difference between methods that are less noticeable at lower permittivity values. The difference between the tangent method and the other methods is probably caused by the displacement of t_1 or t_2. Thus, for the small values of the permittivity, the difference is not that noticeable because the fixed t_1 from the Heimovaara method and the Schwartz method are near the tangent method's t_1. As the permittivity increases, the tangent method's t_1 moves from the other fixed t_1. As for the t_2, it moves the same way in both methods. The t_1 and the t_2 of the Schwartz method can't be obtained from the apparatus, and for this reason, those values can't be compared with the other interpretation methods. Also, in order to develop a trend in the comparison, more tests need to be done at different permittivity levels with the soil. Because using water or other materials doesn't represent the objective of the research, and the obtained trend may be different from the soil.
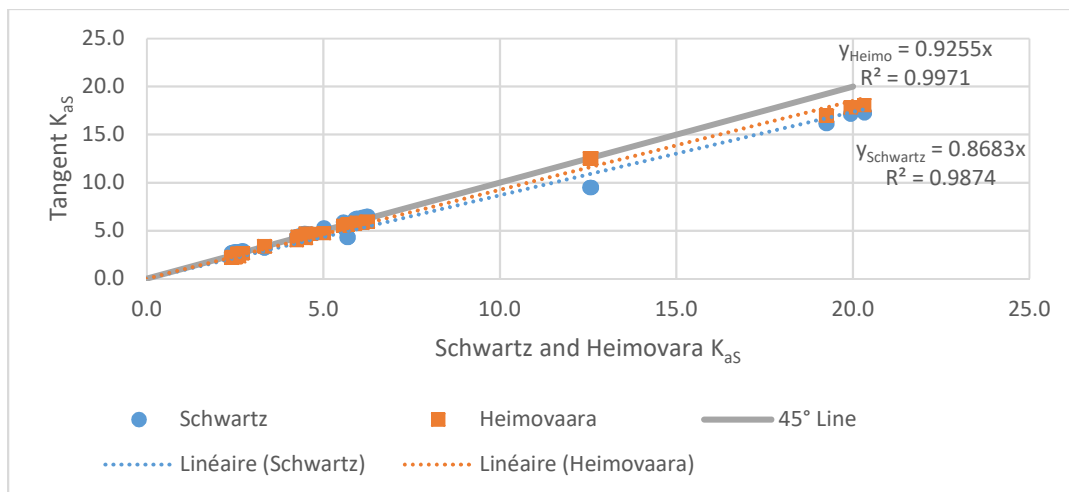
Figure 6.3.1: Tangent method's K_{aS} comparison with Schwartz method and Heimovaara using Setups experiment data

Figure 6.3.2 is another way to visualize how the interpretation method results diverge with the change of the permittivity. The obtained permittivity of each interpretation method from the multiple setups experiment were put together for each soil condition. The K_{aS} points of each TDR position are linked to form a graph that provides better visualization of the values pattern. All graphs have the same y-axis scale, meaning that the graphs with low permittivity variation weren't extended to see those small variations. The graph was separated into four sections: A, B, C and D. Section A contains the K_{aS} of the position *K11L* and *K21L*, section B range is [*K22V* ; *K51V*], section C range is [*K63V* ; *K83V*], and section D range is [*K81L* ; *K102V*]. Those range values can't be used to do an interpolation between points, and the comparison is done vertically.
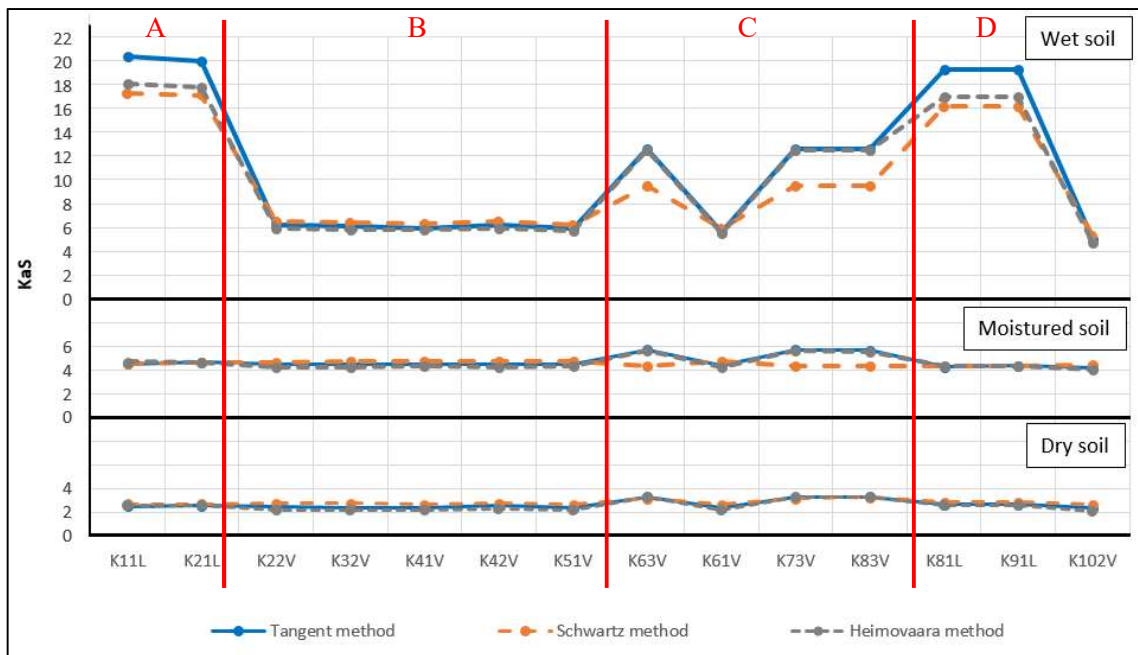
Figure 6.3.2: Obtained K_{aS} graphs for each soil water content

However, the first thing that can be noticed in Figure 6.3.1 is the similarities of the permittivities lower than 6.5, where all the interpretation methods have differences within the +/- 0.5 range. This includes all values of the dry soil, sections B and D of the moist soil graph, and section B of the wet soil. However, for the permittivity above 6.5, the difference between the K_{aS} values increases. In sections A and D of the wet soil graph, the tangent method has the highest permittivity, while the Schwartz method has the lowest permittivity. Furthermore, some differences were similar, like the average difference of 3.1 between the Schwartz method and the Tangent method, which is the

same for sections A, C and D. While the difference between the Heimovaara method and the Tangent method varies between sections A and D and C. In section C, the Heimovaara method's K_{aS} is the same as the tangent method's K_{aS}. On the opposite, in sections A and D, the average difference of the Heimovaara method is 2.2. Most of the points in section C are from TDR#3, while sections A and D are composed mostly of TDR#1 inserted laterally. Those results suggest that the TDR affects the interpretation methods results, but that is not the case. In section C of the moist soil and wet soil, the permittivity of the Heimovaara and Tangent methods are close, which is the same as section B, which has a different TDR. As for the Schwartz method, the difference is probably due to the condition of choosing t_2 by the AWIGF. The differences in sections A and D are probably caused by the calibration of $K_{aB,}$ as shown in Figure 6.3.3. In the figure, the Tangent method and Heimovaara's t_1 and t_2 of each point were plotted in the same way as in Figure 6.3.2 to determine the cause behind the differences below. Hence, it shows vertical variation of t_1 in section A and section D, while the vertical permittivities of the other points show no variations.
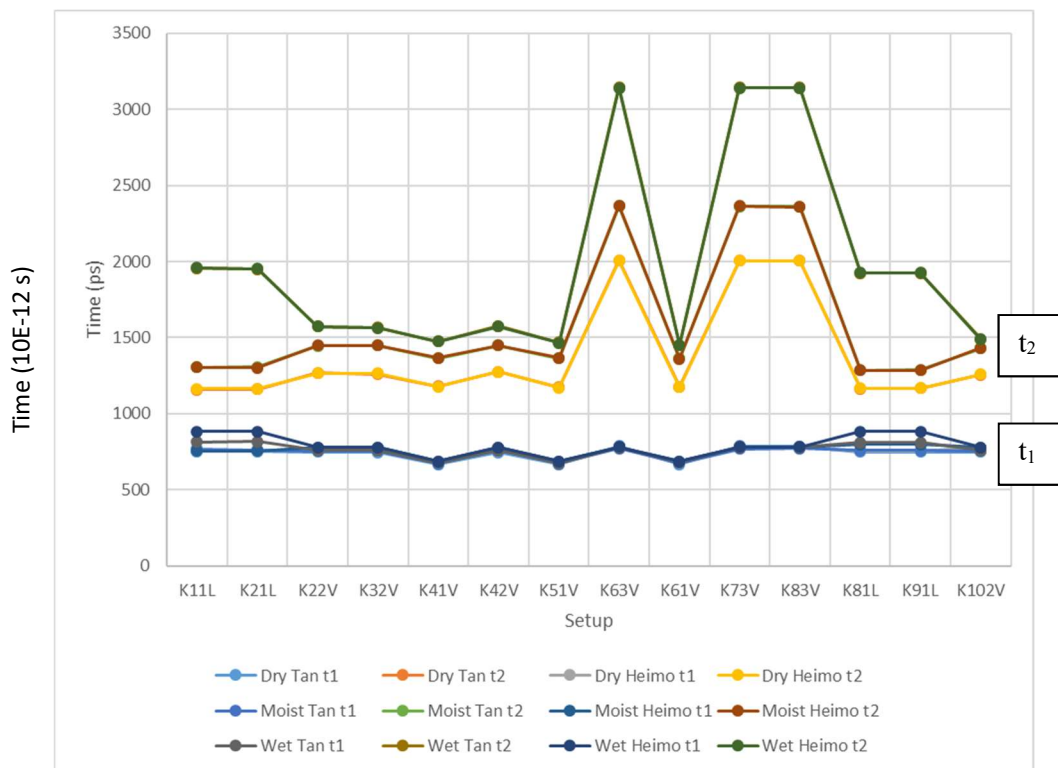
Figure 6.3.3: t_1 and t_2 of the obtained K_{aS} using the Tangent method and the Heimovaara method on soil at different water content

6.4 Gradual lateral insertion

The obtained results of the gradual insertion shown in Table 6.4.1 are presented for each interpretation method. For each insertion increment, the measured distance of the length probe in air L_{rA}, in the cell's border L_{rB} and in the soil L_{rS} are shown. The length of the probe inside the soil is calculated by subtracting the L_{rA} and L_{rB} from the full length of the TDR probe. The error of the measurement is ±0.5 mm for L_{rA} and L_{rB} and ±1.0 mm for L_{rS}. The K_{aS} is obtained by using the refractive index method only by subtracting the air K_a and the cell's border permittivity K_{aB} from the total permittivity K_{aT}. This is due to the obtained negative K_{aB} as discussed earlier. The obtained K_{aS} of each increment is compared with the K_{aS} of the fully inserted lateral probe, called measured K_{aS}. Initially, another TDR was inserted vertically into the top layer, but a difference in soil condition in each layer doesn't give a fair comparison because of the soil condition, and the partial insertion method has proved to be accurate.

Table 6.4.1: Obtained K_{aS} of soil during gradual insertion experiment (Full data in Appendix D Table D.1 to Table D.5)

	L_{rT} m	L_{rA} m	L_{rB} m	L_{rS} m	Tangent K_{aS}	Tangent Meas K_{aS}	Tangent K_{aS} Diff.	Schwartz K_{aS}	Schwartz Meas. K_{aS}	Schwartz K_{aS} Diff.	Heimovaara K_{aS}	Heimovaara Meas. K_{aS}	Heimovaara K_{aS} Diff.
Test 4	0.049	0.033	0.0107	0.0053	11.1	9.9	**1.2**	2.5	8.4	**-5.9**	2.2	8.0	**-5.8**
Test 4	0.049	0.0275	0.0107	0.0108	8.7	9.9	**-1.2**	12.9	8.4	**4.5**	3.9	8.0	**-4.0**
Test 4	0.049	0.018	0.0107	0.0203	15.6	9.9	**5.6**	10.2	8.4	**1.9**	11.6	8.0	**3.7**
Test 4	0.049	0.008	0.0107	0.0303	12.3	9.9	**2.4**	9.6	8.4	**1.3**	9.7	8.0	**1.7**
Test 4	0.049	0	0.0107	0.0383	9.9	9.9	**0.0**	8.4	8.4	**0.0**	8.0	8.0	**0.0**
Test 5	0.049	0.038	0.0107	0.0003	39.0	10.1	**28.9**	305.0	8.6	**296.4**	625.1	8.2	**617.0**
Test 5	0.049	0.0235	0.0107	0.0148	11.0	10.1	**0.9**	10.3	8.6	**1.7**	6.9	8.2	**-1.3**
Test 5	0.049	0.018	0.0107	0.0203	14.9	10.1	**4.8**	9.6	8.6	**1.0**	11.0	8.2	**2.9**
Test 5	0.049	0.008	0.0107	0.0303	12.2	10.1	**2.0**	9.5	8.6	**0.9**	9.6	8.2	**1.4**
Test 5	0.049	0	0.0107	0.0383	10.1	10.1	**0.0**	8.6	8.6	**0.0**	8.2	8.2	**0.0**
Test 6	0.049	0.038	0.0107	0.0003	76.5	9.1	**67.5**	305.0	7.6	**297.4**	529.1	7.2	**521.9**
Test 6	0.049	0.028	0.0107	0.0103	8.0	9.1	**-1.1**	12.9	7.6	**5.3**	3.5	7.2	**-3.7**
Test 6	0.049	0.018	0.0107	0.0203	14.3	9.1	**5.2**	9.3	7.6	**1.7**	10.5	7.2	**3.4**
Test 6	0.049	0.008	0.0107	0.0303	10.2	9.1	**1.1**	8.2	7.6	**0.6**	7.9	7.2	**0.7**
Test 6	0.049	0	0.0107	0.0383	9.1	9.1	**0.0**	7.6	7.6	**0.0**	7.2	7.2	**0.0**

At first, high differences were noticed for the first increments in test #5 and test #6. This is because of the small insertion length into the soil of 0.0003 m. A very small insertion doesn't give an accurate result. When the K_{aS} differences in Table 6.4.1 are compared, a trend is noticed where the difference between both K_{aS} decreases with the insertion of the TDR. The decrease is not necessarily linear because a negative difference happened on the second increment.

With the superposition of the obtained waveforms and the K_{aS} of test #4, the t_2 and t_1 of each waveform were marked to obtain a trend as shown in Figure 6.4.1. The obtained results are the t_2 trend doesn't follow the t_1's trend in order to give the measured K_{aS}. Thus, with the measured K_{aS}, an adjusted t_1 was calculated using equation (6.5) to determine the corrected trend of t_1 to have a better representation.

$$Adjusted\ t1 = t_2 - \frac{2\ (Measured\ K_{aS})^{0.5}\ L_{rS}}{c} \qquad (6.5)$$

Graphically, it is hard to determine the position of the air section and the cell wall section because there is a very small deviation in the waveform. Even more, the adjusted t_1 path doesn't follow the path of that deviation, which represents the transition between layers within the waveform. This subject is discussed in the multilayer experiment chapter.
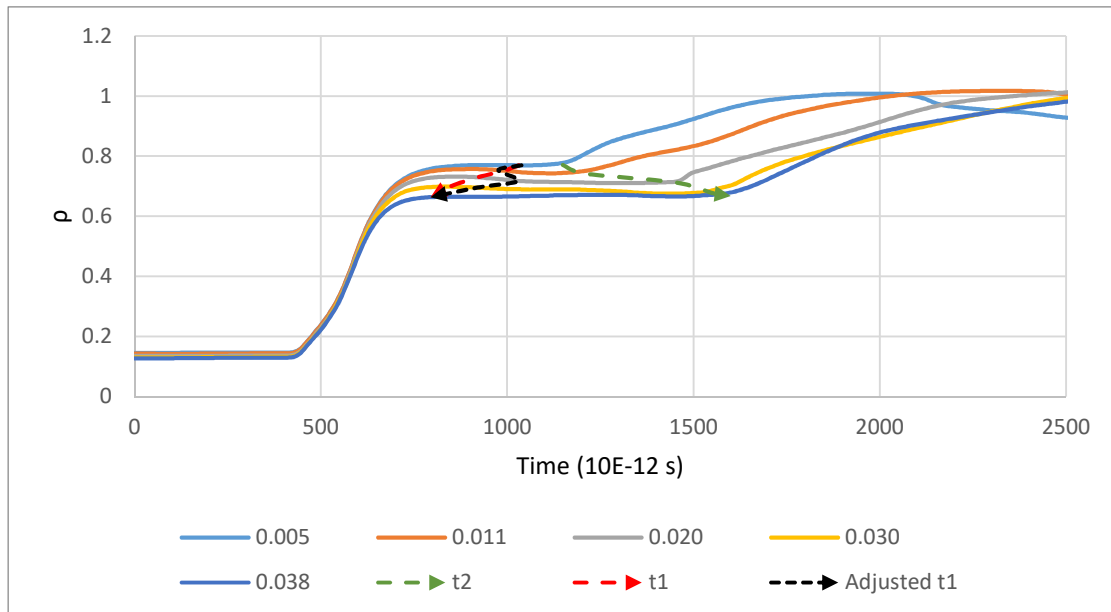
Figure 6.4.1: Obtained waveforms during gradual insertion of test#4

The patterns of both t_1 and t_2 are put together in a time vs probe length into soil L_{rS} in Figure 6.4.2 and Figure 6.4.3 in order to compare the trend. First, the adjusted t_1 and t_2 curves have the same trend with different slopes that are justified by the L_{rS} change during each insertion increment, which is normal. The interesting part of the comparison is the difference in trend between t_1 and the adjusted t_1. As shown in Figure 6.4.1, both t_1 differ where the obtained t_1 has a linear trend compared to the corrected t_1. It is hard to explain that difference, but it can be due to the change in the air section along the probe length. Since there is a change of the permittivity from air to the cell border and then to soil, the waveform doesn't reflect the true apparent length L_a of each layer. Thus, using the K_{aA}, K_{aB} and their L_r to calculate the t_1 of the soil makes the trend linear. Furthermore, because of this problem, it is suggested that the cell border be considered as one layer instead of separated layers. Also, this experiment showed the effect of the layers' dependency. The higher the difference between the permittivity, the higher the variation in the waveform.

To compare the slope of the adjusted t_1 and t_1, a linear trendline was added to the adjusted t_1. The obtained R^2 of 0.8115 is lower than the t_1's R^2 of 0.9994, but it is enough to show that the slopes are about the same for the tangent method in Figure 6.4.2. As for the Heimovaara method in Figure 6.4.3, the same trend is noticeable except for the starting point at L_{rS} of 0.000 m, where t_1 is above t_2, which is inaccurate. This is probably caused by the small insertion into soil that is so small it gives inaccurate results in the calculation of t_1.
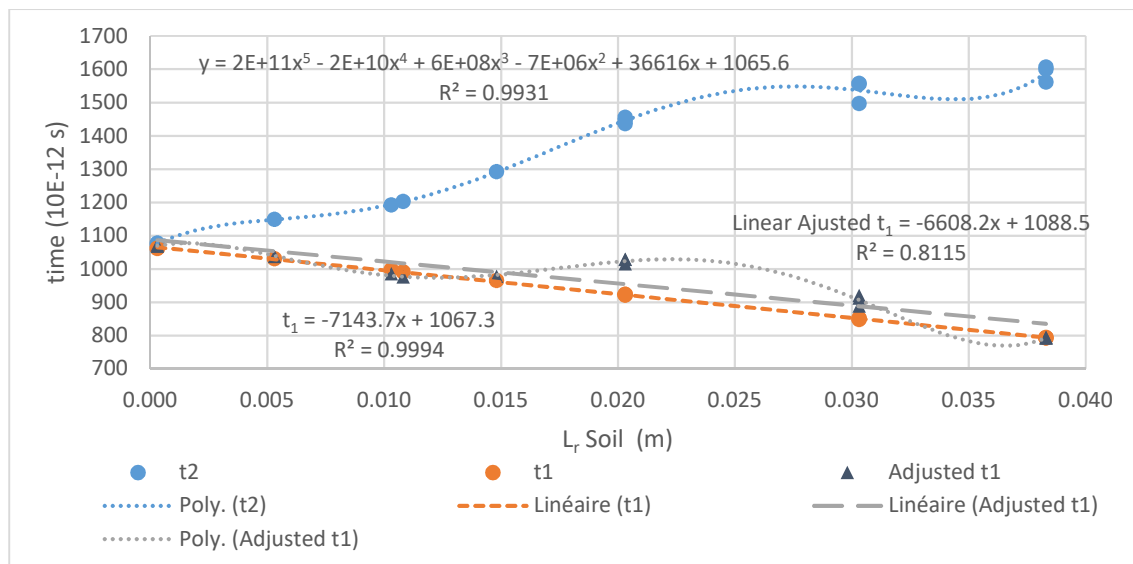
Figure 6.4.2: Variation of Tangent method's t_1, t_2 and adjusted t_1 with the L_{rS} change
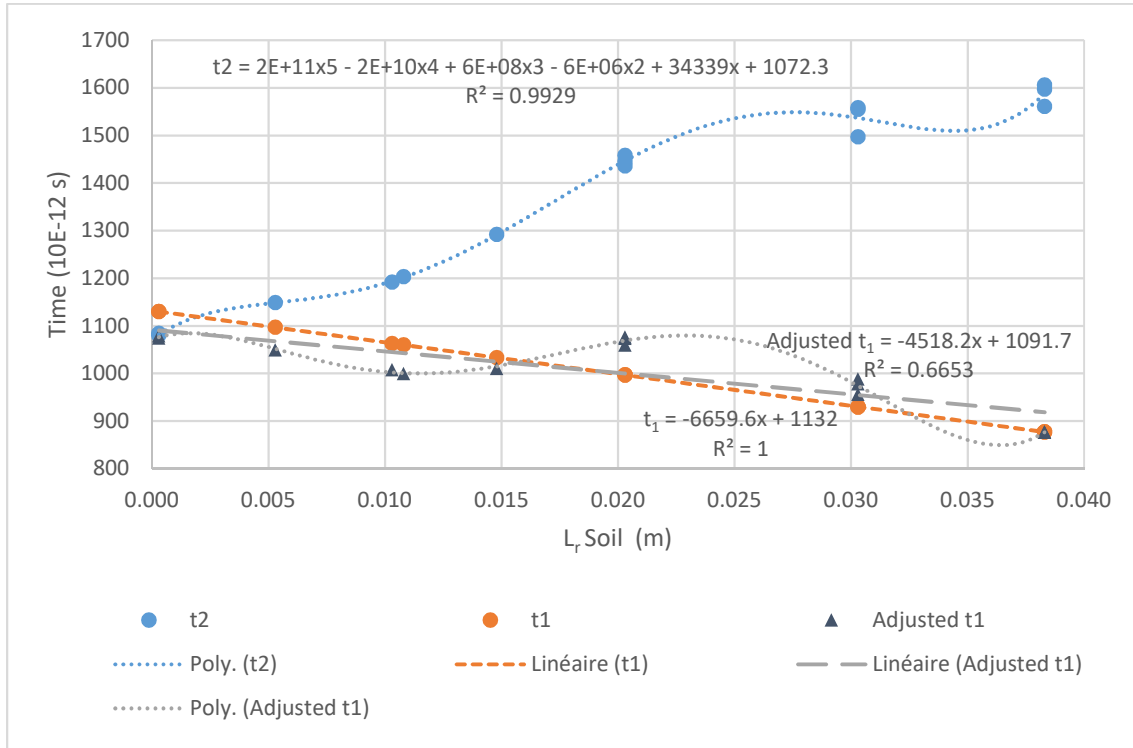
Figure 6.4.3: Variation of Heimovaara method's t_1, t_2 and adjusted t_1 with the L_{rS} change

6.5 Arithmetic Mean and Refractive Index methods comparison

The presented literature section 2.4 is done on different bandwidths and different TDRs. Therefore, it is hard to be confident about the limits between both averaging methods. For our TDR and the experiments that were done, a comparison with deviation analysis is made to calculate the possible error. To do so, the comparison is based on two superposed material layers with respective permittivity K_{a1} and K_{a2} and layers thickness L_{r1} and L_{r2}. In this case, equation (2.15) of the arithmetic mean becomes equation (6.6) and equation (2.16) of the refractive index becomes equation (6.7) as shown below.

$$K_{aT} = K_{a1}\left(\frac{L_{r1}}{L_{rT}}\right) + K_{a2}\left(\frac{L_{r2}}{L_{rT}}\right) \tag{6.6}$$

$$(K_{aT})^n = (K_{a1})^n\left(\frac{L_{r1}}{L_{rT}}\right) + (K_{a2})^n\left(\frac{L_{r2}}{L_{rT}}\right) \tag{6.7}$$

87

$$(K_{aT}) = \left[(K_{a1})^n \left(\frac{L_{r1}}{L_{rT}}\right) + (K_{a2})^n \left(\frac{L_{r2}}{L_{rT}}\right)\right]^{1/n} \qquad (6.8)$$

The equation (6.8) is obtained when K_{aT} from equation (6.7) is separated in order to be used in equation (6.9) by equalizing equation (6.6) to equation (6.8). This allows to analyse the convergence between both functions. Once the equation (6.9) is simplified by factoring $(K_{a1})^n$ on the left function and K_{1a} on the right function to have a function $f(K_{a2}/K_{a1})$, and the equation (6.10) is obtained. The left part of the equation (6.10) is $f_1(K_{a2}/K_{a1})$, and the right part is $f_2(K_{a2}/K_{a1})$.

$$\left[(K_{a1})^n \left(\frac{L_{r1}}{L_{rT}}\right) + (K_{a2})^n \left(\frac{L_{r2}}{L_{rT}}\right)\right]^{1/n} = K_{a1}\left(\frac{L_{r1}}{L_{rT}}\right) + K_{a2}\left(\frac{L_{r2}}{L_{rT}}\right) \qquad (6.9)$$

$$\left[\left(\frac{L_{r1}}{L_{rT}}\right) + \left(\frac{K_{a2}}{K_{a1}}\right)^n \left(\frac{L_{r2}}{L_{rT}}\right)\right]^{\frac{1}{n}} = \left(\frac{L_{r1}}{L_{rT}}\right) + \left(\frac{K_{a2}}{K_{a1}}\right)\left(\frac{L_{r2}}{L_{rT}}\right) \qquad (6.10)$$

At first stance, the functions can be equal when n is equal to 1 or when the relative permittivities ratio is equal to 1 meaning that both lengths L_{r1} and L_{r2} are half of the full length L_{rT}. However, when the experiment's data are put on the $f(K_{a2}/K_{a1})$ equation at $n=0.5$ and plotted in Figure 6.5.1, both data have relatively small differences under K_{a2}/K_{a1} of 5. Most ratios under 5 are from the cell's border and materials: air, dry soil, moist soil and wet soil. For the cell's border and wet soil ratio, the K_a of the cell's border is higher when the cell's border void is wet, which results in a lower ratio. Moreover, the two same soil layers, K_{a2}/K_{a1}, from the multilayer experiment are also <5. A higher obtained ratio of K_{a2}/K_{a1} of 24 has a relative difference to the arithmetic mean of 12.4%. This is between the water inside the cell and the cell's border. The lowest relative difference of 0.0 is between the cell's border and air using the Heimovaara interpretation method.
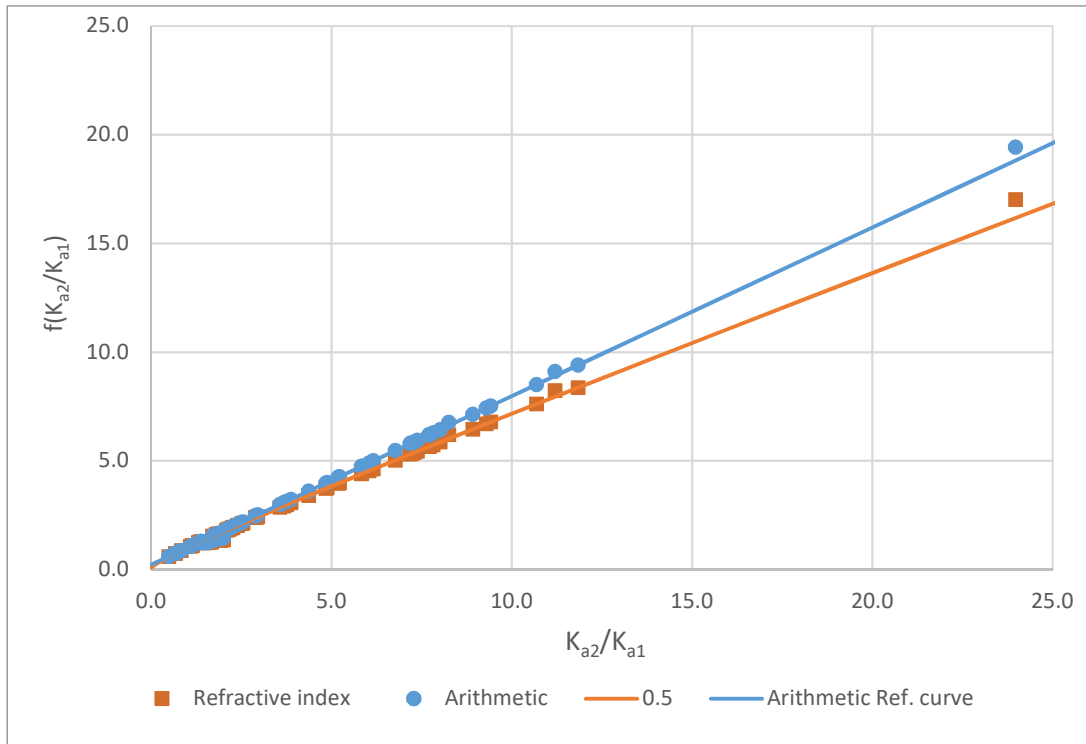
Figure 6.5.1: Obtained data from K_{aB} experiment, setups experiment and multilayer experiment using Arithmetic method and refractive index method

The Figure 6.5.1 shows $f_1(K_{a2}/K_{a1})$ with n=0.5 and $f_2(K_{a2}/K_{a1})$. Nevertheless, an error can be caused by the value of n if it differs from 0.5 since its value is frequency-dependent, as described in the literature. Thus, Figure 6.5.2 graph was traced with different curves of $f(K_{a2}/K_{a1})$ with n starting at -1 to 1 by steps of n=0.25. Mathematically, the function with $n{\approx}0$ is infinite, and it wasn't added to the graph. On the graph, the ratio K_{a2}/K_{a1} axis starts from the ratio of $K_{a\ air}/K_{a\ water}$ of 0.013 to $K_{a\ water}/K_{a\ air}$ of 80. The choice of their extremums is based on these materials because of their gap, and generally, most of the materials used for cells or in geotechnical will have their permittivity in-between. The first highlight is the deviation between positive and negative values of n, and the convergence point is at K_{a2}/K_{a1} of 1. Furthermore, the curves with a higher value of n, or lower negative value of n, get closer compared to lower values of n or higher at lower K_{a2}/K_{a1} ratio.
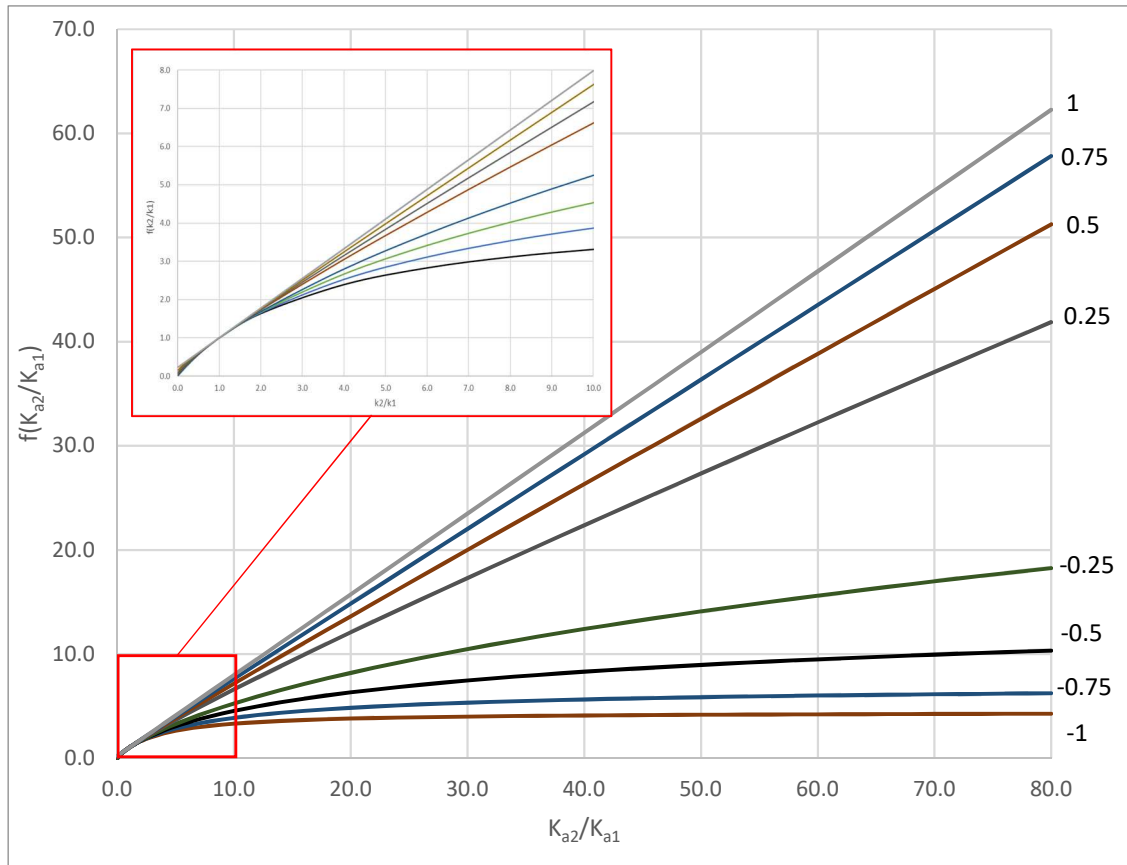
Figure 6.5.2: Function f(k₂/k₁) for different values of n

To have a better representation and comprehension of both Figure 6.5.1 and Figure 6.5.2, the relative difference of function $f_1(K_{a2}/K_{a1})$ to $f_2(K_{a2}/K_{a1})$ was calculated for a specific length fraction L_{ri}/L_{rT}. First, the difference is presented with experiment parameters and then with different generalized parameters. The graph in Figure 6.5.3 is for the experiments with TDRs laterally inserted where L_{r1}/L_{rT} and L_{r2}/L_{rT} fractions are 22.4% and 77.6%, respectively. In the graph, the point of convergence of both equations is at $K_{a2}/K_{a1} = 1$. Same difference when $n = 1$ because $f_1(K_{a2}/K_{a1})$ equal to $f_2(K_{a2}/K_{a1})$ when $n = 1$. On each side of $K_{a1}=K_{a2}$ line, $K_{a1}<K_{a2}$ above 1 and $K_{a1}<K_{a2}$ below 1. In Figure 6.5.3 the part above $K_{a1}=K_{a2}$ line is better represented then Figure 6.5.2 and the differences between n functions are different on each side of the line. When $K_{a1}>K_{a2}$, the negative n values curves have lower differences between them compared to positive n curves. Conversely, in the $K_{a1}<K_{a2}$ part of the graph, the negative n values curves got more dispersed while the positive n values curves got more regrouped. As for the difference with the arithmetic mean method, the curves got closer when $K_{a1}<K_{a2}$. When this graph is reproduced in Figure 6.5.5 with

90

the multilayer experiment length fraction of 50% each, the tendency of the curves is different. Instead of asymmetrical form, the 50% L_{ri}/L_{rT} ratio graph is symmetrical. Figure 6.5.3 and Figure 6.5.4 clearly show how the L_{ri}/L_{rT} ratio affects the curves. Thus, multiple graphs similar to the precedent figures were done at different length fractions. The lengths fraction starts with $L_{r1}/L_{rT}=$ 10% and $L_{r2}/L_{rT}=$ 90%, then the L_{r1}/L_{rT} ratio is increased by 10% for the next graph, and L_{r2}/L_{rT} is decreased by 10%. For each length fraction, the opposite ratio is also shown, meaning that if the first fraction is 10%/90%, the opposite graph of 90%/10% is also presented. This will determine if the fractions above 50%/50% are symmetrical to the opposite fractions. Starting with Figure 6.5.5 and Figure 6.5.6, with fractions of 10%/90% and 90%/10%, respectively, and finishing with Figure 6.5.11 and Figure 6.5.12, with fractions of 40%/60% and 60%/40%, respectively. The curves with negative n values have low differences with each other when the L_{r1}/L_{rT} fraction is small and $K_{a1}>K_{a2}$. With the increase of the L_{r1}/L_{rT} fraction, the difference between the curves increases until it reaches the differences shown in Figure 6.5.6. On the opposite of negative n values curves, the difference between positive n values curves decreases with the increase of L_{r1}/L_{rT} when $K_{a1}>K_{a2}$. At $K_{a1}<K_{a2}$, it's the opposite of $K_{a1}>K_{a2}$ pattern.
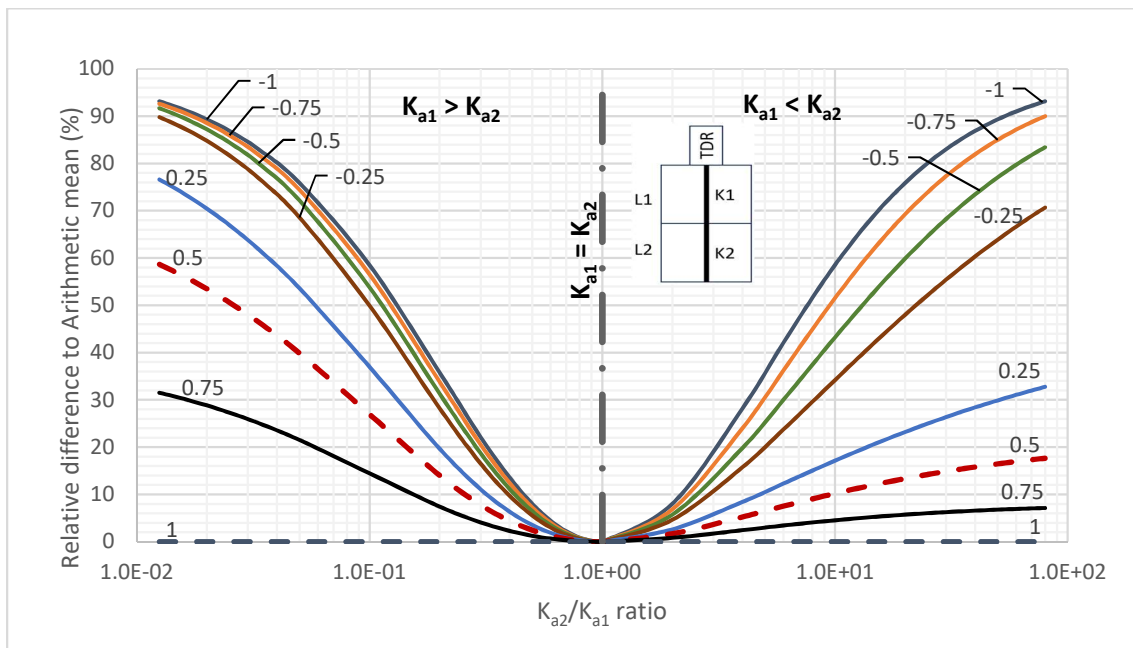
Figure 6.5.3: Relative difference of the refractive index mean for different value of n to the arithmetic mean of k_a when $L_{r1}/L_{rT}=$ 22.4% ; $L_{r2}/L_{rT}=$ 77.6%
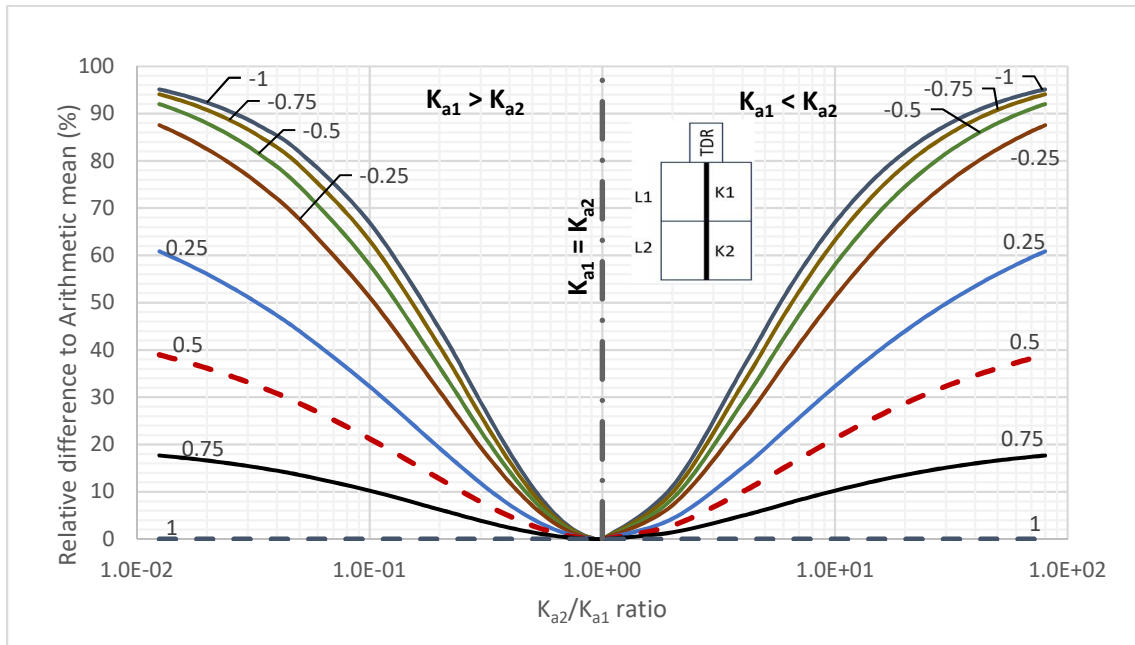
Figure 6.5.4: Relative difference of the refractive index mean for different value of n to the arithmetic mean of k_a when $L_{r1}/L_{rT} = 50\%$; $L_{r2}/L_{rT} = 50\%$
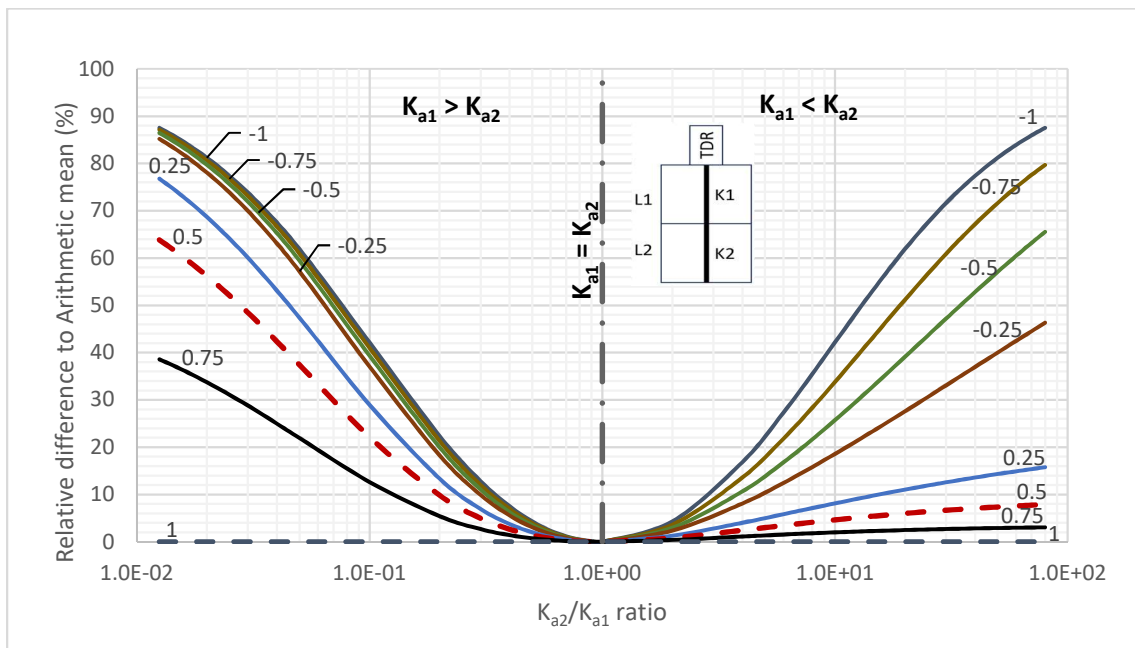
Figure 6.5.5: Relative difference of the refractive index mean for different value of n to the arithmetic mean of k_a when $L_{r1}/L_{rT} = 10\%$; $L_{r2}/L_{rT} = 90\%$
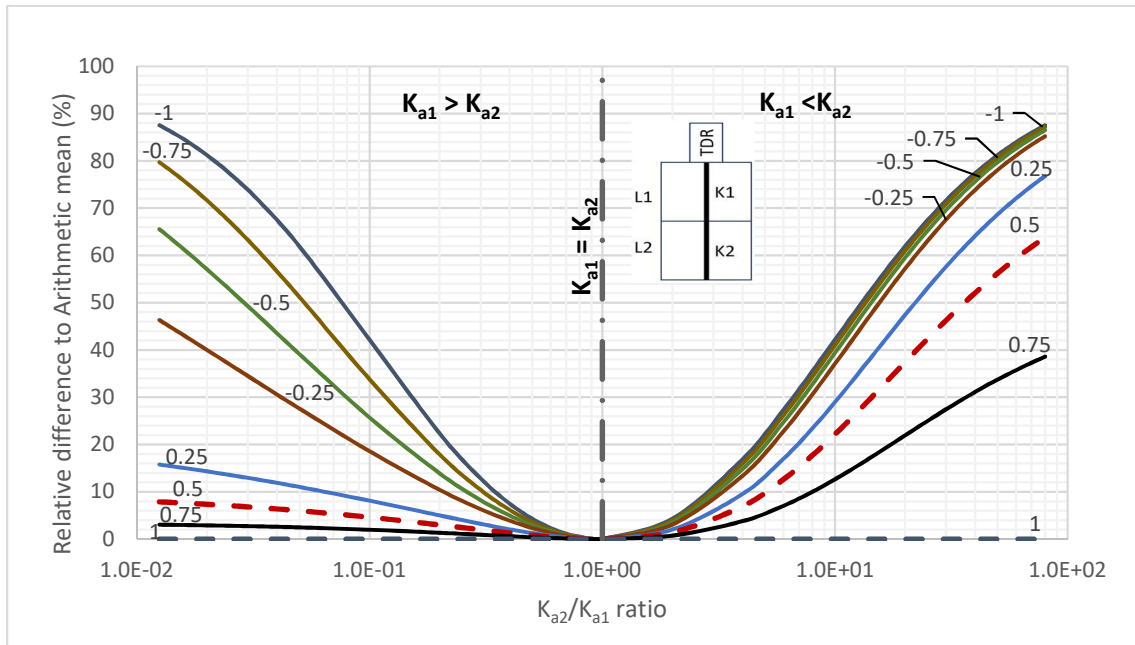
Figure 6.5.6: Relative difference of the refractive index mean for different value of n to the arithmetic mean of k_a when $L_{r1}/L_{rT} = 90\%$; $L_{r2}/L_{rT} = 10\%$
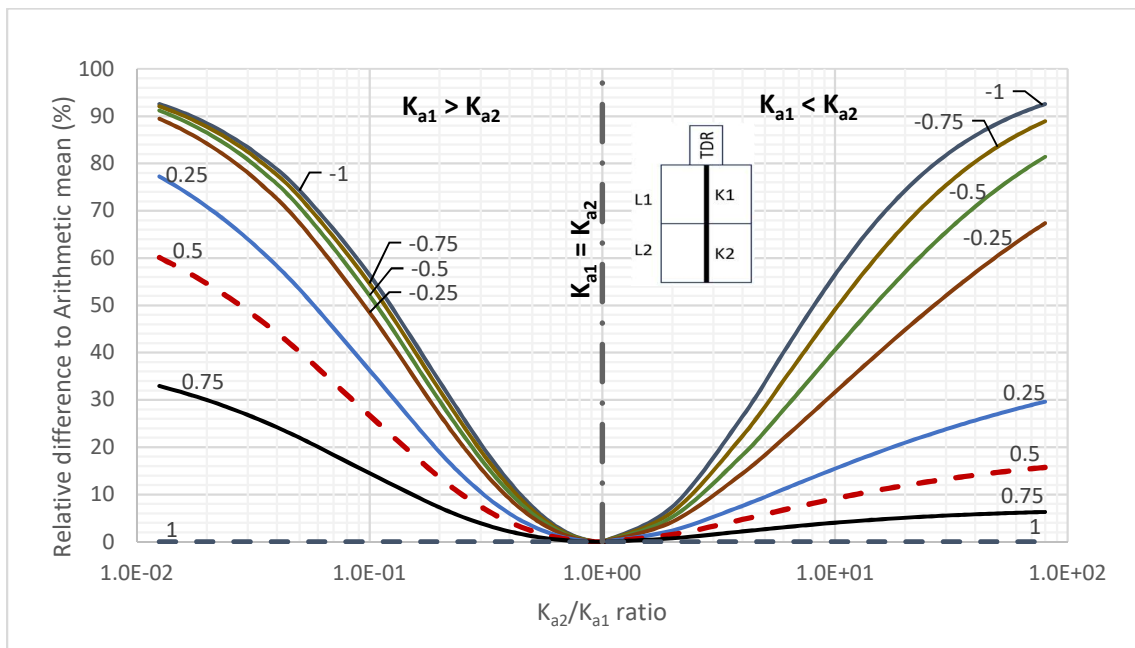
Figure 6.5.7: Relative difference of the refractive index mean for different value of n to the arithmetic mean of k_a when $L_{r1}/L_{rT} = 20\%$; $L_{r2}/L_{rT} = 80\%$
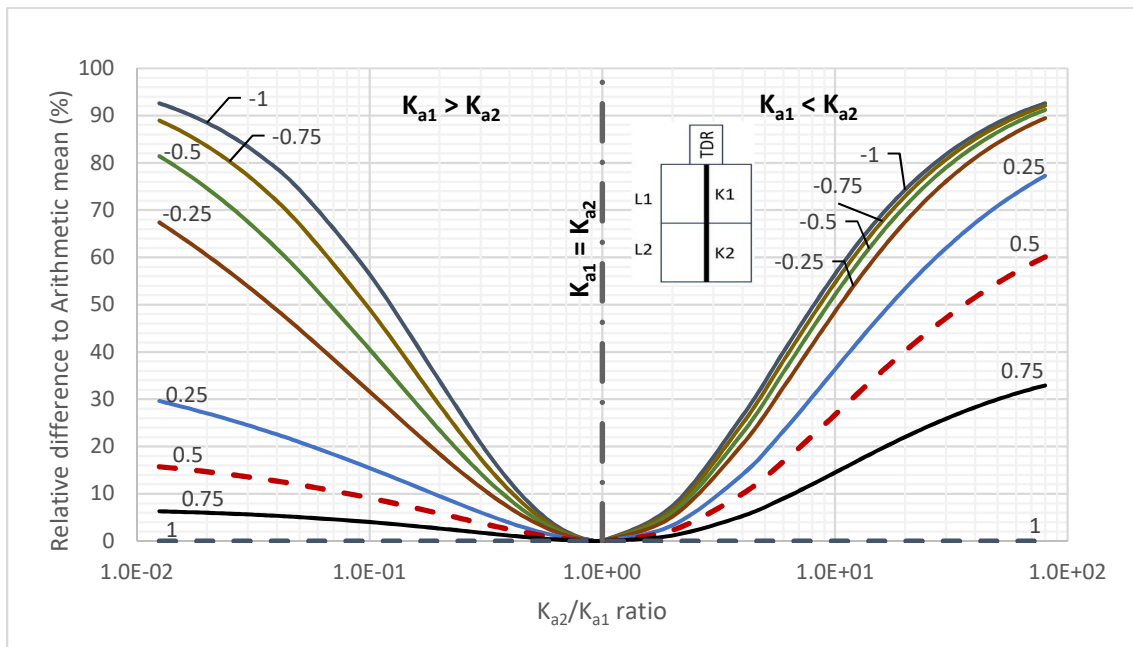
Figure 6.5.8: Relative difference of the refractive index mean for different value of n to the arithmetic mean of k_a when $L_{r1}/L_{rT} = 80\%$; $L_{r2}/L_{rT} = 20\%$
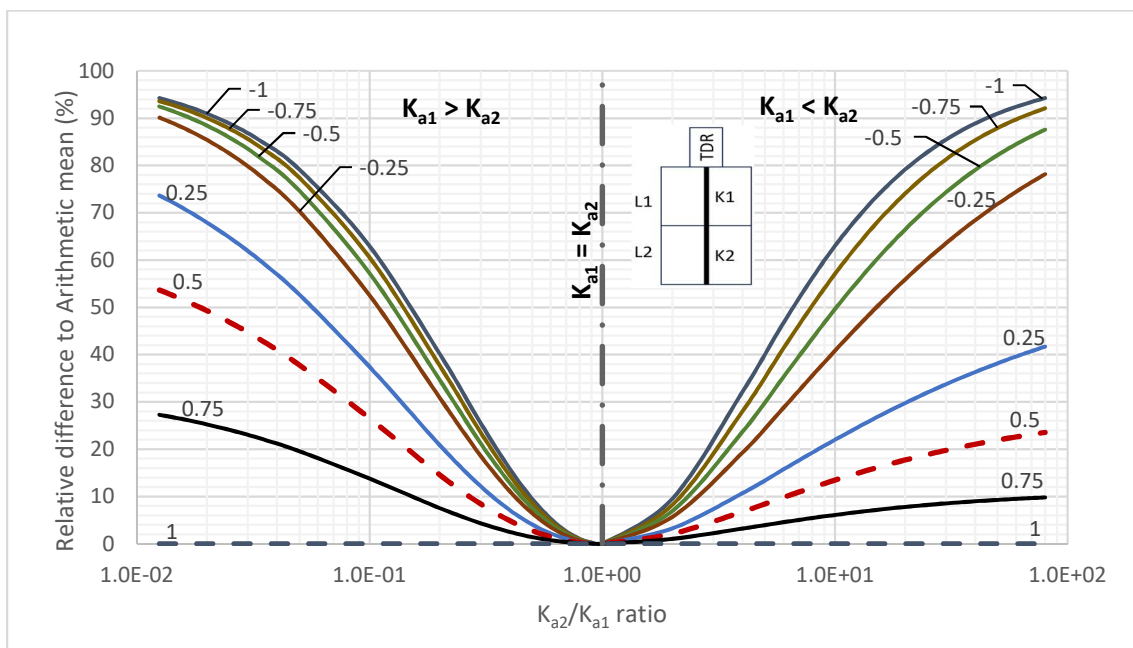
Figure 6.5.9: Relative difference of the refractive index mean for different value of n to the arithmetic mean of k_a when $L_{r1}/L_{rT} = 30\%$; $L_{r2}/L_{rT} = 70\%$
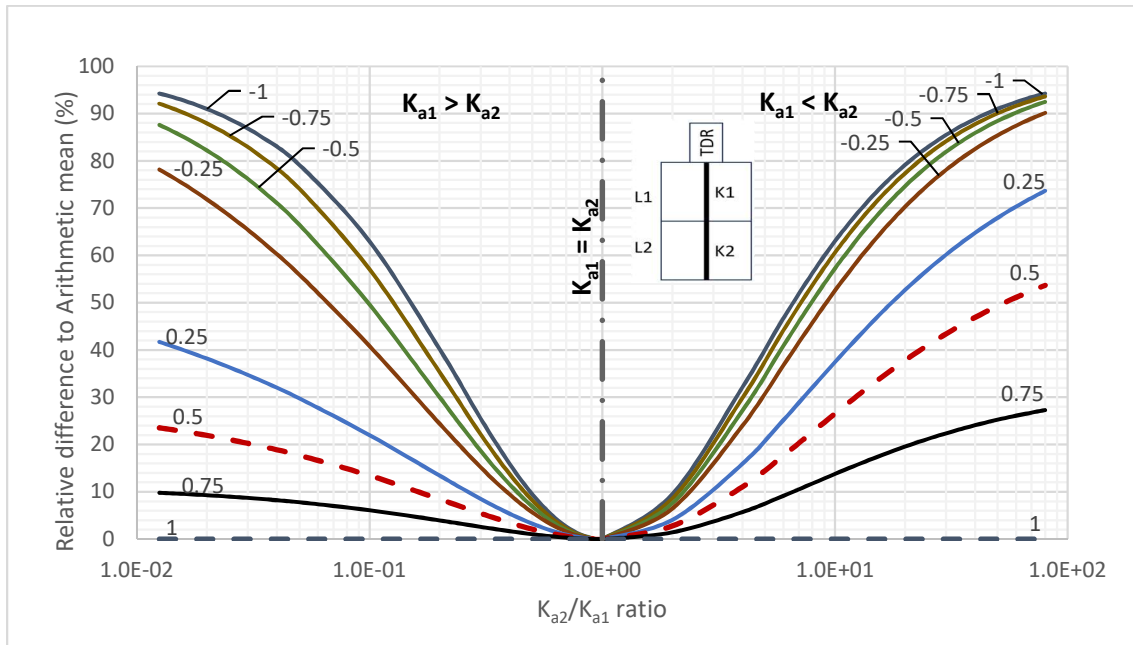
Figure 6.5.10: Relative difference of the refractive index mean for different value of n to the arithmetic mean of k_a when $L_{r1}/L_{rT} = 70\%$; $L_{r2}/L_{rT} = 30\%$
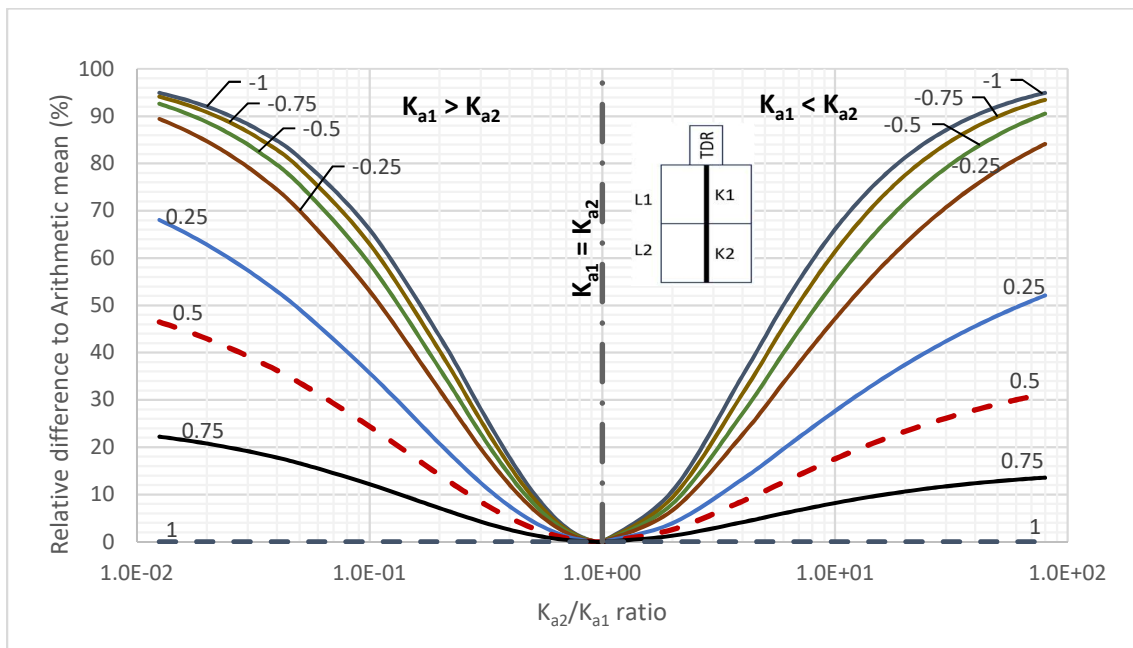
Figure 6.5.11: Relative difference of the refractive index mean for different value of n to the arithmetic mean of k_a when $L_{r1}/L_{rT} = 40\%$; $L_{r2}/L_{rT} = 60\%$
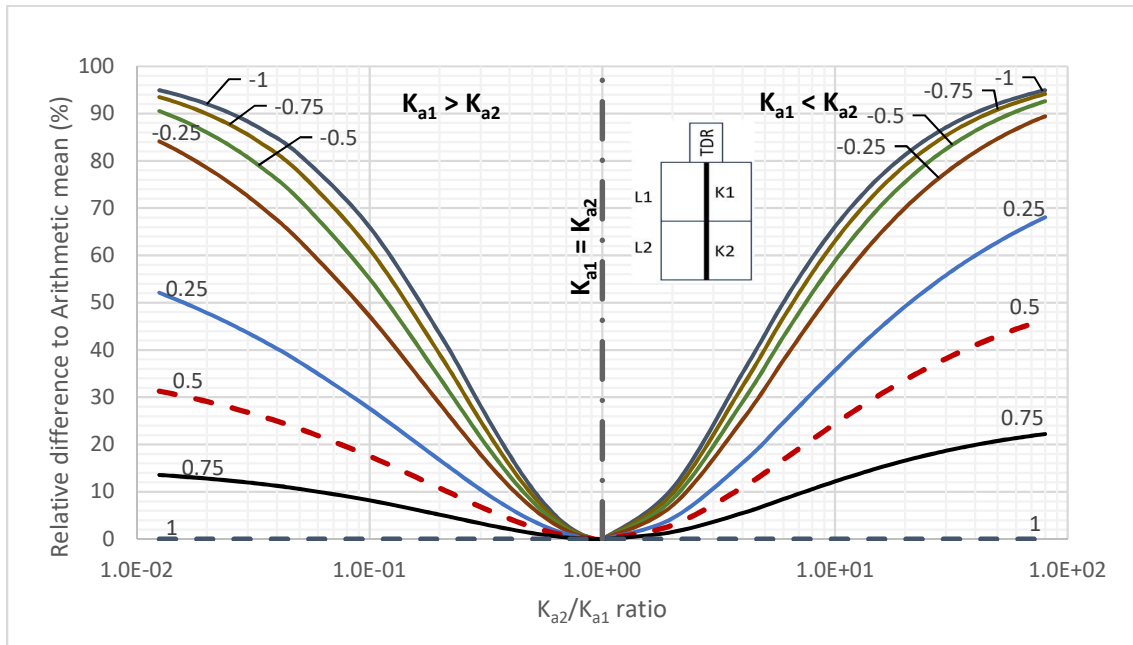
Figure 6.5.12: Relative difference of the refractive index mean for different value of n to the arithmetic mean of k_a when $L_{r1}/L_{rT} = 60\%$; $L_{r2}/L_{rT} = 40\%$

Generally, the curves are symmetrical to the opposite fraction after a fraction of 50%/50%. As for the relative difference, the positive *n* values have a lower difference to the arithmetic mean method. The highest relative difference of the curves with negative n value ranges between 95% and 88% when the length fractions are 50%/50%. The highest relative difference range for the positive *n* value curve when *n*=1 is excluded is 77% to 39% when the lengths fractions are 10%/90% or 90%/10%. Surprisingly, the highest relative differences are not for the same length fractions for negative and positive *n*. Thus, it means that the negative values are less affected by the L_{ri}/L_{rT}. In Figure 6.5.13, the highest relative difference for each *n* at different length fractions is shown, starting from 10%/90% fraction to 90%/10%. In the graph, the negative *n* curves increase until they reach a maximum point and then decrease like the other *n* curves at different length fractions. The opposite to the other curves, the *n*=-1 curve is symmetrical, where the highest relative differences before and after the maximum point at 50/50 are the same. The maximum point gets to a 10/90 length fraction when *n* values are between 0.25 and 0.50. In addition to that, curves starting from *n*=-1 to *n*=0.25 have a maximum highest relative difference of 95.12 %, 94.13 %, 92.62 %, 90.13 % and 77.25 %, respectively. This shows a low increase of the maximum highest relative difference in negative *n* values curves. As for the positive values, the curves decrease from a 10/90

length fraction for curves of $n=0.5$ and above. Thus, the negative n and positive n curves don't decrease in the same manner, and variables such as length fraction and n value have a considerable effect on the highest relative difference. To determine its effects on the curves, the difference between the highest value and the lowest value in Figure 6.5.13 was calculated for each curve, as shown in multilayer experiment data in Table E.1 in the Appendix.

A higher difference means that the effect of the variables on the difference between mean methods is considerable compared to a lower difference. However, it doesn't represent the full range of the K_a ratios, as the difference between the curves shown earlier has little differences closer to $K_{a2}/K_{a1}=1$. The main purpose is to determine the highest possible drop. However, $n=0.25$ has the highest drop of 61.49%, while $n=-1$ has the lowest drop of 7.59%. As for $n=0.5$, which is used for the refractive index, the highest drop is 55.94%. This shows that other than the K_a ratio, the fraction of the length also has a high impact on the difference between both functions, mostly for positive n values.
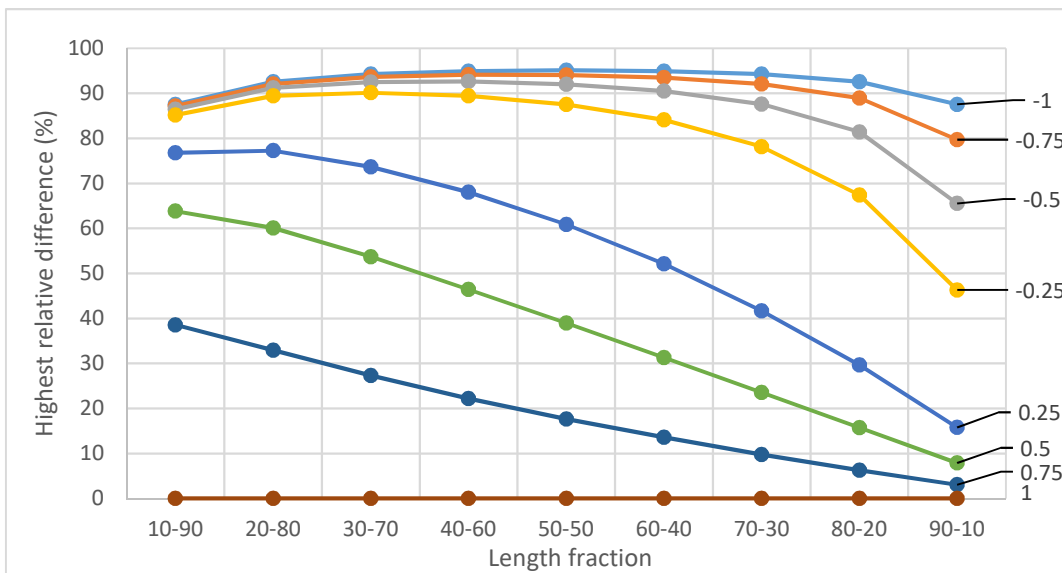
Figure 6.5.13: Highest relative difference when $K_{a1} > K_{a2}$ for different Lengths fractions (data in Appendix E Table E.1)

Knowing that the length fraction can have a high impact on the relative difference to the arithmetic means. The Figure 6.5.14 and Figure 6.5.15 were plotted for $n=0.5$ at different L_{r1}/L_{r2} ratio ranging from 0.1 to 9.0 in order to determine the difference between both methods at different K_a ratios.

The figures were presented in L_{r1}/L_{r2} ratio instead of length fraction to have a better presentation of the graph. However, it is similar to the length fraction. For example, the $L_{r1}/L_{r2} = 9.0$ is when the length fraction is 90%/10%. The comparison showed that there is symmetry when $L_{r1}/L_{r2} = 1$, and the curves of the L_{r1}/L_{r2} ratio above and below 1 are oppositely symmetrical, which is similar to the precedent relative differences figures. Thus, when $K_{a1} > K_{a2}$, the increase in the length ratio decreases the relative difference to the arithmetic mean. On the opposite, when $K_{a1} < K_{a2}$, it increases the relative difference in the same matter as it decreases when $K_{a1} > K_{a2}$.
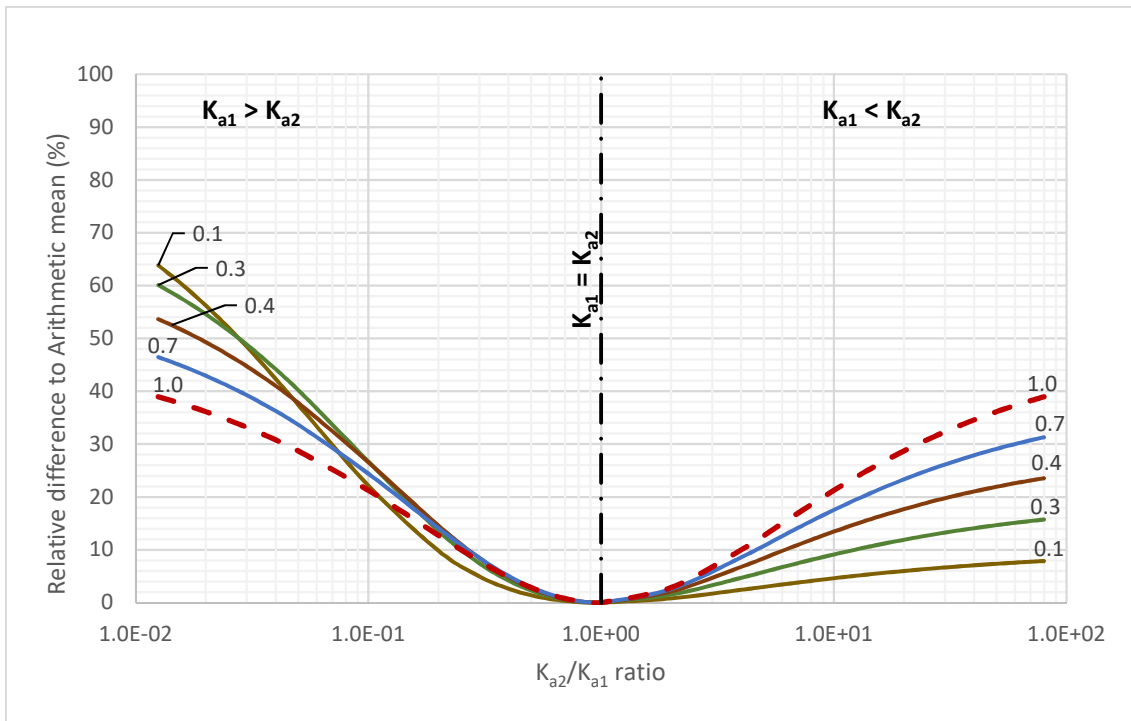
Figure 6.5.14: Relative difference of Refractive index to Arithmetic mean at n=0.5 for L_{r1}/L_{r2} range of L_{r1}/L_{r2} 0 to 1.0
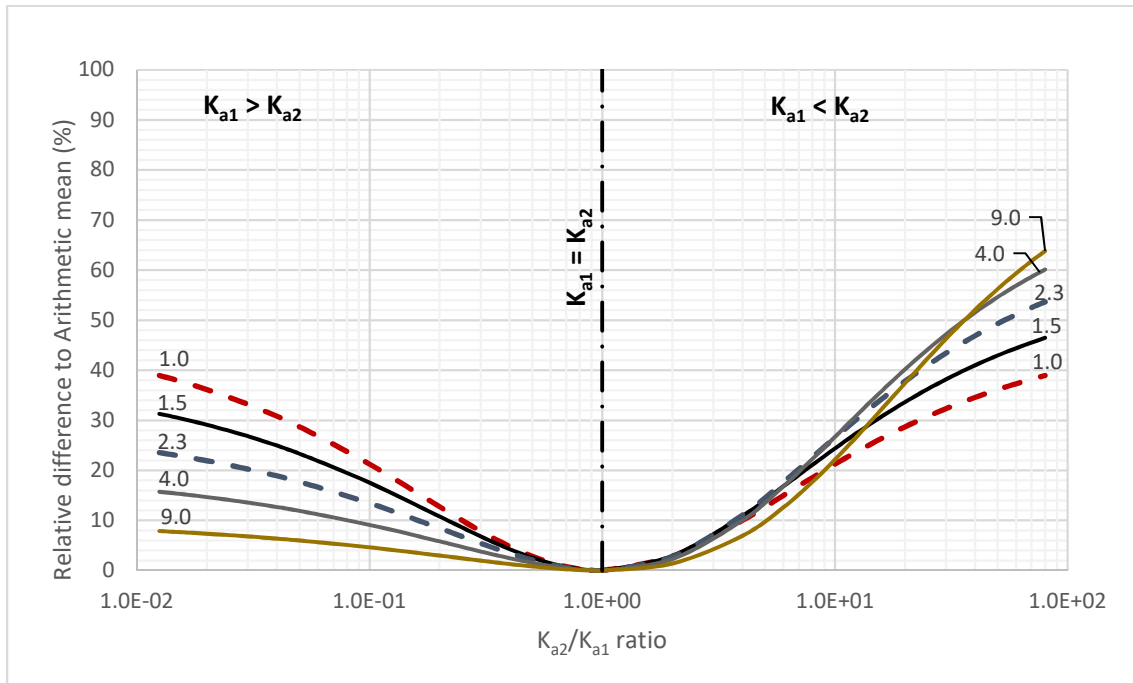
Figure 6.5.15: Relative difference of Refractive index to Arithmetic mean at n=0.5 for L_{r1}/L_{r2} range of L_{r1}/L_{r2} 1.0 to 9.0
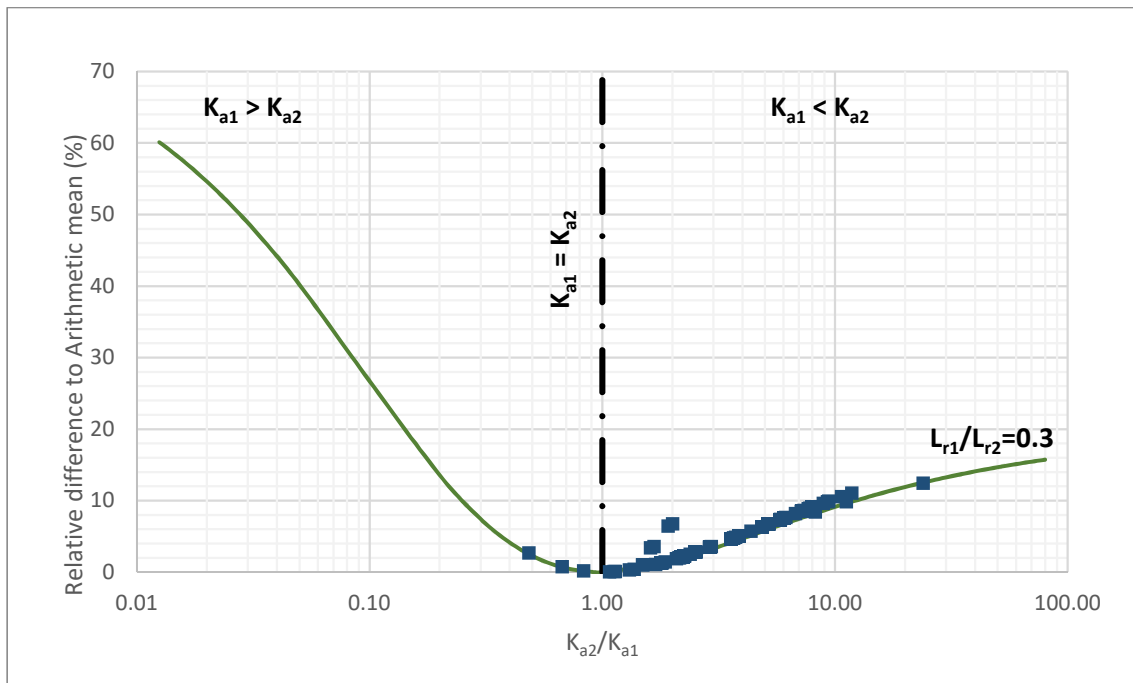
Figure 6.5.16: Relative difference to the arithmetic mean using obtained data when n=0.5

When the experimental data are calculated with $n=0.5$ and plotted in Figure 6.5.16. It shows that the variation between both methods for most of the data is around 10%. Most results have a $K_{a1} < K_{a2}$ because of the cell. Thus, it means that from what was discussed in the preceding comparison, the increase in length ratio, such as increasing the cell's border thickness, will increase the relative difference.

Now the differences between both methods and their effects on the experimental results were discussed. The n values of all the experiments waveform including all interpretation methods were calculated to find the best fit. The calculus was done using equation (6.11) by iteration until the value of n matches the measured waveform's K_{aT}.

$$K_{aT} = K_{a1} \left(\frac{L_{r1}}{L_{rT}} \right)^{1/n} + K_{a2} \left(\frac{L_{r2}}{L_{rT}} \right)^{1/n} \qquad\qquad (6.11)$$

For each experiment's waveform K_{a2}/K_{a1}, the found value of n is traced in Figure 6.5.17. Then, a line of n equal to 0.5 for the refractive index and equal to 1 for the arithmetic mean were traced. At first, the waveforms K_{aT} that was used had a precision of one decimal, the same as n values. Thus, multiple values of n were found to give the same value of K_{aT}, which were added as a range on the figures (vertical lines). For 1 decimal precision in Figure 6.5.17, most of n values have more range in K_{a2}/K_{a1} below 5. Above 5, the majority of points have an n value of 0.5 and have only one value of n to obtain the waveform's K_{aT}. A close-up view of the K_{a2}/K_{a1} range of 0 to 5 shown in Figure 6.5.18 demonstrates the range of n values is higher around 1 and decreases with the increase of the K_{a2}/K_{a1} ratio.
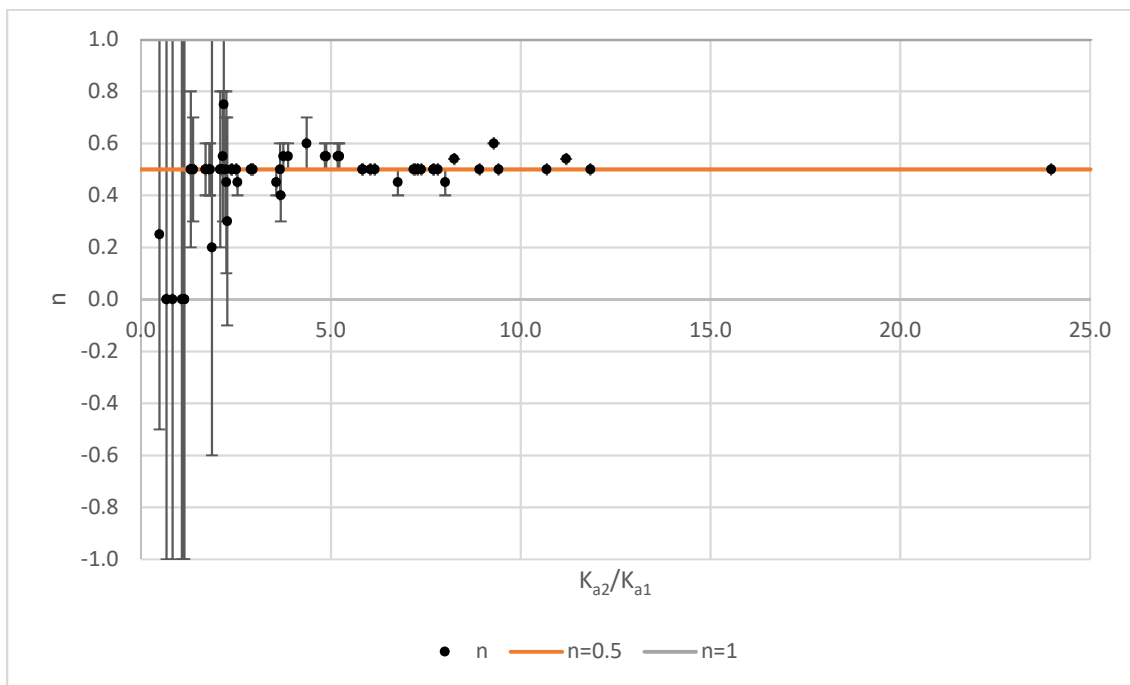
Figure 6.5.17: All experiments waveform's n using 1 decimal precision
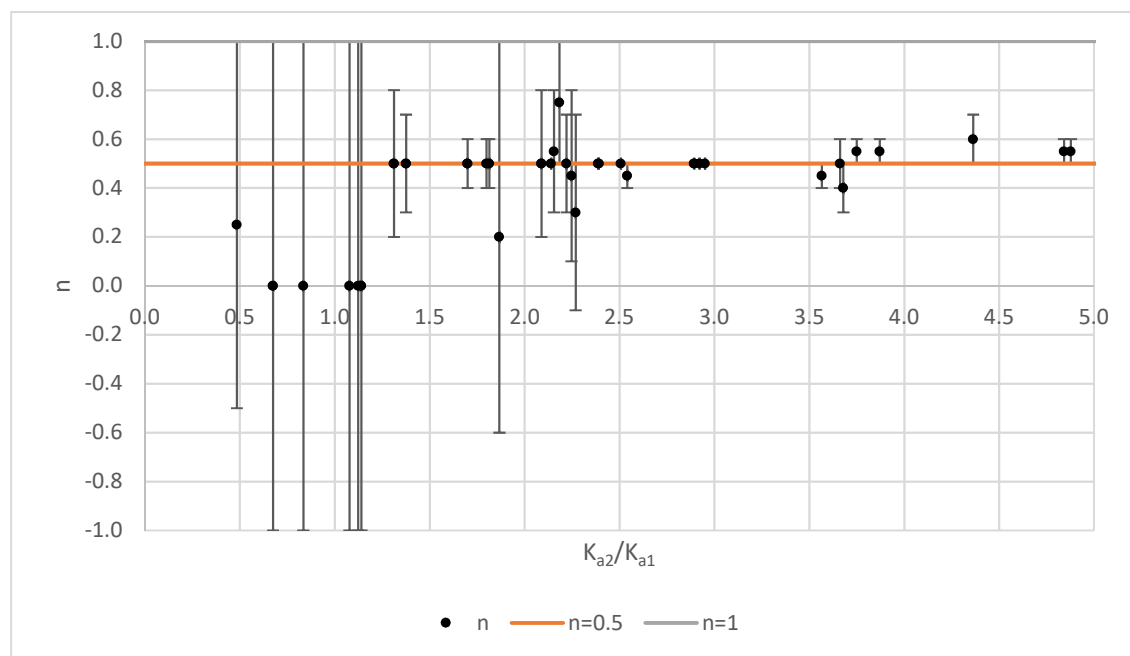
Figure 6.5.18: All experiments waveforms n using 1 decimal precision K_{a2}/K_{a1} range]0.0 ; 5.0]

The higher range of n values is mainly caused by the precision of K_{aT}. So, to lower the effect of the precision, the values of K_{aT} and K_{a2}/K_{a1} were increased to 2 decimals, and the results are shown in Figure 6.5.19 and Figure 6.5.20. Compared to 1 decimal, the 2 decimals value has more points with lower to no range and the n values show clearly that they are around 0.5. Interestingly, it was found that the range of n values increases around K_{a2}/K_{a1} equal to 1. This means K_{aT} is less affected by n values because of the high range, whereas some are in the full range. Furthermore, the refraction index method is the method that fits the waveforms from the experiments.
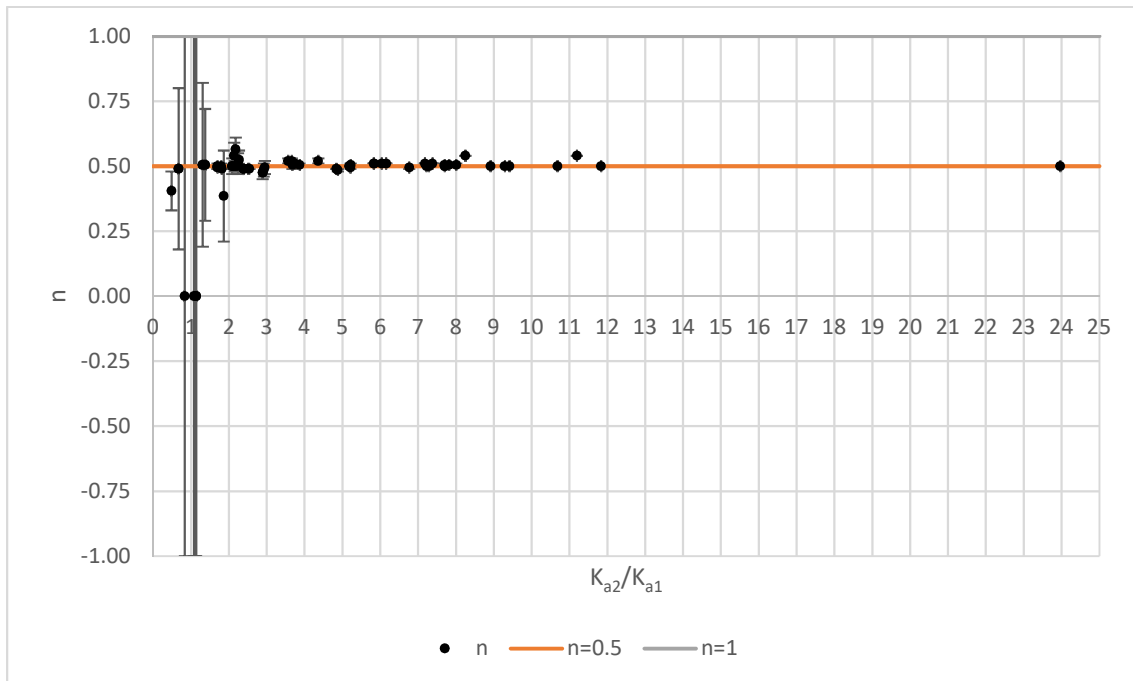
Figure 6.5.19: All experiments waveform's n using 2 decimals precision
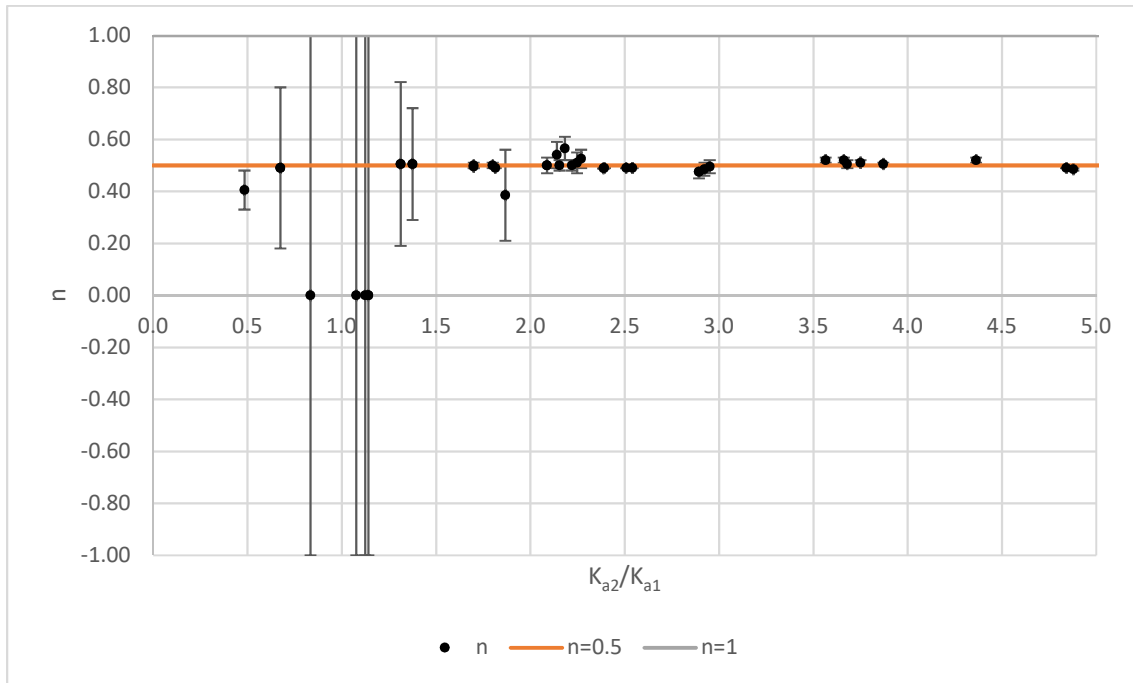
Figure 6.5.20: All experiments waveforms n using 2 decimal precision K_{a2}/K_{a1} range]0.0 ; 5.0]

6.6 Multilayer experiment

The multilayer experiment consists of putting two layers of the same soil with two compaction levels in which one TDR-305 per layer is inserted laterally then, a TDR-310 is inserted vertically through both layers. For each TDR, waveforms are collected in order to compare both methods of insertion and to compare both methods of permittivity averaging. The bottom layer is denser than the upper layer as the compaction energy was affecting it when the upper layer was compacted.

The obtained waveforms from the TDR inserted vertically crossing two soil layers were more difficult to interpret than those obtained from the laterally inserted TDR's crossing the same soil layer. This is caused by the changes in soil properties along the length of the TDR probes.

Figure 6.6.1 shows waveforms of the TDR-310 gradually inserted into two layers in order to detect the changes caused to the waveform by the second layer. During the first insertion, the TDR passes through air and the upper layer and in the obtained waveform, there is a drop in the amplitude when it gets in the upper layer. As the insertion continues, the probe finishes by being fully inserted and passed through the upper and bottom layers only. From which the obtained waveform has a drop

between *L2* and *L1*, shown in the figure 6.6.1. That drop is caused by a difference in soil conditions, resulting in a difference in the permittivities. These drops were noticeable, but in a case where the difference between both layers is small, the differentiation between both layers will be difficult.
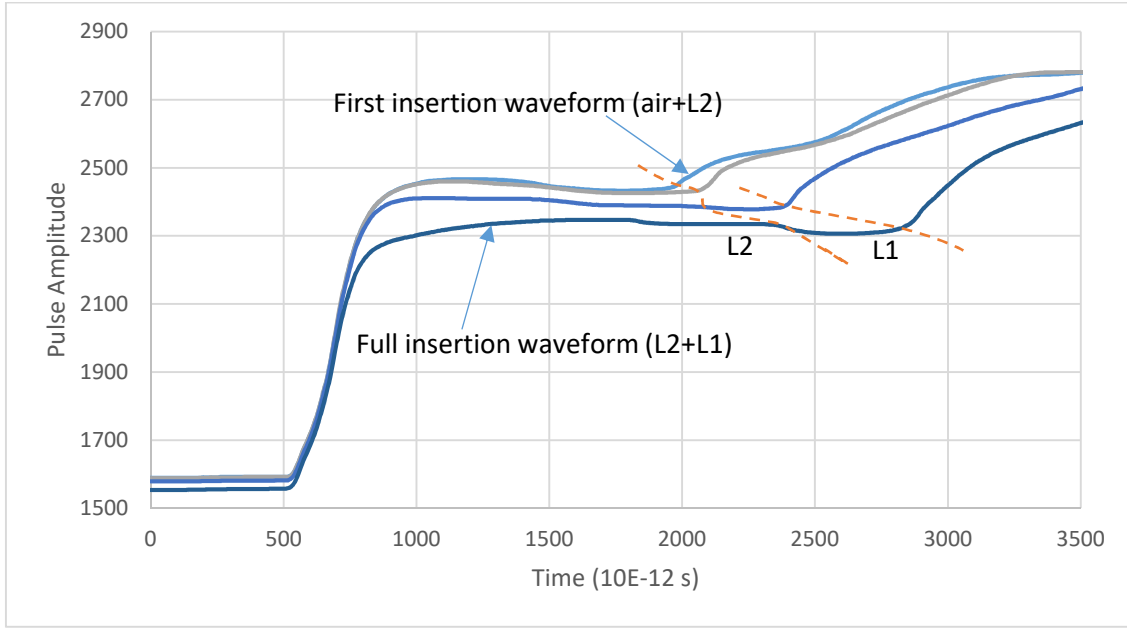
Figure 6.6.1: Gradual insertion of the vertical TDR-310 (#434) in the multilayered soil

Because of this situation, the lateral insertion was used and compared with the vertical insertion. For the three tests that were done in the multilayer experiment, the K_{aS} of the whole waveform obtained from the vertical insertion *V* was determined by using all the interpretation methods. *V* will be used as a reference for comparison to *V1* and *V2*, which will be explained in the following paragraphs.

Then, the obtained waveforms of the lateral insertion in the upper layer *L2* and the bottom layer *L1* are used to determine the K_a of *L1* and *L2*. These two permittivities are then used to determine the permittivity *V1* following the equation below. Depending on the meaning method, the *n* value is equal to 1 for the arithmetic mean and equal to 0.5 for the refractive index.

$$K_{a\,V1} = \left[(K_{a\,L1})^n \left(\frac{L_{r1}}{L_{rT}} \right) + (K_{a\,L2})^n \left(\frac{L_{r2}}{L_{rT}} \right) \right]^{1/n} \qquad (6.12)$$

V1 include only *L1* and *L2* because of the TDR310 length of 100 mm. Since the exact 50 mm layers is not reachable the TDR probe can have couple mm inserted into the base layer. In the waveform, the base layer in not noticeable compared to other layers. Because of this, it is interesting to determine if it impacts the total permittivity *V*. To determine if the base layer impacts *V*, the permittivity of the base layer is calculated using the equation below.

$$K_{aB} = \left[\frac{(K_{aS\,V})^n L_{rT} - (K_{aS\,L1})^n L_{r\,L1} - (K_{aS\,L2})^n L_{r\,L2}}{L_{rB}} \right]^{1/n}$$

(6.13)

If the obtained permittivity is higher than the highest permittivity of a wet soil (~30), it means that the base layer has no impact on the total permittivity. The reason is if the distance is relatively small, it may need an exaggerated permittivity to affect the total permittivity.

Since both layers were noticeable on the waveform, a total permittivity *V2* was calculated using the permittivity of each layer. The layers' permittivity is determined on the waveform: the layer 2 starts from the beginning to the transition and layer 1 from the transition to the end of the waveform as shown in Figure 6.6.1. At the transition, the interception of both tangents is used as the t_2 of layer 2 and t_1 of layer 1. This comparison is done to show the limits of the waveform interpretation when the TDR is inserted through multiple layers. The comparison was done for both meaning methods and only for the Tangent and Heimovaara interpretation methods. This method can't be applied to the Schwartz method of interpretation because it's an automated process that is used to determine two points, t_1 and t_2, and it is complex to try to determine other points. The permittivities of each layer that were obtained to calculate *V1* and *V2* are also compared.

In Table 6.6.1, the results of the obtained permittivities discussed presciently for the three tests are shown. Starting with the vertical insertion waveform total permittivity *V*, the Tangent method and Heimovaara method have low differences from the Schwartz method. That difference is due to t_1, which is not the same because of the methods and procedures. The comparison of the lateral insertion permittivities of each layer showed that there is a low difference between interpretation methods. However, both layers don't have the same permittivity, where the lowest difference is 33% and the highest is 50%. This is due to the experimental procedure where *L1* is probably denser because of the compaction energy received from the *L2* compaction. It is important to note that a 50% difference in permittivity doesn't mean that *L1* is 50% denser than *L2*.

When *V1* was calculated, low differences were noticed in meaning and interpretation methods. Moreover, the highest difference between values is 0.4. When compared to *V*, the Schwartz method has the lowest difference to *V*, ranging from 1.4 to 1.9. This is 22% to 29% lower than *V* and about 50% lower than the other interpretation methods. Moreover, the differences between the other methods' differences to *V* are between 3.1 and 4.1, which is 37% to 46% lower than *V*. This difference is explained later in this chapter. These differences are for this experiment and cannot be generalized. The fact that this experiment's lateral method obtained 25% differences relative to the vertical insertion waveform's total permittivity doesn't mean that it will be the same for other experiments. Thus, further work should be done in order to have a generalized theory on that specific usage.

The obtained base layer permittivities using arithmetic mean have values ranging from 100.4 to 166.4 for Tangent and Heimovaara interpretation methods. The Schwartz method values range from 49.3 to 73.8, which is the lowest of all interpretation methods. When the Refractive index is used, the results are about 5 to 7 times higher than the arithmetic mean for the Tangents and Heimovaara interpretation methods. In comparison, the results of the Schwartz method are 3 to 4 times higher. The test 3 base permittivity is 0 because the probe doesn't reach the base layer. Thus, it can be supposed that the base layer doesn't have an impact on the total permittivity because of the obtained higher permittivity values. If the base layer permittivity was around 10, the total permittivity would be around 5 for the arithmetic mean and refractive index, which is not very different from V1, which includes only two layers.

Table 6.6.1: Multilayer experiment permittivity comparison (Appendix E Table E.2 and Table E.3)

			Arithmetic mean			Refractive Index		
		Layer height	Tangent	Schwartz	Heimo	Tangent	Schwartz	Heimo
		m	K_{aS}	K_{aS}	K_{aS}	K_{aS}	K_{aS}	K_{aS}
Test 1								
Vertical insertion	V	0.100	8.8	6.6	9.0	8.8	6.6	9.0
Lateral insertion K_{aS}	L2	0.047	3.3	3.3	3.4	3.3	3.3	3.4
	L1	0.049	6.6	6.3	6.5	6.6	6.3	6.5
	V1	**0.096**	**5.0**	**4.8**	**5.0**	**4.9**	**4.7**	**4.8**
	ΔV	**-**	**3.8**	**1.8**	**4.0**	**4.0**	**1.9**	**4.1**
Calculated Base	***Base**	**0.004**	**100.4**	**49.3**	**104.7**	**455.0**	**148.5**	**483.9**
Vertical insertion waveform's K_{aS}	L2	0.047	19.1	-	19.5	19.1	-	19.5
	Δ L2	**-**	**-15.8**	**-**	**-16.2**	**-15.8**	**-**	**-16.1**
	L1	0.049	3.5	-	3.5	3.5	-	3.5
	Δ L1	**-**	**3.1**	**-**	**3.0**	**3.1**	**-**	**3.0**
	V2	**0.096**	**11.1**	**-**	**11.3**	**9.6**	**-**	**9.7**
	ΔV	**-**	**-2.3**	**-**	**-2.4**	**-0.8**	**-**	**-0.8**
Test 2								
Vertical insertion	V	0.100	8.3	6.4	8.4	8.3	6.4	8.4
Lateral insertion K_{aS}	L2	0.050	3.9	4.0	4.0	3.9	4.0	4.0
	L1	0.048	6.6	6.1	6.5	6.6	6.1	6.5
	V1	**0.098**	**5.2**	**5.0**	**5.2**	**5.1**	**5.0**	**5.1**
	ΔV	**-**	**3.1**	**1.4**	**3.2**	**3.2**	**1.4**	**3.3**
Calculated Base	***Base**	**0.002**	**159.0**	**73.8**	**166.4**	**1087.4**	**300.1**	**1166.7**
Vertical insertion waveform's K_{aS}	L2	0.050	15.3	-	15.6	15.3	-	15.6
	Δ L2	**-**	**-11.3**	**-**	**-11.6**	**-11.3**	**-**	**-11.6**
	L1	0.048	3.7	-	3.7	3.7	-	3.7
	Δ L1	**-**	**2.8**	**-**	**2.7**	**2.8**	**-**	**2.7**
	V2	**0.098**	**9.6**	**-**	**9.8**	**8.6**	**-**	**8.8**
	ΔV	**-**	**-1.3**	**-**	**-1.4**	**-0.3**	**-**	**-0.3**
Test 3								
Vertical insertion	V	0.100	9.5	7.1	9.6	9.5	7.1	9.6
Lateral insertion K_{aS}	L2	0.053	4.7	4.3	4.6	4.7	4.3	4.6
	L1	0.047	7.0	6.7	6.9	7.0	6.7	6.9
	V1	**0.100**	**5.8**	**5.4**	**5.7**	**5.7**	**5.4**	**5.7**
	ΔV	**-**	**3.7**	**1.7**	**3.9**	**3.8**	**1.7**	**3.9**
Calculated Base	***Base**	**0.0**	**0.0**	**0.0**	**0.0**	**0.0**	**0.0**	**0.0**
Vertical insertion waveform's K_{aS}	L2	0.053	19.1	-	19.3	19.1	-	19.3
	Δ L2	**-**	**-14.4**	**-**	**-14.7**	**-14.4**	**-**	**-14.7**
	L1	0.047	2.7	-	2.7	2.7	-	2.7
	Δ L1	**-**	**4.3**	**-**	**4.2**	**4.3**	**-**	**4.2**
	V2	**0.100**	**11.4**	**-**	**11.5**	**9.5**	**-**	**9.6**
	ΔV	**-**	**-1.9**	**-**	**-1.9**	**0.0**	**-**	**0.0**

L1: Lateral TDR measured KaS of layer 1
L2: Lateral TDR measured KaS of layer 2
V1: Vertical TDR measured KaT
V2: Calculated KaT without base layer
*Base: KaS of base calculated from the measured L1 and L2

Graphically, the layers *L2* and *L1* obtained permittivities have different ratios compared to the lateral permittivities. This means that permittivity values from laterally inserted TDRs have ratios of K_{aS1}/ K_{aS2} ranging from 1.5 to 2.0, while the ratios range from vertically inserted TDRs are between 0.1 and 0.2. As shown in Figure 6.6.2, the length of *L2* of the waveform is 1302 ps, and the length of *L1* is 618 ps. Hence, the length of *L2* is about twice the length of *L1*. This is unrealistic because of the condition of *L1*, which is more compact. When the lateral permittivity of layers is compared to the vertical waveform's permittivity, a difference of -11.3 to -16.2 is found for layer 2, and a difference of 2.7 to 4.3 is found for layer 1. Moreover, *L2* permittivities are about 3.9 to 5.8 times the value of the lateral permittivities, and vertical *L1*'s permittivities are about 0.4 to 0.6 times the lateral permittivities. Other than the differences between permittivities and the fact that the highest permittivity is from the wrong layer, the obtained permittivities of *L2* are unrealistic for the soil condition. Thus, if the apex at 1600 ps is selected, the permittivity of *L2'* will be 2.3, which is also not representative of the soil as it is nearer to the dry sand than moist soil.
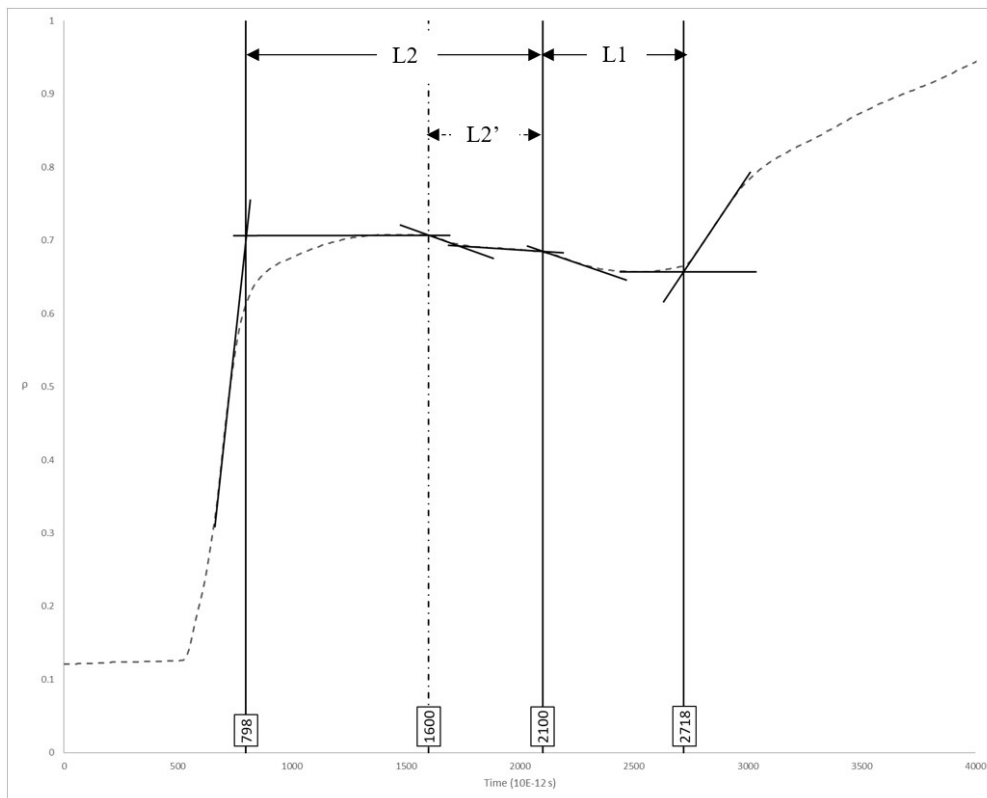
Figure 6.6.2: Layers graphical representation of the vertical insertion (Test 2, Tangent interpretation method)

Another graphic representation of the meaning comparison is shown in Figure 6.6.3 for the Tangent interpretation method and Figure 6.6.4 for the Heimovaara interpretation method. For both methods presented Table 6.6.1, *V* and *VI* total permittivity's times t_1 and t_2 are presented in Table. E.3 and in Table. E.2. Both methods have a difference of 12 ps, which is the equivalent of a permittivity of 0.1 for the tangent method, which is negligible. However, with the vertical waveform, the difference is noticeable.
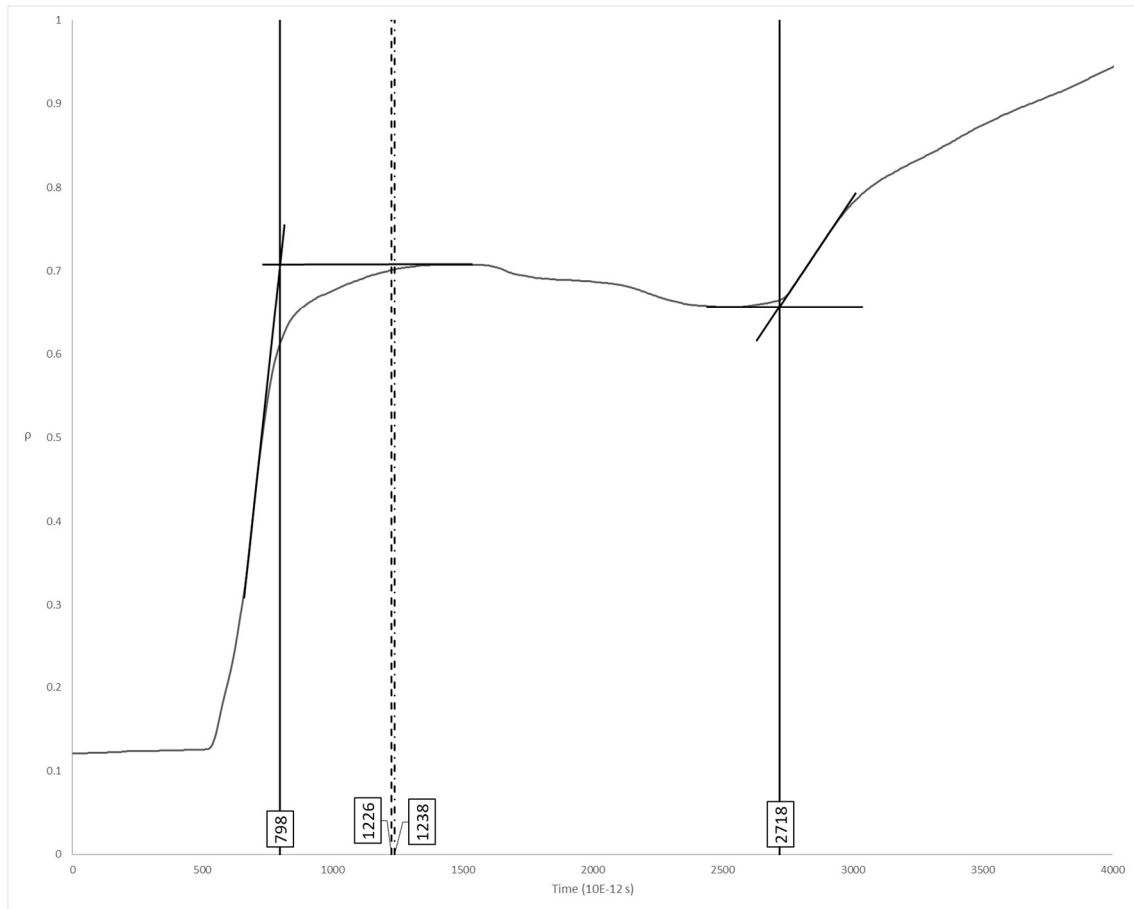
Figure 6.6.3: Graphical representation of the meaning methods to the Graph's Δt_T (Test 2, Tangent interpretation method)
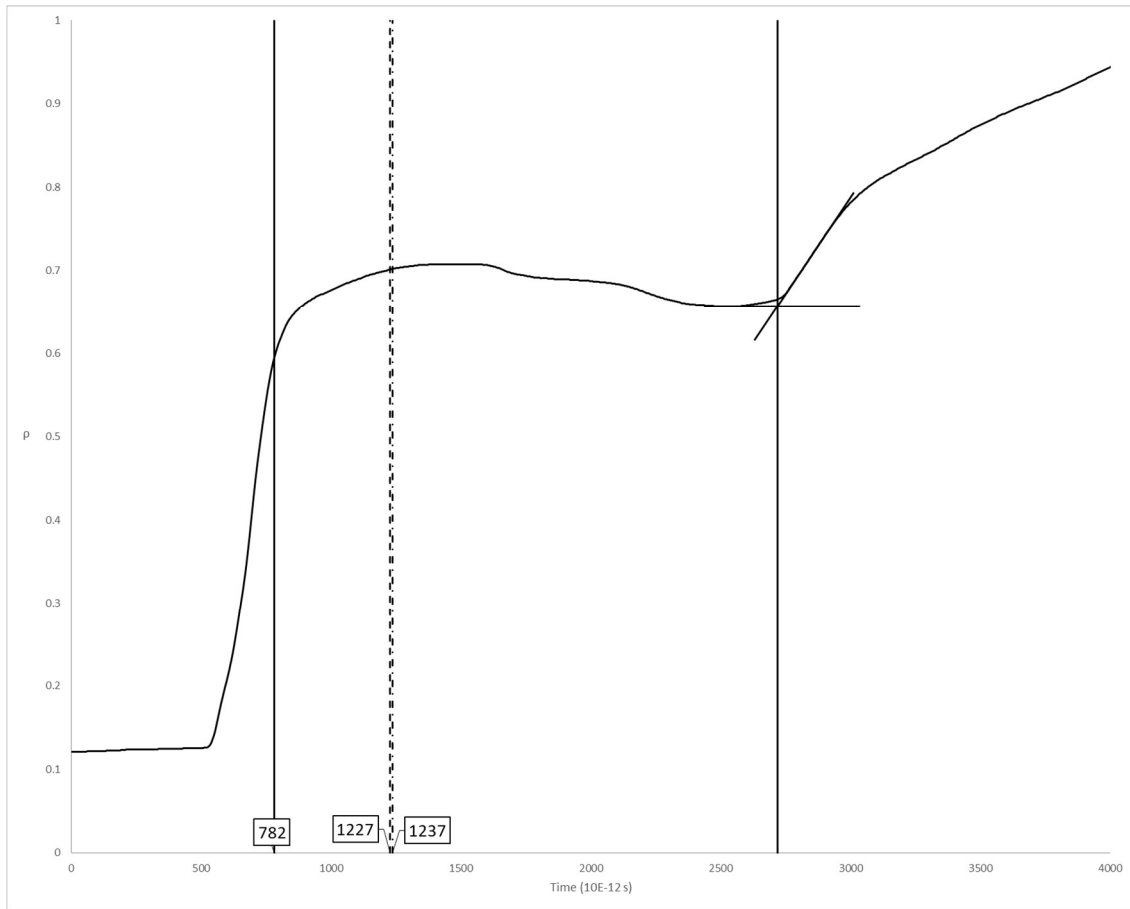
Figure 6.6.4: Graphical representation of the meaning methods to the Graph's Δt_T (Test 2, Heimovaara interpretation method)

These difference between the combination of lateral insertion permittivities and the vertical insertion is due to the signal delay. That delay depends on different factors, such as:

- The number of layers, as shown in Schaap et al. (2003), can affect the meaning method and choosing the wrong method can lead to erroneous results;
- Layers thickness and layers thickness ratio, as demonstrated with the base layer. Since the base layer is smaller than the two other layers, it is not noticeable on the waveform;
- Border in between layers condition can affect the length of the transition in the waveform;
- Layers permittivity ratio; and
- Broadband frequency of can affect the delay by extending it when the frequency is low and by shorten it when the frequency is high depending on the number of layers. Even more, according to Schaap et al. (2003), a narrow band may be sensitive to the number of layers.

Thus, an interpretation of vertical insertion waveform can get more complex because of that delay and probably other factors. Therefore, the lateral insertion is more advantageous if the calibration is done properly. The lateral insertion is a multilayer as the vertical insertion, but the waveform interpretation is done on one layer because of the border fraction of the waveform doesn't change. This, compared to two soils at different conditions, doesn't depend on the thickness of the layers and their permittivities ratio.

6.7 Sources of error

6.7.1 Impact of the column's wall on the waveform interpretation

To demonstrate the necessity of the partial insertion correction, all permittivities obtained from the experiments were compiled and presented in Figure 6.7.1. The curve in Figure 6.7.1 is presented into three types of experiments: water-column W/C, air-column A/C, and soil-column S/C. Since the ratio of permittivity changes with the filling materials, Figure 6.7.1 uses a ratio of the filling material's permittivity K_{a2} to the permittivity of column wall (Plexiglas + O-ring) K_{a1}. This gave three ranges of data where the first one is around a ratio K_{a2}/K_{a1} of 1, which is related mostly to air, the second one is S/C experiments that is between ratios of 1 and 9, and the last one is W/C experiment that is between a ratio of 8 and 24. For the W/C experiments, most of the ratios are between 8 and 12. However, the ratio of 24 is from the tangent interpretation method, where the water permittivity is 79.9, and the column's wall permittivity is 3.3. The impact of the cell was measured by calculating the relative difference of the permittivity of the material inside the column found with the correction method and the total permittivity of the waveform K_{aT} without correction. When the column is empty, the difference ranges from -11% to 20%. On the other hand, W/C experiments have less variation, where the difference ranges from -24% to -29%.

At permittivity ratios below 1, when the ratio gets closer to 0, the relative difference percentage is expected to be infinite because a ratio of 0 can't be reached since there is no permittivity equal to zero. At a higher permittivity, it is supposed that the relative difference percentage stagnates around -30%. At a ratio of 1, both materials are considered as one, and the relative difference is 0%. As for the soil, the curve was separated from Figure 6.7.1 and is presented in Figure 6.7.2. The S/C experiments' relative difference ranges from -5.6% to -28%. Since the lowest ratios are from dry soil and the highest ratios are from wet soil, it is concluded that the column wall has a smaller

effect on dry soil. As the water content increases, the effect increases to 30%. A regression was done in order to obtain a relation between the permittivity ratio and the relative difference percentage, but the obtained equation is not representative since it doesn't cross the 0% difference at a permittivity ratio equal to 1.
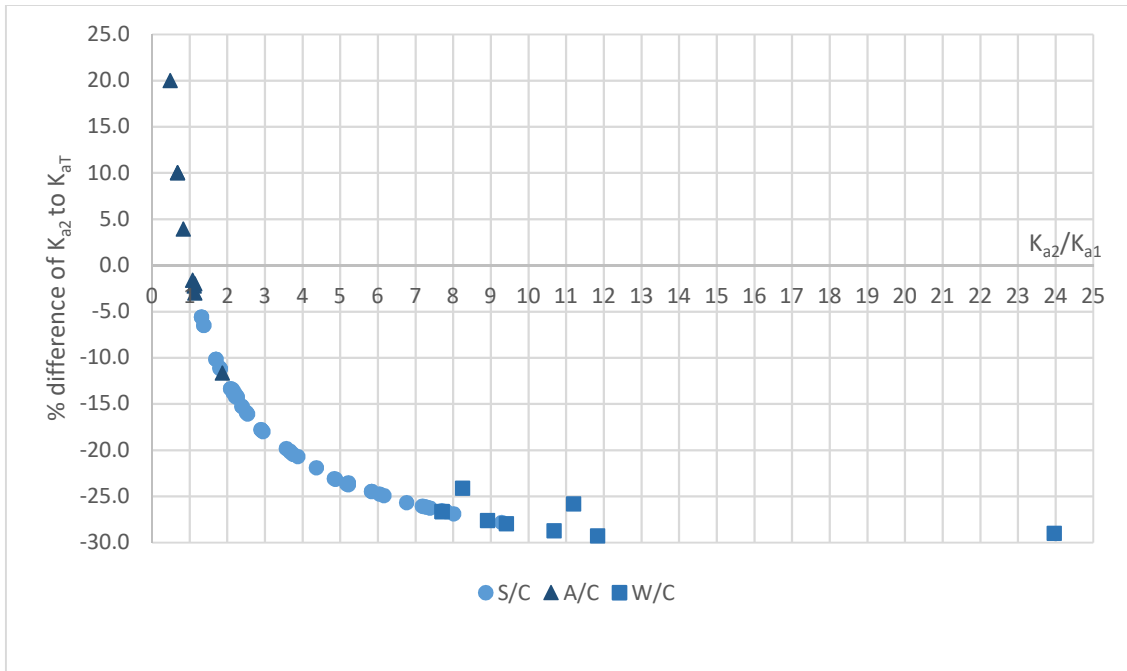
Figure 6.7.1: Difference percentage of permittivity measurement with correction method (K_{a2}) to the permittivity without correction method (K_{aT}) for soil, water and air. (Data in Appendix F Table F.1)
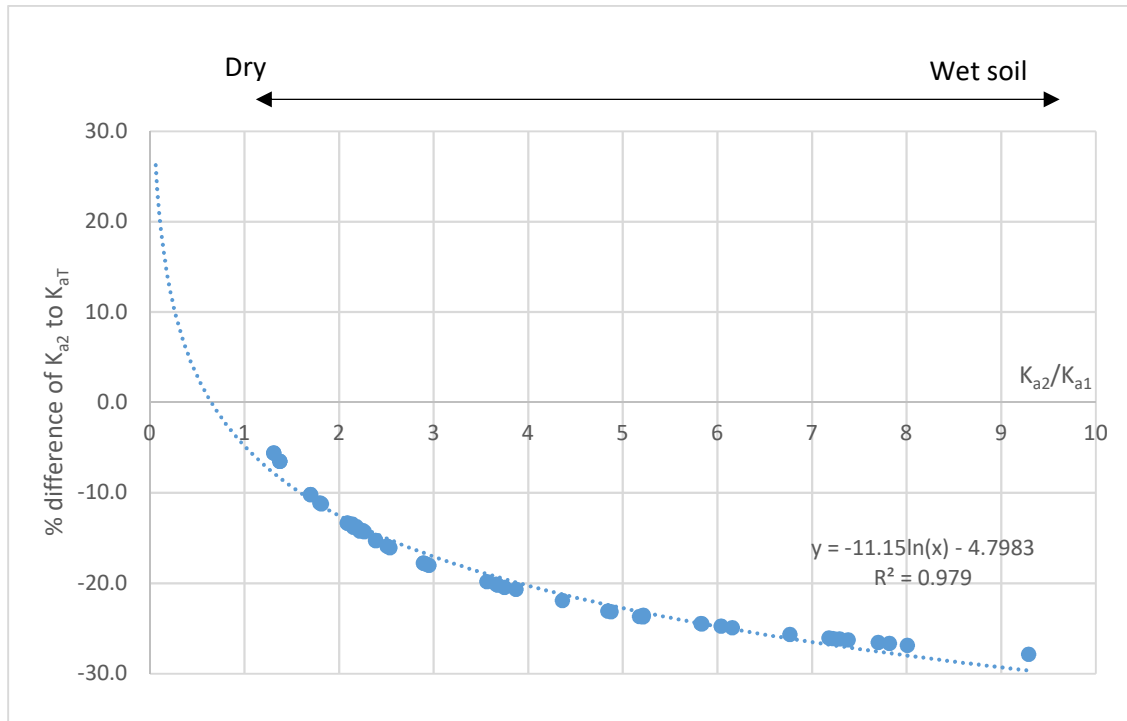
Figure 6.7.2: Difference percentage of permittivity measurement with correction method (K_{a2}) to the permittivity without correction method for soil (K_{aT}) different ratio K_{a1}/K_{a2}

6.7.2 Soil displacement

Due to the design of the TDR, the measurement area is generalized to the whole layer. Thus, if an experiment has variations in a local area, it would be beneficial to consider the TDR placement. The other limitation is the insertion of the TDR probes. The TDR probes are small, and damaging could affect the results obtained. Thus, the level of compaction of the soil should be enough to insert the TDR without damaging the rod. When the soil compaction is too low, a small movement can create space between the TDR probe and soil during the beginning of insertion. When it's fully inserted, the soil is a little bit compacted at the top of the TDR near the plastic head of the TDR. Any movement of the TDR, when it is inserted in a low to non-compacted soil, will cause a void between the soil and the TDR rod. Furthermore, the soil grain size is also limited. In the case of large grains, the TDR can't be inserted. For this reason, why the soil that was used for the experiment has a maximum size between [4.75mm ; 2.36mm]. Even more, the grains are moved by the rods during the insertion, as shown in Figure 6.7.3, which probably affects the density of

113

the soil around the probes. Furthermore, the insertion of the TDR probes can also affect the density around the probes, which can cause false results (Siddiqui et al. 2000).

Figure 6.7.3: Soil Grains displacement during insertion

Movement during insertion can also impact the waveform. This happens when the soil has a high density or a very low density. At high density, the friction on the probe creates the need to apply more force on the TDR. Thus, by adding more force, the TDR can move. At low density, the TDR can move freely and is not supported by the soil, which creates voids along the probes. A small experiment was done to determine the highest impact on the waveform of the wobbling. The results are shown in Figure 6.7.4. The initial waveform prior to wobbling is put on the same graph as the waveform obtained after the wobbling. The t_2 moved from 1400 ps to 1150 ps, changing the permittivity from 4.6 to 1.9. That 17.9% decrease in the t_2 value results in an error of -58.8%, which is significant. For this reason, the TDR should be inserted carefully and stabilized to limit movement during insertion and when it is in its final placement.
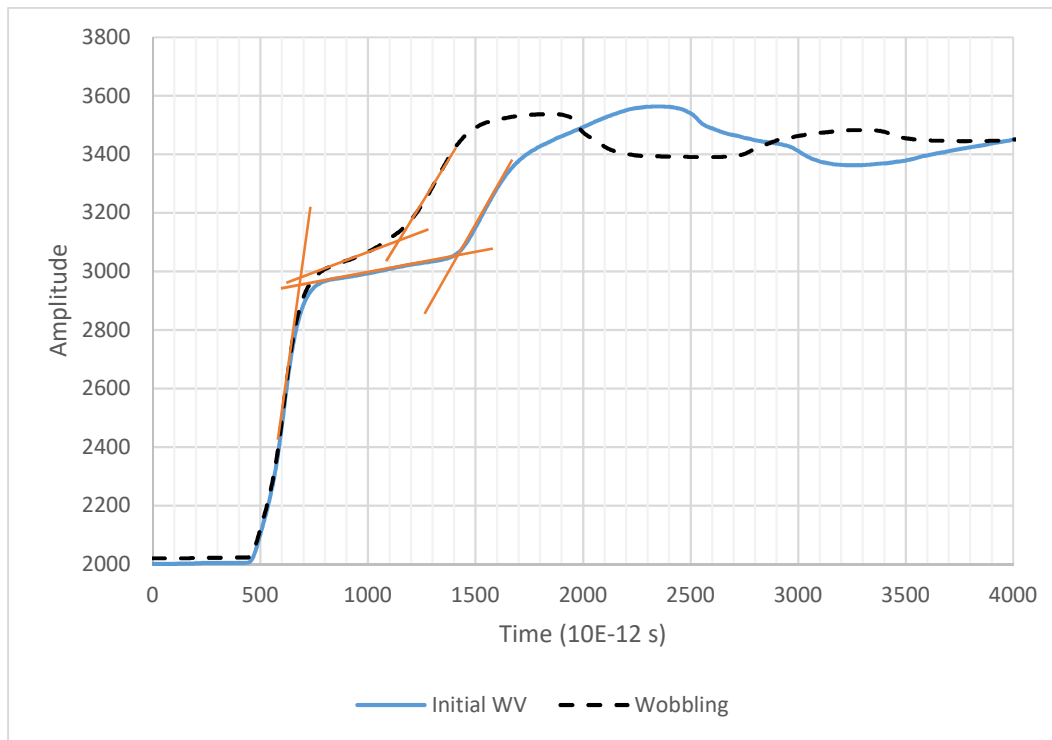
Figure 6.7.4: Effect of TDR wobbling on the waveform obtained from TDR 305

6.7.3 Soil properties

Soil properties can be a source of error because of its mineralogy or when the grain size distribution is less uniform. For these reasons, it's important to know the soils properties such as its grain maximum diameter, grain size distribution and mineralogy in order to interpret the TDR measurement results.

The electrical properties of soil are defined in this case as how the soil affects the magnetic field and how it interacts with other materials. A good example of soil's electrical properties is the presence of magnetic fines in soil, shown in Figure 6.7.5. The figure is a magnetic fine on a magnet that was inserted into the soil. It can affects the permittivity either by increasing or decreasing it by affecting the general polarization molecule of the material (Mohamed and Marwan 2011) . As for soil interaction with other materials present in soil, clay-water interaction is a good example. Because the clay particles' properties are charged, it can affect the orientation and arrangement of water molecules. Moreover, clay is frequency-dependent because the frequency affects its molecule's reorientation.

Figure 6.7.5: Magnetic fines on a magnet after being inserted into soil

The soil's properties, such as the grain size distribution, could also have an effect on results consistency. It is assumed that taking measurements in uniform soils can result in more consistent results than in well-distributed soil. Figure 6.7.6 shows a close view of the border between the TDR probe and two soils with different grain size distributions. The uniform soil has soil grains that are positioned uniformly along the probe. Every time the TDR is inserted in the uniform soil, the chances are the same grain arrangement will be along the probe, resulting in the same void volume. The heterogeneous soil has different grain sizes arranged randomly along the probe. Each time the probe is inserted into the heterogeneous soil, a different grain arrangement is obtained, resulting in a different void volume. Also, permittivity measured in dry or fully saturated soil will obtain a consistent permittivity because the voids are homogeneous when filled with one material, such as air and water. If it is partially saturated, it can be possible to obtain a difference in the measured permittivity. The impact of the materials along the probe is higher and then decreases with the increase of the distance from the TDR probe. However, the impact on permittivity depends on the difference between the material's permittivity and the distance from the probe and the surrounding material, which affects the influence zone of the TDR. In the case of heterogeneous soil, the void will have more impact, especially when the soil is saturated because of the high permittivity of

water. Not as high as the water, but voids in dry soil can also impact the consistency of the permittivity because the permittivity of air is closer to the permittivity of the soil than water. As for the interference zone range, it depends on the surrounding material; the propagation distance of the electrical field is different in each material and depends on the characteristics of the TDR.
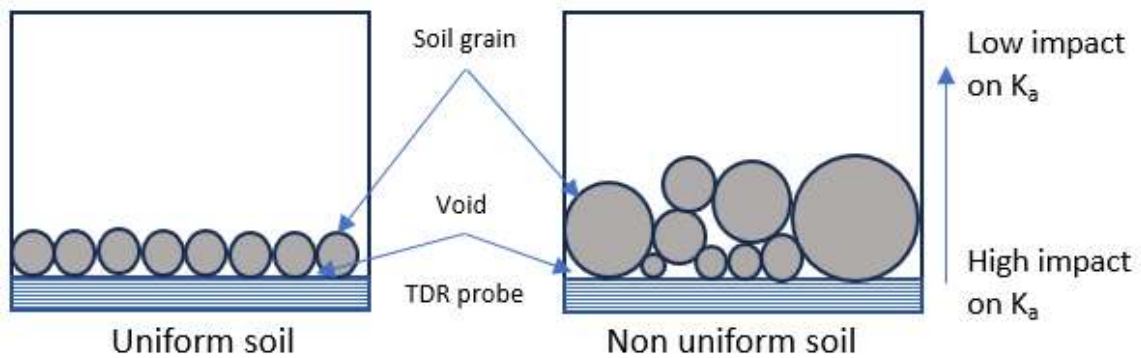
Figure 6.7.6: Grains arrangement near TDR probe representation of a uniform soil and non uniform soil

Chapter 7: Conclusion

7.1 Conclusion

In this research, a method was developed to correct the waveform of a partially inserted TDR into a soil column. When a TDR is laterally inserted into a column filled with soil, it collects a waveform containing the column's wall and the soil in that column that the probes crosses. Therefore, considering the full waveform length may result in erroneous permittivity values due to the influence of the column wall. Literature shows that the column wall effect on the waveform was often either not considered (the authors do not even presented it or discussed it) or was overlooked due to the limited resolution of the waveform. In this study, the analysis of all experimental data demonstrated that neglecting to correct the waveform for partial penetration of the TDR probes in the soil in the column can lead to an underestimation of permittivity up to 30%. To validate the correction method, two Plexiglas columns of same wall thickness but different heights and diameters were built and checked for leakage. The TDRs were then used in multiple set up experiments involving gradual insertion of TDR, multi-setup, and multilayer experiments.

Starting with the correction method where K_{aB} is obtained on columns either empty (air) or filled with water. The permittivity of the column's wall was expected to be just above 3 because of the presence of Plexiglas, rubber O-ring and air. However, the obtained permittivity K_{aB} is different because of the void between the probe and the Plexiglas surface inside the hole. Adjustments during the construction of the column cause that void. The void has a higher effect on K_{aB} when it is filled with water, resulting in a permittivity of up to 10. Consequently, the condition of the void during the experiment has to be considered to use the correct K_{aB}. Otherwise, an erroneous result will be obtained.

The gradual insertion objective was to analyze the soil's t_1 movement and the partial insertion method at different probe lengths in the air and in the soil. In this case, the section of the probe in the air has different lengths, where initially, the TDR probes cross the column's wall, which includes the rubber O-ring. As the probes get inserted, the probe's length in air and soil changes. The experiments showed that a small insertion in soil results in an unrealistic soil permittivity K_{aS}. But, as the probe is being inserted, the results converge to the fully laterally inserted probes. As for the t_1 movement, the measured t_1 didn't follow the linear tendency obtained when the K_{aS} was

calculated with the refractive index. However, when the linear regression was applied to the measured K_{aS}, the linear curve slopes had the same tendency. It was determined that considering the column's wall and air layer as one layer would be more accurate, but the calibration must be done for each length, and a relation with K_{aB} can be made.

In the multi-setup experiment, TDR was used in multiple layouts on the column SC filled with soil at different water contents to study the effect of interferences between TDRs for the specific column, the effect of reinsertion on K_{aS}, the effect of the TDR probes length. This experiment showed that this specific layout has no interferences between TDRs. In fact, verification of TDR interferences with other instruments must be part of the apparatus preparation. The effect of TDR reinsertion at the same position has an effect on the permittivity only when there is small movement during reinsertion. A reinsertion in dry soil affects the permittivity less because of soil grain rearrangement. As for the moist soil, the effect is more pronounced because of the cohesion of soil grains. This showed that wobbling has a noticeable effect on the permittivity because of the void closer to the probe. When the partial insertion was verified in this experiment, it showed a difference between the measured permittivity of the soil and the permittivity of the soil obtained with the correction method ranged from 0.0 to ± 0.2. This proves that the correction method is done accurately and works. The effect of the TDR length on the accuracy of measuring the permittivity was affected by the variations in soil. Longer TDR probes will have more measurement volume, which causes a difference in permittivity with smaller TDR probes in soil with heterogeneous conditions.

In the multi-layer experiment, two layers of the same sandy soil compacted at two different levels were installed into column BC. In the column, one TDR with a probe length of 100 mm was inserted vertically, and two TDR with a probe length of 50 mm were inserted laterally in each layer to compare the lateral insertion to the vertical insertion in a multilayers experiment. It was demonstrated that the waveforms obtained from the vertical insertion are more complex to interpret because of the transition delays between the two layers of unknown dielectric properties. A serious complexity in the case of heterogeneous soil conditions where the waveforms can be of increased complexity to interpret. However, the results obtained from TDR lateral insertion proved to be more reliable when the proposed correction is applied. A base layer was added to facilitate vertical insertion because of the way the column BC was built. In some tests, the vertical TDR probes may be inserted for a maximum depth of 4 mm. That section could have affected the interpretation of

the measured permittivity even if it wasn't noticeable on the vertical insertion waveform. A laterally inserted TDR in the base layer could help to determine the permittivity of that small insertion.

The multi-layer experiment was also used to analyze the refractive index and arithmetic meaning method used to determine the average permittivity. The obtained results showed that for this experiment, there was no difference between methods when the average methods were used on the laterally inserted TDRs results. However, the interpretation of the vertical waveform total permittivity and the average permittivity of the lateral insertion showed that there is a difference ranging from 1.4 to 4.1. This represent 22% to 46% of the vertical waveform total permittivity. It is caused by a signal delay that is affected by the number of layers, layers thickness ratio, condition of the border between both layers, permittivity ratio and the pulse characteristic. A numerical analysis was done to determine how the parameters such as permittivity ratio and length ratio affect the difference between both averaging methods. It was determined that with the length ratio of 0.3 that represents all the experiments in this work, a relative difference of the refractive index to the arithmetic range from 0% to 60% when the layer's permittivity ratio is below 1. Above a permittivity ratio of 1, the relative difference ranges from 0% to 16%. Most of the obtained data with the permittivity ratio between 1 and 10 showed a relative difference between 0% and 10%. As for the waveform fitting, the study showed that the refractive index represents the waveforms better for this thesis experiments.

A total of 167 waveforms were obtained and interpreted using the Tangent method, Heimovaara method, and Schwartz method. The Heimovaara interpretation method use a fixed t_1 obtained with known permittivity materials such as water and air where the obtained t_1 are different. That difference was negligible for TDR with longer probes but not the case for small TDR probes. Because of this, it was decided to use the t_1 obtained in water's waveform because of the accurate waveform interpretation. Then, since water's temperature has an effect on the permittivity, where a variation was noticed in t_1 values which wasn't discussed in Heimovaara (1993). That variation in waveform obtained in moist or wet soil can be negligible, but at lower permittivity, that variation can have an impact on the permittivity precision. Thus, it was decided that the choice of t_1 would be based on the experiment's temperature range, which is between 18°C and 22°C.

The comparison between methods showed that the difference between the tangent method and the Heimovaara and Schwartz methods increases with the permittivity. The difference between the Heimovaara method and the tangent method is explained by the fixed t_1 of the Heimovaara method, as they have the same t_2. Thus, the cause of the difference is the difference between the t_1 of each method. As for the Schwartz method, the difference is explained by the difference of t_2. In the multi-setup experiment, the permittivities below 6 showed no difference between interpretation methods. Conversely, the permittivities above 8 showed noticeable differences up to 25%. It was demonstrated that t_1 doesn't vary as much as t_2, which explains the low difference with the Heimovaara method and the difference with the Schwartz method.

7.2   Recommendations and future work

The correction method was done in the temperature range that doesn't change too much. However, it is recommended that K_{aB} calibration be done at different temperatures during the experiment in order to make an accurate correction. The same can be said with the variation of the column's wall if compressible material is used. These could be used to determine the errors related to the partial insertion of the TDR probes. However, there is still work to be done on the multi-layer field. Thus, future work will be done to study the multilayer waveform analysis.

List of references

Baker, J.M., and Allmaras, R.R. 1990. System for Automating and Multiplexing Soil Moisture Measurement by Time-Domain Reflectometry. Soil Science Society of America Journal, 54(1): 1–6. doi:10.2136/sssaj1990.03615995005400010001x.

Bhuyan, H., Scheuermann, A., Bodin, D., and Becker, R. 2018. Soil moisture and density monitoring methodology using TDR measurements. International Journal of Pavement Engineering, 21(10): 1263–1274. doi:10.1080/10298436.2018.1537491.

Birchak, J.R., Gardner, C.G., Hipp, J.E., and Victor, J.M. 1974. High dielectric constant microwave probes for sensing soil moisture. Proceedings of the IEEE, 62(1): 93–98. doi:10.1109/PROC.1974.9388.

Brown, W.F. 1956. Dielectrics. *In* Dielectrics / Dielektrika. *Edited by* W.F. Brown, W. Franz, and P.W. Forsbergh. Springer, Berlin, Heidelberg. pp. 1–154.

Chan, C.Y., and Knight, R.J. 1999. Determining water content and saturation from dielectric measurements in layered materials. Water Resources Research, 35(1): 85–93. doi:10.1029/1998WR900039.

Chan, C.Y., and Knight, R.J. 2001a. Laboratory measurements of electromagnetic wave velocity in layered sands. Water Resources Research, 37(4): 1099–1105. doi:10.1029/2000WR900356.

Chan, C.Y., and Knight, R.J. 2001b. Laboratory measurements of electromagnetic wave velocity in layered sands. Water Resources Research, 37(4): 1099–1105. doi:10.1029/2000WR900356.

Chung, C.-C., Lin, C.-P., Ngui, Y.J., Lin, W.-C., and Yang, C.-S. 2022. Improved technical guide from physical model tests for TDR landslide monitoring. Engineering Geology, 296: 106417. doi:10.1016/j.enggeo.2021.106417.

Curioni, G., Chapman, D.N., Royal, A.C.D., Metje, N., Dashwood, B., Gunn, D.A., Inauen, C.M., Chambers, J.E., Meldrum, P.I., Wilkinson, P.B., Swift, R.T., and Reeves, H.J. 2019. Time domain reflectometry (TDR) potential for soil condition monitoring of geotechnical assets. Canadian Geotechnical Journal, 56(7): 942–955. doi:10.1139/cgj-2017-0618.

Dobson, M., Ulaby, F., Hallikainen, M., and El-rayes, M. 1985. Microwave Dielectric Behavior of Wet Soil-Part II: Dielectric Mixing Models. IEEE Transactions on Geoscience and Remote Sensing, GE-23(1): 35–46. doi:10.1109/TGRS.1985.289498.

Dowding, C., Huang, F., and McComb, P. 1996. Water Pressure Measurement with Time Domain Reflectometry Cables. Geotechnical Testing Journal, 19(1): 58–64. doi:10.1520/GTJ11408J.

Feng, W., Lin, C.P., Deschamps, R.J., and Drnevich, V.P. 1999. Theoretical model of a multisection time domain reflectometry measurement system. Water Resources Research, 35(8): 2321–2331. doi:10.1029/1999WR900123.

Ghavam-Nasiri, A., El-Zein, A., and Airey, D. 2017. Hydration and desiccation of geosynthetic clay liners in composite lining systems under brine pond conditions: A laboratory investigation.

Greco, R. 2006. Soil water content inverse profiling from single TDR waveforms. Journal of Hydrology, 317(3–4): 325–339. doi:10.1016/j.jhydrol.2005.05.024.

Hasted, J.B. 1973. Aqueous Dielectrics. Chapman and Hall [Distributed in the U.S.A. by Halsted Press, a division of J. Wiley & Sons, New York.

Heimovaara, T.J. 1993. Design of Triple-Wire Time Domain Reflectometry Probes in Practice and Theory. Soil Science Society of America Journal, 57(6): 1410–1417. doi:10.2136/sssaj1993.03615995005700060003x.

Heimovaara, T.J., and Bouten, W. 1990a. A computer-controlled 36-channel time domain reflectometry system for monitoring soil water contents. Water Resources Research, 26(10): 2311–2316. doi:10.1029/WR026i010p02311.

Heimovaara, T.J., Freijer, J.I., and Bouten, W. 1993. The application of TDR in laboratory column experiments. Soil Technology, 6(3): 261–272. doi:10.1016/0933-3630(93)90015-7.

Hilhorst, M.A. 1998. Dielectric characterisation of soil. Wageningen Agricultural University, Wageningen, Netherlands.

Jung, S., Drnevich, V.P., and Abou Najm, M.R. 2013. New Methodology for Density and Water Content by Time Domain Reflectometry. Journal of Geotechnical and Geoenvironmental Engineering, 139(5): 659–670. doi:10.1061/(ASCE)GT.1943-5606.0000783.

Keng, J.C.W., and Topp, G.C. 1983. Measuring water content of soil columns in the laboratory: A comparison of gamma ray attenuation and TDR techniques. Canadian Journal of Soil Science.

Looyenga, H. 1965. Dielectric constants of heterogeneous mixtures. Physica, 31(3): 401–406. doi:10.1016/0031-8914(65)90045-5.

Mohamed, A.-M.O., and Marwan, S.S. 2011. Impact of Soil Magnetic Properties on Moisture Content Prediction Using TDR. Geotechnical Testing Journal, 34(3): 273–278. doi:10.1520/GTJ102792.

Or, D., and Wraith, J.M. 1999. Temperature effects on soil bulk dielectric permittivity measured by time domain reflectometry: A physical model. Water Resources Research, 35(2): 371–383. doi:10.1029/1998WR900008.

Robinson, D.A., Schaap, M., Jones, S.B., Friedman, S.P., and Gardner, C.M.K. 2003. Considerations for Improving the Accuracy of Permittivity Measurement using Time Domain Reflectometry: Air-Water Calibration, Effects of Cable Length. Soil Science Society of America Journal, 67(1): 62–70. doi:10.2136/sssaj2003.6200.

S. R. Evett. 2000. THE TACQ COMPUTER PROGRAM FOR AUTOMATIC TIME DOMAIN REFLECTOMETRY MEASUREMENTS: II. WAVEFORM INTERPRETATION METHODS. Transactions of the ASAE, 43(6): 1947–1956. doi:10.13031/2013.3100.

Schaap, M.G., Robinson, D.A., Friedman, S.P., and Lazar, A. 2003. Measurement and Modeling of the TDR Signal Propagation through Layered Dielectric Media. Soil Science Society of America Journal, 67(4): 1113–1121. doi:10.2136/sssaj2003.1113.

Schanz, T., Nguyen Tuan, L., and Baille, W. 2011. Effects of Temperature on Measurements of Soil Water Content with Time Domain Reflectometry. Geotechnical Testing Journal, 34: in print. doi:10.1520/GTJ103152.

Schwartz, R.C., Casanova, J.J., Bell, J.M., and Evett, S.R. 2014. A Reevaluation of Time Domain Reflectometry Propagation Time Determination in Soils. Vadose Zone Journal, 13(1): vzj2013.07.0135. doi:10.2136/vzj2013.07.0135.

Schwartz, R.C., Evett, S.R., Anderson, S.K., and Anderson, D.J. 2016. Evaluation of a Direct-Coupled Time-Domain Reflectometry for Determination of Soil Water Content and Bulk Electrical Conductivity. Vadose Zone Journal, 15(1): vzj2015.08.0115. doi:10.2136/vzj2015.08.0115.

Schwartz, R.C., Evett, S.R., Pelletier, M.G., and Bell, J.M. 2009. Complex Permittivity Model for Time Domain Reflectometry Soil Water Content Sensing: I. Theory. Soil Science Society of America Journal, 73(3): 886–897. doi:10.2136/sssaj2008.0194.

Stogryn, A.P., Bull, H.T., Rubayi, K., and Iravanchy, S. 1995. The microwave permittivity of sea and fresh water. GenCorp Aerojet, Azusa, CA,.

Technion, S.N. 2023. Is the soil dry density important when using TDR?

Thuro, K., Singer, J., Festl, J., Wunderlich, T., Wasmeier, P., Reith, C., Heunecke, O., Glabsch, J., and Schuhbäck, S. 2010. New landslide monitoring techniques – developments and experiences of the alpEWAS project. Journal of Applied Geodesy, 4(2). doi:10.1515/jag.2010.008.

Topp, G.C., Davis, J.L., and Annan, A.P. 1980. Electromagnetic determination of soil water content: Measurements in coaxial transmission lines. Water Resources Research, 16(3): 574–582. doi:10.1029/WR016i003p00574.

Topp, G.C., Davis, J.L., and Annan, A.P. 1982. Electromagnetic Determination of Soil Water Content Using TDR: I. Applications to Wetting Fronts and Steep Gradients.

Topp, G.C., Zegelin, S., and White, I. 2000. Impacts of the Real and Imaginary Components of Relative Permittivity on Time Domain Reflectometry Measurements in Soils. Soil Science Society of America Journal, 64(4): 1244–1252. doi:10.2136/sssaj2000.6441244x.

Yang, H., Rahardjo, H., Leong, E.C., and Fredlund, D.G. 2004. A study of infiltration on three sand capillary barriers. Canadian Geotechnical Journal, 41(4): 629–643. doi:10.1139/t04-021.

Yu, X., and Drnevich, V.P. 2004. Soil Water Content and Dry Density by Time Domain Reflectometry. Journal of Geotechnical and Geoenvironmental Engineering, 130(9): 922–934. doi:10.1061/(ASCE)1090-0241(2004)130:9(922).

Appendix

List of figures

128

List of tables

A. Thermometer verification

Table. A.1: Thermometer 1 verification results

Thermo 2	Thermo 1		Thermo 3		
Measured T	Measured T	ΔT	Measured T	Round Measured T	ΔT
°C	°C	°C	°C	°C	°C
± 0.1	± 0.1		± 0.01		
5.8	6.1	0.3	5.69	5.7	-0.1
5.8	6.1	0.3	5.69	5.7	-0.1
6.1	6.5	0.4	6.09	6.1	0.0
10.1	9.9	-0.2	10.05	10.1	0.0
10.2	9.9	-0.3	10.12	10.1	-0.1
10.3	10.1	-0.2	10.21	10.2	-0.1
14.9	14.8	-0.1	14.79	14.8	-0.1
15.1	15.0	-0.1	14.94	14.9	-0.2
15.1	15.1	0	15.00	15.0	-0.1
20.2	20.1	-0.1	20.07	20.1	-0.1
20.2	20.1	-0.1	20.07	20.1	-0.1
20.2	20.1	-0.1	20.07	20.1	-0.1
25.1	24.9	-0.2	24.87	24.9	-0.2
25.1	24.9	-0.2	27.87	-	-
25.1	24.9	-0.2	24.88	24.9	-0.2
31.3	31.6	0.3	31.06	31.1	-0.2
31.3	31.6	0.3	31.04	31.0	-0.3
31.2	31.6	0.4	31.05	31.1	-0.1
39.7	39.6	-0.1	39.6	39.6	-0.1
39.9	39.7	-0.2	39.66	39.7	-0.2
39.9	39.7	-0.2	39.72	39.7	-0.2
48.2	48.1	-0.1	48.03	48.0	-0.2
47.7	47.6	-0.1	47.55	47.6	-0.1
48.1	48.1	0	47.99	48.0	-0.1

B. Heimovaara method t_1 and t_2 variation with water temperature variation (TABLES)

Ka Water	a			b	Test																
				Hasted		1		2		3		4		5							
TDR #	Name	Lr	T°	Theo Ka	Δt Hasted	t1	t2	t1	t2	t1	t2	t1	t2	t1	t2	Max var. t1	Max var. t2	Avg t1	Avg t2	Ecart max de t1	Relative Error
		m	°C		ps	ps	ps	ps	ps	ps	ps	ps	ps	ps	ps	ps	ps	ps	ps	ps	%
434																					
	H434-6.1	0.1	6.1	85.33	6158	717	6875	719	6877	715	6873	732	6890	738	6896	23	23	724	6882	23	3.2%
	H434-10.3	0.1	10.3	83.72	6100	740	6840	738	6838	750	6850	745	6845	745	6845	12	12	744	6844	12	1.6%
	H434-15.1	0.1	15.1	81.91	6034	764	6798	766	6800	766	6800	761	6795	761	6795	5	5	764	6798	5	0.7%
	H434-20.2	0.1	20.2	80.03	5964	784	6748	781	6745	781	6745	781	6745	776	6740	8	8	781	6745	8	1.0%
	H434-25.1	0.1	25.1	78.27	5898	804	6702	802	6700	794	6692	797	6695	796	6694	10	10	799	6697	10	1.3%
	H434-31.2	0.1	31.2	76.13	5817	795	6612	787	6604	786	6603	788	6605	790	6607	9	9	789	6606	9	1.1%
	H434-39.9	0.1	39.9	73.18	5703	795	6498	797	6500	804	6507	797	6500	802	6505	9	9	799	6502	9	1.1%
	H434-48.1	0.1	48.1	70.51	5598	740	6338	749	6347	742	6340	737	6335	742	6340	12	12	742	6340	12	1.6%
					Avg	767	6676	767	6676	767	6676	767	6676	769	6678						
					Max Variation	87	537	83	530	89	533	65	555	64	556						
144																					
	H144-5.8	0.049	5.8	85.45	3020	739	3759	740	3760	738	3758	745	3765	750	3770	12	12	743	3762	12	1.6%
	H144-10.2	0.049	10.2	83.76	2990	755	3745	752	3742	750	3740	755	3745	750	3740	5	5	753	3742	5	0.7%
	H144-15.1	0.049	15.1	81.91	2956	768	3724	772	3728	781	3737	774	3730	774	3730	13	13	773	3730	13	1.7%
	H144-20.2	0.049	20.2	80.03	2922	780	3702	774	3696	777	3699	770	3692	770	3692	10	10	774	3696	10	1.3%
	H144-25.1	0.049	25.1	78.27	2890	778	3668	775	3665	785	3675	776	3666	780	3670	10	10	779	3669	10	1.3%
	H144-31.3	0.049	31.3	76.09	2850	789	3639	793	3643	788	3638	784	3634	785	3635	9	9	788	3638	9	1.1%
	H144-39.9	0.049	39.9	73.18	2795	746	3541	753	3548	750	3545	746	3541	748	3543	7	7	749	3544	7	0.9%
	H144-47.7	0.049	47.7	70.64	2746	711	3457	706	3452	709	3455	708	3454	711	3457	5	5	709	3455	5	0.7%
					Avg	758	3654	758	3654	760	3656	757	3653	759	3655						
					Max Variation	78	302	87	308	79	303	76	311	74	313						
152																					
	H152-5.8	0.049	5.8	85.45	3020	676	3696	677	3697	678	3698	673	3693	673	3693	5	5	676	3695	5	0.7%
	H152-10.1	0.049	10.1	83.79	2990	659	3649	672	3662	668	3658	671	3661	668	3658	13	13	667	3658	13	1.9%
	H152-14.9	0.049	14.9	81.98	2958	681	3639	680	3638	689	3647	679	3637	684	3642	10	10	683	3641	10	1.5%
	H152-20.2	0.049	20.2	80.03	2922	684	3606	683	3605	675	3597	671	3593	660	3582	24	24	674	3597	24	3.6%
	H152-25.1	0.049	25.1	78.27	2890	692	3582	691	3581	691	3581	683	3573	692	3582	9	9	690	3580	9	1.3%
	H152-31.3	0.049	31.3	76.09	2850	685	3535	683	3533	683	3533	685	3535	679	3529	6	6	683	3533	6	0.9%
	H152-39.7	0.049	39.7	73.25	2796	691	3487	687	3483	694	3490	685	3481	684	3480	10	10	688	3484	10	1.5%
	H152-48.2	0.049	48.2	70.48	2742	626	3368	618	3360	628	3370	632	3374	625	3367	14	14	625	3368	14	2.2%
					Avg	674	3570	674	3570	676	3572	672	3568	671	3567						
					Max Variation	66	328	73	337	67	328	54	319	67	326						

Figure. B.1: Results Heimovaara method versus water temperature using Hasted (1973) as a reference

Ka Water	a				Storgyn	Test		1		2		3		4		5							
TDR #	Measured Ka	Lr	T°	Ka theo	Δt Storgyn	t1	t2	t1	t2	t1	t2	t1	t2	t1	t2	t1	t2	Max var. t1	Max var. t2	Avg t1	Avg t2	Ecart max de t1	Relative Error
		m	°C		ps	ps	ps	ps	ps	ps	ps	ps	ps	ps	ps	ps	ps	ps	ps	ps	ps	ps	%
434																							
S434-6.1	0.1	6.1	85.49	6164	711	6875	713	6877	709	6873	726	6890	732	6896	23	23	**718**	**6882**	23	3.2%
S434-10.3	0.1	10.3	83.86	6105	735	6840	733	6838	745	6850	740	6845	740	6845	12	12	**738**	**6844**	12	1.6%
S434-15.1	0.1	15.1	82.04	6038	760	6798	762	6800	762	6800	757	6795	757	6795	5	5	**759**	**6798**	5	0.7%
S434-20.2	0.1	20.2	80.15	5968	780	6748	777	6745	777	6745	777	6745	772	6740	8	8	**776**	**6745**	8	1.0%
S434-25.1	0.1	25.1	78.37	5902	800	6702	798	6700	790	6692	793	6695	792	6694	10	10	**795**	**6697**	10	1.3%
S434-31.2	0.1	31.2	76.20	5820	792	6612	784	6604	783	6603	785	6605	787	6607	9	9	**787**	**6606**	9	1.1%
S434-39.9	0.1	39.9	73.22	5705	793	6498	795	6500	802	6507	795	6500	800	6505	9	9	**797**	**6502**	9	1.1%
S434-48.1	0.1	48.1	70.51	5598	740	6338	749	6347	742	6340	737	6335	742	6340	12	12	**742**	**6340**	12	1.6%
				Avg	**764**	**6676**	**764**	**6676**	**764**	**6676**	**764**	**6676**	**765**	**6678**						
				Max Variation	**90**	**537**	**86**	**530**	**94**	**533**	**70**	**555**	**69**	**556**						
144																							
S144-5.8	0.049	5.8	85.61	3023	736	3759	737	3760	735	3758	742	3765	747	3770	12	12	**740**	**3762**	12	1.6%
S144-10.2	0.049	10.2	83.90	2992	753	3745	750	3742	748	3740	753	3745	748	3740	5	5	**750**	**3742**	5	0.7%
S144-15.1	0.049	15.1	82.04	2959	765	3724	769	3728	778	3737	771	3730	771	3730	13	13	**771**	**3730**	13	1.7%
S144-20.2	0.049	20.2	80.15	2924	778	3702	772	3696	775	3699	768	3692	768	3692	10	10	**772**	**3696**	10	1.3%
S144-25.1	0.049	25.1	78.37	2892	776	3668	773	3665	783	3675	774	3666	778	3670	10	10	**777**	**3669**	10	1.3%
S144-31.3	0.049	31.3	76.17	2851	788	3639	792	3643	787	3638	783	3634	784	3635	9	9	**787**	**3638**	9	1.1%
S144-39.9	0.049	39.9	73.22	2795	746	3541	753	3548	750	3545	746	3541	748	3543	7	7	**748**	**3544**	7	0.9%
S144-47.7	0.049	47.7	70.64	2746	711	3457	706	3452	709	3455	708	3454	711	3457	5	5	**709**	**3455**	5	0.7%
				Avg	**757**	**3654**	**757**	**3654**	**758**	**3656**	**756**	**3653**	**757**	**3655**						
				Max Variation	**77**	**302**	**86**	**308**	**78**	**303**	**75**	**311**	**73**	**313**						
152																							
S152-5.8	0.049	5.8	85.61	3023	673	3696	674	3697	675	3698	670	3693	670	3693	5	5	**673**	**3695**	5	0.7%
S152-10.1	0.049	10.1	83.94	2993	656	3649	669	3662	665	3658	668	3661	665	3658	13	13	**665**	**3658**	13	2.0%
S152-14.9	0.049	14.9	82.12	2960	679	3639	678	3638	687	3647	677	3637	682	3642	10	10	**680**	**3641**	10	1.5%
S152-20.2	0.049	20.2	80.15	2924	682	3606	681	3605	673	3597	669	3593	658	3582	24	24	**672**	**3597**	24	3.6%
S152-25.1	0.049	25.1	78.37	2892	690	3582	689	3581	689	3581	681	3573	690	3582	9	9	**688**	**3580**	9	1.3%
S152-31.3	0.049	31.3	76.17	2851	684	3535	682	3533	682	3533	684	3535	678	3529	6	6	**682**	**3533**	6	0.9%
S152-39.7	0.049	39.7	73.29	2797	690	3487	686	3483	693	3490	684	3481	683	3480	10	10	**688**	**3484**	10	1.5%
S152-48.2	0.049	48.2	70.48	2742	626	3368	618	3360	628	3370	632	3374	625	3367	14	14	**625**	**3368**	14	2.2%
				Avg	**673**	**3570**	**672**	**3570**	**674**	**3572**	**671**	**3568**	**669**	**3567**						
				Max Variation	**65**	**328**	**72**	**337**	**66**	**328**	**53**	**319**	**66**	**326**						

Figure. B.2: Results Heimovaara method versus water temperature using Storgyn (1995) as a reference

C. Multi setups data

Table. C.1: Multi setup t_1 and t_2 variation result with the permittivity K_{aS}

	Tangent				Heimovaara			
Dry	ΔtS	Dry Tan t1	Dry Tan t2	Tan KaS	ΔtS	Dry Heimo t1	Dry Heimo t2	Heimo KaS
	ps	ps	ps		ps	ps	ps	
K11L	406	753	1159	2.57	409	756	1165	2.60
K21L	410	752	1162	2.62	409	756	1165	2.60
K22V	518	751	1269	2.51	487	779	1266	2.22
K32V	514	747	1261	2.48	488	779	1267	2.23
K41V	512	668	1180	2.46	491	687	1178	2.26
K42V	528	747	1275	2.61	496	779	1275	2.31
K51V	506	669	1175	2.40	485	687	1172	2.20
K63V	1218	790	2008	3.34	1223	782	2005	3.37
K61V	509	669	1178	2.43	488	687	1175	2.23
K73V	1215	790	2005	3.32	1224	782	2006	3.37
K83V	1220	785	2005	3.35	1223	782	2005	3.37
K81L	416	750	1166	2.70	411	756	1167	2.63
K91L	418	749	1167	2.72	413	756	1169	2.66
K102V	508	749	1257	2.42	481	779	1260	2.17
Moist	ΔtS	Moist Tan t1	Moist Tan t2	Tan KaS	ΔtS	Moist Heimo t1	Moist Heimo t2	Heimo KaS
	ps	ps	ps		ps	ps	ps	
K11L	537	768	1305	4.50	549	756	**1305**	4.69
K21L	546	761	1307	4.65	547	756	**1303**	4.66
K22V	691	755	1446	4.47	671	779	**1450**	4.22
K32V	694	755	1449	4.51	671	779	**1450**	4.22
K41V	690	675	1365	4.46	680	687	**1367**	4.33
K42V	692	758	1450	4.49	671	779	**1450**	4.22
K51V	690	675	1365	4.46	679	687	**1366**	4.32
K63V	1591	772	2363	5.70	1584	782	**2366**	5.65
K61V	688	676	1364	4.44	673	687	**1360**	4.24
K73V	1591	769	2360	5.70	1581	782	**2363**	5.62
K83V	1587	774	2361	5.67	1576	782	**2358**	5.59
K81L	524	760	1284	4.28	529	800	**1285**	4.36
K91L	531	758	1289	4.39	531	800	**1287**	4.39
K102V	673	755	1428	4.24	653	779	**1432**	4.00

Wet	ΔtS	Wet Tan t1	Wet Tan t2	Tan KaS	ΔtS	Wet Heimo t1	Wet Heimo t2	Heimo KaS
	ps	ps	ps		ps	ps	ps	
K11L	1142	814	1956	20.3	1076	882	**1958**	18.0
K21L	1131	819	1950	19.9	1069	882	**1951**	17.8
K22V	815	758	1573	6.2	794	779	**1573**	5.9
K32V	807	759	1566	6.1	786	779	**1565**	5.8
K41V	797	678	1475	6.0	787	687	**1474**	5.8
K42V	817	758	1575	6.3	794	779	**1573**	5.9
K51V	793	675	1468	5.9	780	687	**1467**	5.7
K63V	2366	778	3144	12.6	2358	782	**3140**	12.5
K61V	771	681	1452	5.6	765	687	**1452**	5.5
K73V	2363	779	3142	12.6	2356	782	**3138**	12.5
K83V	2362	780	3142	12.6	2358	782	**3140**	12.5
K81L	1111	812	1923	19.2	1044	882	**1926**	17.0
K91L	1112	811	1923	19.3	1043	882	**1925**	17.0
K102V	732	759	1491	5.0	709	779	**1488**	4.7

D. Gradual insertion experiment data

Table. D.1: Gradual insertion results using tangent method test #4

TDR#	ρb	T	LrT	LrA	LrB	LrS	KaT	ΔtT	ΔtA	ΔtB	**ΔtS**	KaS	Measured KaS	KaS diff
	g/cm3	°C	m	m	m	m		ps	ps	ps	**ps**			
152	1.86	24.7	0.049	0.033	0.0107	0.005	2.05	468	220	130	**118**	11.1	**9.9**	**1.2**
			0.049	0.0275	0.0107	0.011	2.59	526	183	130	**212**	8.7	**9.9**	**-1.2**
			0.049	0.018	0.0107	0.020	5.76	784	120	130	**534**	15.6	**9.9**	**5.6**
			0.049	0.008	0.0107	0.030	7.47	893	53	130	**709**	12.3	**9.9**	**2.4**
			0.049	0	0.0107	0.038	8.19	935	0	130	**805**	9.9	**9.9**	**0.0**

Table. D.2: Gradual insertion results using tangent method test #5

TDR#	ρb	T	LrT	LrA	LrB	LrS	KaT	ΔtT	ΔtA	ΔtB	**ΔtS**	KaS	Measured KaS	KaS diff
	g/cm3	°C	m	m	m	m		ps	ps	ps	**ps**			
152	1.9	24.8	0.049	0.038	0.0107	0.000	1.47	396	253	130	**12**	39.0	**10.1**	28.9
			0.049	0.0235	0.0107	0.015	3.53	614	157	130	**327**	11.0	**10.1**	0.9
			0.049	0.018	0.0107	0.020	5.60	773	120	130	**523**	14.9	**10.1**	4.8
			0.049	0.008	0.0107	0.030	7.39	888	53	130	**704**	12.2	**10.1**	2.0
			0.049	0	0.0107	0.038	8.33	943	0	130	**813**	10.1	**10.1**	0.0

Table. D.3: Gradual insertion results using tangent method test #6

TDR#	ρb	T	LrT	LrA	LrB	LrS	KaT	ΔtT	ΔtA	ΔtB	**ΔtS**	KaS	Measured KaS	KaS diff
	g/cm3	°C	m	m	m	m		ps	ps	ps	**ps**			
152	1.9	24.9	0.049	0.038	0.0107	0.000	1.51	401	253	130	**17**	76.5	9.1	67.5
			0.049	0.028	0.0107	0.010	2.45	511	187	130	**194**	8.0	9.1	-1.1
			0.049	0.018	0.0107	0.020	5.44	762	120	130	**512**	14.3	9.1	5.2
			0.049	0.008	0.0107	0.030	6.44	829	53	130	**645**	10.2	9.1	1.1
			0.049	0	0.0107	0.038	7.57	899	0	130	**769**	9.1	9.1	0.0

Table. D.4: Gradual insertion results using Schwartz method for test#4, test#5 and test#6

	TDR#	ρb	T	LrT	LrA	LrB	LrS	KaT	ΔtT	ΔtA	ΔtB	**ΔtS**	KaS	Measured KaS	KaS diff
		g/cm3	°C	m	m	m	m		ps	ps	ps	**ps**			
Test 4	152	1.86	24.7	0.049	0.033	0.0107	0.005	2.3	495	220	220	**56**	2.5	**8.4**	**-5.9**
				0.049	0.0275	0.0107	0.011	4.1	661	183	220	**258**	12.9	**8.4**	**4.5**
				0.049	0.018	0.0107	0.020	5.6	773	120	220	**433**	10.2	**8.4**	**1.9**
				0.049	0.008	0.0107	0.030	7.6	901	53	220	**627**	9.6	**8.4**	**1.3**
				0.049	0	0.0107	0.038	8.6	958	0	220	**738**	8.4	**8.4**	**0.0**
	TDR#	ρb	T	LrT	LrA	LrB	LrS	KaT	ΔtT	ΔtA	ΔtB	**ΔtS**	KaS	Measured KaS	KaS diff
		g/cm3	°C	m	m	m	m		ps	ps	ps	**ps**			
Test 5	152	1.9	24.8	0.049	0.038	0.0107	0.000	1.8	438	253	220	**-35**	305.0	**8.6**	**296.4**
				0.049	0.0235	0.0107	0.015	4.5	693	157	220	**316**	10.3	**8.6**	**1.7**
				0.049	0.018	0.0107	0.020	5.4	759	120	220	**419**	9.6	**8.6**	**1.0**
				0.049	0.008	0.0107	0.030	7.5	895	53	220	**621**	9.5	**8.6**	**0.9**
				0.049	0	0.0107	0.038	8.8	969	0	220	**749**	8.6	**8.6**	**0.0**
	TDR#	ρb	T	LrT	LrA	LrB	LrS	KaT	ΔtT	ΔtA	ΔtB	**ΔtS**	KaS	Measured KaS	KaS diff
		g/cm3	°C	m	m	m	m		ps	ps	ps	**ps**			
Test 6	152	1.9	24.9	0.049	0.038	0.0107	0.000	1.8	438	253	220	**-35**	305.0	**7.6**	**297.4**
				0.049	0.028	0.0107	0.010	4	653	187	220	**247**	12.9	**7.6**	**5.3**
				0.049	0.018	0.0107	0.020	5.3	752	120	220	**412**	9.3	**7.6**	**1.7**
				0.049	0.008	0.0107	0.030	6.8	852	53	220	**579**	8.2	**7.6**	**0.6**
				0.049	0	0.0107	0.038	8	924	0	220	**704**	7.6	**7.6**	**0.0**

Table. D.5: Gradual insertion results using Heimovaara method for test#4, test#5 and test#6

	TDR#	ρb	T	LrT	LrA	LrB	LrS	KaT	ΔtT	ΔtA	ΔtB	**ΔtS**	KaS	Measured KaS	KaS diff
		g/cm3	°C	m	m	m	m		ps	ps	ps	**ps**			
Test 4	152	1.86	24.7	0.049	0.033	0.0107	0.005	2.00	462	220	190	**52**	2.2	7.9	-5.8
				0.049	0.0275	0.0107	0.011	2.50	516	183	190	**143**	3.9	7.9	-4.0
				0.049	0.018	0.0107	0.020	5.57	771	120	190	**461**	11.6	7.9	3.6
				0.049	0.008	0.0107	0.030	7.11	871	53	190	**628**	9.7	7.9	1.7
				0.049	0	0.0107	0.038	7.76	910	0	190	**720**	7.9	7.9	0.0
	TDR#	ρb	T	LrT	LrA	LrB	LrS	KaT	ΔtT	ΔtA	ΔtB	**ΔtS**	KaS	Measured KaS	KaS diff
		g/cm3	°C	m	m	m	m		ps	ps	ps	**ps**			
Test 5	152	1.9	24.8	0.049	0.038	0.0107	0.000	1.45	393	253	190	**-50**	635.2	8.1	627.1
				0.049	0.0235	0.0107	0.015	3.43	605	157	190	**258**	6.9	8.1	-1.3
				0.049	0.018	0.0107	0.020	5.40	759	120	190	**449**	11.0	8.1	2.9
				0.049	0.008	0.0107	0.030	7.06	868	53	190	**625**	9.6	8.1	1.4
				0.049	0	0.0107	0.038	7.91	919	0	190	**729**	8.1	8.1	0.0
	TDR#	ρb	T	LrT	LrA	LrB	LrS	KaT	ΔtT	ΔtA	ΔtB	**ΔtS**	KaS	Measured KaS	KaS diff
		g/cm3	°C	m	m	m	m		ps	ps	ps	**ps**			
Test 6	152	1.9	24.9	0.049	0.038	0.0107	0.000	1.48	397	253	190	**-46**	538.4	7.2	531.2
				0.049	0.028	0.0107	0.010	2.39	505	187	190	**128**	3.5	7.2	-3.7
				0.049	0.018	0.0107	0.020	5.26	749	120	190	**439**	10.5	7.2	3.3
				0.049	0.008	0.0107	0.030	6.15	810	53	190	**567**	7.9	7.2	0.7
				0.049	0	0.0107	0.038	7.16	874	0	190	**684**	7.2	7.2	0.0

E. Multilayer experiment data

Table. E.1: Maximum relative difference to the arithmetic mean method for each n and length fraction when K1>K2

L fraction\n	Max relative difference							
	-1	-0.75	-0.5	-0.25	0.25	0.5	0.75	1
10-90	87.53	87.14	86.47	85.20	76.77	63.82	38.58	0.00
20-80	92.58	92.08	91.20	89.46	77.25	60.11	32.93	0.00
30-70	94.25	93.62	92.48	90.13	73.65	53.66	27.28	0.00
40-60	94.93	94.13	92.62	89.42	68.06	46.46	22.22	0.00
50-50	95.12	94.08	92.01	87.54	60.86	38.96	17.68	0.00
60-40	94.93	93.48	90.53	84.12	52.09	31.29	13.56	0.00
70-30	94.25	92.09	87.59	78.17	41.71	23.54	9.79	0.00
80-20	92.58	88.94	81.41	67.39	29.63	15.73	6.30	0.00
90-10	87.53	79.70	65.54	46.32	15.76	7.88	3.05	0.00
Variation	**7.59**	**14.43**	**27.08**	**43.81**	**61.49**	**55.94**	**35.53**	**0.00**

Maximum point before value decrease

Table. E.2: V and V1 total permittivity's t1 and t2 using Tangent method

	Test #	LrT	KaT	Δt	t1	t2
		m		ps	ps	ps
Graphically	Test 1	0.100	8.8	1981	797	2778
	Test 2	0.100	8.3	1920	798	2718
	Test 3	0.100	9.5	2059	790	2849
Arithmetic	Test 1	0.096	5.0	1433	1345	2778
	Test 2	0.098	5.2	1492	1226	2718
	Test 3	0.100	5.8	1605	1244	2849
Refractive index	Test 1	0.096	4.9	1412	1366	2778
	Test 2	0.098	5.1	1480	1238	2718
	Test 3	0.100	5.7	1597	1252	2849

Table. E.3: V and V1 total permittivity's t1 and t2 using Heimovaara method

	Test #	LrT	KaT	Δt	t1	t2
		m		ps	ps	ps
Graphicaly	Test 1	0.100	9.0	1996	782	2778
	Test 2	0.100	8.4	1936	782	2718
	Test 3	0.100	9.6	2067	782	2849
Arithmetic	Test 1	0.096	5.0	1428	1350	2778
	Test 2	0.098	5.2	1491	1227	2718
	Test 3	0.100	5.7	1594	1255	2849
Refractive index	Test 1	0.096	4.8	1409	1369	2778
	Test 2	0.098	5.1	1481	1237	2718
	Test 3	0.100	5.7	1587	1263	2849

F. Column's wall impact analysis data

Table. F.1: Percentage error data of the impact of the column's wall

*Layer 1: cell's wall

Exp	Int method	Column	*Layer 2 Material 2	Cell LT (m)	L1/LT	K1	Material L2/LT	K2	K2/K1	KT (WV)	ΔK	ΔK/K2 %
Kab	Tangent	SC	Air	0.049	0.204	1.2	0.796	1.0	0.8	1.0	**0.0**	**3.9**
	Tangent	SC	Water	0.049	0.198	3.3	0.802	79.9	24.0	56.7	**-23.2**	**-29.0**
	Tangent	BC	Air	0.049	0.224	0.9	0.776	1.0	1.1	1.0	**0.0**	**-3.0**
	Tangent	BC	Air	0.049	0.224	0.9	0.776	1.0	1.1	1.0	**0.0**	**-2.0**
	Tangent	BC	Water	0.049	0.224	7.6	0.776	81.7	10.7	58.2	**-23.5**	**-28.7**
	Tangent	BC	Water	0.049	0.224	9.0	0.776	80.6	8.9	58.3	**-22.3**	**-27.6**
	Schwartz	SC	Air	0.049	0.224	2.1	0.776	1.0	0.5	1.2	**0.2**	**20.0**
	Schwartz	SC	Water	0.049	0.204	9.5	0.796	78.7	8.2	59.7	**-19.0**	**-24.1**
	Schwartz	BC	Air	0.049	0.224	1.5	0.776	1.0	0.7	1.1	**0.1**	**10.0**
	Schwartz	BC	Air	0.049	0.224	1.5	0.776	1.0	0.7	1.1	**0.1**	**10.0**
	Schwartz	BC	Water	0.049	0.224	10.2	0.776	78.8	7.7	57.8	**-21.0**	**-26.7**
	Schwartz	BC	Water	0.049	0.224	10.2	0.776	78.8	7.7	57.8	**-21.0**	**-26.7**
	Heimo	SC	Air	0.049	0.204	0.9	0.796	1.0	1.1	1.0	**0.0**	**-2.2**
	Heimo	SC	Water	0.049	0.204	7.1	0.796	79.2	11.2	58.7	**-20.5**	**-25.8**
	Heimo	BC	Air	0.049	0.224	0.5	0.776	1.0	1.9	0.9	**-0.1**	**-11.7**
	Heimo	BC	Air	0.049	0.224	0.9	0.776	1.0	1.1	1.0	**0.0**	**-1.6**
	Heimo	BC	Water	0.049	0.224	6.7	0.776	79.4	11.8	56.1	**-23.3**	**-29.3**
	Heimo	BC	Water	0.049	0.224	8.4	0.776	79.4	9.4	57.2	**-22.2**	**-28.0**
Setups Dry	Heimo	SC	Dry SF-1	0.049	0.224	0.9	0.776	2.6	2.9	2.1	**-0.5**	**-17.8**
	Heimo	SC	Dry SF-1	0.049	0.224	0.9	0.776	2.6	2.9	2.1	**-0.5**	**-17.8**
	Heimo	SC	Dry SF-1	0.049	0.224	0.9	0.776	2.6	2.9	2.2	**-0.5**	**-17.9**
	Heimo	SC	Dry SF-1	0.049	0.224	0.9	0.776	2.7	3.0	2.2	**-0.5**	**-18.0**
	Schwartz	SC	Dry SF-1	0.049	0.224	2.1	0.776	2.8	1.3	2.6	**-0.2**	**-5.6**
	Schwartz	SC	Dry SF-1	0.049	0.224	2.1	0.776	2.8	1.3	2.6	**-0.2**	**-5.6**
	Schwartz	SC	Dry SF-1	0.049	0.224	2.1	0.776	2.9	1.4	2.7	**-0.2**	**-6.5**
	Schwartz	SC	Dry SF-1	0.049	0.224	2.1	0.776	2.9	1.4	2.7	**-0.2**	**-6.5**
Setups Dry	Tangent	SC	Dry SF-1	0.049	0.224	1.2	0.776	2.6	2.1	2.2	**-0.3**	**-13.5**
	Tangent	SC	Dry SF-1	0.049	0.224	1.2	0.776	2.6	2.2	2.3	**-0.4**	**-13.7**
	Tangent	SC	Dry SF-1	0.049	0.224	1.2	0.776	2.7	2.2	2.3	**-0.4**	**-14.2**
	Tangent	SC	Dry SF-1	0.049	0.224	1.2	0.776	2.7	2.3	2.3	**-0.4**	**-14.3**
Setups Moist	Heimo	SC	Moist SF-1	0.049	0.224	0.9	0.776	4.7	5.2	3.6	**-1.1**	**-23.7**
	Heimo	SC	Moist SF-1	0.049	0.224	0.9	0.776	4.7	5.2	3.6	**-1.1**	**-23.7**
	Heimo	SC	Moist SF-1	0.049	0.224	0.9	0.776	4.4	4.8	3.4	**-1.0**	**-23.1**
	Heimo	SC	Moist SF-1	0.049	0.224	0.9	0.776	4.4	4.9	3.4	**-1.0**	**-23.2**
	Schwartz	SC	Moist SF-1	0.049	0.224	2.1	0.776	4.5	2.2	3.9	**-0.6**	**-13.8**
	Schwartz	SC	Moist SF-1	0.049	0.224	2.1	0.776	4.7	2.2	4.0	**-0.7**	**-14.2**
	Schwartz	SC	Moist SF-1	0.049	0.224	2.1	0.776	4.4	2.1	3.8	**-0.6**	**-13.4**
	Schwartz	SC	Moist SF-1	0.049	0.224	2.1	0.776	4.4	2.1	3.8	**-0.6**	**-13.4**
	Tangent	SC	Moist SF-1	0.049	0.224	1.2	0.776	4.5	3.8	3.6	**-0.9**	**-20.5**
	Tangent	SC	Moist SF-1	0.049	0.224	1.2	0.776	4.6	3.9	3.7	**-1.0**	**-20.7**
	Tangent	SC	Moist SF-1	0.049	0.224	1.2	0.776	4.3	3.6	3.4	**-0.8**	**-19.8**
	Tangent	SC	Moist SF-1	0.049	0.224	1.2	0.776	4.4	3.7	3.5	**-0.9**	**-20.1**

147

Exp	Int method	Column	*Layer 2 Material 2	Cell LT (m)	L1/LT	K1	Material L2/LT	K2	K2/K1	KT (WV)	ΔK	ΔK/K2 %
Setups Wet	Heimo	SC	Wet SF-1	0.049	0.224	7.1	0.776	18.0	2.5	15.1	**-2.9**	**-16.1**
	Heimo	SC	Wet SF-1	0.049	0.224	7.1	0.776	17.8	2.5	15.0	**-2.8**	**-15.9**
	Heimo	SC	Wet SF-1	0.049	0.224	7.1	0.776	17.0	2.4	14.4	**-2.6**	**-15.3**
	Heimo	SC	Wet SF-1	0.049	0.224	7.1	0.776	17.0	2.4	14.4	**-2.6**	**-15.3**
	Schwartz	SC	Wet SF-1	0.049	0.224	9.5	0.776	17.2	1.8	15.3	**-1.9**	**-11.2**
	Schwartz	SC	Wet SF-1	0.049	0.224	9.5	0.776	17.1	1.8	15.2	**-1.9**	**-11.1**
	Schwartz	SC	Wet SF-1	0.049	0.224	9.5	0.776	16.1	1.7	14.5	**-1.6**	**-10.2**
	Schwartz	SC	Wet SF-1	0.049	0.224	9.5	0.776	16.1	1.7	14.5	**-1.6**	**-10.2**
	Tangent	SC	Wet SF-1	0.049	0.224	3.3	0.776	20.3	6.2	15.3	**-5.1**	**-24.9**
	Tangent	SC	Wet SF-1	0.049	0.224	3.3	0.776	19.9	6.0	15.0	**-4.9**	**-24.8**
	Tangent	SC	Wet SF-1	0.049	0.224	3.3	0.776	19.2	5.8	14.5	**-4.7**	**-24.5**
	Tangent	SC	Wet SF-1	0.049	0.224	3.3	0.776	19.3	5.8	14.5	**-4.7**	**-24.5**
Multi L	Tangent	BC	SF-1	0.049	0.224	0.9	0.776	3.3	3.7	2.6	**-0.7**	**-20.2**
T1	Tangent	BC	SF-1	0.049	0.224	0.9	0.776	6.6	7.4	4.9	**-1.7**	**-26.3**
T2	Tangent	BC	SF-1	0.049	0.224	0.9	0.776	3.9	4.4	3.1	**-0.9**	**-21.9**
T2	Tangent	BC	SF-1	0.049	0.224	0.9	0.776	6.6	7.3	4.8	**-1.7**	**-26.2**
T3	Tangent	BC	SF-1	0.049	0.224	0.9	0.776	4.7	5.2	3.6	**-1.1**	**-23.5**
T3	Tangent	BC	SF-1	0.049	0.224	0.9	0.776	7.0	7.8	5.2	**-1.9**	**-26.7**
T1	Heimo	BC	SF-1	0.049	0.224	0.5	0.776	3.4	6.8	2.5	**-0.9**	**-25.7**
T1	Heimo	BC	SF-1	0.049	0.224	0.9	0.776	6.5	7.2	4.8	**-1.7**	**-26.1**
T2	Heimo	BC	SF-1	0.049	0.224	0.5	0.776	4.0	8.0	2.9	**-1.1**	**-26.9**
T2	Heimo	BC	SF-1	0.049	0.224	0.9	0.776	6.5	7.2	4.8	**-1.7**	**-26.1**
									9.3	3.4	**-1.3**	**-27.9**
T3	Heimo	BC	SF-1	0.049	0.224	0.5	0.776	4.6	7.2	4.8	**-1.7**	**-26.1**
T3	Heimo	BC	SF-1	0.049	0.224	0.9	0.776	6.9	7.7	5.1	**-1.8**	**-26.6**

G. Column's wall permittivity waveforms correction

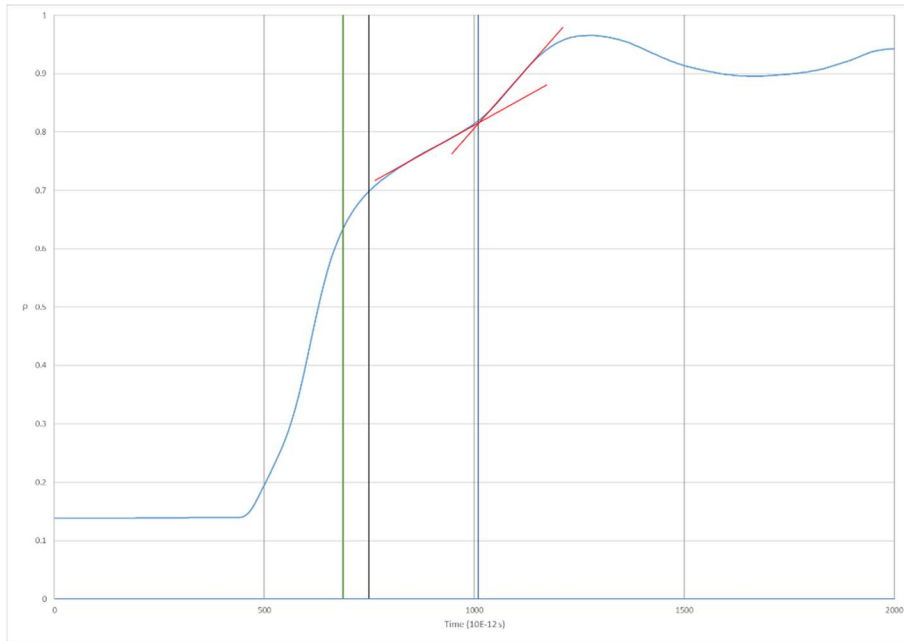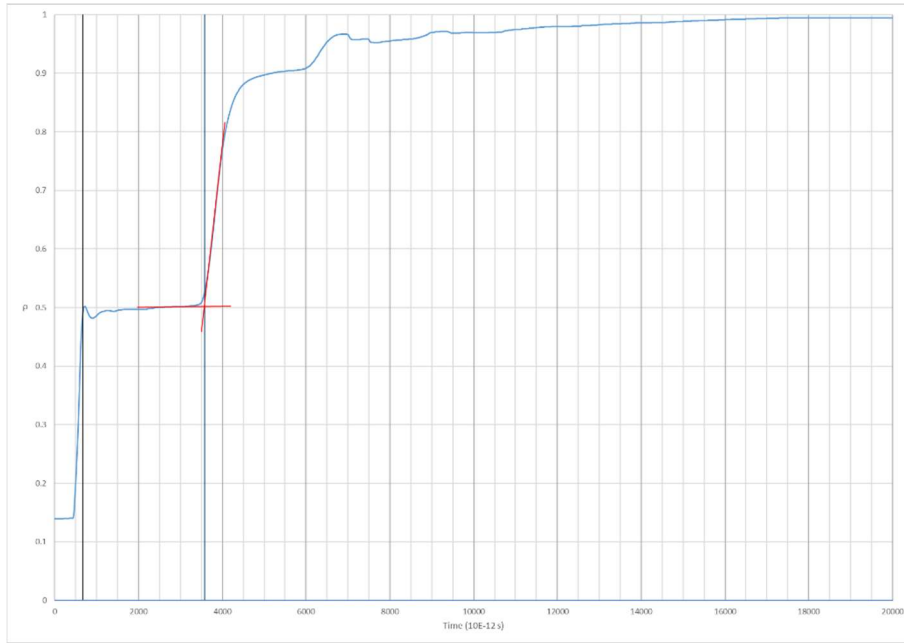## G.1   Column's wall of permittivity SC correction (waveforms)
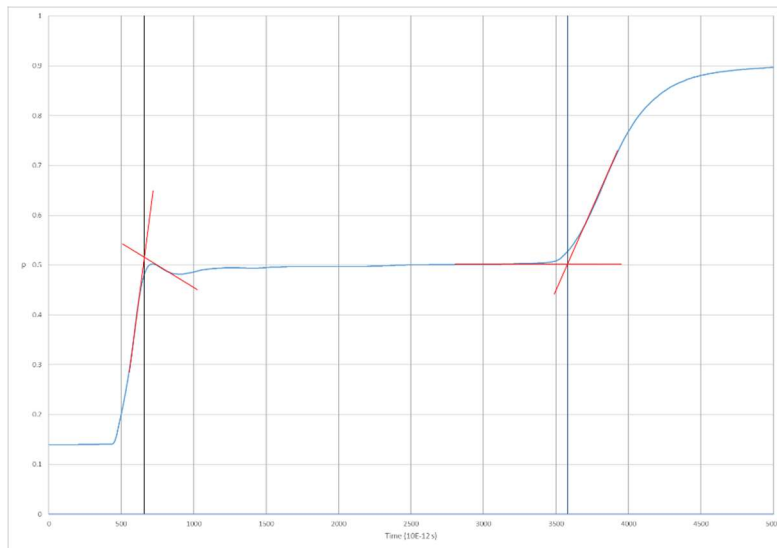
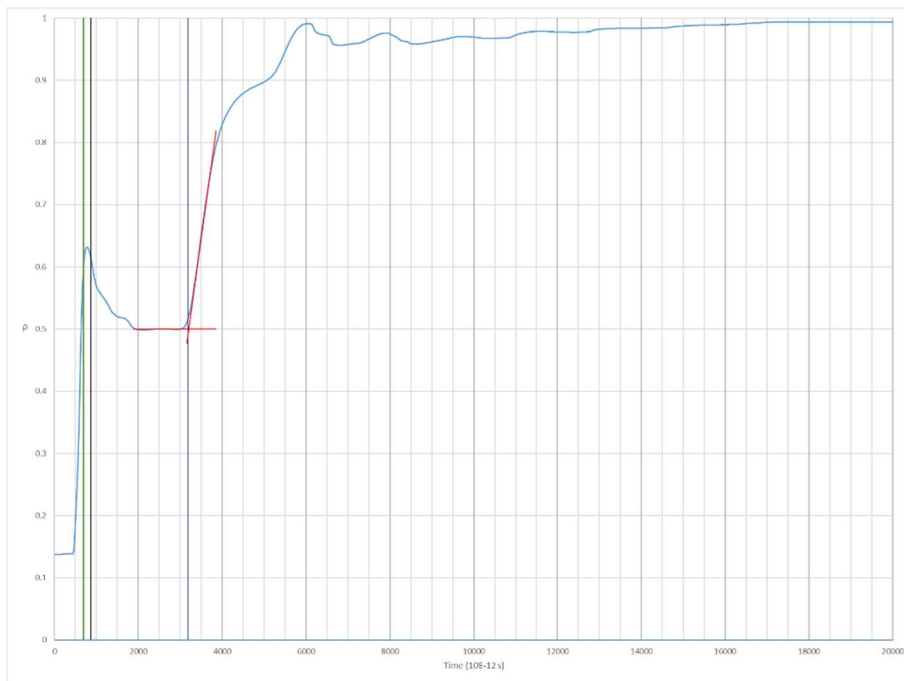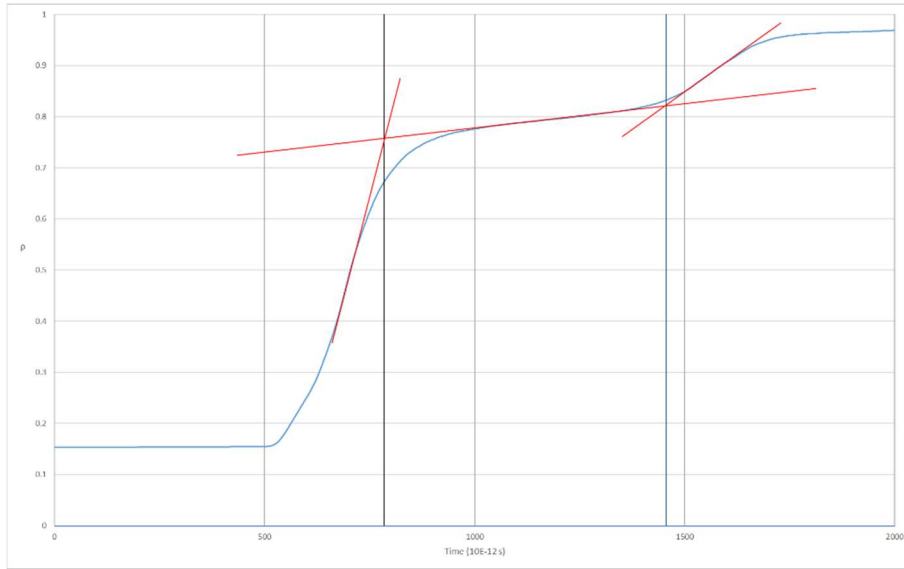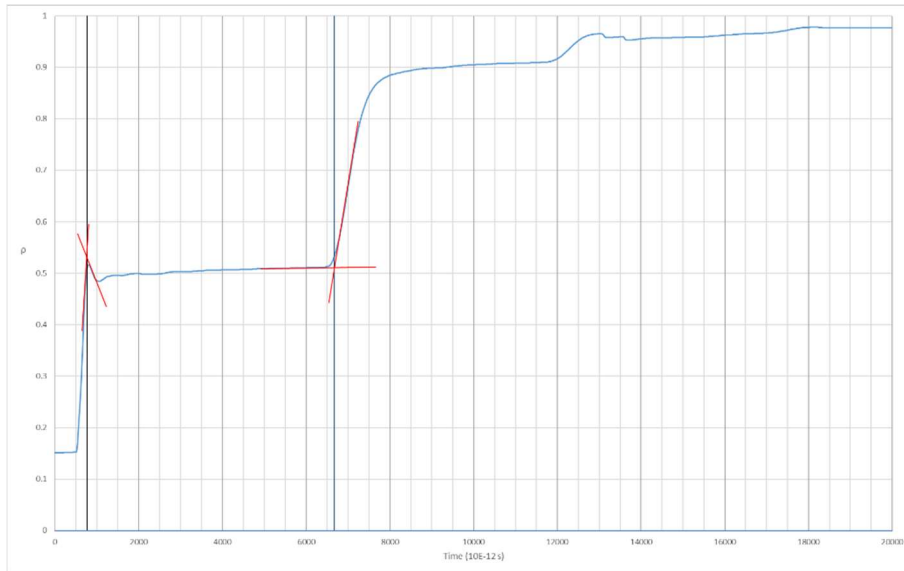*Figure. G.1: Waveform obtained in water with TDR 305, interpretation using tangent method*
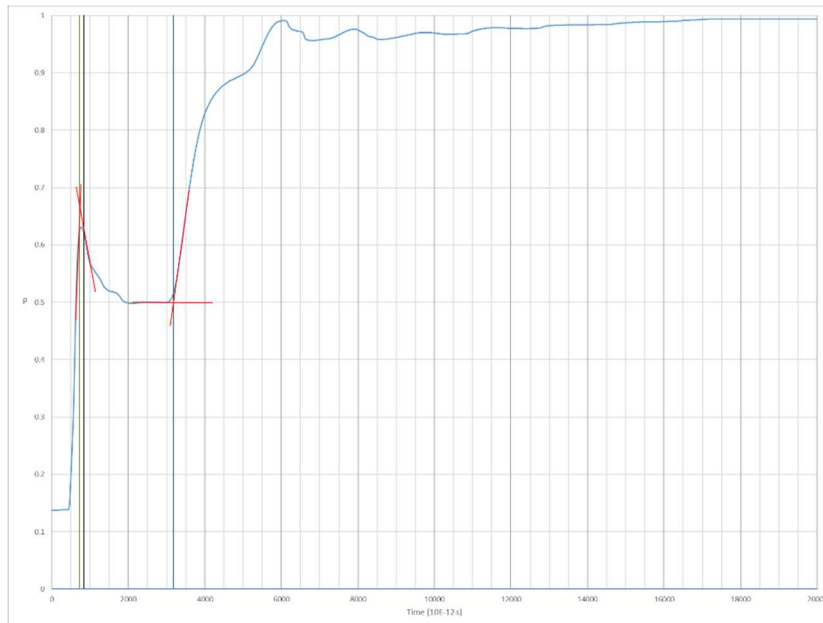
Figure. G.2: Waveform obtained from TDR 305 crossing the Column SC column's wall and water. Interpretation using tangent method
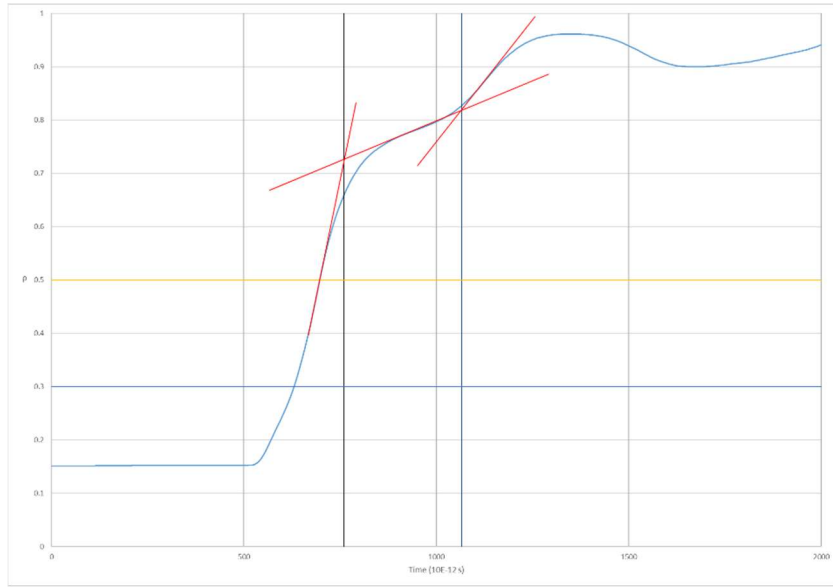
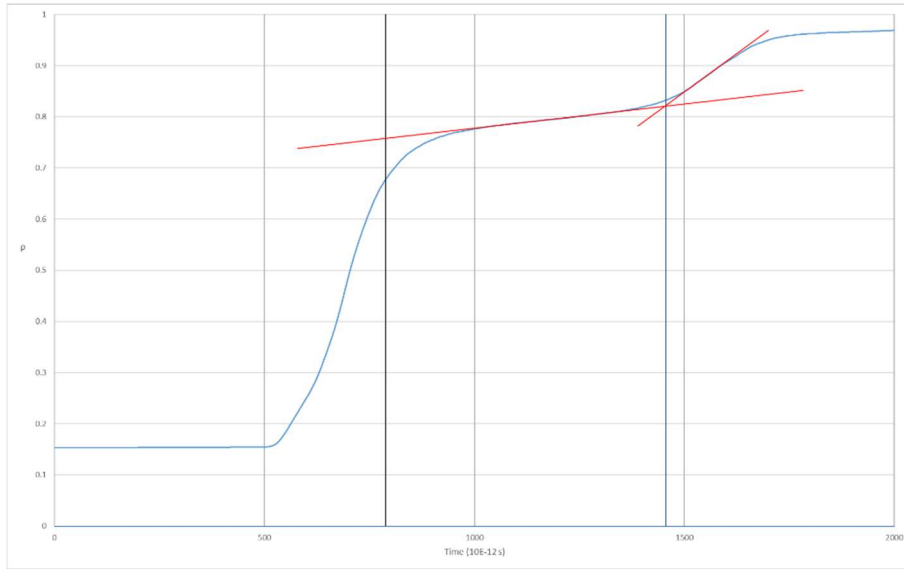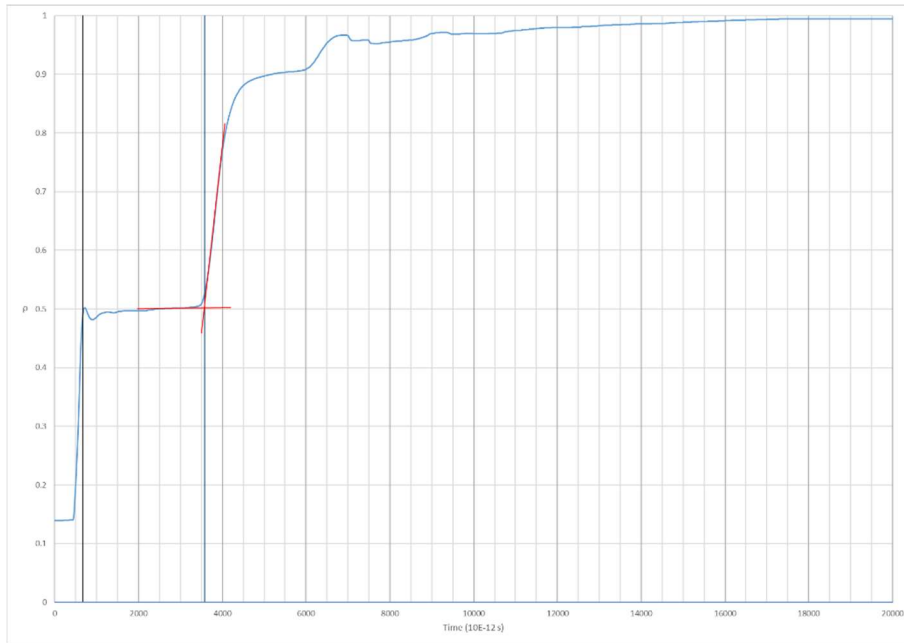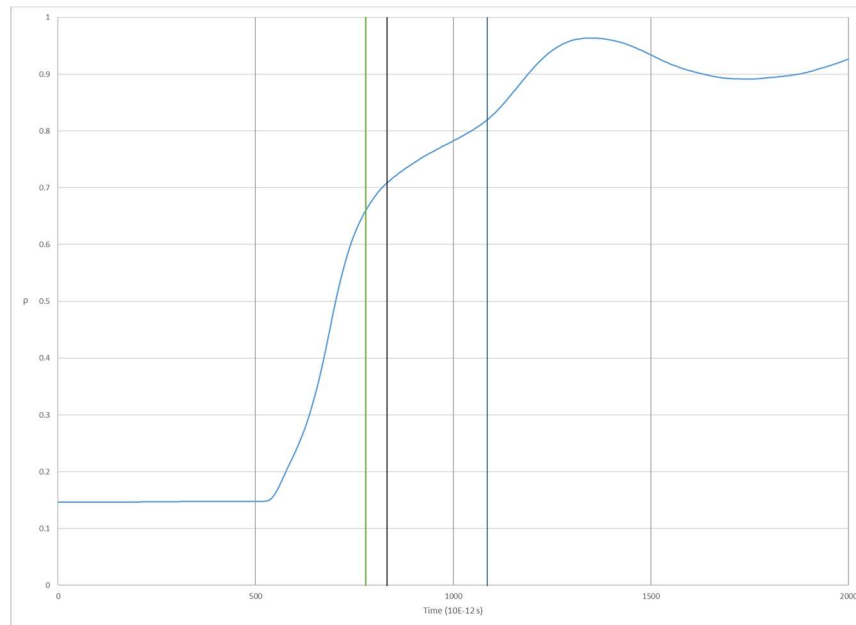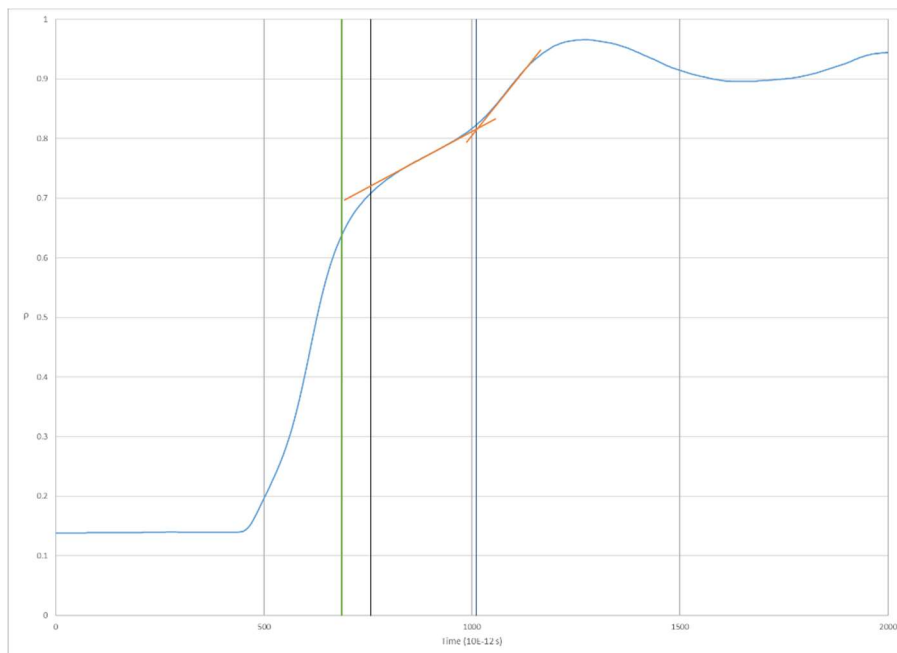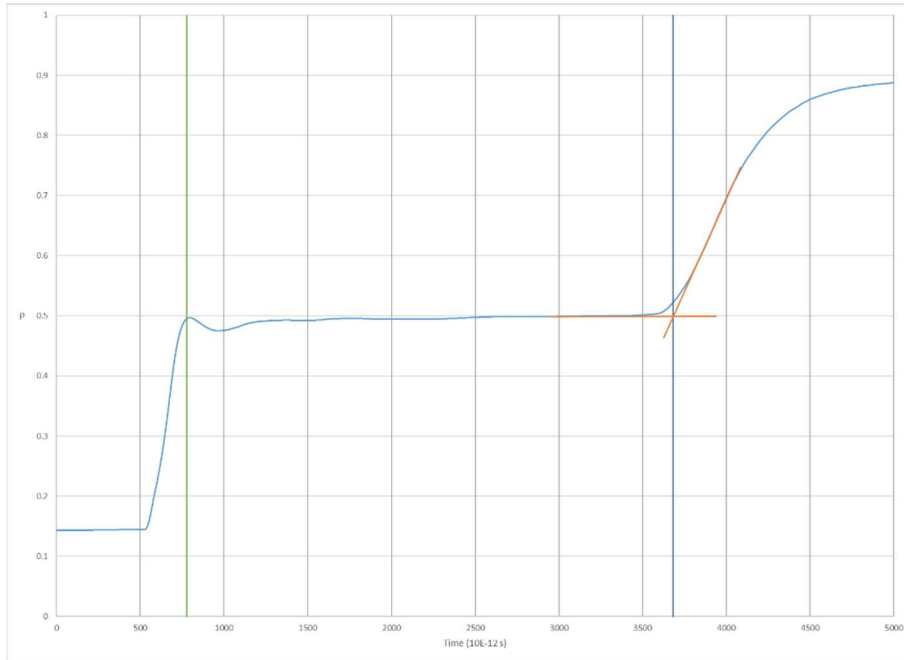*Figure. G.3: Waveform obtained in air with TDR 305, interpretation using tangent method*
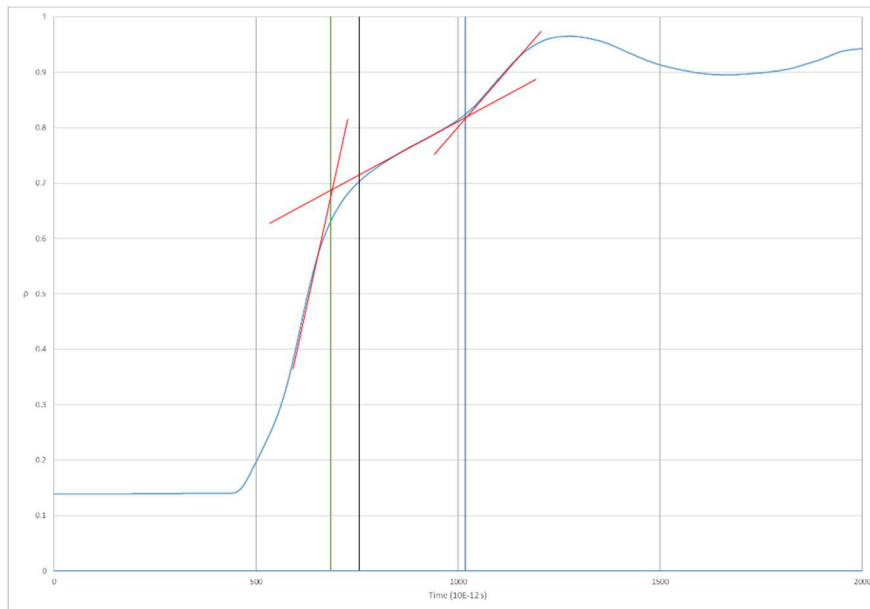
Figure. G.4: Waveform obtained from TDR 305 crossing the Column SC column's wall and air.
Interpretation using tangent method
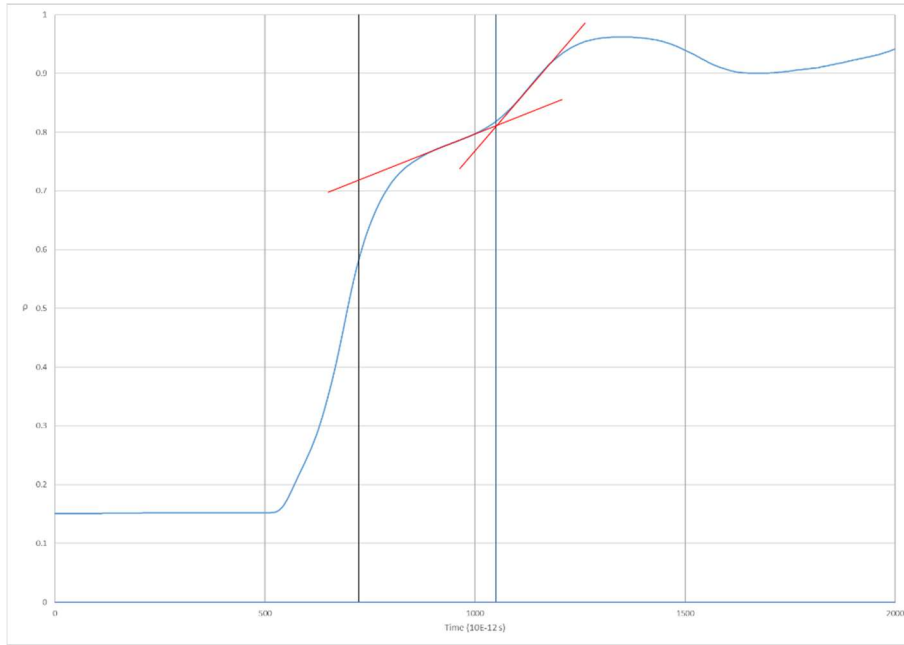
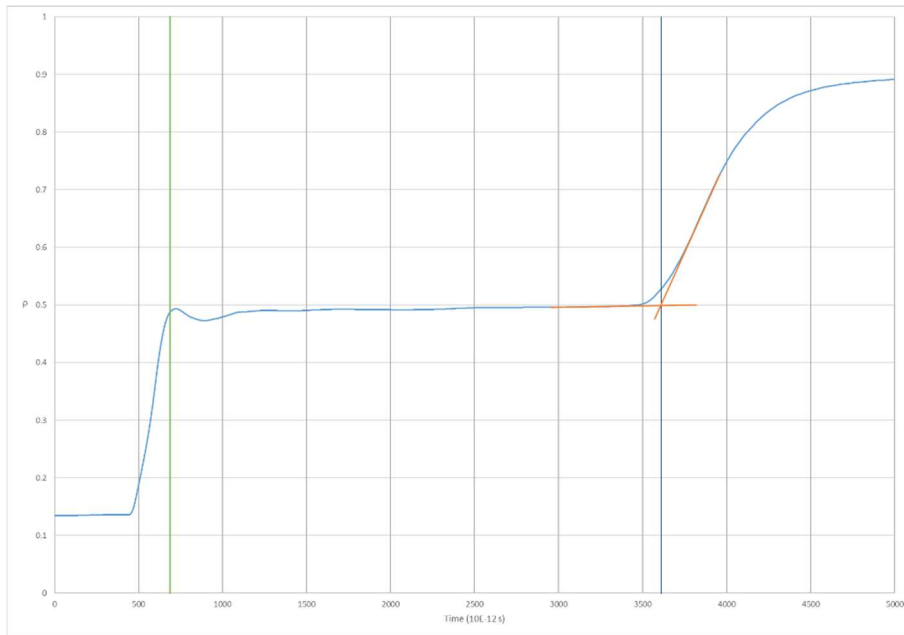*Figure. G.5: Waveform obtained in air with TDR 305, interpretation using Heimovaara method*

Figure. G.6: Waveform obtained from TDR 305 crossing the Column SC column's wall and air.
Interpretation using Heimovaara method

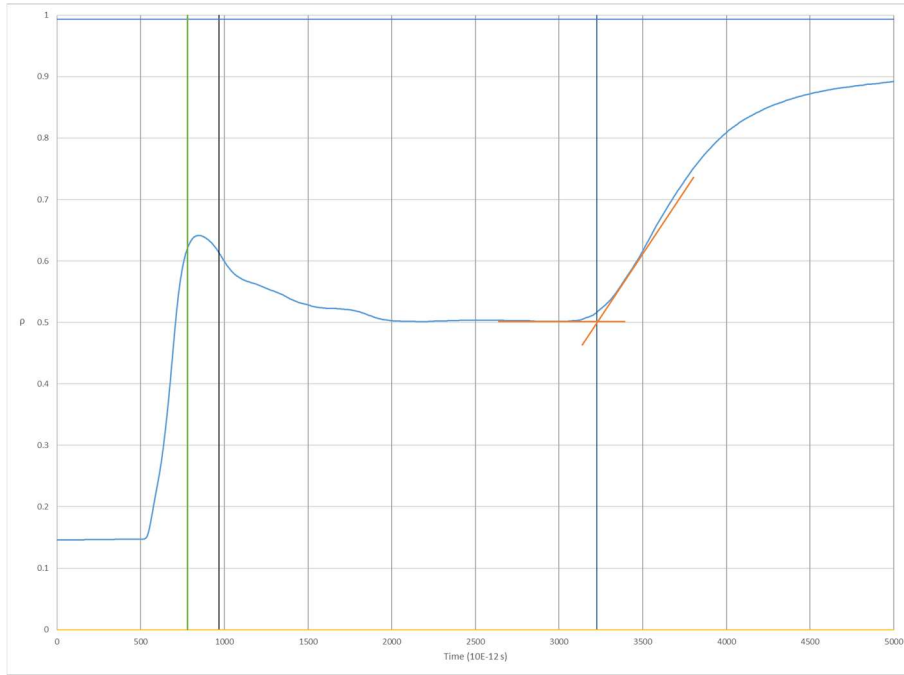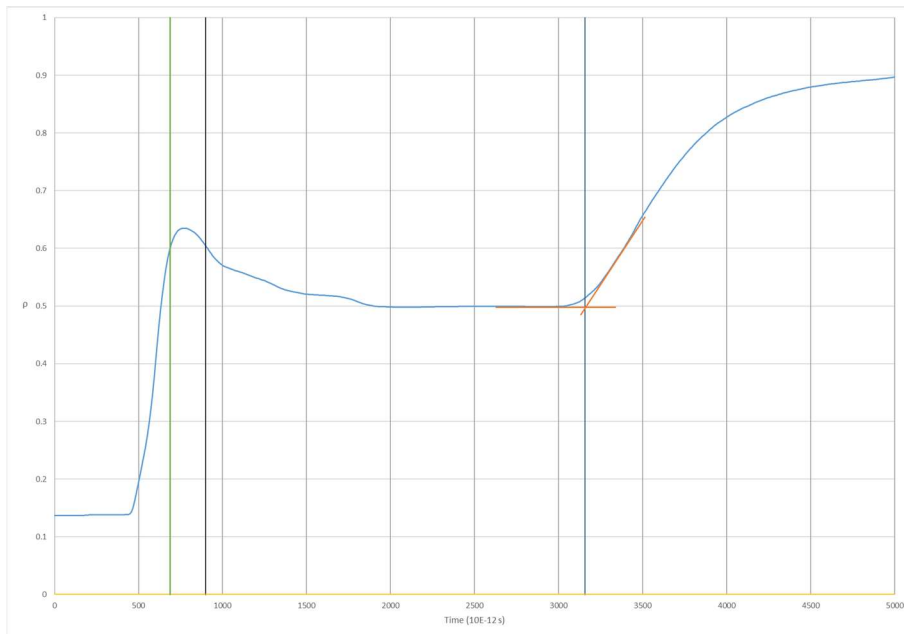*Figure. G.7: Waveform obtained in water with TDR 305, interpretation using Heimovaara method*

Figure. G.8: Waveform obtained from TDR 305 crossing the Column SC column's wall and water. Interpretation using Heimovaara method
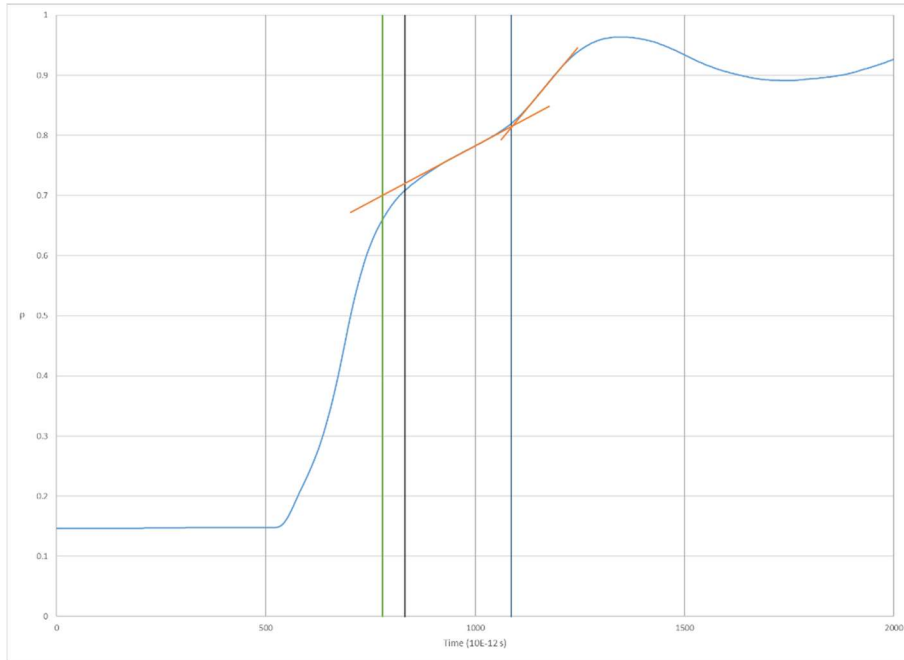
Figure. G.9: Waveform obtained in air with TDR 310, interpretation using tangent method

Figure. G.10: Waveform obtained in water with TDR 310, interpretation using tangent method

154

Figure. G.11: Waveform obtained in air with TDR 310, interpretation using Heimovaara method

Figure. G.12: Waveform obtained in water with TDR 310, interpretation using Heimovaara method

G.2   Column's wall of permittivity BC correction (waveforms)

Figure. G.13: Waveform obtained from TDR 305-144 crossing the Column BC column's wall and air. Interpretation using Heimovaara method method
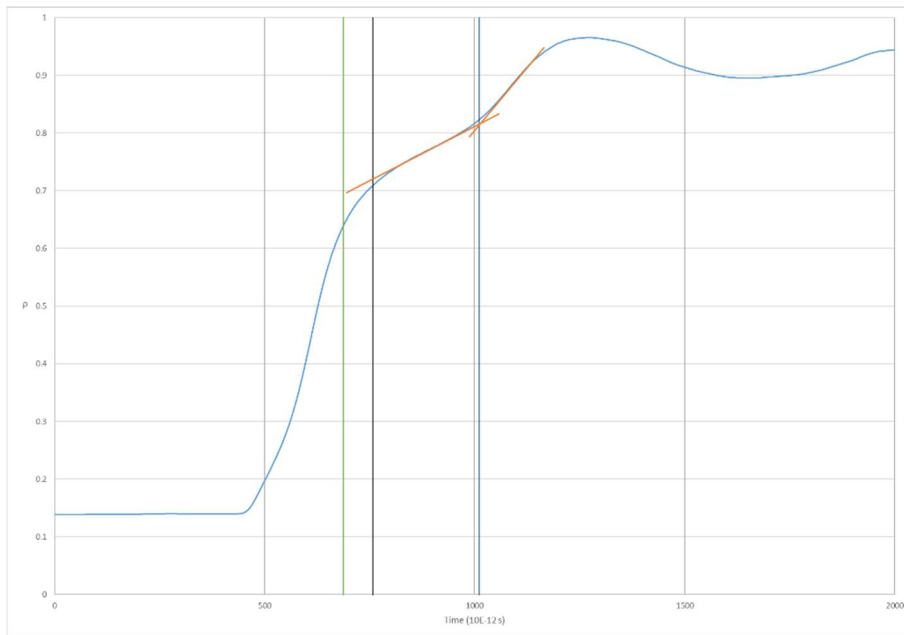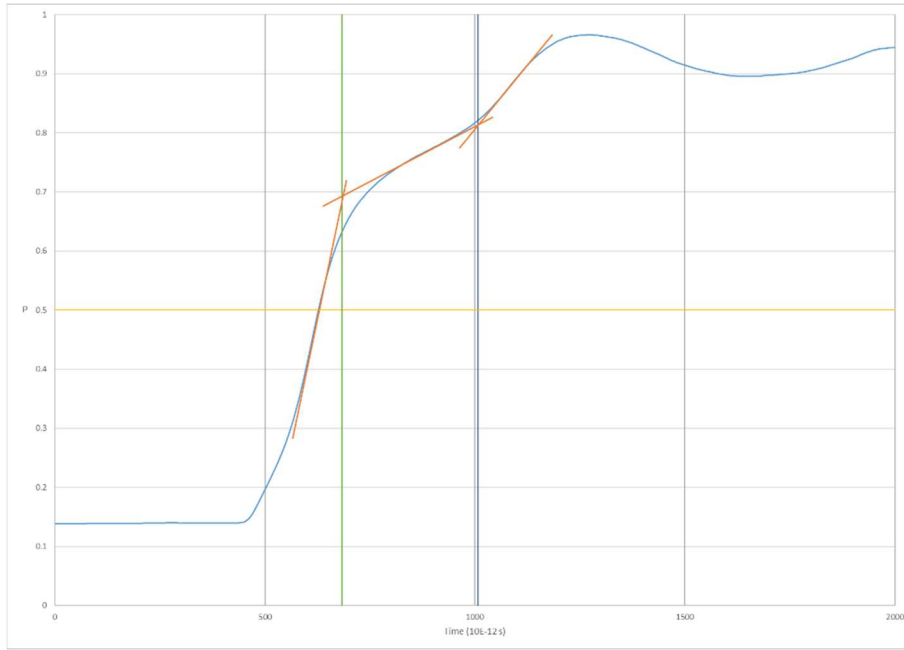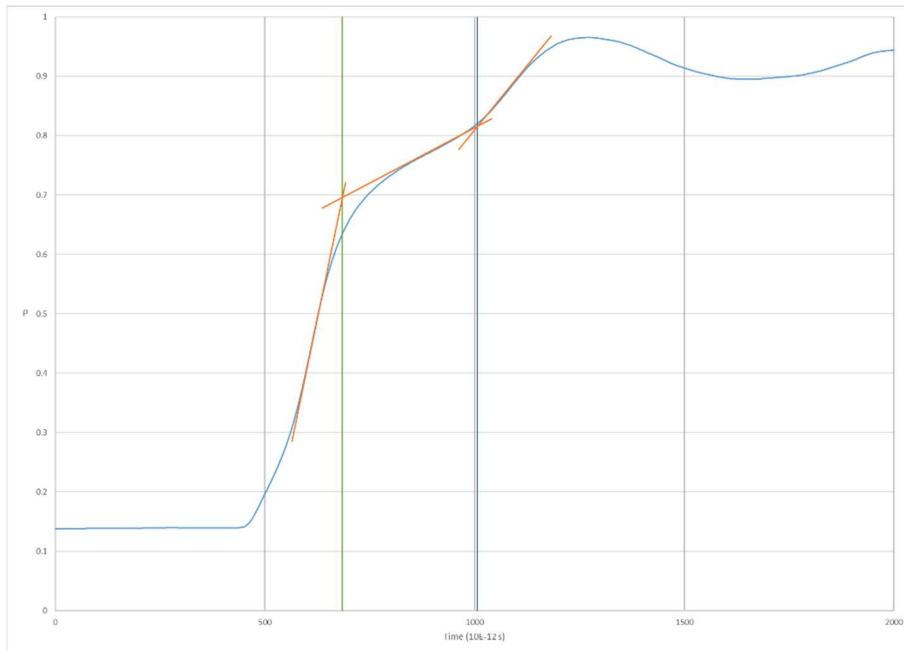

Figure. G.14:Waveform obtained from TDR 305-152 crossing the Column BC column's wall and air. Interpretation using Heimovaara method
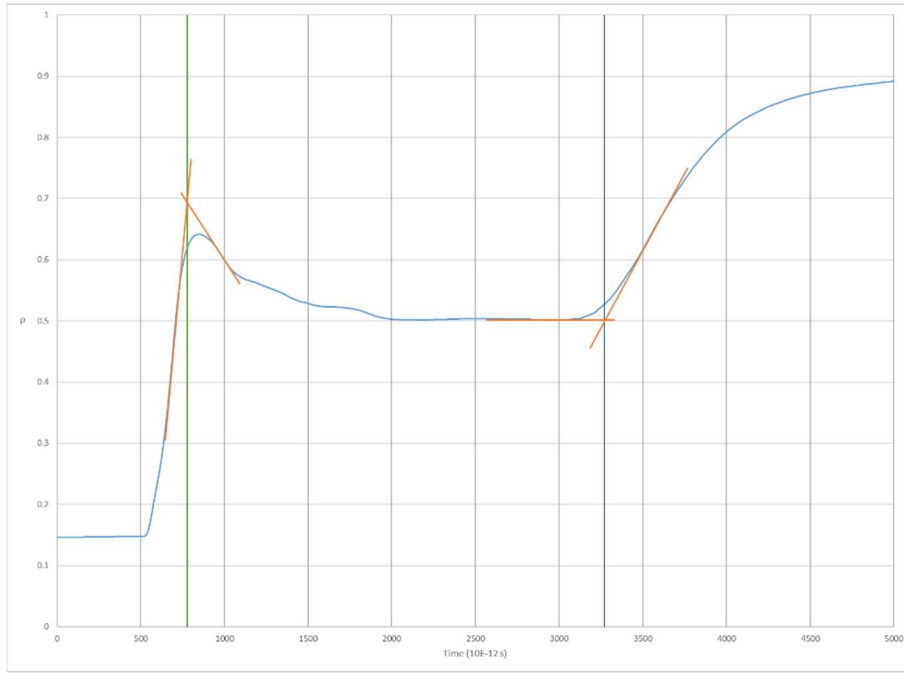
Figure. G.15: Waveform obtained in water with TDR 305-152, interpretation using Heimovaara

Figure. G.16:Waveform obtained in water with TDR 305-144, interpretation using Heimovaara

Figure. G.17: Waveform obtained from TDR 305-144 crossing the Column BC column's wall and water. Interpretation using Heimovaara method

Figure. G.18: Waveform obtained from TDR 305-152 crossing the Column BC column's wall and water. Interpretation using Heimovaara method

Figure. G.19: Waveform obtained from TDR 305-144 crossing the Column SC column's wall and air. Interpretation using Heimovaara method

Figure. G.20: Waveform obtained from TDR 305-152 crossing the Column SC column's wall and air. Interpretation using Heimovaara method
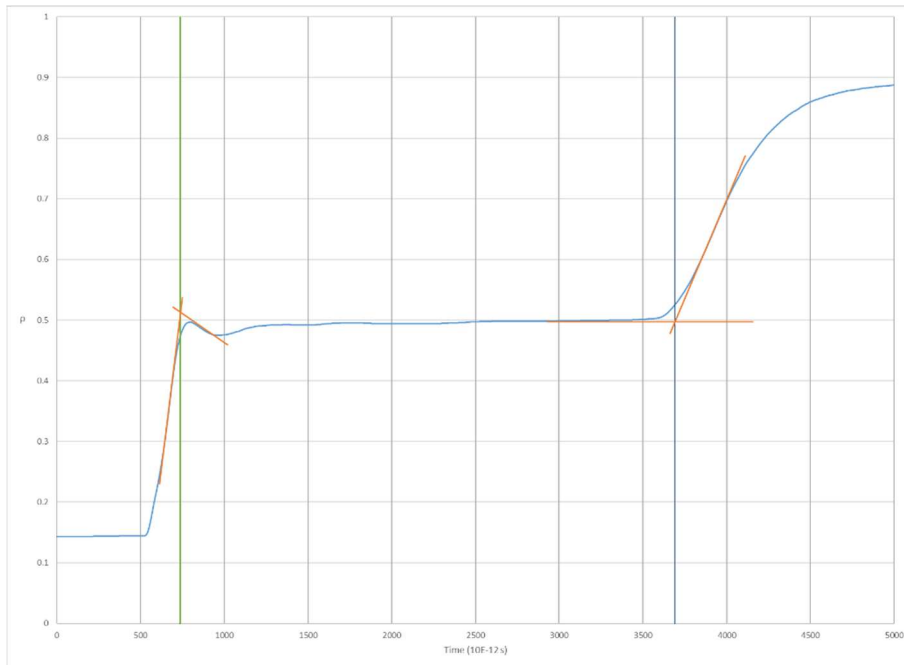
159

Figure. G.21: Waveform obtained from TDR 305-144 crossing the Column SC column's wall and air. Interpretation using tangent method

Figure. G.22:Waveform obtained from TDR 305-152 crossing the Column SC column's wall and air. Interpretation using tangent method

160

Figure. G.23: Waveform obtained from TDR 305-144 crossing the Column BC column's wall and water. Interpretation using Tangent method

Figure. G.24: Waveform obtained from TDR 305-144 in water. Interpretation using Tangent method
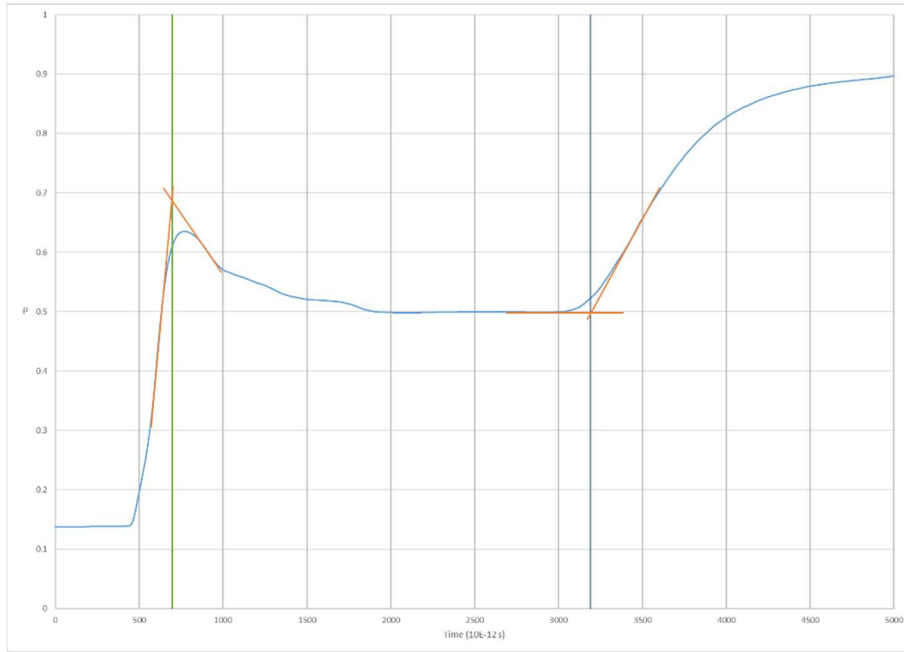
161

Figure. G.25: Waveform obtained from TDR 305-152 crossing the Column BC column's wall and water. Interpretation using Tangent method
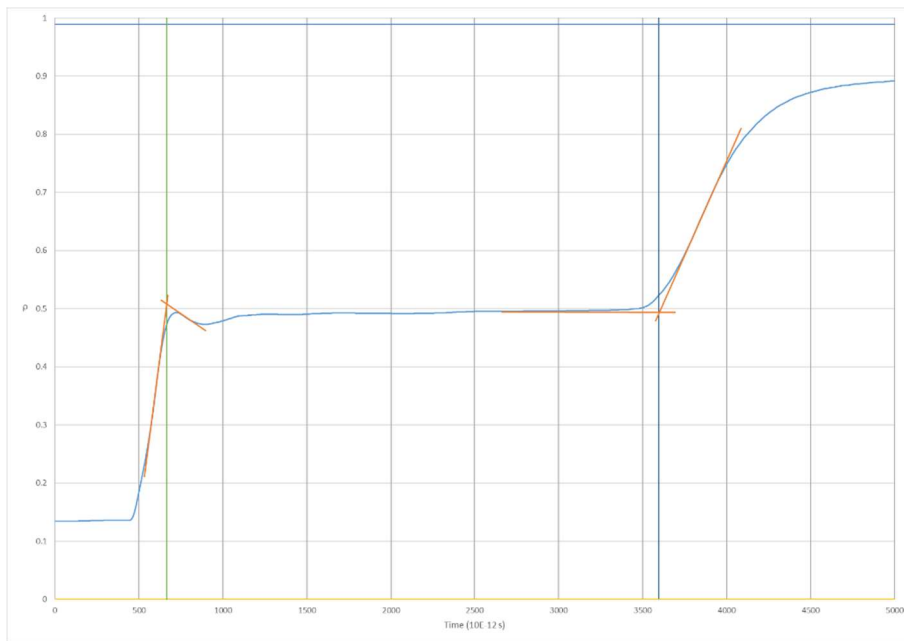

Figure. G.26: Waveform obtained from TDR 305-152 in water. Interpretation using Tangent method